Development of an indirect bridge health monitoring approach using moving sensors

by

JIANTAO LI

B.Sc., M.Sc.

A thesis submitted in partial fulfilment of the requirements for the

Degree of Doctor of Philosophy

University of Technology Sydney

Faculty of Engineering and Information Technology

September 2019

CERTIFICATION OF ORGINAL AUTHORSHIP

I, Jiantao Li, declare that this thesis is submitted in fulfilment of the requirements for the award of Degree of PhD., in the Faculty of Engineering and Information Technology at the University of Technology Sydney.

This thesis is wholly my own work unless otherwise referenced or acknowledged. In addition, I certify that all information sources and literature used are indicated in the thesis.

This document has not been submitted for qualifications at any other academic institution.

This research is supported by the Australian Government Research Training Program.

Production Note:
Signature: Signature removed prior to publication.

Date: 31/01/2020

ACKNOWLEDGEMENTS

First and foremost, I would like to express my sincere gratitude to my principal supervisor, Prof. Xinqun Zhu, for his patience, insightful motivation and continuous support of my PhD study. Professor Zhu has offered much invaluable academic and personal advice to me. His immense knowledge and great personality have impressed and affected me greatly.

I also would like to thank my other supervisors, Prof. Bijan Samali, Prof. Jianchun Li and Prof. Siu-seong Law for their advice and guidance during my PhD study. Especially, Prof. Siu-seong Law's guidance helped me a lot in my research and paper writing. Without their help this thesis would not have been possible. I also wish to express my gratitude to Prof. Ying Lei and Dr. Lijun Liu of Xiamen University who have provided great help and guidance to me since long time ago. Their help has had a profound influence in my life.

The help from Mr. Robert Marshall in Western Sydney University for the arrangement and setting up the experimental testbed in the structural lab is much appreciated. I also very much appreciate the help from lab technicians Mr. Murray Bolden and Mr. Ali Ghari Zadeh during my experimental tests. The instrumentation system and data management on the actual cable-stay bridge are done by Data 61 and some experimental tests on the bridge were arranged by Dr. Makki Alamdari Mehrisadat. Their help is also greatly appreciated. I would also thank the staff in Centre for Infrastructure Engineering in Western Sydney University and School of Civil and Environmental Engineering in University of Technology Sydney who were always helpful and supportive when I needed help during my research.

Many thanks are given to my dear friends whom I am shared all those times with on the path to a PhD. I would like to express my gratitude towards the group of fellow students who have made the leisure time of the journey pleasant and enriched my daily life.

Last but not least, many thanks go to my family including my parents, my sister and my parents-in-law for their understanding and support. Special thanks is given to my wife, Dr. Siyi Lu, who is always by my side, encouraging me and trusting me. The love and smile from them make me strong, and this thesis is dedicated to them.

This research is supported by research funding of the Australian Research Council Discovery Project (DP160103197).

LIST OF PUBLICATIONS

Journal papers

1. Li J.T., Zhu X.Q., Law S.S. and Samali B. (2019) Indirect bridge modal parameters identification with one stationary and one moving sensors and stochastic subspace identification. *Journal of Sound and Vibration* 446: 1-21.

2. Li J.T., Zhu X.Q., Law S.S. and Samali B. (2019) Drive-by blind modal identification with singular spectrum analysis. *Journal of Aerospace Engineering ASCE* 32(4): 04019050.

3. Li J.T., Zhu X.Q., Law S.S. and Samali B. (2019) A two-step indirect bridge damage detection using vehicle axle responses by Dual Kalman Filter. *Mechanical Systems and Signal Processing* (submitted on 16 May 2019)

4. Li J.T., Zhu X.Q., Law S.S. and Samali B. (2019) Time-varying characteristics of bridges under passage of vehicles. *Mechanical Systems and Signal Processing* (submitted on 8 July 2019)

Conference papers

1. Li J.T., Zhu X.Q. and Samali B. (2017) "Extraction of bridge modal parameters using a moving instrumented vehicle by SSI technique." *Proceedings of the 8th International Conference on Structural Health Monitoring of Intelligent Infrastructure*, 5-8 December 2017, Brisbane, Australia.

2. Zhu X.Q., Li J.T. and Samali B. (2018) "Estimation of bridge frequency from the vibration measurements of a moving vehicle by using blind source separation technique."

Proceedings of the 7th World Conference on Structural Control and Monitoring, 22-25 July 2018, Qingdao, China.

3. Li J.T. and Zhu X.Q. (2018) "Condition assessment of highway bridges under traffic loadings." *Proceedings of the 15th International Symposium on Structural Engineering*, 24-27 October 2018, Hangzhou, China.

4. Li J.T., Zhu X.Q. and Samali B. (2018) "Bridge operational modal identification using sparse blind source separation." *Proceedings of the 25th Australasian Conference on the Mechanics of Structures and Materials*, 4-7 December 2018, Brisbane, Australia.

5. Li J.T. and Zhu X.Q. (2019) "Bridge Damage Identification via Interaction Forces of the Vehicle-bridge System using Vehicle Axle Responses." *Proceedings of the 9th International Conference on Structural Health Monitoring of Intelligent Infrastructure*, 4-7 August 2019, ST. Louis, USA.

6. Li J.T. and Zhu X.Q. (2019) "Drive-by bridge parameter identification: an overview." *Proceedings of the 16th East Asia-Pacific Conference on Structural Engineering & Construction (EASEC16)*, 3-6 December 2019, Brisbane, Australia.

ABSTRACT

The inevitable deterioration and damage of bridge infrastructures due to repeated and excess traffic loading, environmental erosion and ageing are of great concern worldwide. Bridge structural health monitoring (SHM) is critical to obtain structural health information and early warning for potential damage. Most of the current SHM strategies measure vibration responses from sensors installed at different locations on the bridge. This direct approach poses several challenges, such as the high cost of the installation and maintenance of sensors, the need for extensive data processing and the insufficient spatial information. To seek a more economical and flexible way to monitor bridges, an indirect approach that measures responses of a passing vehicle has recently drawn great attention. This strategy involves the use of instrumented vehicles as a moving sensory system to capture bridge dynamic information via vehicle-bridge interaction (VBI). Sensors are installed on the vehicle axles or body. However, the responses from sensors on a moving vehicle are nonstationary, noisy and significantly affected by the surface roughness of the bridge. Therefore, most of the classical output-only system identification approaches based on the assumption of white noise excitation may fail to extract accurate structural dynamic properties.

This research aims to establish a framework for bridge SHM using vehicle-based mobile sensory systems. Indirect structural identification methods that consider the intrinsic nonstationary characteristics of VBI responses are proposed to extract the bridge dynamic parameters from vehicle acceleration responses. Firstly, a Short-time Stochastic Subspace Identification (STSSI) strategy was proposed to identify bridge modal frequencies and mode shapes. This method combines conventional SSI with a rescale procedure to estimate the bridge modal parameters using the responses of two instrumented vehicles.

Secondly, based on the sequential implementation of singular spectrum analysis (SSA) and blind source separation (BSS), a method named drive-by blind modal identification with singular spectrum analysis (SSA-BSS) was proposed to extract the response components from a single set of vehicle vibration responses. The bridge frequencies can be identified from the obtained bridge related components.

Numerical and experimental results clearly demonstrated the feasibility and effectiveness of the proposed methods for indirect identification of bridge modal frequencies and mode shapes. To gain insight on the time-dependent features of VBI system, a time-frequency (TF) analysis method called Synchroextracting transform (SET) was used to analyse the vehicle and bridge responses in TF domain. The instantaneous frequencies (IFs) of the system revealed the time-varying characteristics of the VBI system. Besides the indirect bridge modal identification, a two-step drive-by bridge damage detection strategy using vehicle axle responses was proposed. Dual Kalman filter (DKF) was applied to identify the interaction forces between vehicle and bridge. With the interaction forces, a sensitivity analysis was performed with regularization technique to identify the bridge damage. The proposed two-step damage detection method effectively identified the location and extent of the damages using vehicle axle responses, which demonstrated its great potential for drive-by bridge damage detection. Moreover, the SSA-BSS and the TF analysis strategy were successfully applied to analyse the responses from an in-situ VBI system.

In summary, an indirect bridge SHM technique using vehicle-based moving sensing system was developed in this study. Bridge modal identification and damage detection were conducted successfully using vehicle responses. Results further demonstrated that it can be a convenient and cost-effective alternative or a promising complement to conventional bridge SHM.

TABLE OF CONTENTS

LIST OF ABBREVIATIONS

SHM	Structural Health Monitoring
VBI	Vehicle-Bridge Interaction
SSI	Stochastic Subspace Identification
STSSI	Short-Time Stochastic Subspace Identification
SSA	Singular Spectrum Analysis
BSS	Blind Source Separation
TF	Time-Frequency
TFA	Time-Frequency Analysis
SET	Synchroextracting Transform
IFs	Instantaneous frequencies
DKF	Dual Kalman Filter
FDD	Frequency Domain Decomposition
RDT	Random Decrement Technique
DOFs	Degrees of Freedom
PCA	Principal Component Analysis
FFT	Fast Fourier Transform
HHT	Hilbert-Huang Transform
HT	Hilbert Transform
EMD	Empirical Mode Decomposition
IMFs	Intrinsic Mode Functions
CWT	Continuous Wavelet Transformation
STFT	Short-time Fourier Transform
NExT	Natural Excitation Technique
IMFs	Intrinsic Mode Functions
IAS	Instantaneous Amplitude Squared
Ref-SSI	Reference-based SSI

SDOF	Single-Degree-of-Freedom
PSD	Power Spectral Density
MAC	Modal Assurance Criterion
DMF	Dynamic Magnification Factor
SOBI	Second-Order Blind Identification
BMID	Blind Modal IDentification
CS	Compressive Sensing
JAD	Joint Approximate Diagonalization
SVD	Singular Value Decomposition
SST	Synchrosqueezing Transform
TFR	Time-Frequency Representation
SNR	Signal-to-Noise Ratio
AKF	Augmented Kalman Filter
ZOH	Zero-Order-Hold
RPE	Relative Percentage Error

LIST OF FIGURES

LIST OF TABLES

CHAPTER 1 INTRODUCTION

1.1 Research background and motivation

Bridge infrastructures play an increasingly important role in modern transportation systems. They are inevitably degraded due to the effect of excess loading, environmental erosion, ageing and other stresses during their designed service life. According to the Australia Infrastructure Report Card (Engineers Australia, 2010), a large proportion of bridge infrastructure in New South Wales is in average to poor conditions. Those in the USA are in similar conditions. According to the ASCE recent Infrastructure Report Card (American Society of Civil Engineers, 2017), 40% of bridges in the USA are more than 50 years old and 9.1% of them are structurally deficient. Recent catastrophic collapse of bridges around the world, such as that of the Minnesota River Bridge (USA) in 2007, the Washington State Bridge (USA) in 2013, and Genoa Bridge (Italy) in 2018, to name a few, highlights the necessity and significance of monitoring the health condition of bridges.

Many studies have been conducted on bridge structural health monitoring (SHM) in the last few decades. Traditional visual-based bridge inspection methods are not adequate for bridge SHM and maintenance management due to the high variation and low resolution of the methods (Malekjafarian et al., 2015). Hence, vibration-based SHM methods were developed to identify structural dynamic parameters, which are widely used for structural condition assessment of bridges. Most of the current vibration-based bridge SHM approaches record the vibration responses of an instrumented bridge (Zhu and Law, 2015). Sensors are directly installed on different locations of the bridge structure to monitor its dynamic responses. The approach using these responses for SHM is referred to as direct

methods. Since the locations of existing damages or possible damage occurrence are not known, the inclusion of more spatial information can greatly enhance the accuracy of health assessment. Generally, the sensor network for the direct approach is fixed on the bridge structure, and response from each sensor contains spatial information at the measured point only. A large number of sensors is therefore needed in pursuit of the detailed spatial information. This poses a number of challenges, such as involuntary damage of the installed equipment, high installation and maintenance cost of sensors, and extensive data processing and management (Law and Zhu 2009). Clearly, there is an urgent need to improve current practices and explore a more cost-effective means for bridge SHM.

Research using vehicle responses for structural health monitoring became an attractive topic recently with the aim for a quick scan on the health status of a large volume of bridges. Indirect bridge SHM strategy utilising an instrumented vehicle as a moving sensory system has the potential to meet this purpose. Instead of recording the dynamic response of the bridge, the dynamic responses of the vehicle are measured during its passage over the bridge deck. These measurements contain VBI information from which vital bridge-related dynamic information can contribute to the bridge condition assessment (Yang et al. , 2004). Bridge SHM using vehicle responses has certain merits over responses directly measured from the bridge structures. Firstly, the instrumented vehicle serves as a moving sensor and/or a moving exciter, which is flexible and convenient. Secondly, the installation and maintenance of the vehicle sensory system is more rapid and cost-effective than that of fixed sensors on bridge. Thirdly, and most importantly, the moving sensors can collect data at different locations – this is equivalent to having a dense array of sensors along the bridge deck with each collecting data close to the excitationpoint for a short duration. This means that rich spatial data can be

obtained using relatively less sensors. Moreover, by using local responses collected from a moving sensor, the local damage can be more quickly and accurately identified due to higher local sensitivity.

Despite its attractive features, there are key issues in vehicle-based bridge monitoring systems. The dynamic responses from the moving vehicle are sensitive to the bridge surface roughness which would induce the vehicle frequency components dominantly in the response spectrum (Yang et al. 2012a). In other words, the frequency spectrum is smeared which is not good for the identification of bridge dynamic parameters and damage detection. This is one of the main challenges for the successful extraction of bridge modal parameters in practice to eliminate or reduce the effect of road surface roughness (Hester and González, 2017). Additionally, the responses from the moving vehicle are intrinsically nonstationary and noisy. Most of the classical output-only system identification approaches are based on the assumption of white noise excitation and they may fail to extract accurate structural dynamic parameters from the vehicle response (Zhu and Law, 2015). To date, research on the indirect bridge damage detection including the localization and severity identification with vehicle responses is rare.

1.2 Research objectives

This research aims to develop a rapid, accurate and cost-effective bridge SHM approach for dynamic parameter identification and damage detection. To overcome the shortcomings of direct bridge monitoring systems involving fixed sensor networks and the limitations of current direct approach, an indirect approach that uses responses of passing vehicles is developed in this thesis. Wireless sensors are installed on the vehicle to form a wireless sensory system. Compared to conventional approaches, the proposed

system requires fewer sensors and provides richer spatial data vital to bridge condition assessment.

The following objectives will be pursued in this research:

1) Develop an indirect approach for extracting the bridge dynamic parameters from vehicle responses;

2) Study the time-varying characteristics of the VBI system;

3) Develop an approach for bridge damage detection using a passing instrumented vehicle.

1.3 Significance of the study

The project is to develop indirect bridge structural health monitoring approach for accurate, rapid, and cost-effective assessments of a large population of bridges using the data collected from a passing vehicle equipped with sensors. Owing to the fact that ageing bridge infrastructures are still in service in Australia and around the world, the proposed approach will make a significant contribution to monitor the structural conditions and in protecting the structure and human lives, as well as developing an economic infrastructure asset management scheme. Outcomes of the project include:

- Several novel indirect bridge modal identification methods are proposed to identify bridge modal parameters from responses of passing vehicles. The nonstationary features of the vehicle-bridge interaction are taken into account.
- A new time-frequency analysis technique is adopted to study the time-varying characteristics of the vehicle-bridge interaction system. The vehicle and bridge instantaneous frequencies are extracted for analysis.

- A new two-step drive-by bridge damage identification method is proposed. The interaction forces are estimated from axle responses of a passing vehicle. The location and severity of bridge damages are subsequently identified.

1.4 Structure of the thesis

This thesis is organized into nine chapters. Chapter 1 introduces the background, motivation and objectives of the research.

Chapter 2 presents a comprehensive review of previous research work on the vibration-based bridge SHM methods. The review is conducted in different perspectives of the direct and indirect methods in the bridge modal identification and damage detection. Research on VBI and its influence on the time-varying characteristic of the system are also reviewed.

In Chapter 3, short-time stochastic subspace identification (STSSI) is proposed for indirect bridge modal identification using two instrumented vehicles. One vehicle is moving over the bridge and the other one remains stationary as reference sensor. White-noise support excitation is included in the vehicle-bridge system to simulate the presence of multiple operational excitations. Vehicle responses are divided into several segments and each response segment is assumed stationary due to the relative short measuring time. The combination of SSI and a rescaling procedure estimates the bridge modal frequencies and mode shapes from the response segments.

In Chapter 4, a model vehicle with one sensor is assumed moving over the bridge. The drive-by blind modal identification with singular spectrum analysis (SSA-BSS) is proposed to decompose vehicle response and extract bridge-related components. The

method can reduce the effect of bridge surface roughness and measurement noise to enhance the identification accuracy on the bridge modal frequencies.

In Chapter 5, a time-frequency analysis technique called SET is used to study the time-dependent features of the VBI system. A multi-ridge detection algorithm is used to extract the IFs of the system. Effects of the system parameters on time-varying characteristics are investigated.

Chapter 6 presents the experimental verification of the proposed methods in Chapters 3 and 4. The time-dependent features of the VBI process discussed in Chapter 5 are also studied experimentally. A VBI test bed is built in the laboratory. A two-span continuous steel beam is used to model the bridge. Vehicle models with different configurations are fabricated. A wireless sensory system is setup for monitoring the responses.

Chapter 7 proposes a two-step drive-by bridge damage detection approach using dual Kalman filter. The interaction forces between vehicle and bridge are firstly identified. Sensitivity analysis based on the interaction forces is performed to detect the bridge damage. Single- and multi-damage cases are considered wherein the damage is defined as a change in the elemental flexural stiffness of the beam.

In Chapter 8, the method and analytical procedures discussed in Chapters 4 and 5 are applied to a vehicle-bridge system in the field. Drive-by bridge modal frequency identification is conducted using the responses of an instrumented vehicle. The time-varying characteristics of the bridge frequencies due to the interaction with a truck are studied.

Chapter 9 presents the summary of this research along with concluding remarks. Recommendations for future study and potential research directions are also discussed.

CHAPTER 2 LITERATURE REVIEW

2.1 Overview

This chapter critically reviews the vibration-based bridge SHM with emphasis on the methods based on VBI, which has played an important role in the field of bridge modal identification and damage detection. First, direct approaches were evaluated. Then, a survey of indirect approaches with focus on dynamic parameter identification and damage assessment was performed. Available literature about the vehicle-bridge system identification using both the vehicle and bridge dynamic responses measured from a wireless sensory system as well as the time-dependent behaviour of VBI were assessed in detail. Finally, the key findings of this literature review was summarized and the technical challenges involved in indirect bridge health assessment approaches were presented.

2.2 Vibration based bridge structure health monitoring

2.2.1 Vibration based bridge structural damage detection

In the field of SHM, structural damage can be defined as the degradation of its physical properties, such as mass, stiffness and damping. The changes in these physical properties are difficult or impossible to directly measure. On the other hand, the dynamic properties of structures (modal frequency, damping and mode shape) can be extracted with less effort from vibration measurement. In fact, vibration-based approaches have been applied for decades in bridge SHM (Doebling et al. , 1998; Carden and Fanning, 2004; Abdeljaber et al., 2017). Essentially, changes in physical properties due to damage causes variations in the structural dynamic properties, and consequently structural damage can be predicted

by measuring the change in dynamic properties (Malekjafarian et al. , 2015). Farrar and Jauregui (1998a) compared five damage identification methods using experimental modal data from undamaged and damaged bridges. These methods show varying levels of success when damage was relatively less. The variability in bridge modal properties and statistical analysis were discussed in an accompanying numerical study (Farrar and Jauregui, 1998b). Pines and Aktan (2002) reviewed the developments in the field of SHM and its application to long-span bridges in the USA. Various SHM technologies were reviewed and it was envisioned that the cost of the monitoring system were expected to protect the much greater investment in the bridge construction and user costs. A series of natural frequencies of the structure in intact and damaged states measured from an on-line instrumentation system of a cable-stayed bridge were used in a multi-stage scheme for damage detection (Ko et al., 2002). Based on changes of mode shapes, Huth et al. (2005) proposed a damage indicator called mode shape area index for a prestressed concrete bridge. Cruz and Salgado (2009) evaluated the performance of vibration-based damage detection methods for bridges. The performance of the damage detection methods were susceptible to noise and the effects of noise to the response of bridges were difficult to predict. Bedon and Morassi (2014) conducted dynamic testing and parameter identification of a base-isolated bridge, and highlighted the typical properties of this type of bridge. The vibration characteristics and damage detection of a suspension bridge were studied (Wickramasinghe et al., 2016). A mode shape component specific damage index was proposed to detect and locate damage in the main cables of the suspension bridge. A comparative study with different vibration-based damage detection methods were presented (Das et al., 2016). Time series analysis was proved to be effective in the case of damage detection that even small damages could be detected.

2.2.2 Output-only bridge modal identification

Various methods have been proposed for bridge modal identification using vibration responses. Without knowledge or measurement of the input excitation of the structure under normal operating conditions, output-only modal identification techniques such as stochastic subspace identification (SSI) (Boonyapinyo and Janesupasaeree, 2010), frequency domain decomposition (FDD) (Brincker et al., 2001) and random decrement technique (RDT) (Asmussen et al., 1998) have been extensively applied. The deviations in modal properties (*e.g.*, frequency changes, mode shape changes and mode shape curvature changes) relative to the intact structure have been used for damage detection (Fan and Qiao, 2011). Generally, white noise input is assumed in output-only identification. Therefore, this approach does not comprise operational variations of excitations and disregards the correlation between excitation processes at different locations on the bridge (Chen et al. , 2009). The inclusion of vehicle-bridge interaction information can reduce the uncertainties and enhance the accuracy of bridge dynamic parameter identification (Kim et al. , 2011). Extensive studies have been done for vibration-based bridge SHM and the methods based on VBI are the primary concern of this thesis.

2.2.3 Importance of vehicle-bridge interaction to bridge structural health monitoring

Generally, the process of vibration-based structural damage detection consists of recording structural vibration, extracting modal properties and identifying damages based on changes in structural dynamic properties. In vibration data recording, the source of excitation can be generated from a specific vibrating machine (Farrar and Jauregui, 1998a), ambient loading (Zhang, 2007) or operational loading (Zhu and Hao, 2012).

Among these three excitation sources, operational loading in the form of passing vehicles has obvious advantages given that it does not require specific or expensive vibration devices and it provides sufficient excitation forces compared to ambient loads. Furthermore, it enables the monitoring of target bridges under operating conditions whilst fulfilling the objectives of design verification, structural maintenance and traffic management (Sumitoro et al., 2001). Because of these benefits, there has been a dramatic increase of the interest in VBI-based bridge SHM.

When a vehicle crosses a bridge with an assumption that the wheels remain in contact with the bridge deck, there is a complex dynamic coupling between the vehicle and the bridge. The dynamic coupling is referred to as "vehicle-bridge interaction" (Yang and Lin, 1995). Sensors can be installed on the different locations on the bridge to record structural vibration responses. Structural dynamic properties can then be extracted for structural damage detection. This kind of method is referred to as a "direct approach". To determine the structural modal parameters, many sensors must be mounted on the entirety of the bridge structure. This process incurs high cost due to sensor installation and maintenance. In the VBI system, the vehicle serves as a moving exciter to the bridge structure and at the same time, it can be instrumented to form a moving sensory system. Some researchers have proposed to install the sensors on the moving vehicle and to use the dynamic responses from the vehicle to extract bridge modal properties indirectly (Yang et al. , 2004; Yang et al. , 2009a; Oshima et al. , 2014; Marulanda, 2016). These methods are referred to as "indirect approach." Only a few sensors are needed to equip the vehicle, and none or a few bridge instrumentation is required. The dynamic responses from either the bridge structure or the vehicle can be used for structural identification. The relatively low cost of VBI-based approach makes it an attractive option for bridge

SHM. VBI-based bridge SHM can be classified into two types, *i.e.*, direct and indirect, which are discussed in Section 2.3.

2.3 Bridge structural health monitoring based on VBI

2.3.1 Direct approach

2.3.1.1 Structural health monitoring from bridge responses under traffic excitations

In VBI system, the vehicle moving along the bridge provides equal opportunities for different locations to be excited. Piombo et al. (2000) studied the interaction between a three-span supported bridge and a seven degrees of freedom (DOFs) vehicle. The dynamic responses of the bridge excited by the vehicle were used to obtain the dynamic properties using wavelet technique. Lee et al. (2002) measured the vertical accelerations of the bridge deck under traffic conditions. The modal parameters were identified from the vertical response measurements, and the parameters were utilised to develop a method to assess damages based on neural networks. Carden and Fanning (2004) reviewed different methods used for vibration-based structural condition monitoring. The modal parameter shifts due to localised damage would be not sensitive or measurable for the damage detection. Marchesiello et al. (2009) applied continuous wavelet transform and a modified version of the stochastic subspace identification to extract the instantaneous frequency of a bridge subjected to a crossing train. Lu and Liu (2011) used a response sensitivity-based finite element model updating approach to identify both the bridge damages and the vehicle parameters from the bridge dynamic responses. Gökdağ (2013) presented a method to identify cracks in a beam under moving vehicle. The method utilised the difference of the measured and the calculated responses as the objective function using the particle swarm optimization technique. Li et al. (2013) reported improvement in damage detection on bridge infrastructures subjected to moving loads

numerically and experimentally. The impulse response function of the bridge responses was calculated and damage detection was conducted based on the response reconstruction. O'Brien et al. (2015) used a method based on moving load identification to detect structural damage, and reported that the load was sensitive to the local damages of the bridge. Matarazzo and Pakzad (2016) introduced structural identification using expectation maximization (STRIDE), and identified structural modal properties using the dynamic responses of two actual bridges in ambient vibration conditions. The method used Kalman filtering and Rauch-Tung-Striebel smoothing equations to produce estimates of the unobserved states and identified the state-space modal parameters in an iterative procedure. Multivariate statistical analysis techniques were applied to data for the monitoring of a long-span arch bridge (Comanducci et al., 2016). The techniques that were used included dynamic regression models, linear and local principal component analysis (PCA), and combinations thereof (e.g. the combination of dynamic multiple linear regressions and local principal component analysis). Bridge acceleration responses were also used to identify parameters of moving vehicle (Wang et al., 2017). Particle filter was adopted to estimate bridge pavement roughness using responses of sensor equipped vehicle and vehicle mass was then estimated using bridge responses.

2.3.1.2 Bridge damage identification using advanced signal processing techniques

This section reviews some of the most extensively used signal processing techniques for bridge health assessment. Traditionally, the fast Fourier transform (FFT) is used for parameter identification from measured vibration response time history. FFT converts a signal from the time domain to a representation in the frequency domain to obtain structural frequencies. However, the damage information may be masked by different errors during signal measurement if parameter identification is not properly conducted

(Zhu and Law, 2016). To improve results, some recent studies used (a) the Hilbert-Huang transform (HHT) and (b) wavelet analysis to extract useful damage features from the measured responses. HHT, which was first proposed by Huang et al. (1998), is generally recognized as an analysis tool for nonlinear and nonstationary signals. Data processing with HHT consists of two stages: empirical mode decomposition (EMD) and Hilbert spectral analysis. The EMD decomposes data into a finite set of intrinsic mode functions (IMFs) usually arranged from high to low frequencies. Huang et al. (2005) adopted this method for bridge structure health monitoring. Kunwar et al. (2013) applied HHT to analyse data from sensors installed on the bridge deck. Damages were more easily identified from sensors located closer to the point of damage.

Wavelet analysis is used to transform signals in time domain to time-frequency domain, and this technique has been used for bridge damage identification. Zhu and Law (2006) proposed a method based on wavelet analysis to identify cracks in bridge structures under a moving load. The continuous wavelet transformation (CWT) of the response measurements was used for locating the cracks and the damage index, formed from the wavelet coefficient, indicated the extent of damage. The use of WT-related bridge damage identification has also been reported by other studies (Hester and González, 2012; Hester and González, 2017; Manuel et al., 2013).

2.3.2 Indirect approach

2.3.2.1 The identification of bridge modal properties using vehicle responses

Due to the obvious advantages of indirect bridge SHM methods over conventional direct methods, recent research has focused on drive-by bridge structural identification. The method of identifying bridge modal frequency from the dynamic response of a moving

vehicle was first proposed by Yang et al. (2004). In their study, the vehicle was modelled as a sprung mass system while the bridge was a simply-supported beam that yielded only the first mode of vibration. The results ascertained that information about the natural frequency of the bridge was contained in the vehicle's dynamic response. Through further investigation, Yang and Lin (2005) determined that the vehicle response in a VBI system contained three frequency components, *i.e.*, driving frequency, vehicle frequency, and bridge frequency. Among these, bridge frequency is relevant to bridge SHM. Experimental verification and further parametric studies were also conducted by the same research group (Lin and Yang, 2005; Yang and Chang 2009a), which confirmed the potential and feasibility of indirect bridge frequency identification. Moving on a rough bridge deck, vehicle frequency usually appeared as a dominant peak in the Fourier response spectra of the vehicle response which makes the bridge frequencies invisible. Yang and Chen (2009b) applied EMD to pre-process the response data of a vehicle passing over the bridge to generate the IMFs. Then, FFT was used to extract the bridge frequency. Yang et al. (2012b) applied two connected vehicles and simulated their dynamic responses as they passed over the bridge. By subtracting the acceleration frequency spectrum of one vehicle from that of the other, a residual spectrum was obtained where the vehicle frequency contributed from the road surface roughness had been basically removed. Yang et al. (2013b) also used three different filtering techniques to eliminate vehicle frequency and improve the identification of bridge modal frequencies. Nguyen (2015) investigated the dynamic behaviour of a cracked beam when it was excited by a moving vehicle and earthquake excitation. The appearance of cracks led to changes in bridge natural frequency during vibration. The wavelet spectrum was used to analyse the change in frequency. A modified SSI technique was proposed for the extraction of bridge modal frequencies using an moving instrumented vehicle (Yang and

Chen, 2015). A truck-trailer vehicle system with accelerometers installed at the axles of the trailer was used to detect variations of damping of a bridge due to local damages (González et al. , 2012; Keenahan et al., 2014). Yang et al. (2019) identified bridge damping ratio using a two-axle moving test vehicle, equipped with uniformly spaced accelerometers and laser sensors.

A small number of researchers have estimated the bridge mode shapes from vehicle responses. Techniques such as short-time frequency domain decomposition (FDD) and Hilbert transform (HT) were adopted to extract bridge mode shapes from the response measurements of the moving vehicles (Yang et al. , 2014; Malekjafarian and O'Brien, 2017). In short-time FDD, the quality of the estimated mode shape depended on the singular value at a selected frequency obtained by the peak-picking method (Malekjafarian and O'Brien, 2014). Of note, in this approach, some prior knowledge of the modal frequencies was required. A method using a test vehicle consisting of a tractor and two following trailers was proposed by Kong et al. (2016). The residual response between the two trailers was obtained in the time domain instead of in the frequency domain. Fast Fourier transformation (FFT) and short-time Fourier transformation (STFT) were applied to the residual responses to identify the bridge modal frequencies and mode shape squares, respectively. However, the extraction of bridge mode shapes was not satisfactory. This proposed method was recently verified by using the measurement data of an existing field bridge (Kong et al. , 2017). Two types of test vehicles were proposed and compared for their capacity in bridge modal identification. Marulanda et al. (2016) used two sensors – mobile and stationary – to record the acceleration of a simply supported beam. The frequencies of the beam were easily obtained from the stationary sensor, and the data from both mobile and stationary sensors were used to identify mode shapes. The proposed ambient vibration-based modal identification method using mobile

sensors was based on a matrix formulation of the natural excitation technique (NExT) (Ill, et al. , 1993; James et al. , 1995). However, the effect of the properties of moving sensor was not studied, and the study did not consider vehicle-induced bridge vibration. Tan et al. (2019) used vehicle responses to extract the bridge damping ratio and mode shapes by the Hilbert transform. A low and constant vehicle speed was required for the identification and higher damping affected the accuracy of the mode shape identification negatively.

Some relatively new indirect bridge SHM techniques have shown potential in structural damage identification. Generalized pattern search algorithm was successfully applied to identify bridge stiffness and to obtain modal frequencies from vehicle responses (Li et al. , 2014). Lederman et al. (2017a) proposed a novel supervised-classification-based method to monitor rail infrastructure from the acceleration records of the train's cabin in its revenue-service. A new feature extracted from vibration signals, signal-energy, was the most effective, compared to temporal-frequency, spatial-frequency and spatial-domain for detecting track changes in simulations as well as operational data. They also proposed a sparse method to analyse vibration data collected from the operational train (Lederman et al., 2017b). This method detected the magnitude and location of bumps, which were used as indicators of the state of the tracks. These two methods (i.e., supervised-classification and sparse) emerged as promising approaches to help enable bridge monitoring by using in-service vehicles. Kim et al. (2017) conducted an experimental verification using moving vehicles as sensors to extract bridge frequencies. They also studied the changes of spectral distribution pattern due to damages on the bridge.

2.3.2.2 Bridge damage detection using the instrumented vehicle as a moving sensor

1) Response-Based Methods

A new method based on wavelet transform was presented for detecting damages in a multi-cracked beam from vehicle dynamic response (Nguyen and Tran, 2010). The cracks were identified via small distortions in the dynamic response. The crack locations were determined from the locations of the peaks in the wavelet transform of dynamic response. However, roughness was not included in the vehicle-bridge system. Similarly, Khorram et al. (2012) used the wavelet-based damage detection approach and compared the effectiveness of determining damage from fixed (sensors installed on the bridge) and moving (sensors installed on the vehicle) systems. Their results showed that the moving sensor was more effective than the fixed one. Zhang et al. (2012) installed an accelerometer on a moving robot equipped with a tapping device to get health information of the bridge deck basing on extracted mode shape squares. Furthermore, the operating deflection shape of the bridge was extracted using a moving device (Zhang et al. , 2013), and its curvature for damage detection was obtained via a pre-filtering based on wavelet decomposition. Kim et al. (2014) validated the potential of bridge condition assessment by comparing patterns of dynamic parameters that have been periodically monitored using a drive-by inspection system. Chen et al. (2014) applied a multiresolution classification framework with semi-supervised learning on graphs to the indirect bridge structural health monitoring. Kong et al. (2014) proposed a bridge damage detection method based on the response transmissibility of moving vehicles in the VBI system. Two moving sensors were used to record the dynamic response of the sensing vehicles when the bridge was subjected to traffic excitation. Damage indicators were constructed and compared based on the transmissibility from both bridge and vehicles. O'Brien et al. (2017) applied EMD to analyse vehicle speed pseudo-frequency component extracted

from vehicle response. They pin-pointed damages on the bridge by checking the difference of Intrinsic Mode Functions (IMFs) of the responses before and after the occurrence of damage. Zhang et al. (2018) extracted the driving component of the contact-point response and calculated the instantaneous amplitude squared (IAS) using Hilbert transform. The IAS peaks were used as the indicators of crack locations.

2) Model-based damage detection method

Of note, it has been observed that variations in bridge responses due to damage were enlarged by moving loads (Bilello and Bergman, 2004). The sensor on the moving vehicle collects data at different locations along the structure. This means that damages in a region passed by the vehicle can be identified with greater accuracy. Bu et al. (2006) proposed a method to directly use the acceleration time histories of vehicle in a sensitivity-based model updating method. The damage index, which was defined as the flexural stiffness reduction, was identified with good accuracy. Furthermore, Li and Au (2014) presented a multistage damage detection method using the modal strain energy and the genetic algorithm. O'Brien et al. (2014) developed a drive-by highway bridge inspection system by analyzing vehicle acceleration responses using moving force identification technique. The bridge surface roughness and the bridge stiffness were obtained. This method was further verified by experimental study in laboratory (McGetrick et al., 2015). Results indicated that an instrumented vehicle had potential to be an economical approach for periodic checking of stiffness of short- to medium-span bridges. Zhu et al. (2018) proposed an approach to identify local anomalies in a bride using an instrumented vehicle as a moving sensory system. Interaction forces were obtained from the measured axle and body accelerations of the vehicle. Results further showed that interaction forces were more sensitive to local damages than acceleration responses from the vehicle. Malekjafarian et al. (2015) and Yang and Yang (2018)

performed critical reviews of indirect methods for bridge SHM, and the potential of indirect methods was well illustrated. Some challenges, such as the road profile, the limited VBI time and environmental effects, needs to be overcome for successful implementation of drive-by inspection in practice.

2.3.3 Wireless sensory network for vehicle-bridge structural identification

Mobile sensors simultaneously record data in time while moving in space. This feature allows mobile sensory systems to provide rich spatial information with fewer sensors than fixed systems. Moreover, the availability of spatial information significantly enhances the accuracy of structural health assessment. Kim and Kawatani (2008) proposed a simplified VBI model using a pseudo-static formulation by removing the stationary assumption to detect changes in bridge element stiffness. The method of Kim and Kawatani (2008) was later verified in a laboratory study (Chang et al., 2014b). Meanwhile, Chen et al. (2009) proposed a video-assisted approach to obtain traffic information. Data of passing vehicles were incorporated with acceleration responses collected from the bridge deck to evaluate structural properties. Caicedo and Casas (2013) used mobile sensors to collect dynamic structure properties with enhanced spatial resolution. With this method, mode shapes with high spatial density were extracted using a reduced number of sensors. Zhu et al. (2010) developed a novel SHM approach using an specially designed mobile sensing node. The effectiveness of the mobile sensory network was first validated through damage identification on a steel frame, and its performance was further assessed through modal identification of a field pedestrian bridge (Zhu et al. , 2012). The system was proven capable of structural modal identification by measuring vibrations in discrete points. A mobile sensing platform using sensor cart was developed for identifying structural dynamic properties. The Truncated Physical Model was proposed to process mobile

sensor data and the Structural Identification using Expectation Maximization algorithm was selected to identify the modal parameters (Horner et al., 2015).

For the implementation of the mobile wireless sensory system in the bridge-vehicle system identification, Kim et al. (2011) explored the truck-based mobile wireless sensor network to identify the dynamic interaction between the bridge and vehicle. Wireless sensors were installed on both the moving truck and bridge to obtain time-synchronized VBI dynamic data. The dynamic characteristics of the bridge and the time varying vehicular loading imposed on the bridge were isolated using a two-stage system identification approach (Kim and Lynch 2012). Bridge dynamic parameters were identified using the free-vibration responses of the structure in the first stage. In the second stage, the vehicle and bridge responses measured during interaction were used to estimate the load matrix of the system.

2.4 Time-varying behaviour of the vehicle-bridge interaction system

The VBI-based approach enables monitoring and assessment of target bridges under operational conditions. For the majority of indirect bridge frequency identification, the frequencies of the vehicle and bridge are assumed constant. However, this assumption is appropriate only when the VBI effect is negligible. If vehicle mass were substantial compared to the bridge mass – for instance, in the case of a heavy vehicle passing over a short-span bridge – system frequency variation due to VBI must be taken into account. Several experimental investigations (Farrar et al., 1997; Zhang et al., 2002; Kim and Lynch, 2012) have confirmed that significant variation in bridge frequencies occur due to vehicular loadings.

Significant research efforts have been devoted to evaluate the measured instantaneous bridge frequencies in the VBI system. Li et al. (2003) theoretically studied the natural frequency of railway girder bridges under vehicular load. Bridge frequency varied periodically as the vehicle passed over it. Kim et al. (2003) studied the effect of vehicle mass on the bridge natural frequencies under traffic-induced excitation. A change of 5.4% in the natural frequencies was noted in the monitored short span bridge with a 3.8% vehicle-to-bridge mass ratio. Law and Zhu (2004) studied the effect of bridge cracks on instantaneous frequency under moving vehicular loads. The frequency variations due to a moving mass and a moving oscillator were compared. The changes were sensitive to the mass of vehicle as well as the frequency ratio of the vehicle and bridge. Yang et al. (2013a) presented a theoretical framework with closed-form solutions on the instantaneous frequencies of the VBI system considering only the first bridge vibration mode. Both the vehicle and bridge frequencies varied in a roughly half sine wave form with respect to vehicle location. A larger vehicle/bridge mass ratio yielded larger frequency deviations. When the vehicle-bridge frequency ratio was close to unity, the vehicle and bridge frequencies deviated drastically from their natural values. Chang et al. (2014a) studied the variability in bridge frequency due to a parked vehicle theoretically and experimentally. The frequency variation should be considered in bridge-related engineering. Cantero et al. (2017) conducted field tests on the evolution of bridge modal properties (bridge frequencies and vibration modes) during the passage of truck. They also assessed the non-stationary and non-linear features of the vehicle responses in a VBI test bed (Cantero et al., 2019). Despite the abovementioned efforts, the non-stationary properties of bridge vibration under passing vehicle that results to the time-dependent system frequencies are not yet fully explored and elucidated in bridge SHM (Xiao et al., 2017).

2.5 Summary

This chapter provided an overview of the field of VBI-based bridge SHM. Indirect methods have potential to provide richer data over direct methods with lower installation and maintenance cost. Among different approaches, vehicle-based drive-by health monitoring systems emerged as a cost-efficient way to monitor the bridge infrastructures. However, vehicle-based monitoring has several key problems. Particularly, the bridge-vehicle system often exhibits nonstationary features due to the interaction. Also, the existence of road roughness obfuscates the determination of bridge frequency. Furthermore, the signals captured from the passing vehicle is naturally noisy, and inclusive of VBI data that is not necessary for bridge SHM. These limitations due to noise, roughness, and time-variance of signals must be overcome so that drive-by bridge inspection can be reliably implemented in practice.

CHAPTER 3 Indirect bridge modal parameters identification with short-time stochastic subspace identification

3.1 Overview

This chapter presents indirect bridge modal identification using vehicle responses. A new method called STSSI is proposed to identify the bridge modal frequencies and mode shapes.

Stochastic subspace identification is widely used for operational modal analysis to capture structural dynamic parameters from bridge responses only (Hong et al., 2012). Meanwhile, Reference-based Covariance-Driven SSI (Ref-SSI) was developed (Peeters and De Roeck, 1999) to obtain global structural mode shapes. In this approach, measurements from a large structure are divided into multiple setups with overlapping reference sensors. Stabilization diagrams are used to separate the true system poles from the spurious numerical poles.

In this chapter, the reference-based stochastic subspace identification method is combined with a rescaling procedure to obtain bridge mode shapes from acceleration responses of a stationary as well as a moving instrumented vehicle. The methodology is as follows: the stationary vehicle serves as the reference sensor, whereas the moving vehicle serves as the sensor moving over the deck. External excitations such as ongoing traffic and wind load are considered as white noise excitations at bridge supports. Measurements from the two vehicles are divided into segments corresponding to the same number of physical segments of the deck. The local mode shape values for each bridge segment are obtained from the corresponding measured data segment. These values are rescaled to get the

global mode shape vectors. The effectiveness and performance of the proposed strategy are investigated numerically.

The rest of this chapter is organised as follows: First, the modelling of the VBI system is presented considering the extra support excitations followed by the derivation of the state space formulation of the VBI system. Then, the identification of bridge mode shapes from multiple measurement setups using Ref-SSI is reported. Finally, numerical case studies are conducted to demonstrate the overall effectiveness and performance of the proposed strategy. The effect of different vehicle speeds and physical parameters of vehicle on the identified results are evaluated.

3.2 Vibration of the vehicle-bridge system

3.2.1 Equation of motion of the vehicle

Considering a VBI system as shown in Figure 3.1, the vehicle was modelled as a single-degree-of-freedom (SDOF) quarter-car model and the bridge deck is simulated as a simply supported Euler-Bernoulli beam. The vehicle was assumed to move along the bridge deck at a constant velocity v. The equation of motion for the vehicle can be written as

$$m_v\ddot{d}_v(t)+c_v\dot{d}_v(t)+k_v d_v(t)=\left\{c_v[\dot{d}_b(x,t)+vr'(x)]+k_v\left[d_b(x,t)+r(x)\right]\right\}_{x=vt} \tag{3.1}$$

where m_v, k_v, c_v are the mass, stiffness and damping of the vehicle respectively, $d_v(t)$ is the vertical displacement of the vehicle, $d_b(x,t)$ is the vertical displacement of the bridge at the contact point x and time t, and $r(x)$ is the road surface roughness with $r'(x) = dr(x)/dx$.

3.2.2 Equation of motion of the bridge deck

According to the Euler-Bernoulli beam theory, the governing equation for flexural vibrations of a bridge deck under a moving vehicle can be written as (Yang et al. 2020):

$$EI\frac{\partial^4 d_b(x,t)}{\partial x^4}+\rho\frac{\partial^2 d_b(x,t)}{\partial t^2}+\mu\frac{\partial d_b(x,t)}{\partial t}=-F(t)\delta(x-vt) \tag{3.2}$$

where E is the Young's modulus of a material, I is the moment of inertia of deck cross-section, EI is the flexural rigidity of deck, ρ is the mass of the material per unit length, μ is the viscous damping parameter,$F(t)$is the interaction force between the bridge and vehicle with $F(t)=m_v g+m_v\ddot{d}_v(t)$, where g is the acceleration of gravity, and δ is the Dirac function.

The displacement response of the deck can be expressed with modal superposition (Clough and Penzien, 2003)

$$d_b(x,t)=\sum_{i=1}^{n}\phi_i(x)\eta_i(t) \tag{3.3}$$

where n is the number of modes considered. $\phi_i(x)=\sqrt{\frac{2}{\rho L}}\sin\frac{i\pi x}{L}\in R^{n\times 1}$ is the *ith* vibration mode shape, and $\eta_i(t)$ is the *ith* modal coordinate. L is the length of the beam.

Substituting Eq. (3.3) into Eq. (3.2) and applying the orthogonality conditions of vibration modes, Eq. (3.2) becomes

$$\ddot{\eta}_i(t)+2\zeta_i\omega_i\dot{\eta}_i(t)+\omega_i^{\,2}\eta_i(t)=-F(t)\phi_i(vt) \tag{3.4}$$

where $2\zeta_i\omega_i=\mu/\rho$ and $\omega_i^{\,2}=\frac{EI}{\rho}\left(\frac{i\pi}{L}\right)^4$.

A bridge deck is subjected, in general, to multiple excitations which may include the ongoing traffic, ground motion, wind excitation, and others. In this study, these excitations were modelled as white noise time series applied at the right and left bridge supports denoted as $\ddot{d}_r(t)$ and $\ddot{d}_l(t)$, respectively. The equation of motion for the *ith* vibration mode of the deck subject to a moving vehicle and support excitations can be written as

$$\ddot{\eta}_i(t)+2\zeta_i\omega_i\dot{\eta}_i(t)+\omega_i^2\eta_i(t)=-F(t)\phi_i(vt)+P_i(t) \tag{3.5}$$

where $P_i(t)=-\ddot{d}_l(t)\int_0^L \rho(1-\frac{x}{L})\phi_i(x)\,dx-\ddot{d}_r(t)\int_0^L \rho\frac{x}{L}\phi_i(x)\,dx$.

Combining Eq. (3.1) and Eq. (3.5), the equation of motion of the VBI system can be obtained in matrix form as

$$\mathbf{M}\ddot{\mathbf{d}}+\mathbf{C}\dot{\mathbf{d}}+\mathbf{K}\mathbf{d}=\mathbf{F} \tag{3.6}$$

in which

$$\mathbf{M}=\begin{bmatrix}1 & 0 & \cdots & 0 & m_v\phi_1(x)\\ 0 & 1 & \cdots & 0 & m_v\phi_2(x)\\ \vdots & \vdots & \ddots & 0 & \vdots\\ 0 & 0 & \cdots & 1 & m_v\phi_n(x)\\ 0 & 0 & 0 & 0 & m_v\end{bmatrix},\quad \mathbf{C}=$$

$$\begin{bmatrix}2\zeta_1\omega_1 & 0 & \cdots & 0 & 0\\ 0 & 2\zeta_2\omega_2 & \cdots & 0 & 0\\ \vdots & \vdots & \ddots & 0 & \vdots\\ 0 & 0 & \cdots & 2\zeta_n\omega_n & 0\\ -c_v\phi_1(x) & -c_v\phi_2(x) & \cdots & -c_v\phi_n(x) & c_v\end{bmatrix},$$

$$\mathbf{K}=\begin{bmatrix}\omega_1^2 & 0 & \cdots & 0 & 0\\ 0 & \omega_2^2 & \cdots & 0 & 0\\ \vdots & \vdots & \ddots & 0 & \vdots\\ 0 & 0 & \cdots & \omega_n^2 & 0\\ -c_v\dot{\phi}_1(x)-k_v\phi_1(x) & -c_v\dot{\phi}_2(x)-k_v\phi_2(x) & \cdots & -c_v\dot{\phi}_n(x)-k_v\phi_n(x) & k_v\end{bmatrix},$$

$$\mathbf{d} = \begin{bmatrix} \eta_1(t) \\ \eta_2(t) \\ \vdots \\ \eta_n(t) \\ d_v(t) \end{bmatrix}, \qquad \mathbf{F} = \begin{bmatrix} -\phi_1 m_v \mathrm{g} + P_1(t) \\ -\phi_2 m_v \mathrm{g} + P_2(t) \\ \vdots \\ -\phi_n m_v \mathrm{g} + P_n(t) \\ k_v r(x) + c_v v r'(x) \end{bmatrix}$$

The dynamic response of the vehicle can be calculated as the "measured" data by time-stepping integration from Eq.(3.6) using the explicit Newmark-β method (Liu et al., 2014a). The measured data are used to estimate the bridge modal parameters in this study.

3.2.3 Road surface roughness

Bridge surface roughness has great effect on indirect bridge modal identification. To better simulate the VBI system, road surface roughness is considered and described by a periodically modulated random process. It is specified by its power spectral density function (PSD) given by (ISO 8608)

$$G_d(n_s) = G_d(n_0) \cdot (n_s/n_0)^{-w} \tag{3.7}$$

where n_0 $(= 0.1\ \text{cycles/m})$ is the reference spatial frequency; w is the exponent of the PSD, and n_s is the spatial frequency (cycles/m). The value of $G_d(n_0)$ gives an estimate of the degree of the roughness of the road. This classification is made by assuming a constant vehicle velocity PSD and taking w equal to 2. Based on this ISO specification, the road surface roughness in time domain can be simulated by applying the inverse fast Fourier transformation on $G_d(n_s)$ (Henchi et al., 1998)

$$r(x) = \sum_{i=1}^{N_f} \sqrt{4G_d(n_{s,i})\Delta n} \cos(2\pi n_i x + \theta_i) \tag{3.8}$$

where $n_{s,i} = i\Delta n$ is the spatial frequency, $\Delta n = \frac{1}{N_f \Delta}$; Δ is the distance interval between successive ordinates of the surface profile; N_f is the number of data points and $\theta_i$is a set

of independent random phase angle uniformly distributed between 0 and 2π. Different classes of road surface are given in the standard, and thus Class A and Class B surface roughness were considered in the simulation.

3.3 Formulation of VBI system in state space

The VBI model in state space is introduced in this section (Van Overschee and De Moor, 2012). When written in state space, Eq. (3.5) becomes

$$\begin{Bmatrix} \dot{\boldsymbol{\eta}}(t) \\ \ddot{\boldsymbol{\eta}}(t) \end{Bmatrix} = \begin{bmatrix} \mathbf{0} & \mathbf{I}_n \\ -\omega_i^2 \mathbf{I}_n & -2\zeta_i \omega_i \mathbf{I}_n \end{bmatrix} \begin{Bmatrix} \boldsymbol{\eta}(t) \\ \dot{\boldsymbol{\eta}}(t) \end{Bmatrix} - \begin{bmatrix} \mathbf{0} \\ m_v \mathbf{I}_n \end{bmatrix} \begin{bmatrix} \mathbf{0} & \boldsymbol{\Phi}(vt) \end{bmatrix} \begin{Bmatrix} \dot{d}_v(t) \\ \ddot{d}_v(t) \end{Bmatrix} + \begin{bmatrix} \mathbf{0} \\ m_v \mathbf{I}_n \end{bmatrix} g\boldsymbol{\Phi}(vt) + \begin{bmatrix} \mathbf{0} \\ \mathbf{P}(t) \end{bmatrix} \tag{3.9}$$

where $\boldsymbol{\eta}(\mathrm{t}) = [\eta_1(t) \quad \cdots \quad \eta_i(t) \quad \cdots \quad \eta_n(t)] \in R^{n\times 1}$,

$\boldsymbol{\Phi}(vt) = [\phi_1(vt) \quad \cdots \quad \phi_i(vt) \quad \cdots \quad \phi_n(vt)] \in R^{n\times 1}$,

$\mathbf{P}(\mathrm{t}) = [P_1(t) \quad \cdots \quad P_i(t) \quad \cdots \quad P_n(t)] \in R^{n\times 1}$, and $\mathbf{I}_n$ is a unit matrix of size *n*.

Eq. (3.9) can then be written as

$$\dot{\mathbf{X}}(t) = \mathbf{A}_\mathbf{c}\mathbf{X}(t) - \mathbf{B}_\mathbf{c}\mathbf{L}(t)\dot{\mathbf{Z}}(t) + \mathbf{B}_\mathbf{c} g\boldsymbol{\Phi}(vt) + \mathbf{P}_\mathbf{c}(t) \tag{3.10}$$

where

$$\mathbf{X}(t) = \begin{Bmatrix} \boldsymbol{\eta}(t) \\ \dot{\boldsymbol{\eta}}(t) \end{Bmatrix} \in R^{2n\times 1},\ \mathbf{Z}(t) = \begin{Bmatrix} d_v(t) \\ \dot{d}_v(t) \end{Bmatrix} \in R^{2\times 1},\ \mathbf{A}_\mathbf{c} = \begin{bmatrix} \mathbf{0} & \mathbf{I}_n \\ -\omega_i^2 \mathbf{I}_n & -2\zeta_i \omega_i \mathbf{I}_n \end{bmatrix} \in R^{2n\times 2n}$$

$$\mathbf{B}_\mathbf{c} = \begin{bmatrix} \mathbf{0} \\ m_v \mathbf{I}_n \end{bmatrix} \in R^{2n\times n},\ \mathbf{L}(t) = [\mathbf{0} \quad \boldsymbol{\Phi}(vt)] \in R^{n\times 2},\ \mathbf{P}_\mathbf{c}(t) = \begin{bmatrix} \mathbf{0} \\ \mathbf{P}(t) \end{bmatrix} \in R^{2n\times 1}$$

Incorporating an exponential matrix for transformation, Eq. (3.10) can be rewritten in a discretised recursive form as

$$\mathbf{X}_{k+1} = \mathbf{A}\mathbf{X}_k - \mathbf{B}\mathbf{L}_k\mathbf{Z}_k + \mathbf{B}g\mathbf{\Phi}_k + \mathbf{P}_k \tag{3.11}$$

where $\mathbf{A} = \exp(\mathbf{A}_\mathbf{c} \cdot \Delta t)$, $\mathbf{BL}_k = \mathbf{A}_\mathbf{c}^{-1}(\mathbf{A} - \mathbf{I})\mathbf{B}_\mathbf{c}\mathbf{L}(t)$, $\mathbf{P}_k = \mathbf{A}_\mathbf{c}^{-1}(\mathbf{A} - \mathbf{I})\mathbf{P}_\mathbf{c}(t)$ and Δt is the time step interval. The second term on the right-hand side of Eq. (3.11) is the system input related to dynamic response $\mathbf{Z}_k$ of the moving vehicle. The third term is the input related to the mass of the vehicle, and the fourth term is the ambient excitation. This study simulated a light vehicle with significantly smaller excitation than on-going traffic. The ambient excitation $\mathbf{P}_k$, which may consist of the on-going traffic excitation, was the dominant factor. The last three terms on the right-hand side in Eq. (11) can then be approximated by a stochastic process $\mathbf{v}_k$.

Substituting Eq. (3.3), Eq. (3.1) can be written in the state space as

$$\begin{Bmatrix} \dot{d}_v(t) \\ \ddot{d}_v(t) \end{Bmatrix} = \begin{bmatrix} 0 & 1 \\ -k_v/m_v & -c_v/m_v \end{bmatrix} \begin{Bmatrix} d_v(t) \\ \dot{d}_v(t) \end{Bmatrix} + \begin{bmatrix} 0 & 0 \\ c_v/m_v & k_v/m_v \end{bmatrix} \begin{bmatrix} v\dot{\mathbf{\Phi}}^T(vt) & \mathbf{\Phi}^T(vt) \\ \mathbf{\Phi}^T(vt) & 0 \end{bmatrix} \begin{Bmatrix} \boldsymbol{\eta}(t) \\ \dot{\boldsymbol{\eta}}(t) \end{Bmatrix} + \begin{bmatrix} 0 & 0 \\ k_v/m_v & c_v v/m_v \end{bmatrix} \begin{Bmatrix} r(vt) \\ r'(vt) \end{Bmatrix} \tag{3.12}$$

or

$$\dot{\mathbf{Z}}(t) = \mathbf{D}_\mathbf{c}\mathbf{Z}(t) + \mathbf{E}_\mathbf{c}\mathbf{\Phi}_\mathbf{c}(t)\mathbf{X}(t) + \mathbf{F}_\mathbf{c}\mathbf{R}(t) \tag{3.13}$$

with $\mathbf{Z}(t)=\begin{Bmatrix} d_v(t) \\ \dot{d}_v(t) \end{Bmatrix}$, $\mathbf{D_c}=\begin{bmatrix} 0 & 1 \\ -k_v/m_v & -c_v/m_v \end{bmatrix}\in R^{2\times 2}$, $\mathbf{E_c}=\begin{bmatrix} 0 & 0 \\ c_v/m_v & k_v/m_v \end{bmatrix}\in R^{2\times 2}$,

$\mathbf{\Phi_c}(t)=\begin{bmatrix} v\dot{\mathbf{\Phi}}^T(vt) & \mathbf{\Phi}^T(vt) \\ \mathbf{\Phi}^T(vt) & 0 \end{bmatrix}\in R^{2\times 2n}$, $\mathbf{F_c}=\begin{bmatrix} 0 & 0 \\ k_v/m_v & c_v v/m_v \end{bmatrix}\in R^{2\times 2}$ and

$\mathbf{R}(t)=\begin{Bmatrix} r(vt) \\ r'(vt) \end{Bmatrix}\in R^{2\times 1}$

Eq. (3.13) can be discretised as

$$\mathbf{Z}_{k+1}=\mathbf{D}\mathbf{Z}_k+\mathbf{E}\mathbf{\Phi}_k\,\mathbf{X}_k+\mathbf{F}\mathbf{R}_k \tag{3.14}$$

with $\mathbf{D}=\exp(\mathbf{D_c}\cdot\Delta t)$, $\mathbf{E\Phi}_k=\mathbf{D}_c^{-1}(\mathbf{D}-\mathbf{I})\mathbf{E_c}\mathbf{\Phi}_c(t)$ and $\mathbf{F}=\mathbf{D_c^{-1}}(\mathbf{D}-\mathbf{I})\mathbf{F_c}$.

Let $\mathbf{Y}_k=\mathbf{Z}_{k+1}-\mathbf{D}\mathbf{Z}_k$ and $\mathbf{E\Phi}_k=\mathbf{H}_k$, and the road surface roughness related term, $\mathbf{FR}_k$, is represented by a random stochastic process $\mathbf{W}_k$. The equation of motion for the VBI system in state space can be written as

$$\mathbf{X}_{k+1}=\mathbf{A}\mathbf{X}_k+\mathbf{v}_k \tag{3.15a}$$

$$\mathbf{Y}_k=\mathbf{H}_k\mathbf{X}_k+\mathbf{w}_k \tag{3.15b}$$

The bridge modal frequencies can be obtained from the vehicle responses in Eq. (3.15) using the SSI method.

3.4 Identification of bridge mode shapes with a stationary and a moving sensor

The application of the Ref-SSI method (Peeters and De Roeck, 1999) requires dynamic responses at different locations of the structure to provide sufficient spatial information to identify bridge mode shapes. In this study, the presence of a large group of sensors along the deck was mimicked using two instrumented vehicles. One vehicle, which was

located at a pre-selected location on the deck, served as the reference sensor. Another vehicle moved over the deck with a constant velocity. The bridge length was divided into N physical segments. Signals from these two vehicles were also divided into N corresponding segments. The signal from each segment of the deck was assumed to represent the local dynamic behaviour of the deck. Two signal segments from the two vehicles form a pair of data record, and consequently there were N pairs of records. All the observed output were put together as

$$\mathbf{Y} = \left\{ \underbrace{\begin{pmatrix} \mathbf{Y}^{(1,ref)} \\ \mathbf{Y}^{(1,mov)} \end{pmatrix}}_{\text{Record } 1} \underbrace{\begin{pmatrix} \mathbf{Y}^{(2,ref)} \\ \mathbf{Y}^{(2,mov)} \end{pmatrix}}_{\text{Record } 2} \cdots \underbrace{\begin{pmatrix} \mathbf{Y}^{(j,ref)} \\ \mathbf{Y}^{(j,mov)} \end{pmatrix}}_{\text{Record } j} \underbrace{\begin{pmatrix} \mathbf{Y}^{(N,ref)} \\ \mathbf{Y}^{(N,mov)} \end{pmatrix}}_{\text{Record } N} \right\} \tag{3.16}$$

where, $\boldsymbol{Y}^{(j,ref)}$ and $\boldsymbol{Y}^{(j,mov)}$ are the observed output vectors from the reference and the moving sensors of the *jth* segment of the deck, respectively.

Excitation within the duration of each record was assumed stationary within the short period of measurement. The state space formulation of the system including the deck, the reference vehicle and the moving vehicle for the *jth* data record $\left(j = 1,...,N\right)$ can be written as

$$\begin{cases} \mathbf{X}_{k+1}^{(j)} & = \bar{\mathbf{A}}\mathbf{X}_k^{(j)} + \mathbf{V}_k^{(j)} \\ \mathbf{Y}_k^{(j,ref)} & = \mathbf{H}^{(j,ref)}\mathbf{X}_k^{(j)} \\ \mathbf{Y}_k^{(j,mov)} & = \mathbf{H}^{(j,mov)}\mathbf{X}_k^{(j)} \end{cases} \tag{3.17}$$

where $\mathbf{X}_k$ is the state vector at time instant k, $\mathbf{H}^{(j,ref)}$ is the observation matrix from the reference sensor, $\mathbf{H}^{(j,mov)}$ is the observation matrix from the moving sensor, $\bar{\mathbf{A}}$ is the state transition matrix, $\mathbf{V}_k$ is the unknown stationary noise and $\mathbf{Y}_k^j = \begin{pmatrix} \mathbf{Y}_k^{(j,ref)} \\ \mathbf{Y}_k^{(j,mov)} \end{pmatrix}$ is the vector

of observed output. Due to the stationary assumption, the observation matrix in Eq. (3.17) becomes time-invariant within each record segment.

The Ref-SSI is then applied to the system in Eq. (3.17) in the following steps:

1) Determine the output covariance matrices between all outputs and references by

$$\mathbf{R}_i^{ref} = \mathbf{E}[\mathbf{Y}_{k+i}\ \mathbf{Y}_k^{(ref)^T}] \tag{3.18}$$

2) Form a block Toeplitz matrix using the covariance matrices

$$\mathbf{T}_i^{ref} = \begin{bmatrix} \mathbf{R}_i^{ref} & \mathbf{R}_{i-1}^{ref} & \cdots & \mathbf{R}_1^{ref} \\ \mathbf{R}_{i+1}^{ref} & \mathbf{R}_i^{ref} & \cdots & \mathbf{R}_2^{ref} \\ \cdots & \cdots & \cdots & \cdots \\ \mathbf{R}_{2i-1}^{ref} & \mathbf{R}_{2i-2}^{ref} & \cdots & \mathbf{R}_i^{ref} \end{bmatrix} \tag{3.19}$$

The block matrix can then be decomposed as

$$\mathbf{T}_i^{ref} = \begin{pmatrix} \mathbf{H} \\ \mathbf{H}\bar{\mathbf{A}} \\ \cdots \\ \mathbf{H}\bar{\mathbf{A}}^{\boldsymbol{i-1}} \end{pmatrix} (\bar{\mathbf{A}}^{\boldsymbol{i-1}}\mathbf{G} \quad \bar{\mathbf{A}}^{\boldsymbol{i-2}}\mathbf{G} \quad \cdots \quad \bar{\mathbf{A}}\mathbf{G} \quad \mathbf{G}) = \boldsymbol{O}_i \boldsymbol{C}_i^{ref} \tag{3.20}$$

where $\boldsymbol{C}_i^{ref} = (\bar{\mathbf{A}}^{\boldsymbol{i-1}}\mathbf{G} \quad \bar{\mathbf{A}}^{\boldsymbol{i-2}}\mathbf{G} \quad \cdots \quad \bar{\mathbf{A}}\mathbf{G} \quad \mathbf{G})$ is the controllability matrix, $\mathbf{G} = \mathbf{E}[\mathbf{X}_{k+1}\ \mathbf{Y}_k^{(ref)^T}]$ and $\boldsymbol{O}_i = (\mathbf{H} \quad \mathbf{H}\bar{\mathbf{A}} \quad \cdots \quad \mathbf{H}\bar{\mathbf{A}}^{\boldsymbol{i-1}})^T$ is the observability matrix.

3) Calculate the observability matrix $\boldsymbol{O}_i$ and controllability matrix $\boldsymbol{C}_i^{ref}$ by applying the singular-value decomposition to the block Toeplitz matrix

$$\mathbf{T}_i^{ref} = \boldsymbol{U}\boldsymbol{S}\boldsymbol{V}^T = (\boldsymbol{U}_1 \quad \boldsymbol{U}_2) \begin{pmatrix} \boldsymbol{S}_1 & \mathbf{0} \\ \mathbf{0} & \mathbf{0} \end{pmatrix} \begin{pmatrix} \boldsymbol{V}_1^T \\ \boldsymbol{V}_2^T \end{pmatrix} \tag{3.21}$$

where $\boldsymbol{U}$ and $\boldsymbol{V}$ are orthonormal matrices and $\boldsymbol{S}$ is a diagonal matrix containing the singular values in descending order. The zero singular values and corresponding singular vectors are omitted in Eq. (3.21). Matrix $\boldsymbol{S}_1$ is diagonal, containing non-zero singular values. Matrices $\boldsymbol{U}_1, \boldsymbol{U}_2, \boldsymbol{V}_1$ and $\boldsymbol{V}_2$ are portions of $\boldsymbol{U}$ and $\boldsymbol{V}$ related to $\boldsymbol{S}_1$, respectively.

The system order can be determined by inspecting the number of non-zero singular values. A stabilisation diagram is constructed to eliminate spurious mode due to noise. Inspection on Eqs. (3.20) and (3.21) gives

$$\boldsymbol{O}_i = \boldsymbol{U}_1 \boldsymbol{S}_1^{1/2} \tag{3.22a}$$

$$\boldsymbol{C}_i^{ref} = \boldsymbol{S}_1^{1/2} \boldsymbol{V}_1^T \tag{3.22b}$$

Once $\boldsymbol{O}_i$ and $\boldsymbol{C}_i^{ref}$ are obtained, the state matrix $\overline{\mathbf{A}}$ can then be retrieved to obtain the eigenvalues and eigenvectors ($\lambda_j, \boldsymbol{\varphi}_{\lambda,j}$) of the system (Döhler et al., 2010).

The Reference-based SSI method was applied to each data record $j\,(= 1,\ldots, N)$ to obtain the local mode shape values at the mid-point of each deck segment. Since the reference sensor is the same for all records, the observation matrix $H^{(ref)}$ was the same for all measurement records.

A progressive rescaling procedure was developed to identify the global mode shapes. This procedure is similar to the normalization procedure in experimental modal analysis of a structure. After the local mode shape values of each segment are obtained, they are re-scaled with respect to the reference DOF to form the global mode shape. For example, when the bridge is divided into five segments as shown in Figure 3.2, data from the two vehicles is likewise divided into five pairs of data records. For the first data set, the local mode shape value for the first bridge segment and reference location are $\boldsymbol{\varphi}_{1,1}$ and $\boldsymbol{\varphi}_{1,ref}$, respectively. If the reference sensor is located at the middle of the first segment, the local mode shape values of the first data set from the moving and reference sensors are measured at the same time. Therefore, they can be treated as the global mode shape values with $\boldsymbol{\Phi_1} \approx \boldsymbol{\Phi}_{ref}$. For the second data set, the local mode shape value for the second and reference segments are obtained as $\boldsymbol{\varphi}_{2,2}$ and $\boldsymbol{\varphi}_{2,ref}$ respectively. To obtain the global

mode shape of the second segment $\boldsymbol{\Phi_2}$, a rescaling factor is used with $\boldsymbol{\Phi}_2 = \frac{\boldsymbol{\Phi}_{ref}}{\boldsymbol{\varphi}_{2,ref}} \boldsymbol{\varphi}_{2,2}$.

The calculated local mode shape value in each segment can be rescaled to the global values as

$$\boldsymbol{\Phi}_j = \frac{\boldsymbol{\Phi}_{ref}}{\boldsymbol{\varphi}_{j,ref}} \boldsymbol{\varphi}_{j,j}, \qquad (j = 2,3,\cdots N) \tag{3.23}$$

where $\boldsymbol{\Phi}_j$ is the global mode shape value for the *jth* segment. The accuracy of this approach depends on the number of sub-divided segments of the recorded signal. Therefore, a suitable number of segments must be chosen to balance the required spatial information for the analysis and the accuracy of the identified global mode shapes.

3.5 Numerical simulations

The numerical example by (Yang and Chen, 2015) was adopted to validate the proposed method. In this study, damping of the bridge was neglected because it was insignificant to the forced vibration of the bridge under moving vehicle action (Yang et al., 2014). The physical properties of the undamped bridge were: $L = 30\ m, \rho = 10700\ kg/m, I = 0.494\ m^4, E = 29.43\ GPa$. The first three modal frequencies of the bridge were 2.03, 8.12 and 18.27 Hz. The properties for the undamped vehicle were: $m_v = 100\ kg, k_v = 170\ kN/m$. The modal frequency of the vehicle was 6.50 Hz and its speed was 2 m/s. Data sampling was 15 seconds at the rate of 1000 Hz. The amplitude of ambient excitation at the support was 0.02 m/s^2. These abovementioned parameters are adopted throughout the study unless otherwise stated.

3.5.1 Modal frequency identification using one instrumented vehicle

A previous study (Chang et al., 2010) emphasized that vehicle response is sensitive to bridge surface roughness. Therefore, Classes A and B road surface roughness were considered in this study. The vehicles start moving 50 m from the bridge entrance, wherein the road surface roughness is assumed the same as that of the bridge. The dynamic responses of the vehicle are given in Figure 3.3(a), and the corresponding spectra are shown in Figure 3.3(b). The vehicle frequency is noticeably dominating the spectra. The peak-picking method for FDD was insufficient to obtain the bridge modal frequencies from the spectra. The stabilization diagram with Class A road roughness from the SSI analysis shown in Figure 3.4(a) features the first two bridge modal frequencies as well as the vehicle modal frequency. The third bridge modal frequency was, however, too small to be distinguished. When the vehicle moves on deck with Class B road roughness, the stabilization diagram in Figure 3.4(b) shows only the vehicle frequency, and the bridge frequencies are not present.

3.5.2 Identification of bridge mode shapes using two instrumented vehicles

The acceleration responses from sensors on both vehicles were analysed. The reference vehicle was located at mid- and quarter-span to capture a large modal amplitude to identify the first and second mode shapes, respectively. This segmentation scheme was selected to ensure that the vibration amplitude at the midpoint of each segment is not equal to zero. This configuration was adopted in this study unless otherwise stated. The Modal Assurance Criterion (MAC) was used to compare calculated and theoretical mode shapes.

3.5.2.1 Two vehicles on a smooth road surface

In the first case, the bridge deck was divided into five and nine segments. The dynamic responses of the two vehicles and their spectra with the smooth deck are shown in Figure 3.5. The two time histories were likewise divided into five and nine segments, and the corresponding $\mathbf{\Phi}_{ref}$ are $\mathbf{\Phi}_{3,ref}$,$\mathbf{\Phi}_{5,ref}$ at mid-span, respectively. For the identification of the second mode shape, the dynamic responses of the two vehicles were divided into six or ten segments, and the corresponding $\mathbf{\Phi}_{ref}$ are $\mathbf{\Phi}_{2,ref}$,$\mathbf{\Phi}_{4,ref}$ at quarter-span, respectively.

The Ref-SSI method was applied to each data segment to obtain the local mode shape value at each bridge segment. The first and second mode shapes, identified after the rescaling process, are given in Figure 3.6. Excellent agreement was found for the first mode shape with MAC values equal to 0.998 and 0.999 for the cases with five and nine segments, respectively. For the second mode shape in Figure 3.6 (b), the agreement between the theoretical and identified results was slightly poorer. It was, however, noted that the MAC value increased as the number of segments increased. It may be concluded that a suitable number of segments must be selected to balance the need of spatial information and the accuracy of the identified mode shapes in the analysis.

3.5.2.2 Two vehicles on a rough road surface

The effects of Class A and Class B bridge surface roughness were studied using nine and ten segments for the first and second modes, respectively. The dynamic responses of two vehicles with Class A surface roughness when the reference vehicle was at mid-span of the deck are shown in Figure 3.7. The identified first mode shape is given in Figure 3.8(a). The MAC value slightly decreased with roughness. The identified second mode shape is

given in Figure 3.8(b), likewise the MAC value slightly decreased with roughness. However, when a Class B bridge road surface roughness was considered, the MAC values for the identified first and second mode shapes were 0.7409 and 0.4843, respectively, indicating poor agreement of calculated and theoretical results.

3.5.2.3 The effect of measurement noise

The realistic vehicle-bridge system with "contaminated" measurements (i.e., noisy) was studied in closer detail. The VBI system with Class A bridge surface roughness was studied using nine and ten segments for the first and second modes, respectively. White noise was added to the calculated acceleration response of the vehicle to simulate the contaminated measurements as

$$acc_m = acc_{cal} + E_p \bullet N_{oise} \bullet \sigma(acc_{cal}) \tag{3.24}$$

where acc_{cal} is the calculated acceleration response, E_p is the noise level, N_{oise} is a vector consisting of random values with zero mean and unit standard deviation, and $\sigma(acc_{cal})$ is the standard deviation of the calculated acceleration response. Three noise levels, *i.e,* 5%, 10% and 15%, were considered. The corresponding signal-to-noise ratios were 26, 20 and 16, respectively.

The first and second mode shapes identified from the proposed method are shown in Figure 3.9 (a) and (b), respectively. Of note, the accuracy of the identified mode shapes decreased as the noise level increased. When the noise level was less than 10%, the accuracy of the identified mode shapes was acceptable and the MAC value (0.990) was at the lowest. When the noise level was 15%, the dynamic information of a few bridge

segments was masked by the noise effect, and the overall mode shapes cannot be identified. It may be concluded that the noise effect must be minimized before the proposed method is applied to enhance accuracy.

3.5.3 The effect of moving speeds and vehicle parameters

Class A road surface roughness and 5% white noise were applied in all numerical studies in this section unless otherwise stated.

3.5.3.1 Effect of the vehicle speed

Moving speeds of 2, 4 and 6 m/s were studied. The sampling frequency was 1000 Hz for 2 and 4m/s, and 3000 Hz for 6m/s to ensure sufficient number of data in the sub-divisions. The identified first and second mode shape value for each segment are shown in Figure 3.10 (a) and (b), respectively. When the moving speed was increased to 4m/s, the MAC values were 0.979 and 0.987 for the first two mode shapes, respectively. When the speed was 6 m/s, the MAC values were 0.953 and 0.923. All the MAC values were larger than 0.9, and they notably dropped with increasing speed. It may be concluded that a low vehicle speed may be advantageous to the identification of mode shapes using the proposed indirect method.

3.5.3.2 Effect of vehicle parameters

Previous studies on this topic have shown the feasibility of the proposed method to obtain the bridge modal shapes from measured vehicle responses. The effects of vehicle parameters on the identification are discussed in this section. There are three parameters

in the SDOF vehicle model, *i.e.* mass m_v, stiffness k_v and damping c_v. Eq. (3.1) can be rewritten as

$$m_v\ddot{d}_v(t)+c_v\dot{d}_v(t)+k_v d_v(t)=f_b(t)+f_r(t) \tag{3.25}$$

where $f_b(t)=\left\{c_v[\dot{d}_b(x,t)]+k_v[d_b(x,t)]\right\}_{x=vt}$ and $f_r(t)=\left\{c_v[vr'(x)]+k_v[r(x)]\right\}_{x=vt}$. The response spectrum of the vehicle can be obtained as

$$D_v(w)=H_v(w)F_b(w)+H_v(w)F_r(w) \tag{3.26}$$

where $H_v(w)=\dfrac{m_v}{1-w^2+2j\xi_v w_v w}$ is the frequency response function of the vehicle. $\omega_v=\sqrt{k_v/m_v}$ and $\xi_v=\dfrac{c_v}{2m_v w_v}$ are the vehicle frequency and damping ratio respectively. $F_b(w)$ is the input spectrum due to the bridge vibration and $F_r(w)$ is the spectrum due to the road surface roughness.

Figure 3.11 shows the amplitudes of the frequency response function with three different damping ratios (0.1, 0.25 and 0.5). The frequency ratio is defined as the ratio between the excitation frequency and the vehicle modal frequency. For the vehicle to effectively capture bridge vibration components, it is preferable that the dynamic magnification factor (DMF) is not less than unity. Figure 3.11 shows that when the frequency ratio is less than 0.2, the DMF was almost unity and the effects of damping can be neglected. When the frequency ratio ranged from 0.2 to 1.5, a larger damping ratio notably led to a smaller dynamic magnification factor. When the frequency ratio was larger than 1.5, the magnification factors were all less than unity. The effect of damping ratio became negligible when the frequency ratio continually increased up to 2.0. These results indicate

that the selection of vehicle parameters should be considered carefully for a good identification accuracy.

Another study on the effects of vehicle parameters was also conducted. The reference vehicle was at mid-span and quarter-span the identification of the first and second mode shapes, respectively. Cases with nine and ten segments were studied. Class A road surface roughness and 5% noise were considered, and the sampling rate was 1000 Hz.

a) Effect of vehicle mass

Three vehicle masses, *i.e.*, 100, 200 and 500 kg, were studied. Vehicle speed was maintained at 2.0 m/s. The corresponding mass ratios between the vehicle and the bridge deck were 3.12×10^{-4}, 6.23×10^{-4} and 1.56×10^{-3}, respectively. The frequency ratios between the fundamental frequency of the deck and the vehicle frequency were 0.31, 0.44 and 0.69 for the first bridge frequency, and 1.24, 1.75 and 2.77 for the second bridge frequency.

The identified results are presented in Figure 3.12 (a) and (b). The identified first mode shape from the 100 kg vehicle was closer to the true mode shape than those from 200 and 500 kg vehicles. The MAC values were 0.998, 0.997 and 0.991 for 100, 200 and 500 kg vehicles, respectively. The MAC value of the first mode shape notably decreased as vehicle mass increased. This was due to the proximity of the bridge and vehicle modal frequencies making the identification difficult. Results for the second mode shape were similar as shown in Figure 3.12 (b) with the corresponding MAC values equal to 0.995, 0.991 and 0.992, respectively. Figure 3.13 clearly shows that the dynamic magnification factor is reduced when the frequency ratio increases within the range of 0.2 to 1.5. Furthermore, Eq. (3.9) implies that the effect of the vehicle mass on the total excitation

term cannot be ignored when it is large. Overall, the results suggest that a lighter vehicle should be used with the proposed method.

b) Effect of vehicle stiffness

Three values for vehicle stiffness were studied, *i.e.*, 70, 340 and 700 kN/m), while vehicle mass, damping ratio and moving speed were maintained at 100 kg, 0.10 and 2.0 m/s respectively. The three vehicle stiffness values corresponded to modal frequencies of 6.50, 9.19 and 13.19 Hz, respectively.

The identified first and second mode shapes are shown in Figure 3.13 (a) and (b), respectively. The MAC values for the first mode shape were 0.998, 0.996 and 0.999, respectively, which matched well with the true values. The MAC values for the second mode shape were 0.995, 0.982 and 0.977. Results show that MAC value decreased when the vehicle stiffness increased. This is because the vehicle with the high stiffness also captures the high frequency noise that includes the effect of road surface roughness. This effect has been shown as the second term in Eq. (3.26).

c) Effect of vehicle damping

Three different damping ratios were studied, *i.e.*, 0.10, 0.25 and 0.40. The vehicle mass, stiffness and speed were 100 kg, 170 kN/m and 2.0m/s, respectively.

The identified first and second bridge mode shapes are presented in Figure 3.14 (a) and (b), respectively. The identified results in Figure 3.14(a) were very close to each other with a high MAC value relative to the theoretical ones. In this study, the frequency ratio was 0.31, and the effect of the damping ratio was negligible as shown in Figure 3.11. The identified second bridge mode shape is shown in Figure 3.14 (b). The frequency ratio corresponding to the second bridge frequency was 1.24 with a magnification factor close

to unity as shown in Figure 3.11. When the damping ratio is considered, the accuracy of the identified results decreases with larger damping as discussed in Section 3.5.3.2.

3.6 Summary

The effectiveness of a multiple-setup Reference-based SSI method to identify the bridge modal parameters using two instrumented vehicles was proposed and numerically evaluated. In this method, one vehicle remained stationary during the whole procedure as the reference sensor, while another vehicle measured the dynamic response while moving over the bridge simultaneously. Numerical results showed that the method was effective and robust to identify the bridge modal parameters from dynamic responses of two vehicles. When the bridge surface roughness was Class A and noise was less than 10%, the bridge mode shapes can be identified with high accuracy. However, when the bridge has a Class B surface roughness, it was necessary to reduce the effect of the road roughness prior to the application of the method. Of note, decreasing vehicle speed and mass enhanced the accuracy of the results.

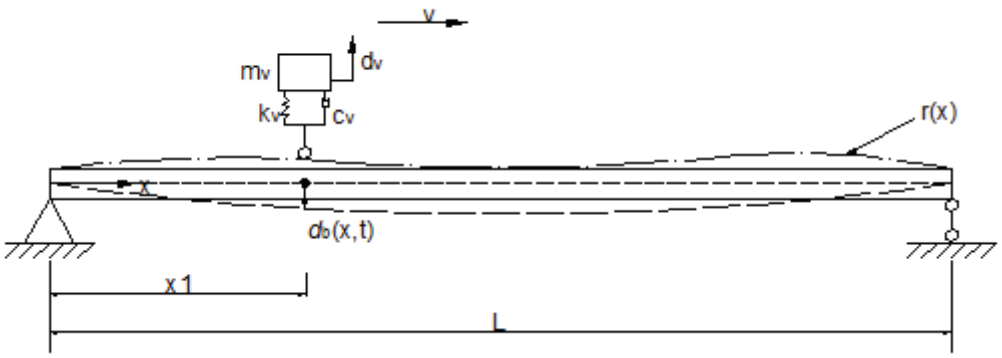

Figure 3.1 Vehicle-bridge system

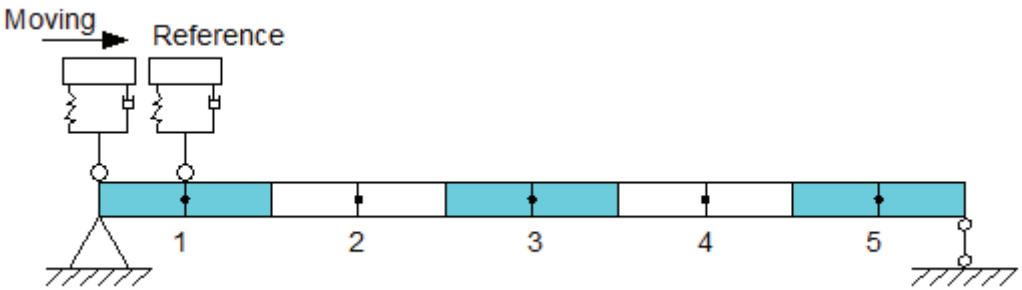

Figure 3.2 Measurement setup

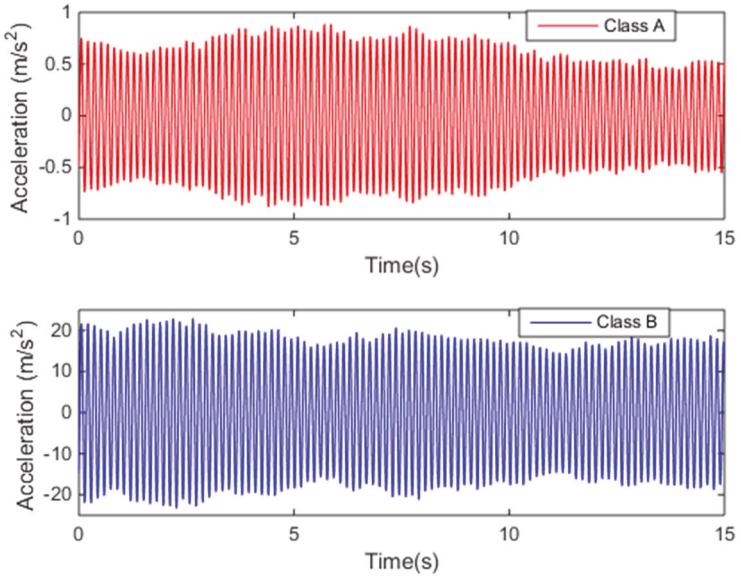

(a) Dynamic responses of the vehicles

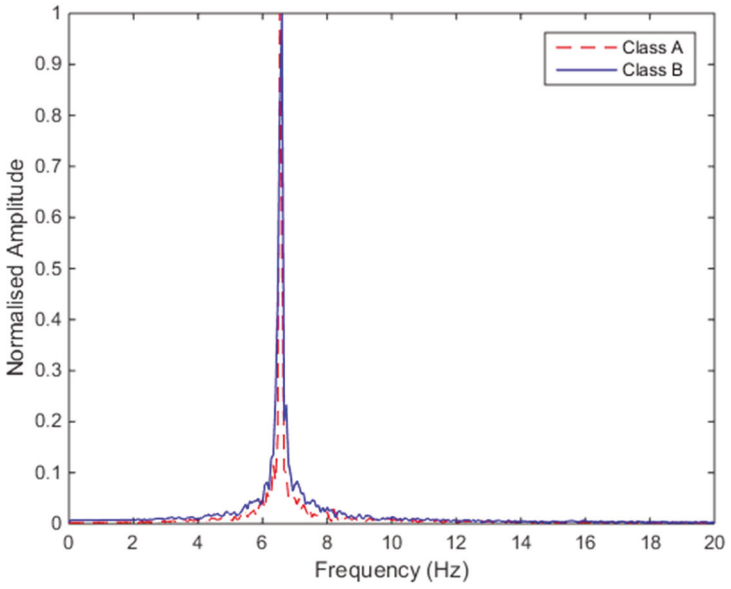

(a) Normalised spectrum of the vehicle responses

Figure 3.3 Dynamic responses and their spectrum of the vehicle moving on the bridge with Classes A and B surface roughness

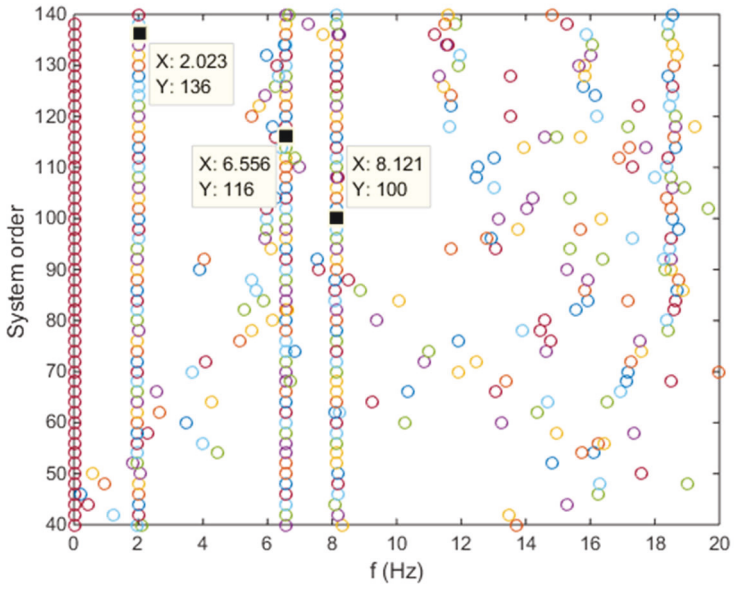

(a) Stabilization diagram with Class A surface roughness

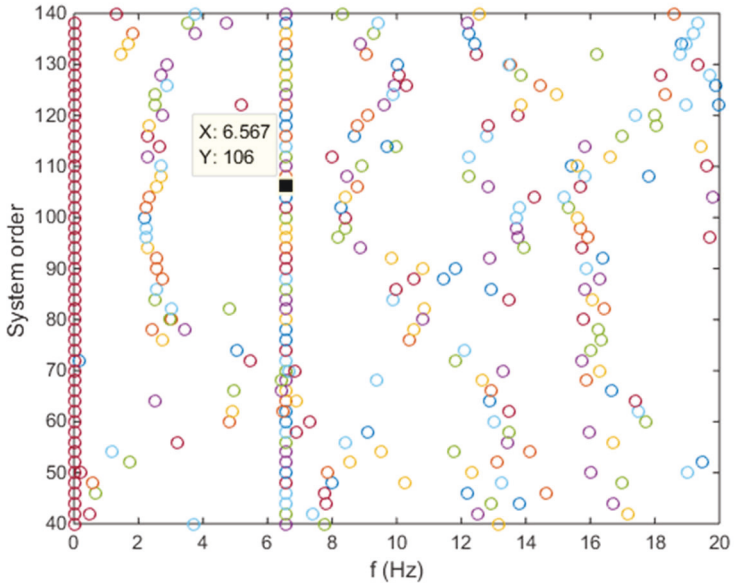

(b) Stabilization diagram with Class B surface roughness

Figure 3.4 Identified results of the bridge from the response of one vehicle

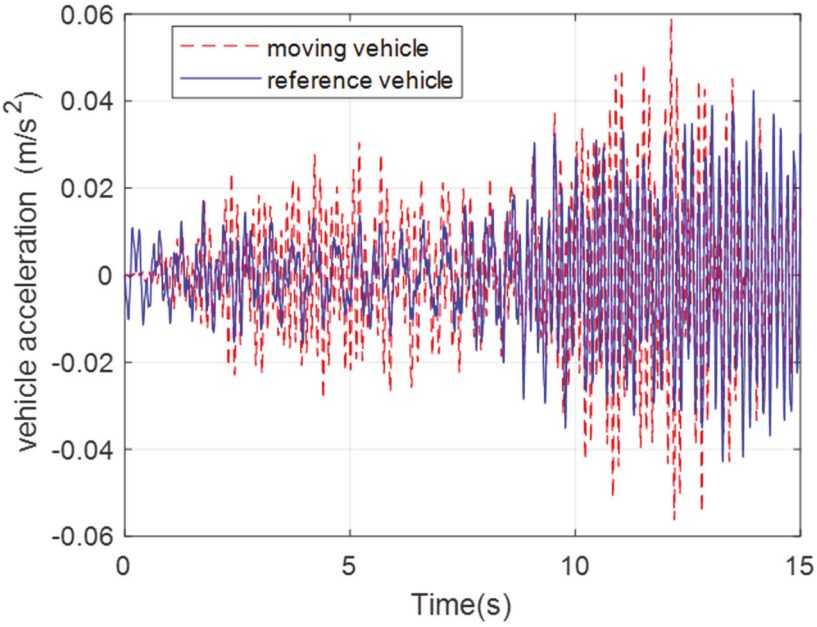

(a) Dynamic responses of two vehicles

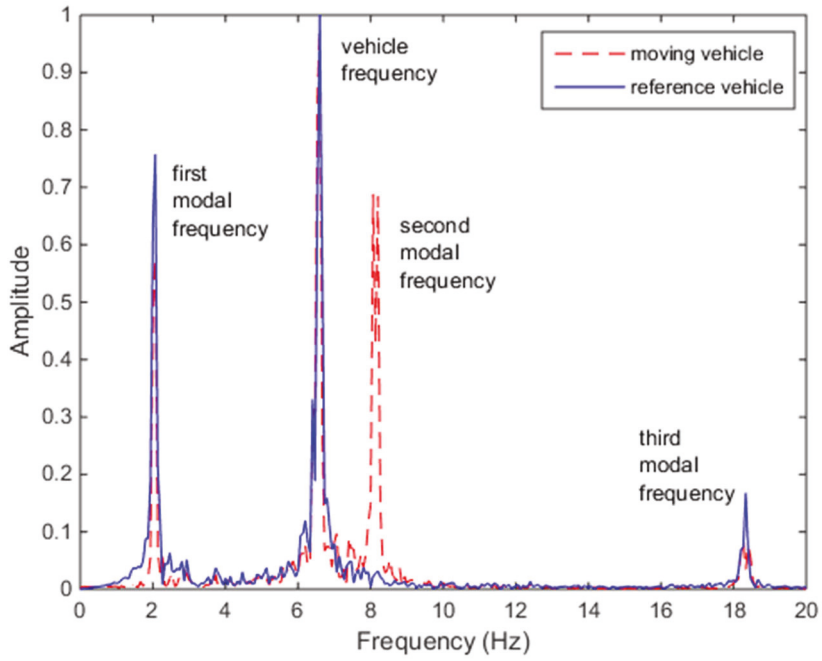

(b) Their spectra

Figure 3.5 Dynamic responses of the moving and reference vehicles and their spectra

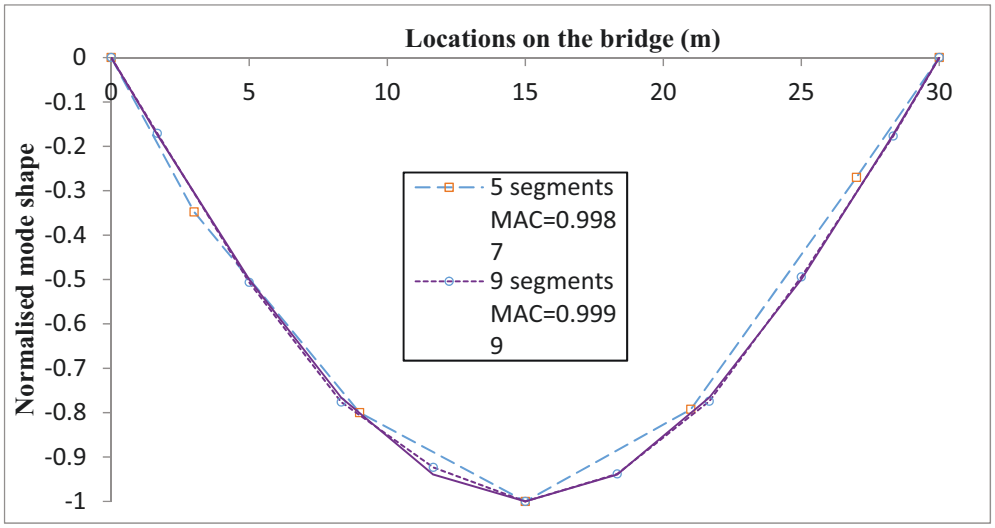

(a) Identified first mode shape with 5 and 9 segments

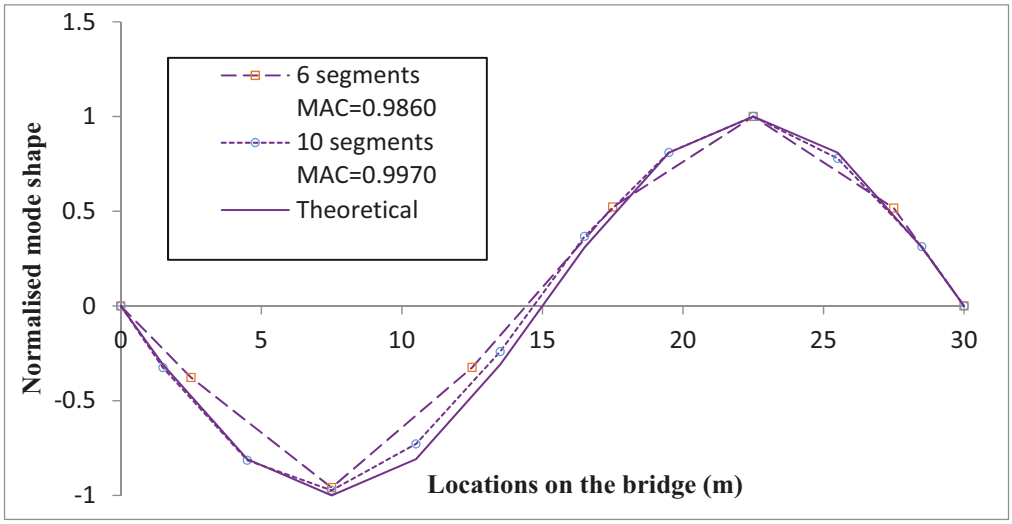

(b) Identified second mode shapes with 6 and 10 segments

Figure 3.6 Identified mode shapes with different segment numbers

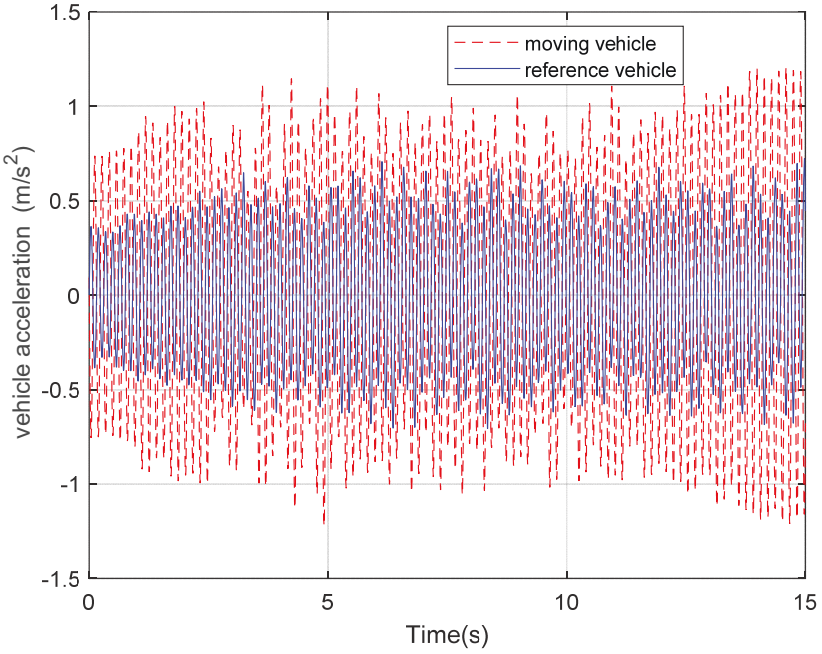

Figure 3.7 Dynamic responses of the vehicles when the surface roughness is Class A

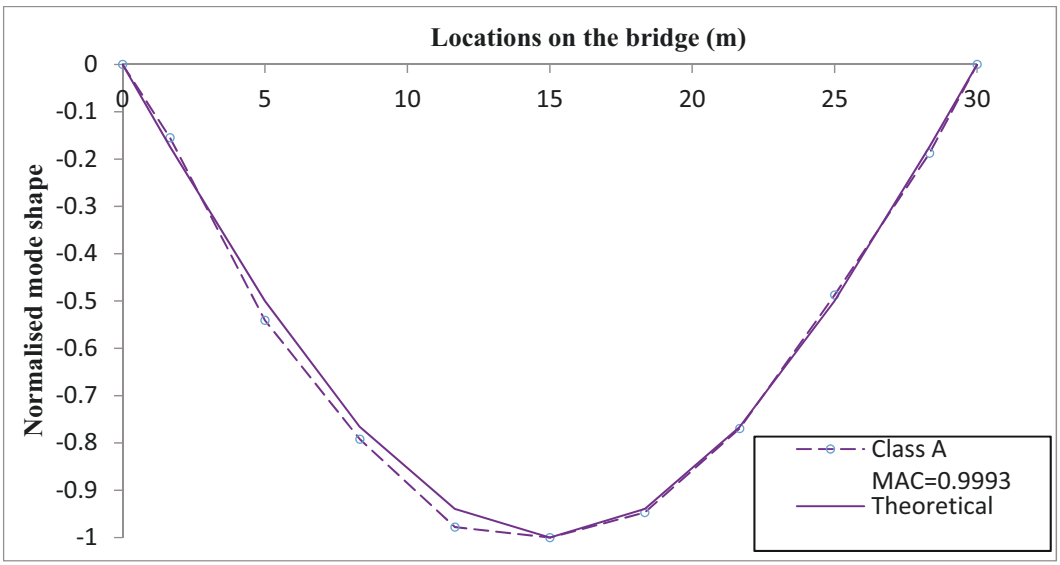

(a) Identified first mode shape

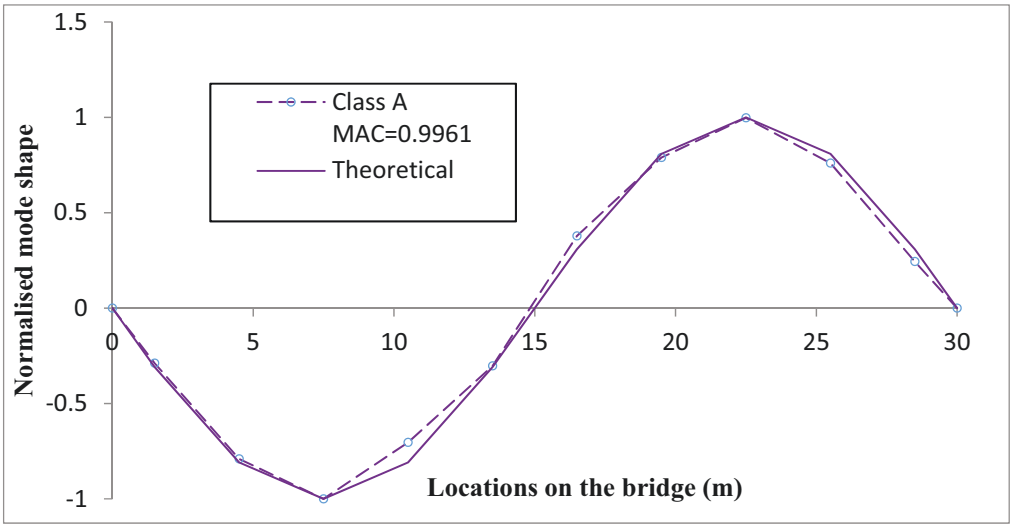

(b) Identified second mode shape

Figure 3.8 Identified mode shapes of the bridge with Class A roughness

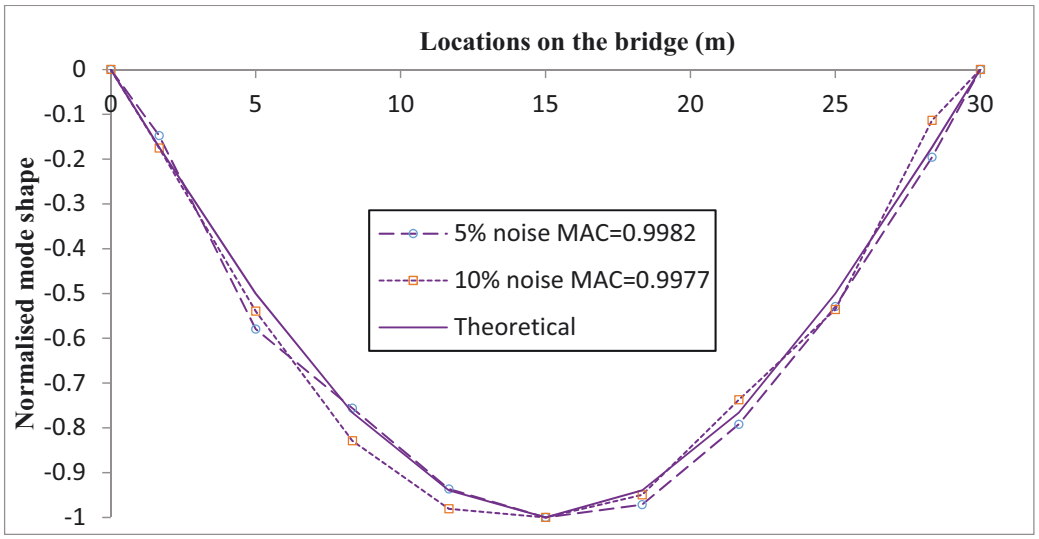

(a) Identified first mode shape

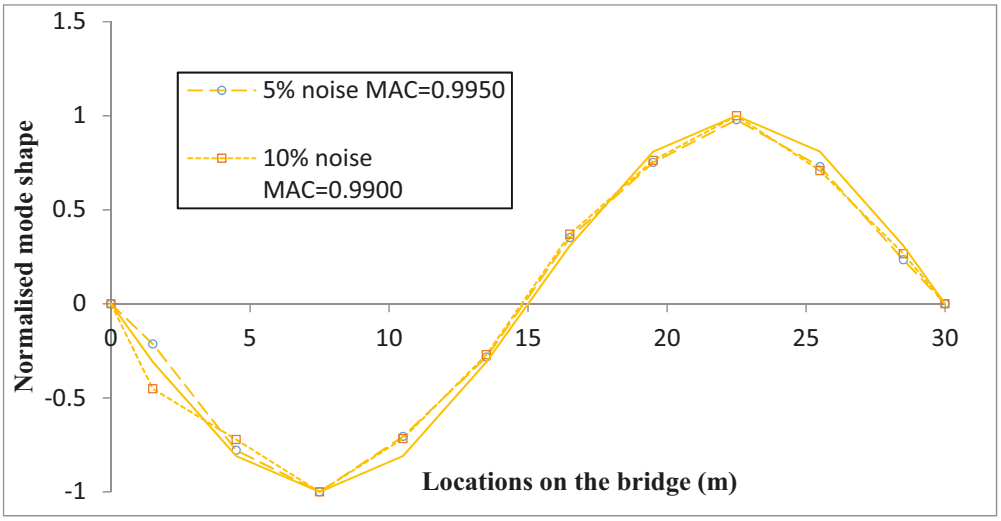

(b) Identified second mode shape

Figure 3.9 Effect of measurement noise on identified results

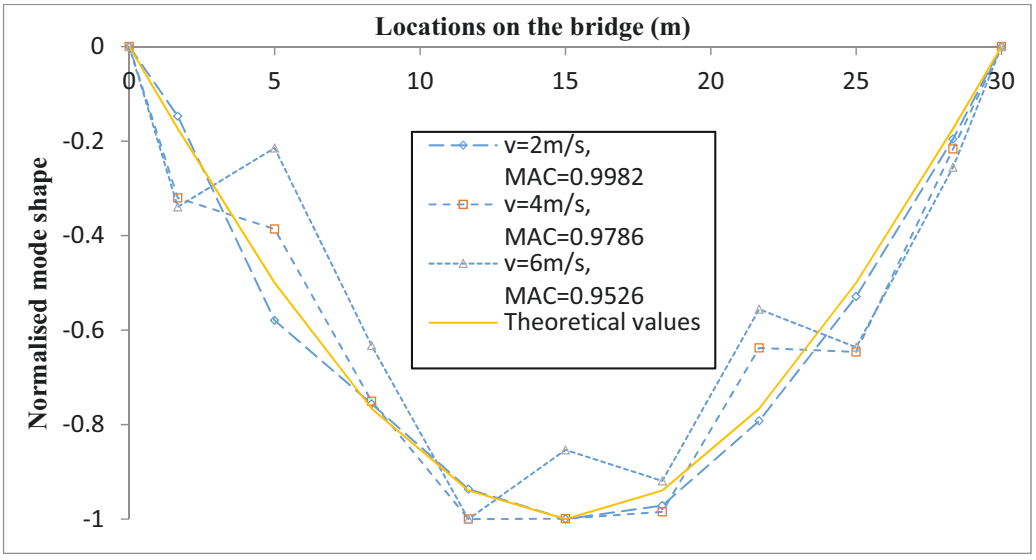

(a) Identified first mode shape

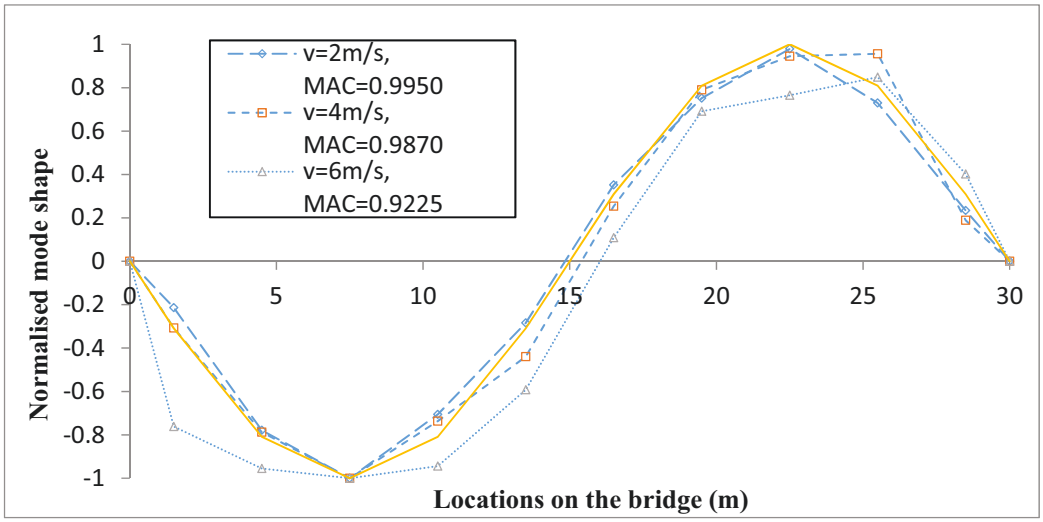

(b) Identified second mode shape

Figure 3.10 Effect of vehicle speeds on identified results

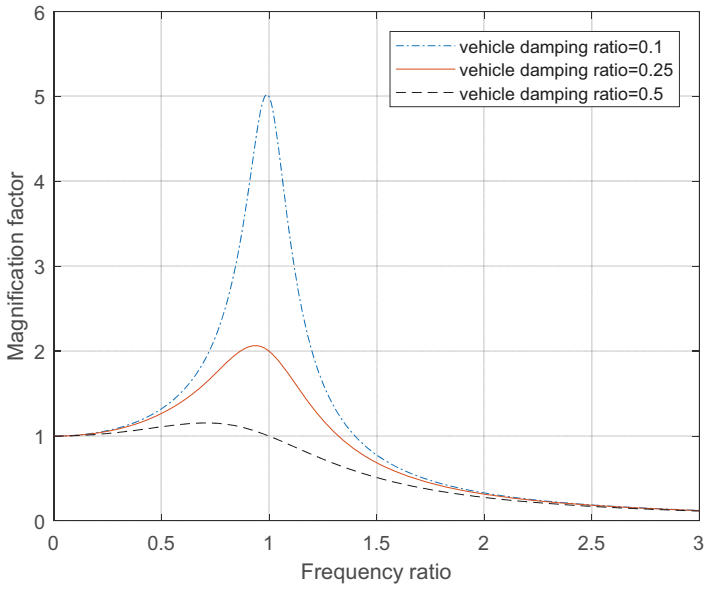

Figure 3.11 Relation between Magnification Factor with the frequency ratio for different damping ratios

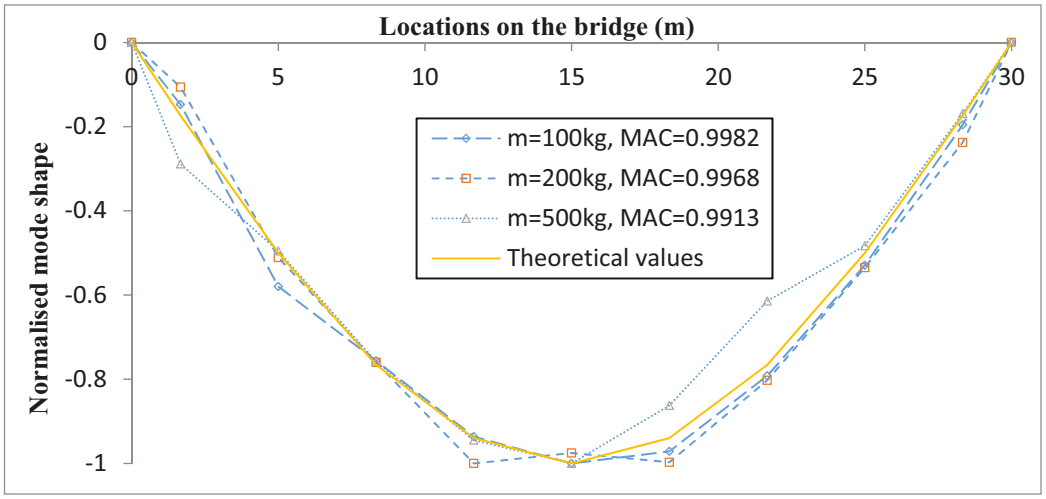

(a) Identified first mode shape

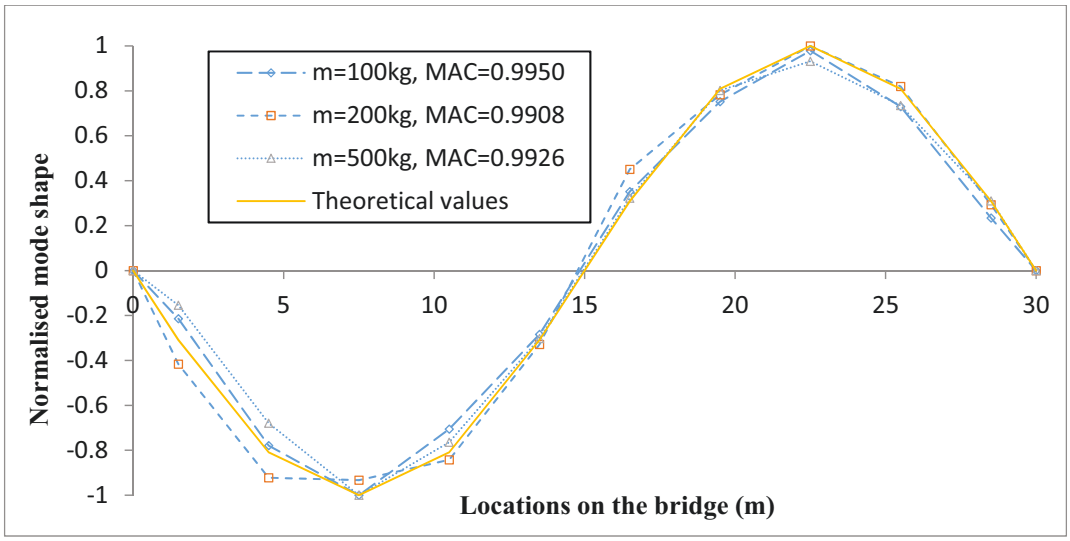

(b) Identified second mode shape

Figure 3.12 Effect of vehicle weights on identified mode shapes

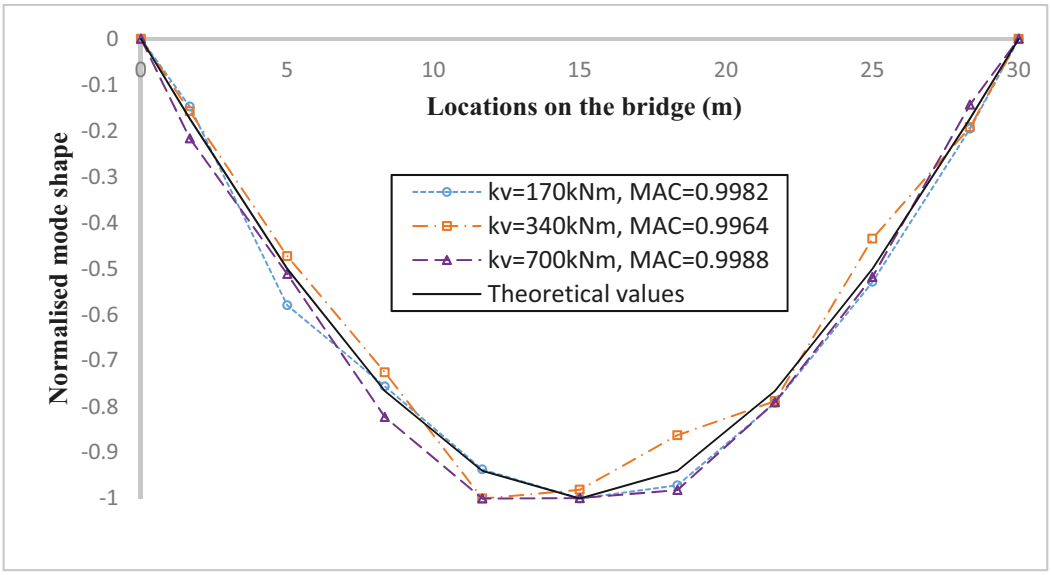

(a) Identified first mode shape

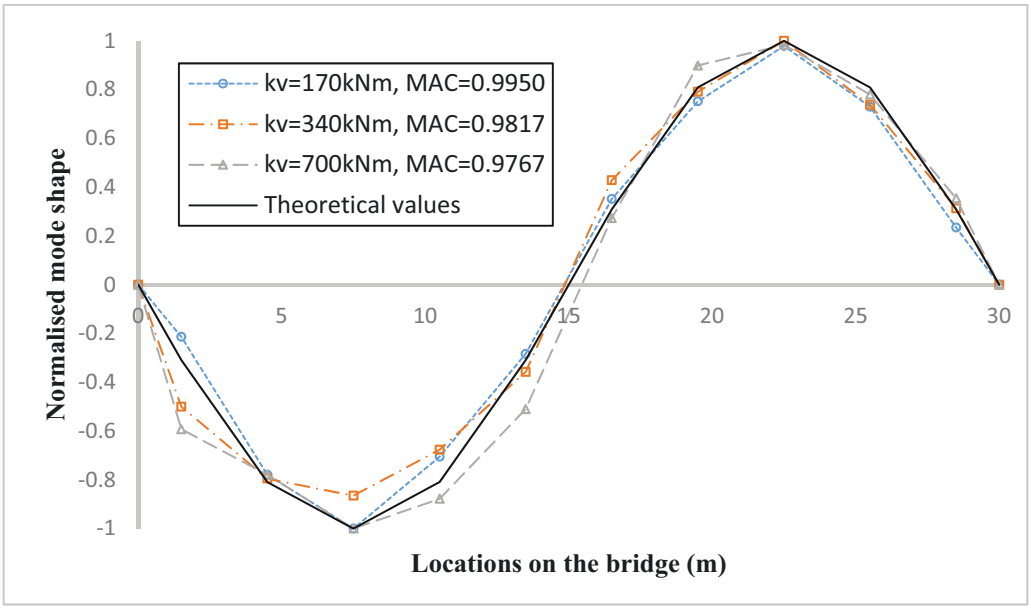

(b) Identified second mode shape

Figure 3.13 Effect of vehicle stiffness on identified mode shapes

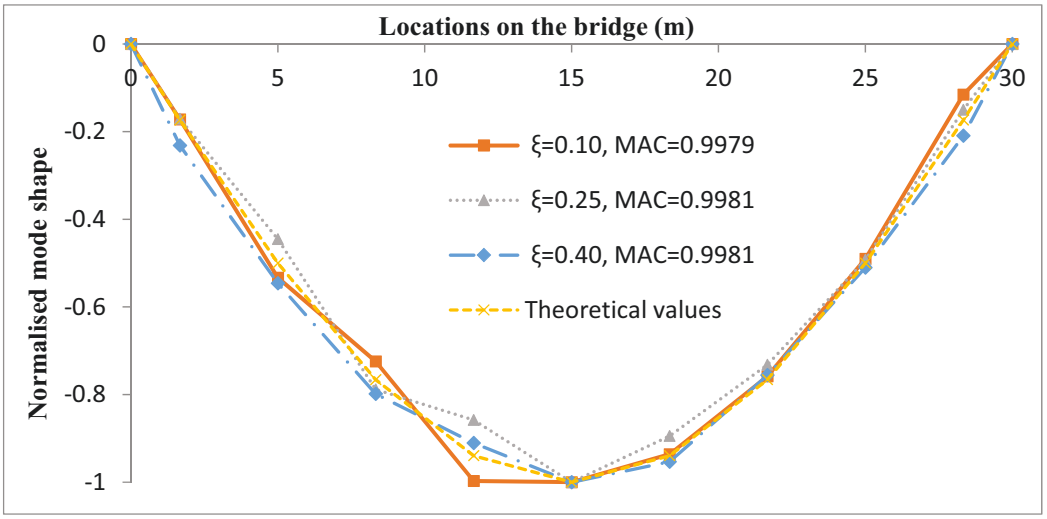

(a) Identified first mode shape

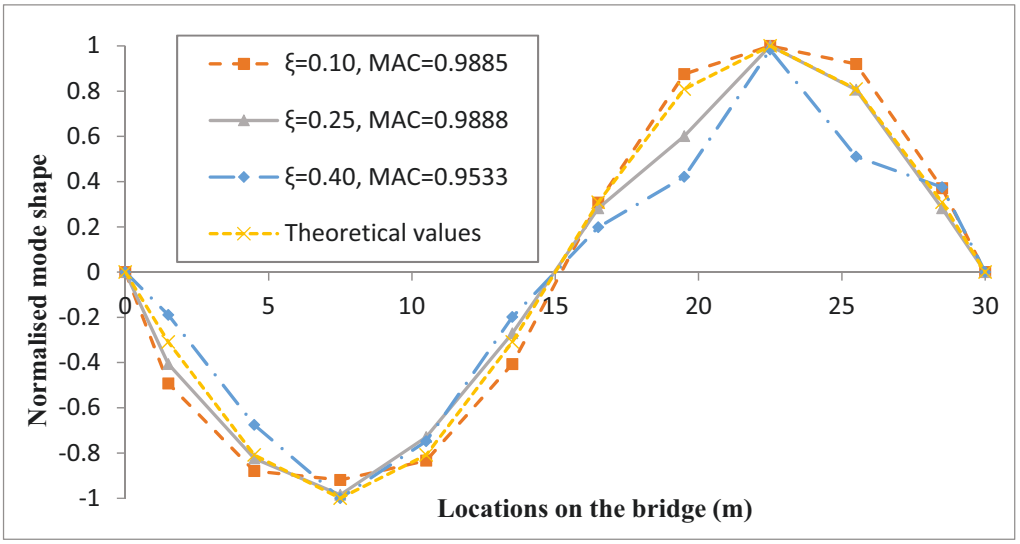

(b) Identified second mode shape

Figure 3.14 Comparison of identified mode shapes considering different vehicle damping ratio

CHAPTER 4 Drive by blind modal identification with Singular Spectrum Analysis

4.1 Overview

An instrumented vehicle passing over a bridge deck captures dynamic information of the bridge structure without bridge closure and on-site instrumentation. The vehicle dynamic response includes components associated with bridge surface roughness as well as vehicle-bridge vibration. Separating these components and extract the bridge modal parameters from the vehicle response is a challenging exercise. In this chapter, a novel drive-by blind modal identification with singular spectrum analysis method called SSA-BSS is proposed to extract the bridge modal frequencies from the vehicle dynamic response.

In the last decade, BSS has emerged as a promising tool for the output-only modal identification (Sadhu et al., 2017). BSS was originally used to recover special source components from the measured data, and the second-order blind identification (SOBI) is used to solve the BSS problem (Antoni, 2005). The mathematical equivalence between the modal expansion theorem and the BSS methods has been previously studied (Kerschen et al., 2007; Poncelet et al., 2007). The SOBI algorithm produces components that are mathematically equivalent with structural modal responses from measured data without any modifications (Zhou and Chelidze, 2007). A framework for output-only blind modal identification (BMID) was developed basing on the SOBI (McNeill and Zimmerman, 2008). Structural modal frequencies and damping ratios were estimated from modal response related components. Recently, BSS has been modified and applied to non-stationary problems (Hazra et al., 2009; Yang and Nagarajaiah, 2012). These

studies found that the number of sensors should be equal or greater than the number of modes. In drive-by bridge modal parameter identification using one instrumented vehicle, only one sensor is installed on the vehicle and one single channel of measurement is available. To solve the underdetermined problems in which the number of observations is less than the number of active components, the sparsity of sources was widely exploited in time-frequency domain (Zhen et al., 2017). Wang and Hao (2013) further proposed a structural damage identification method based on compressive sensing (CS). The application of CS relies on the sparsity of signals in a transform domain. This study took one step further by proposing to extract the independent components for the bridge modal frequency identification with one moving sensor in time domain. To overcome the limitations of previous methods, pre-process method was used to construct multi-channel datasets from the single channel measurement prior to applying the BMID method.

SSA is a technique that can decompose a set of time-series data into a finite number of interpretable components in time-domain ordered by their corresponding singular values (Liu et al., 2014b). The obtained components can be in the form of the trends, oscillation, noise and other undesired signal components. When a vehicle moves over a rough deck surface, the spectrum of the vehicle response contains a dominant component related to vehicular frequency. This component is taken as the "trend" which masks the bridge-related frequencies in the spectrum (Yang et al., 2013b). Yang et al. (2013b) used SSA to filter the vehicle response component and improved the visibility of bridge response components. However, under- or over-filtering may happen depending on the grouping step in SSA.

This chapter discusses how SSA was applied to decompose vehicle response into a multi-channel dataset, which was further analysed with BSS method to isolate bridge modal frequencies. Numerical studies were conducted to verify the proposed method. The

effects of system parameters, specifically road surface roughness, vehicle mass, vehicle stiffness and vehicle speed on the effectiveness of the combined process were also investigated.

4.2 Theoretical background

Recall the equation of motion of vehicle model in Eq. (3.1), the right-hand-side of the equation can be rewritten as

$$f(t) = \left\{c_v\left[\dot{d}_b(x,t) + vr'(x)\right] + k_v[d_b(x,t) + r(x)]\right\}_{x=vt} \tag{4.1}$$

With the Duhamel's integral, the dynamic response of the vehicle can be obtained as

$$d_v(t) = h_v(t) \otimes f(t) \tag{4.2}$$

where $h_v(t)$ is impulse response function of the vehicle system and $\otimes$ is the convolution operator.

Ignoring the effect of the road surface roughness and the vehicle damping, the vehicle response can be written as

$$d_v(t) = h_v(t) \otimes \left\{k_v\left[\sum_{i=1}^{N} \phi_i(vt)\,\eta_i(t)\right]\right\} \tag{4.3}$$

which is the convolution of the impulse response function and the bridge response. In other words, Eq. 4.3 includes both vehicle and bridge response components. The vehicle response becomes more complicated when vehicle damping and road surface roughness

are considered, therefore there is a critical need for an effective tool to extract the bridge response components only.

4.3 Drive by blind modal identification with singular spectrum analysis

The proposed method mainly consists of two steps. The first step is to decompose the vehicle response into a set of independent time series data. The second step is to extract the modal responses through the BSS for the identification of the bridge modal frequencies. Only the dynamic response measurement of the vehicle when crossing the bridge deck is used in the identification of bridge modal frequencies.

4.3.1 Decomposition of the vehicle response using SSA

In this step, the single-channel vehicle response is decomposed into a multi-channel dataset using SSA. SSA has two stages, namely decomposition and reconstruction. The first stage decomposes the time series into a set of elementary matrices based on two separate steps: embedding and singular value decomposition (SVD). The second stage extracts the constituting components based on the grouping and diagonal averaging steps. In this study, two stages of SSA performed as follows:

1) Embedding

A measurement data vector $\mathbf{d_v}(t) = [d_0, d_1, d_2, \dots, d_{N-1}]$ with length N can be divided into L lagged vectors X_i as $\{X_i = [d_{i-1}, d_i,\ d_{i+1} \cdots d_{i+N_L-2}]^T,\ \ i = 1,2, \dots L\}$, where N_L is the window length, which is an integer between 1 and N, and $L = N - N_L + 1$. These L vectors can further be formed into a trajectory matrix $\mathbf{X}$

$$\mathbf{X} = [\mathbf{X}_1, \mathbf{X}_2, \cdots \mathbf{X}_L\ ] = \begin{bmatrix} d_0 & d_1 & \cdots & d_{L-1} \\ d_1 & d_2 & \cdots & d_L \\ \vdots & \vdots & \ddots & \vdots \\ d_{N_L-1} & d_{N_L} & \cdots & d_{N-1} \end{bmatrix} \tag{4.4}$$

where the $(i,j)th$ element of $\mathbf{X}$ in Eq. (4.4) is $x_{ij} = d_{i+j-2}$. Hence, the trajectory matrix $\mathbf{X} \in R^{N_L \times L}$ is a Hankel matrix.

2) Singular value decomposition

Let $\mathbf{S} = \mathbf{X}\mathbf{X}^T$, which is a $N_L \times N_L$ square matrix. The N_L eigenvalues and the corresponding eigenvectors of matrix $\mathbf{S}$ are denoted as $\lambda_1, \lambda_2, \ldots, \lambda_{N_L}$ ($\lambda_1 > \lambda_2 > \cdots > \lambda_{N_L}$) and $\mathbf{U}_1, \mathbf{U}_2, \ldots, \mathbf{U}_{N_L}$, respectively. If N_s is the number of positive eigenvalues ($N_s \leq N_L$), the square root of these eigenvalues, *i.e.* $\sqrt{\lambda_1}, \sqrt{\lambda_2}, \ldots, \sqrt{\lambda_{N_s}}$, are referred to as the singular values of the trajectory matrix $\mathbf{X}$. Extremely small singular values are ignored in the decomposition process. Ignoring these small values does not affect the accuracy. The elementary matrix $\mathbf{X}_{si}$ for a $\sqrt{\lambda_i}$ is

$$\mathbf{X}_{si} = \sqrt{\lambda_i}\mathbf{U}_i\mathbf{V}_i^T \tag{4.5}$$

where $\mathbf{V}_i = \mathbf{X}^T\mathbf{U}_i/\sqrt{\lambda_i}$; and $\mathbf{U}_i$ and $\mathbf{V}_i$ are the left and right singular vectors, respectively. The trajectory matrix $\mathbf{X}$ can then be expressed as the summation of the N_s elementary matrices as

$$\mathbf{X} = \mathbf{X}_{s1} + \mathbf{X}_{s2} + \cdots + \mathbf{X}_{sN_s} \tag{4.6}$$

The trajectory matrix $\mathbf{X}$ is then decomposed into N_s elementary matrices of rank 1 with a norm equal to the singular value.

3) Grouping

All elementary matrices obtained in the previous step can be arranged into N_{g} groups using preset criteria. The grouping criteria depends on the expected function of the SSA, *e.g.*, denoising, smoothing, harmonic component extracting, and others. The elementary matrices in the same group are summed up, and N_{g} resultant matrices, *i.e.* $\mathbf{X}_{\mathrm{g}1}, \mathbf{X}_{\mathrm{g}2}, \ldots \mathbf{X}_{\mathrm{g}N_{\mathrm{g}}}$, can be obtained. The original trajectory matrix $\mathbf{X}$ can then be expressed as

$$\mathbf{X} = \mathbf{X}_{\mathrm{g}1} + \mathbf{X}_{\mathrm{g}2} + \cdots + \mathbf{X}_{\mathrm{g}N_{\mathrm{g}}} \tag{4.7}$$

The groups can be formed based on the information contained into the singular vectors (Hassani, 2007). Because the singular values are arranged in a descending order, the first few elementary matrices contribute more to the trajectory matrix than the others. Therefore, each major elementary matrix forms one group for the reconstruction in the proposed method.

4) Skew diagonal averaging

Each resultant matrix in the last step is converted into a new set of time-series data with the same length as the original dataset. A skew diagonal averaging procedure is adopted to recover the time series. Let $\mathbf{Y}$ be any of the resultant matrixes $\mathbf{X}_{\mathrm{g}l}$, with the elements denoted as $y_{ij}, i = 1, 2, \ldots, N_L,\ j = 1, 2, \ldots, L$. For$N_L < L$, the recovered time series data $\mathbf{d}^{(l)} = [d_0^{(l)}, d_1^{(l)}, \ldots d_{N-1}^{(l)}]$ are given by

$$d_k^{(l)} = \begin{cases} \dfrac{1}{k+1}\displaystyle\sum_{m=1}^{k+1} y_{m,k-m+2} & \text{for } 0 \le k < N_L - 1 \\ \dfrac{1}{N_L}\displaystyle\sum_{m=1}^{N_L} y_{m,k-m+2} & \text{for } N_L - 1 \le k \le L \\ \dfrac{1}{N-k}\displaystyle\sum_{m=k-L+2}^{N-L+1} y_{m,k-m+2} & \text{for } L < k \le N - 1 \end{cases} \tag{4.8}$$

For $N_L > L$, the length N_L should be switched with L in the preceding expressions. There are N_g sets of time series data $\{\mathbf{d}^{(l)},\ l = 1,2,\dots N_\mathrm{g}\}$ obtained from $\mathbf{d}_{\boldsymbol{v}}(t)$ and the new data vector $\mathbf{d}(t)$ after the SSA becomes $\mathbf{d}(t) = \sum_{l=1}^{N_\mathrm{g}} \mathbf{d}^{(l)}$.

4.3.2 Blind modal identification with SSA

The multichannel dataset from SSA is used as the input into BSS for modal parameter identification. Suppose the dataset includes N_g sets of time series data $\mathbf{d} = \{\mathbf{d}^{(l)},\ l = 1,2,\dots,N_\mathrm{g}\}^T$. Each set of time series data $\mathbf{d}^{(l)}$ is a linear mixture of n components $\{\mathbf{s}_{\boldsymbol{i}}, i = 1,2,\dots,n\}$. The relation between the components and the measured data can be written as

$$\mathbf{d} = \mathbf{A}\mathbf{s} \tag{4.9}$$

where $\mathbf{A}$ =$N_\mathrm{g} \times n$ mixing matrix, $\mathbf{s} = \{\mathbf{s}_1, \mathbf{s}_2, \cdots, \mathbf{s}_\mathrm{n}\}^T$and $\mathbf{d}$={ $\mathbf{d}^{(1)}$, $\mathbf{d}^{(2)}$, … $\mathbf{d}^{(Ng)}$}^{T}, and both $\mathbf{A}$ and $\mathbf{s}$ are unknown.

Assuming that the components $\mathbf{s} = [\mathbf{s}_1, \mathbf{s}_2, \cdots, \mathbf{s}_\mathrm{n}]^T$are statistically independent, they can be determined by the second-order blind identification for the overdetermined case of ($N_g > n$) as (Belouchrani et al., 1997)

$$\mathbf{s} = \mathbf{W}\mathbf{d} \tag{4.10}$$

where the de-mixing matrix $\mathbf{W}$ is the inverse of the mixing matrix $\mathbf{A}$, and needs to be estimated. There are two steps in the SOBI algorithm: data whitening and estimation of the mixing and de-mixing matrices. For the observed data $\mathbf{d}(t)$, the time-shifted covariance matrix can be written as $\boldsymbol{R}_d(\tau) = E\{\boldsymbol{d}(t)\boldsymbol{d}(t+\tau)^T\}$. The eigenvalue decomposition of $\mathbf{R}_d(0)$ can be computed as $\mathbf{R}_d(0) = \mathbf{E}\mathbf{D}\mathbf{E}^T$, where $\mathbf{E}$ is the orthogonal matrix of eigenvectors and $\mathbf{D}$ is the diagonal matrix of eigenvalues. The whitening matrix $\mathbf{W}_m$ is then calculated as

$$\mathbf{W}_m = \mathbf{D}^{-1/2}\mathbf{E} \tag{4.11}$$

where the observed data $\mathbf{d}$ are whitened to form the whitened data vector which has a unitary covariance matrix. The whitened data are then computed as $\mathbf{z} = \mathbf{W}_m\mathbf{d}$ with $E\{\mathbf{z}\mathbf{z}^T\} = \mathbf{I}$ (McNeill and Zimmerman, 2008). A matrix $\boldsymbol{\Psi}$ that approximately diagonalizes several time-shifted covariance matrices can be obtained using the joint approximate diagonalization (JAD) technique (Belouchrani et al., 1997). The de-mixing and mixing matrices can then be computed as

$$\mathbf{W} = \boldsymbol{\Psi}^T\mathbf{W}_m \tag{4.12a}$$

$$\mathbf{A} = \mathbf{W}_m^{-1}\boldsymbol{\Psi} \tag{4.12b}$$

The dynamic responses of the vehicle $\mathbf{d}_v$ in Eq. (4.3) can then be expressed as

$$\mathbf{d}_v = \boldsymbol{\Phi}\mathbf{q} \tag{4.13}$$

where $\mathbf{q}$ = vector of vibration modes; and the modal matrix $\mathbf{\Phi}$ is equal to the mixing matrix $\mathbf{A}$ in Eq. (4.12b). The modal responses can be estimated similar to Eq. (4.10) using BSS as

$$\mathbf{q} = \mathbf{\Phi^{-1}} \mathbf{d}_v \tag{4.14}$$

where $\mathbf{\Phi^{-1}}$ is equal to the de-mixing matrix $\mathbf{W}$ in Eq. (4.12a).

McNeill and Zimmerman (2008) proposed a framework for blind modal identification with application of the SOBI algorithm on an expanded and pre-treated dataset. This helps to improve the quality of the estimated modal responses. This framework is adopted in this study for the blind modal identification. The measured data, denoted $\mathbf{d}_0$, are supplemented by $90°$ phase-shifted data, $\mathbf{d}_{90}$, to double the size of the estimation problem as

$$\begin{bmatrix} \mathbf{s}_0^{(n\times 1)} \\ \mathbf{s}_{90}^{(n\times 1)} \end{bmatrix} = \mathbf{W}^{(2n\times 2N_g)} \begin{bmatrix} \mathbf{d}_0^{(N_g\times 1)} \\ \mathbf{d}_{90}^{(N_g\times 1)} \end{bmatrix} \tag{4.15}$$

where $\mathbf{s}_{90}$ = $90°$ phased-shifted components of $\mathbf{s}_0$. The modal responses are

$$\mathbf{q} = \frac{1}{\sqrt{2}} [\mathbf{s}_0 + \mathbf{s}_{90}] \tag{4.16}$$

For a linear vehicle-bridge system, the dominant vehicle or bridge frequencies in the Fourier spectrum of the response component can be identified by curve-fitting. For a nonlinear system, Hilbert transform could be used to estimate the instantaneous frequency and damping from $\mathbf{q}(t)$ (McNeill and Zimmerman, 2008).

4.3.3 Drive by blind modal identification

The step-by-step procedure of the proposed method is as follows:

1) The single-channel measurement of the vehicle response $\mathbf{d}_v(t)$ is separated into a multi-channel dataset $\mathbf{d} = \{\mathbf{d}^{(l)},\ l = 1,2,\dots N_g\}$ using SSA based on Eqs. (4.4) to (4.8). The dataset is denoted as $\mathbf{d}_0$.

2) The dataset is phase shifted $90°$ to get the supplement dataset, $\mathbf{d}_{90}$. It is combined with $\mathbf{d}_0$ to form an expanded set of observed data $\mathbf{d(t)} = \begin{bmatrix}\mathbf{d}_0 \\ \mathbf{d}_{90}\end{bmatrix}$.

3) The whitening matrix $\mathbf{W}_m$ is computed from Eq. (4.11). The whitened data $\mathbf{z} = \mathbf{W}_m\mathbf{d}(t)$. The joint diagonalizer $\mathbf{\Psi}$ can be obtained by applying the JAD technique to the whitened data $\mathbf{z} = \mathbf{W}_m\mathbf{d}$. Then the de-mixing matrix $\mathbf{W}$ and the mixing matrix $\mathbf{A}$ can be obtained from Eq. (4.12).

4) The components $\mathbf{s}_0$ and $\mathbf{s}_{90}$ are then obtained based on Eq. (4.15).

5) The modal responses $\mathbf{q}$ are estimated from Eq. (4.16). The bridge modal frequencies are obtained from the modal responses.

A flow chart of the proposed method is shown in Figure 4.1.

4.4 Numerical study

Numerical simulations were performed with the following parameters of the bridge deck: $L = 30m, \rho = 1000\,kg/m,\ I = 0.175m^4, E = 27.5GPa$. The first two natural frequencies of the deck were 3.83 and 15.32 Hz, respectively. The properties for the vehicle were: $m_v = 200kg,\ k_v = 170\,kN/m$. The vehicle modal frequency was 4.64 Hz. Damping of the bridge and vehicle were not considered in this study. The speed of the

vehicle was constant at $2.0\,m/s$, and time step was set to 0.001s in the simulation. Class A road surface roughness was used. Ongoing traffic was modelled as white-noise excitation at supports of the deck with an amplitude of 0.02m/s^2. The aforementioned parameters were used for all numerical studies in this paper unless otherwise stated. The dynamic response of the vehicle and its frequency spectrum are presented in Figure 4.2, which shows that vehicle frequency is dominant in the spectrum.

4.4.1 Selection of window length

The window length is one of the most important parameters in the SSA technique, and it has a large effect on the decomposition (Harmouche et al., 2018). There are some recommendations on the selection of window length (Golyandina, 2010; Hassani et al., 2011). A larger value of L makes longer-period oscillations to be solved, but too large a value may involve many eigentriples and miss some important principal components with high contributions. Although many trial applications and various methods have been discussed for the selection of optimal values of L, there is still a lack of theoretical regulation for window length selection. In this chapter, three typical values from small to large were selected to show the effect of the window length.

The dynamic response of the vehicle contains information about both the vehicle and bridge, and the first two bridge modes and one vehicle mode are targeted components for extraction. The unsupervised component grouping method based on hierarchical clustering is adopted for the automatic selection of the elementary matrices to compose the desired dataset from the vehicle response (Harmouche et al., 2018). Each elementary matrix is used as one group and it does not need the grouping selection. In the following

sections, the time series data with the top 20% of eigenvalues reconstructed from the SSA are adopted as input to the BSS to estimate the three targeted components.

Three different window lengths, *i.e.*, 100, 500 and 1000, were selected for the study. The first three time series data and their spectra from the SSA decomposition are presented in Figure 4.3. The frequency of the first time series data for all window lengths was 4.73 Hz, which was very close to the vehicle frequency 4.64Hz. The second time series data, from 500 and 1000 window lengths, have only one distinct peak, at 3.73 Hz which was close to the first bridge mode, at 3.83Hz. The amplitude of the time series data is much larger from using 1000 window length. Neither the vehicle nor bridge modes were found in the third time series data in Figure 4.3.

The components decomposed from the BSS are presented in

Figure 4.4. The components corresponding to the vehicle and bridge modal frequencies were clearly separated for all window lengths, and the larger window length provided better separation results. The third component in Figure 5 was related to the second bridge modal frequency, 15.32 Hz, which was more notable than that directly from the SSA method. The proposed method is less sensitive to the effect of window length, and the bridge modal frequencies can be better isolated than by simply application of the SSA only. The window length was selected to be 1000 in the following studies.

4.4.2 Effect of road surface roughness

The road surface roughness has significant effect on the indirect bridge modal identification. Figure 4.5 shows the vehicle response and its corresponding spectrum when the road surface roughness is Class B. There was only one peak in Figure 4.5 (b), at 4.67Hz, which was close to the vehicle mode, 4.64 Hz, and the bridge mode cannot be

identified from the spectrum. Figure 4.6 shows the first two components from the proposed method. The first bridge mode can be identified from the peak of the first component in Figure 4.6 (b), 3.77 Hz, and the vehicle mode was related to the peak of the second component in Figure 4.6(b), 4.67 Hz. The proposed method has the capability to separate the components related to the vehicle and first bridge modal frequency even when the road surface roughness is Class B.

4.4.3 Effect of vehicle mass

Three different vehicle masses, *i.e.*, 200, 500 and 1000 kg, were investigated with the vehicle speed 2.0 m/s. Other parameters are the same as those stated previously. The vehicle modal frequencies were 4.64, 2.93 and 2.08 Hz, respectively, for the different vehicle masses. Figure 4.7 shows the identified first three response components and their frequency spectra. The frequencies of the first components in Figure 4.7 (a) were 3.77, 2.90 and 2.03 Hz for vehicle masses 200, 500 and 1000 kg, respectively. The latter two frequencies corresponded to the vehicle frequency. The first frequency corresponded to the frequency of the first bridge mode. The corresponding vehicle mode at 4.70 Hz was noted in the second component as shown in Figure 4.7(b). The first bridge modal frequency was noted in the second components in Figure 4.7 (b) for the 500 and 1000 kg vehicles as 3.90 and 3.83 Hz, respectively. Figure 4.7 (c) shows the third response component; the peak frequency is around 15.27 Hz, corresponding to the second bridge mode. Comparing the spectrum of the bridge-related components, the spectrum amplitude increased with the vehicle mass. This may suggest that a heavier testing vehicle may amplify the bridge vibration, which is beneficial for the drive-by bridge modal frequency identification.

4.4.4 Effect of vehicle stiffness

A moderate vehicle mass 500 kg was selected with vehicle stiffness of 340, 680 and 1360 kN/m and speed of 2.0 m/s. The corresponding vehicle modal frequencies were 4.15, 5.87, and 8.30 Hz, respectively. Figure 4.8 shows the components of the responses and their spectra with different stiffness values. The peak frequencies were 3.77 and 15.43 Hz as shown in Figure 4.8 (a) and (c), and these frequencies related to the first and second bridge modes. Figure 4.8(b) shows the three frequencies, *i.e.,* 4.33, 5.90 and 8.20 Hz, which corresponded to the vehicle modes with different stiffness, respectively. These results show that the vehicle stiffness does not have a large effect on the identified results.

4.4.5 Effect of vehicle speed

The vehicle parameters were selected as $m_v = 500\ kg$ and $k_v = 170\ kN/m$, with other parameters the same as stated previously (Section 4.4). The vehicle frequency was 2.90 Hz. Vehicle speeds 2.0, 4.0 and 8.0 m/s were studied. Figure 4.9 presents the decomposed components and their spectra. Figure 4.9 (a) shows the first component, with a frequency at around 2.90 Hz for all vehicle speeds. Figure 4.9 (b) and (c) are the second and third components, with frequencies at 3.87 and 15.27 Hz, respectively. These two frequencies corresponded to the first and second bridge modal frequencies. Because the frequency resolution increased with a lower speed as the time record length for the vehicle moving on the deck is increased, the accuracy of identified frequency can be improved with a lower vehicle speed. Therefore, a moderate vehicle speed is recommended when identifying higher-order modal frequencies.

4.4.6 Effect of measurement noise

Practical measurement is always contaminated with noise. Therefore, in this study, white noise was added to the calculated acceleration response to simulate the polluted measurement. The vehicle speed was 4.0 m/s and other parameters were the same as those in Section 4.4.5. Three different noise levels, *i.e.*, 5, 10 and 20%, were simulated. Figure 4.10 shows the identified results. The identified response components and spectra at different noise levels were close together indicating that the proposed method is insensitive to measurement noise. This is mainly due to the fact that only the first 20% of SSA components were adopted as the input to BSS to obtain the first three targeted components of BSS. SSA components with low singular values were removed to reduce the white noise effects.

4.5 Identification of instantaneous frequencies of the VBI system

The vehicle can also be used as an actuator to excite the bridge structure, and the vehicle-induced vibration is a type of non-stationary process (Kim et al., 2014). Hilbert transform may be used to extract instantaneous frequencies of the VBI system in the indirect bridge modal identification. The vehicle parameters were selected as $m_v = 1000\ kg$ and $k_v = 170\ kN/m$, and other parameters were the same as those stated previously in Section 4.4. The natural frequency of the vehicle was 2.08 Hz. The dynamic response and the spectrum of the vehicle are given in Figure 4.11. There are two peaks in the spectrum; the first peak corresponded to the vehicle mode at 2.07 Hz, and the second peak was related to the first bridge mode at 3.87 Hz. The first and second response components are shown in Figure 4.12(a) and the corresponding instantaneous frequencies obtained from HT are presented in Figure 4.12(b). The average values of the first and second components were 2.08 and 3.87 Hz, which were the vehicle frequency and the first bridge modal frequency,

respectively. The oscillations at the beginning and end of the instantaneous frequency were due to the Gibbs phenomenon with record length of the data. The middle part of the time history oscillated between 3.79 and 3.98Hz. Because the vehicle speed was 2.0 m/s and the bridge length was 30 m, the driving frequency was about 0.07 Hz. This instantaneous frequency was modulated by the driving frequency. The result shows that the driving frequency could also be identified by the proposed method.

4.6 Summary

A drive-by blind modal identification method with singular spectrum analysis was developed to extract the bridge modal frequencies from the dynamic response of a passing vehicle. The proposed method was less sensitive to the window length compared with the direct SSA. The vehicle and bridge modal frequencies can be separated easily with the proposed method even with the Class B road surface roughness. The effects of vehicle parameters on the identification were investigated numerically. Results showed that a heavier vehicle can amplify the bridge vibration to enhance the drive-by bridge modal identification and a lower speed can identify the frequency with greater accuracy. The proposed method was also robust to measurement noise. Further analysis with the HT showed that the proposed method can be used to identify the instantaneous frequency of the VBI system.

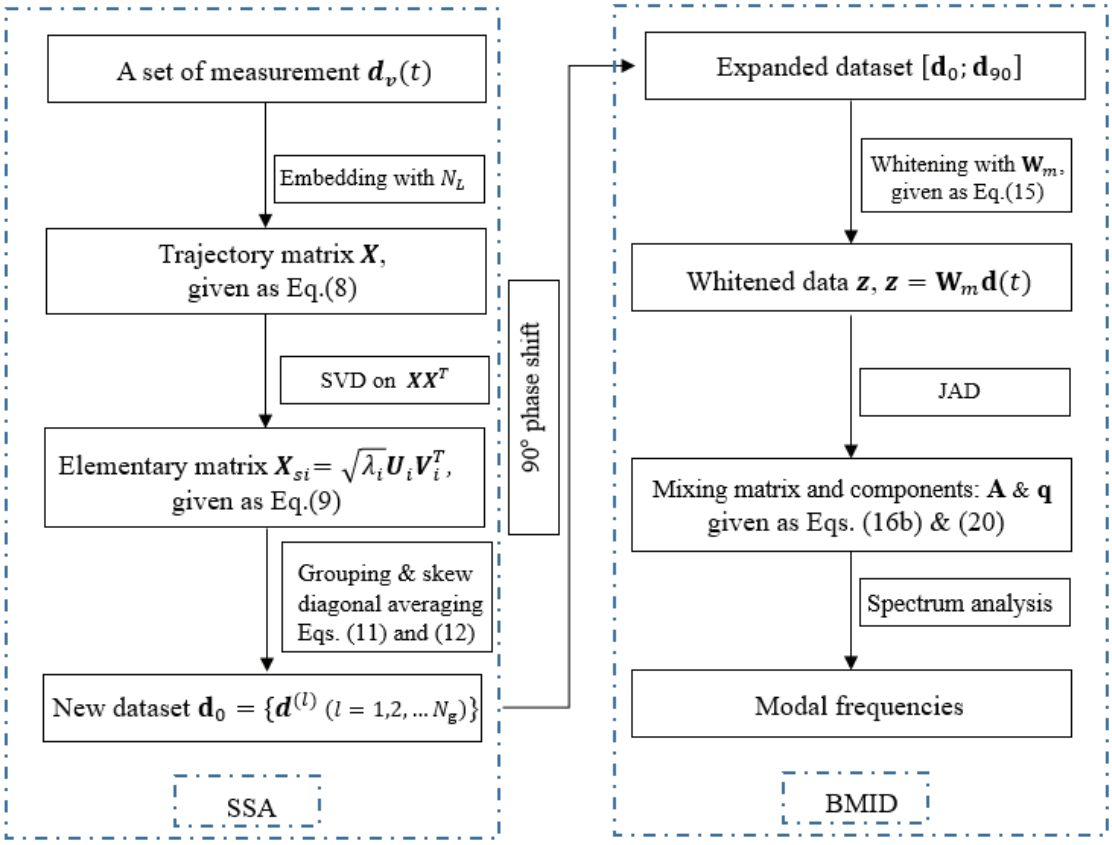

Figure 4.1 Flow chart of proposed method

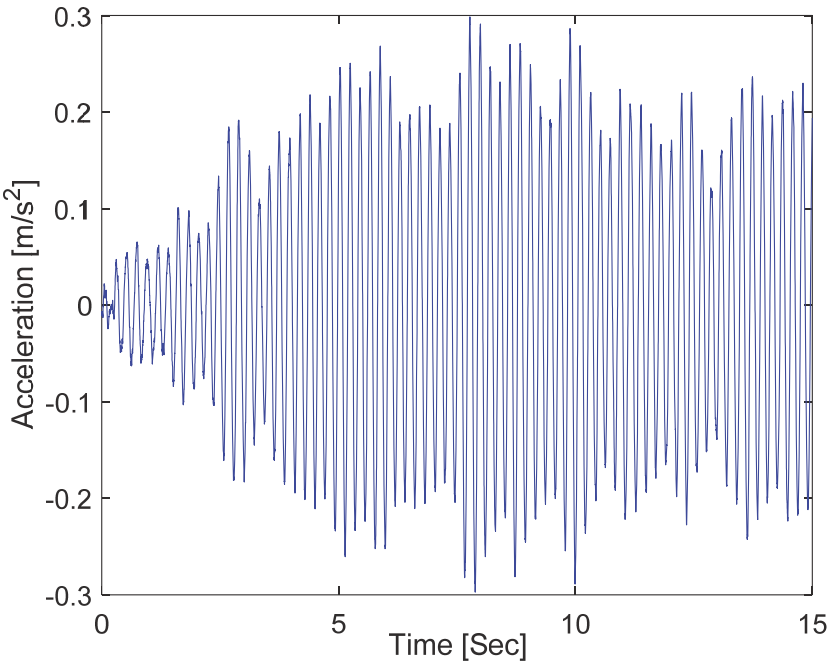

(a) The acceleration response of vehicle

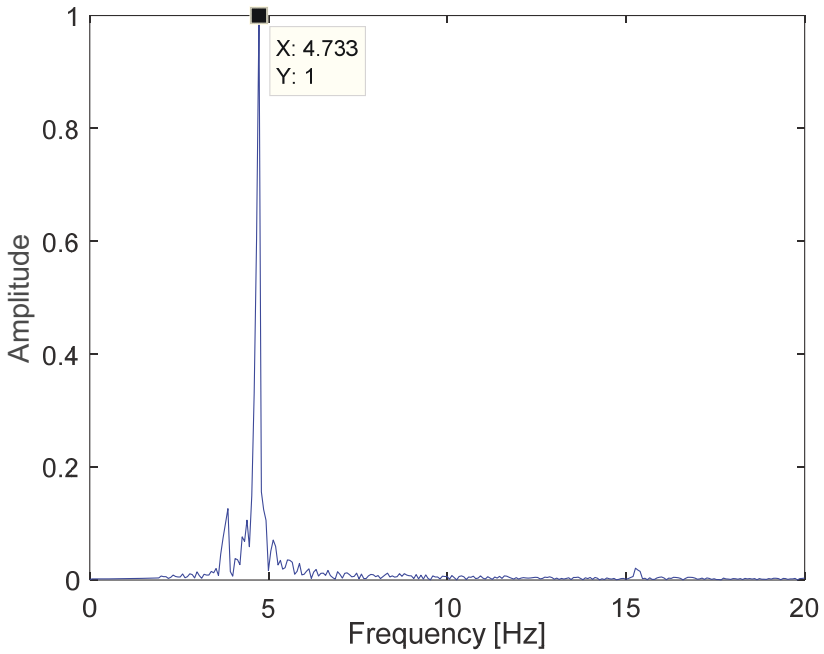

(b) The spectrum

Figure 4.2 Vehicular response and its spectrum when moving on top of bridge deck

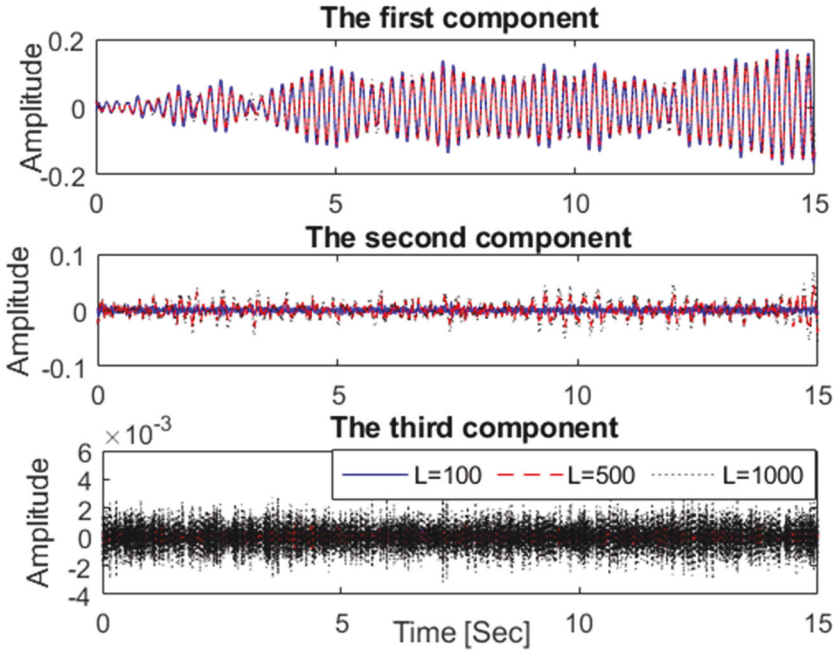

(a) The dataset

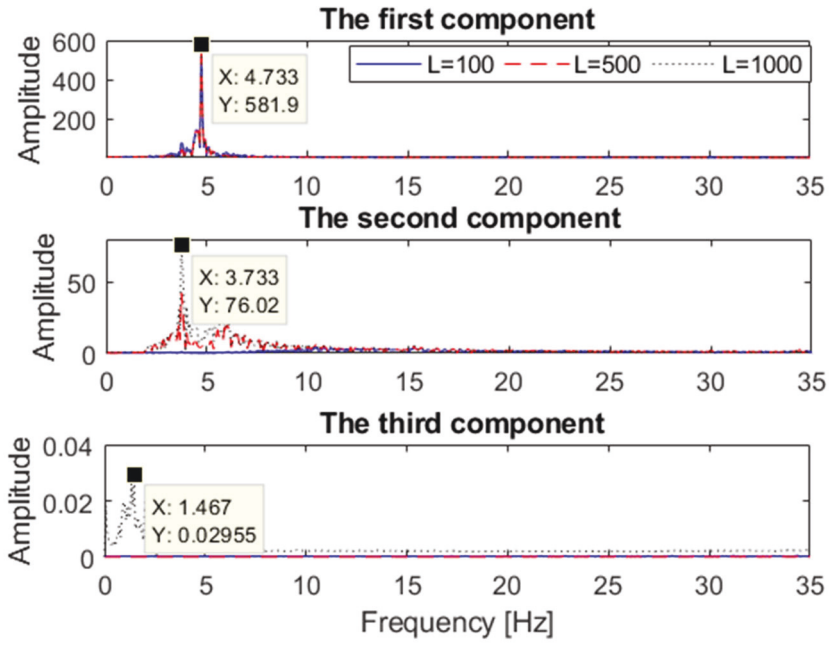

(b) Their spectra

Figure 4.3 Dataset and their spectra by SSA

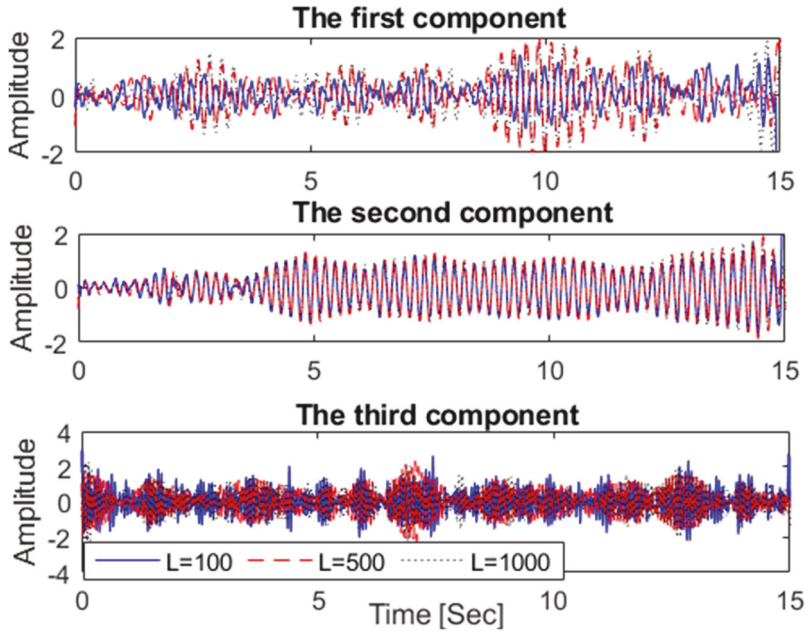

(a) The response components

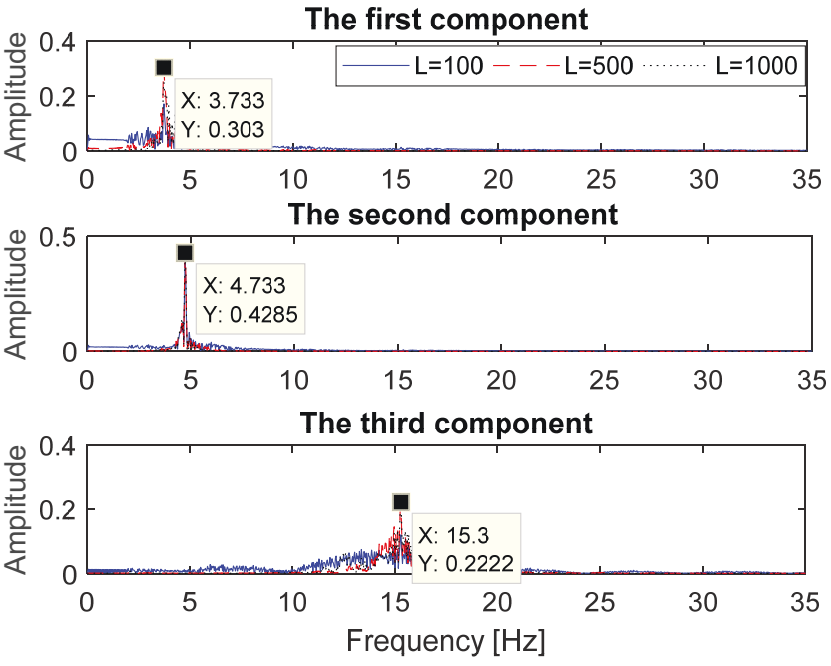

(b) Their spectra

Figure 4.4 Response components and their spectra by the proposed method

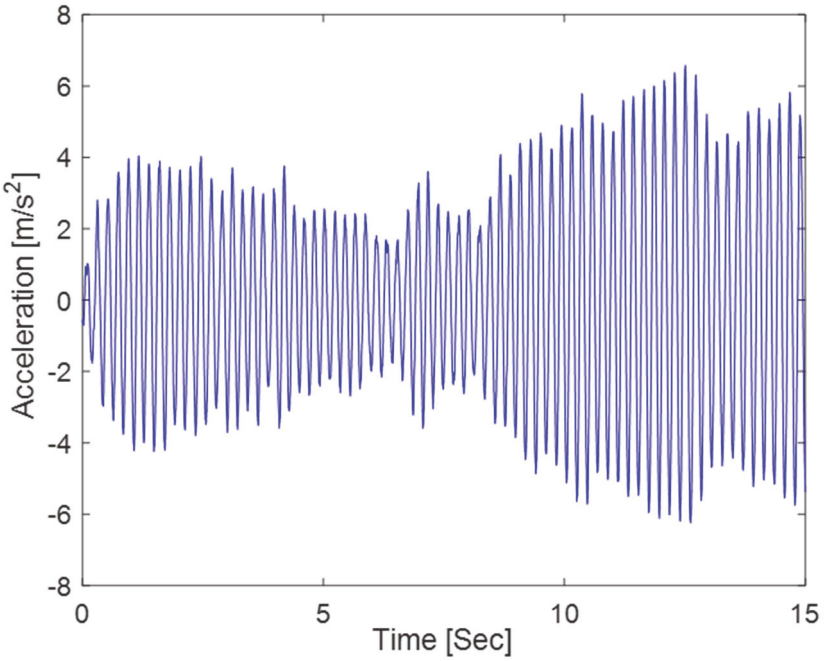

(a) The acceleration response of vehicle

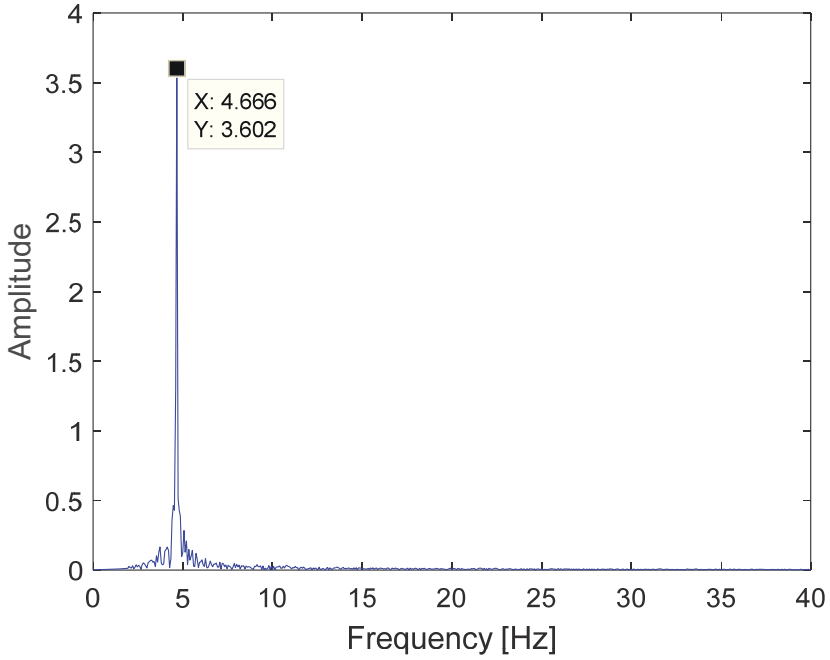

(b) The spectrum

Figure 4.5 Vehicular response and its spectrum for Class B road surface roughness

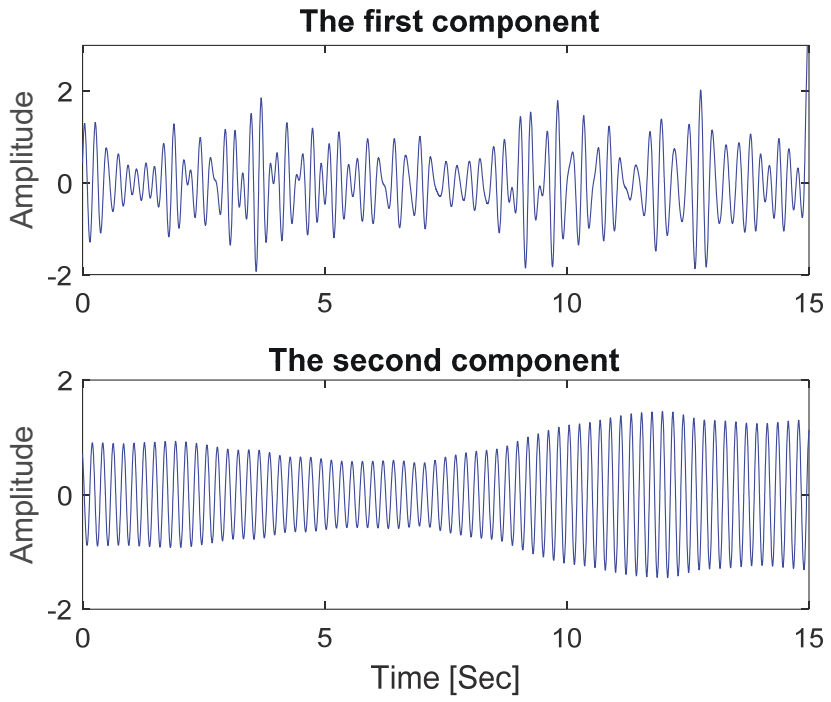

(a) The response components

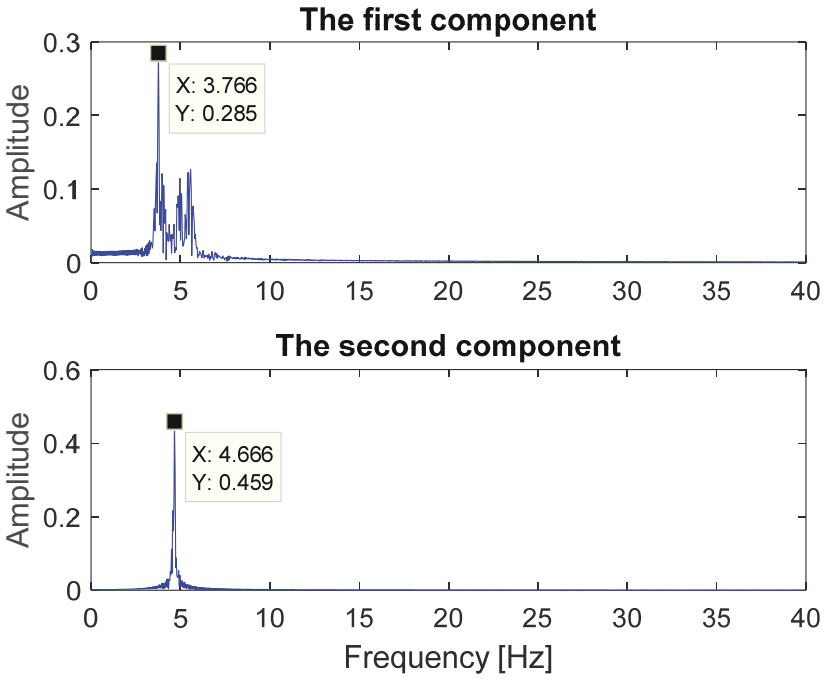

(b) The spectra

Figure 4.6 The first two components and their spectra by the proposed method

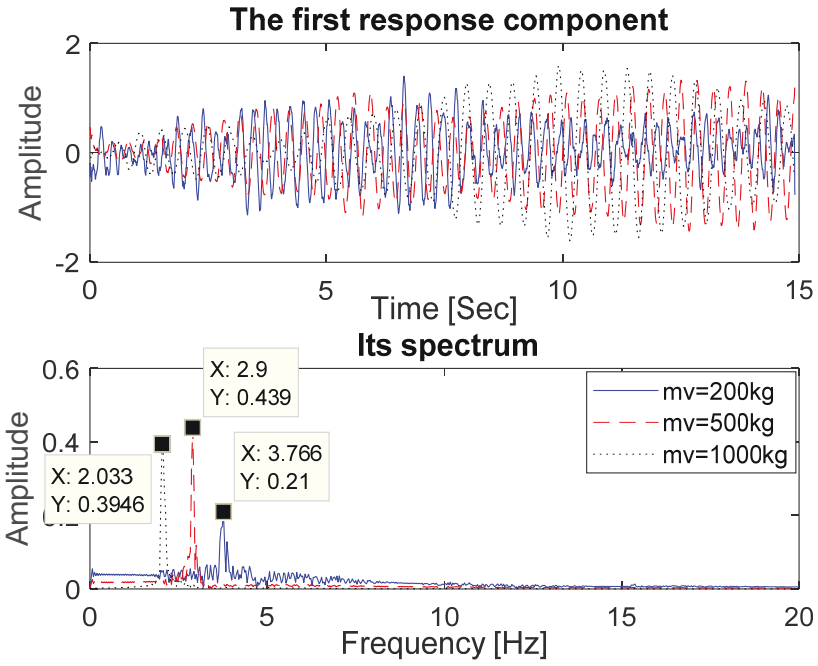

(a) The first response component

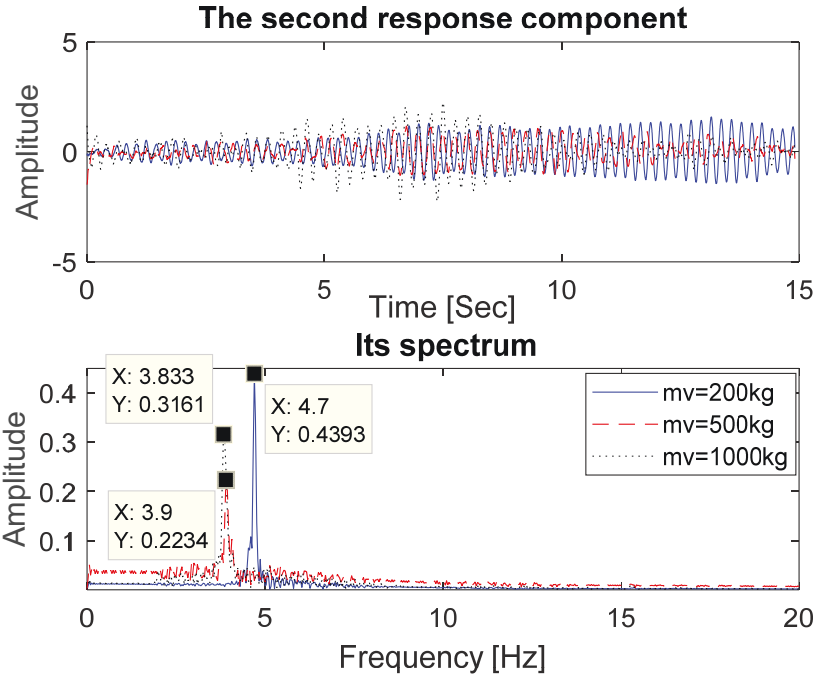

(b) The second response component

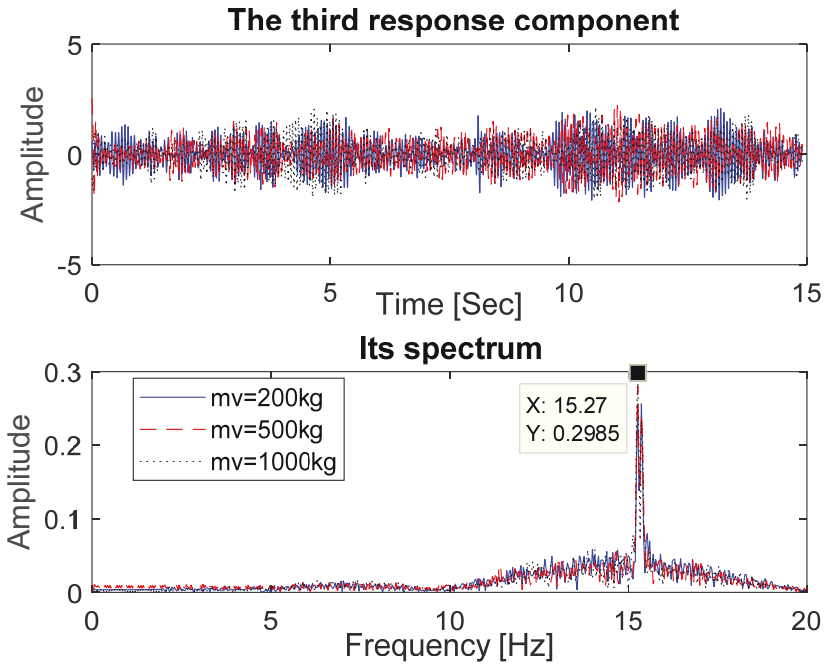

(c) The third response component

Figure 4.7 Response components and their spectra with different vehicle mass

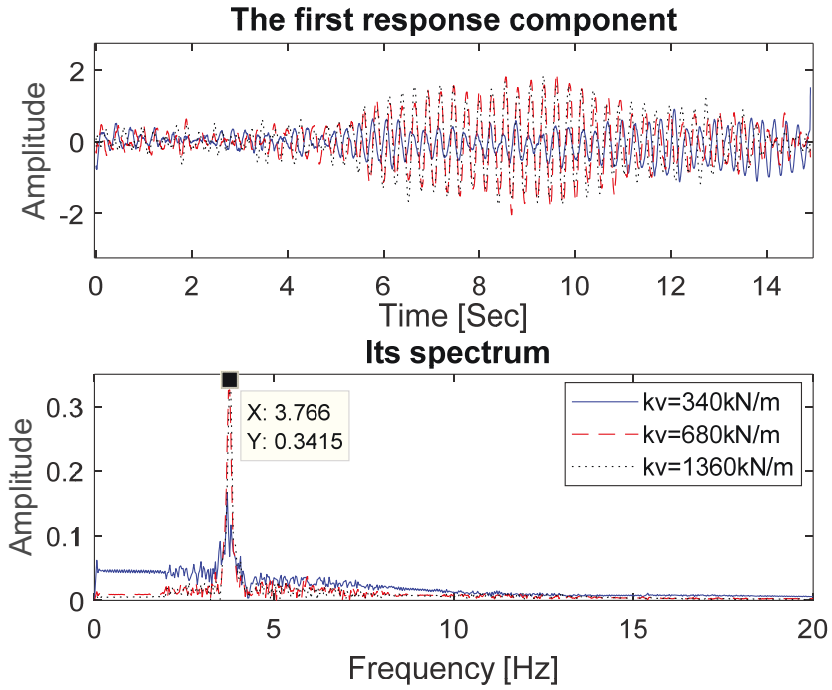

(a) The first response component

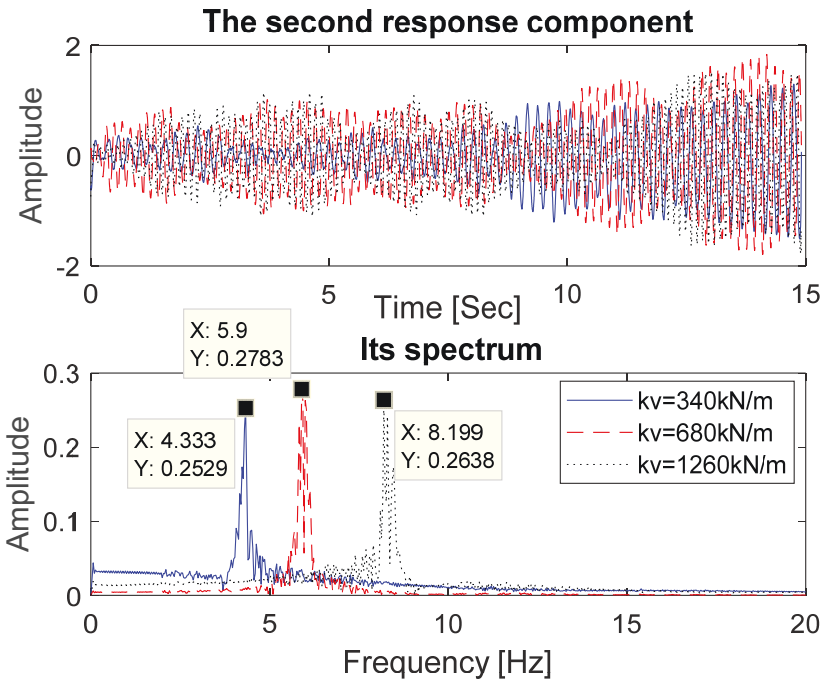

(b) The second response component

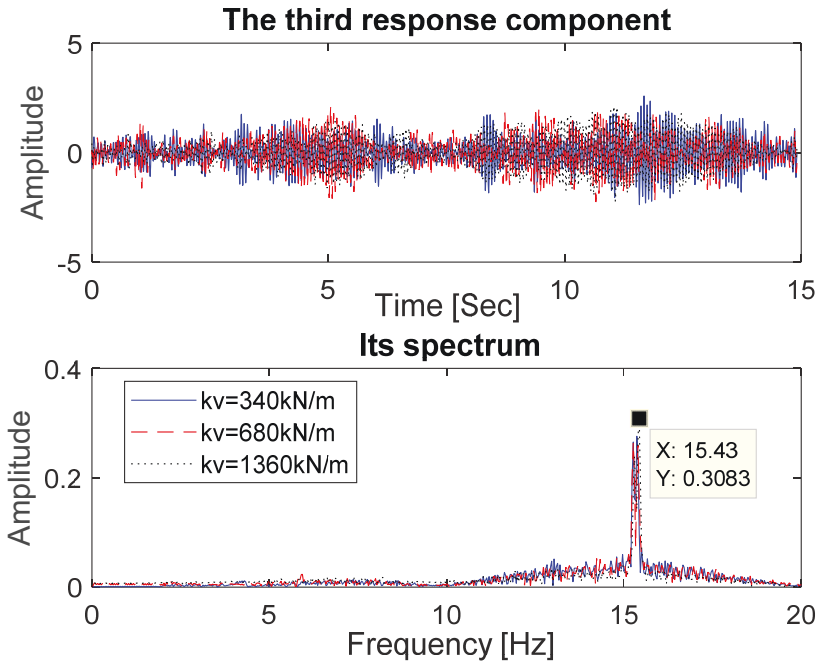

(c) The third response component

Figure 4.8 Response components and their spectra with different vehicle stiffness

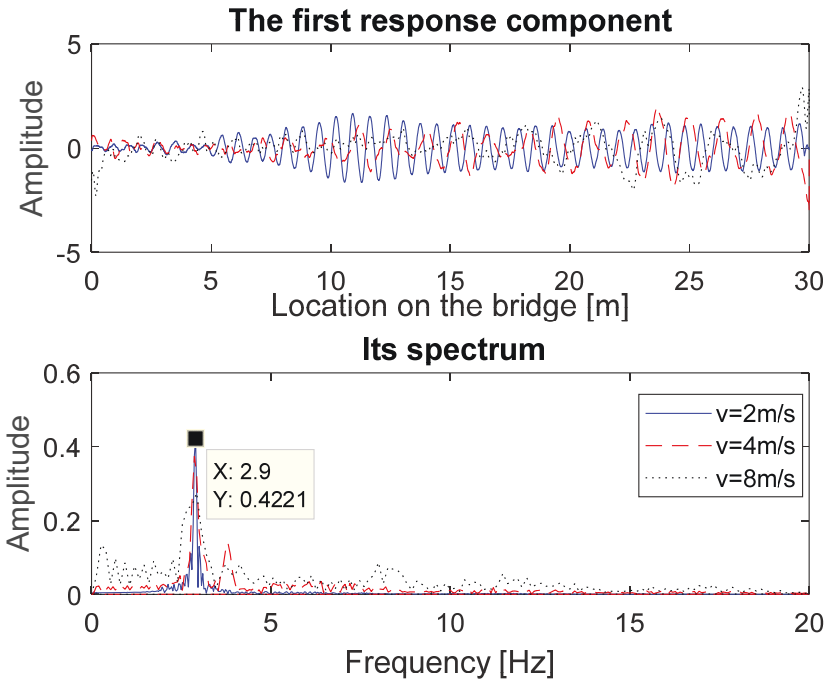

(a) The first response component

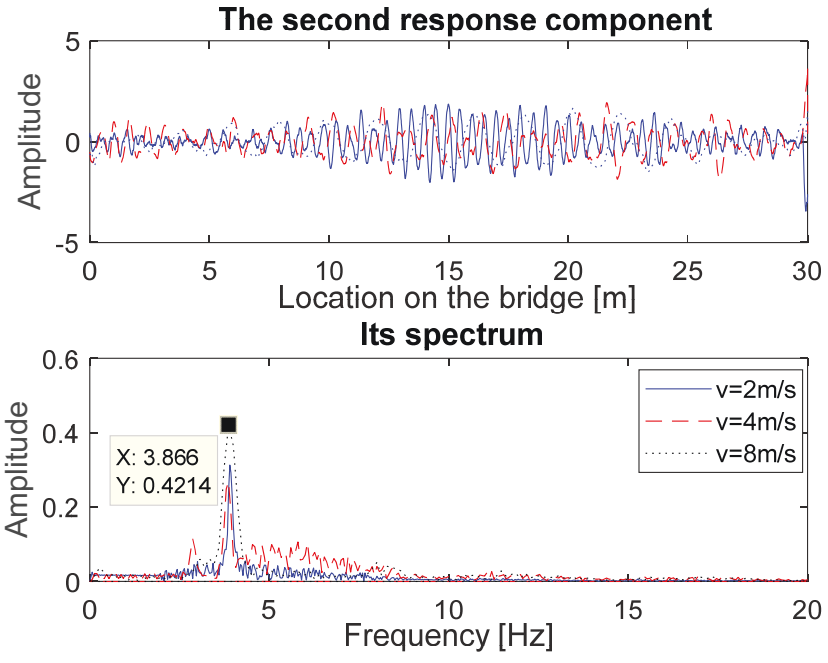

(b) The second response component

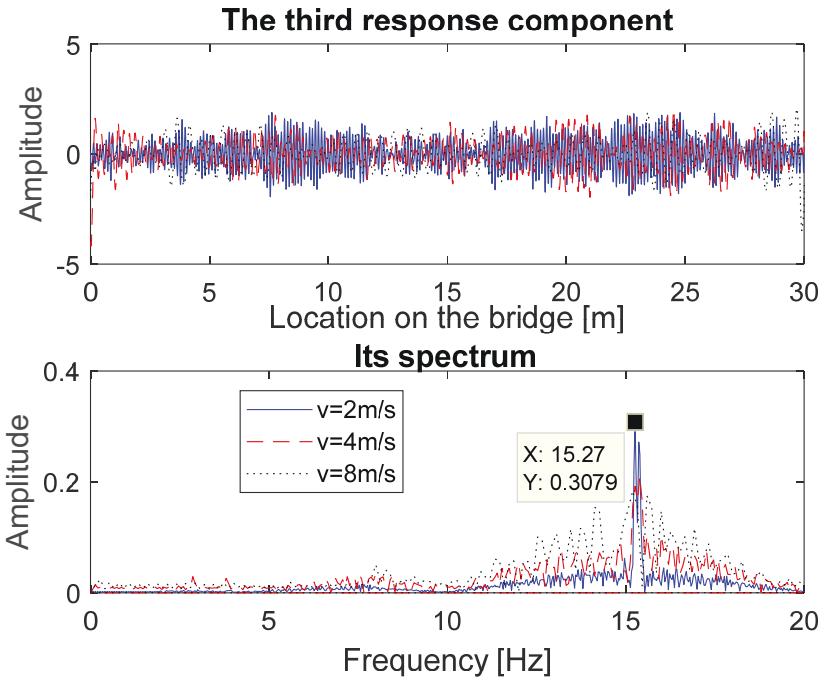

(c) The third response component

Figure 4.9 Response components and spectra considering different vehicle speed

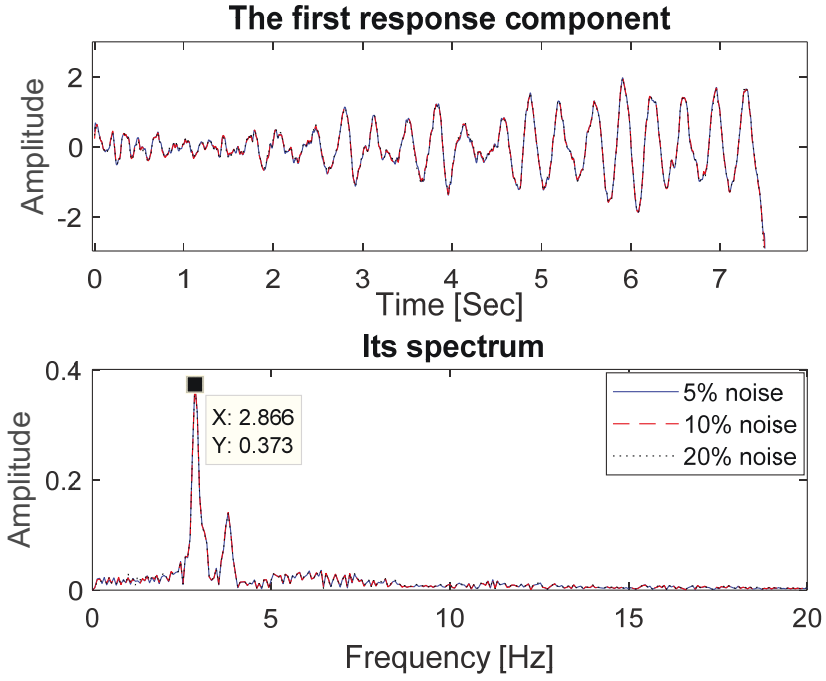

(a) The first response component

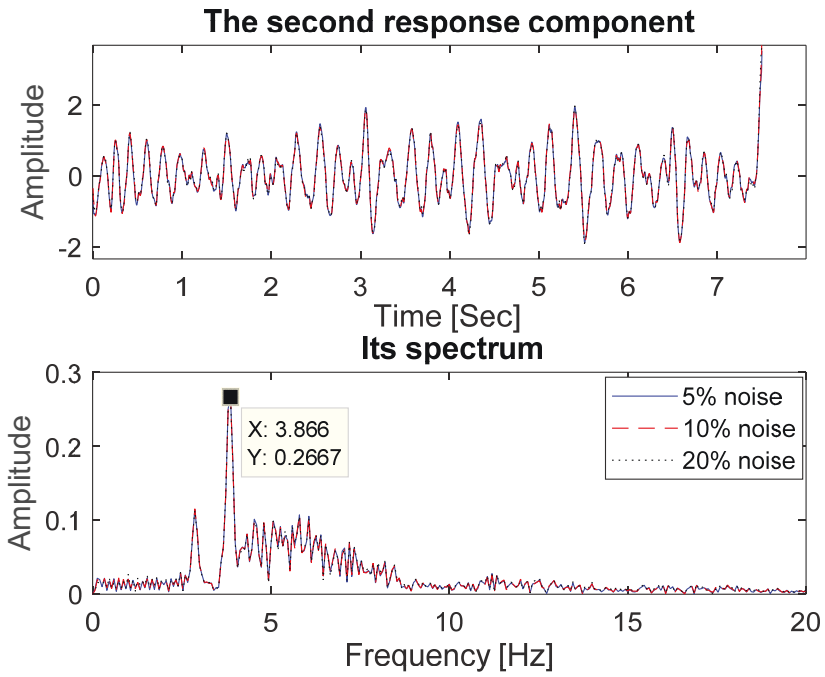

(b) The second response component

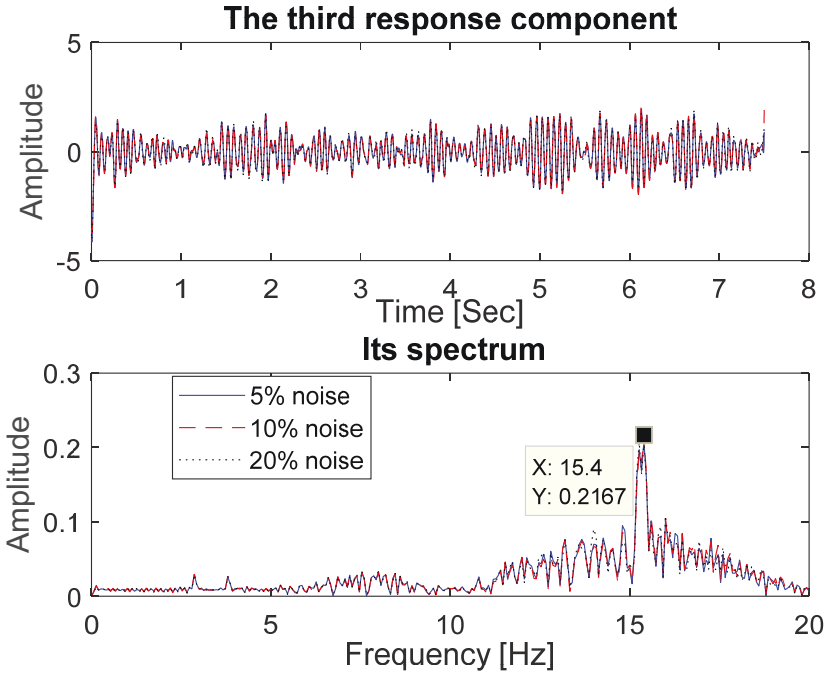

(c) The third response component

Figure 4.10 Response components and their spectra with different noise levels

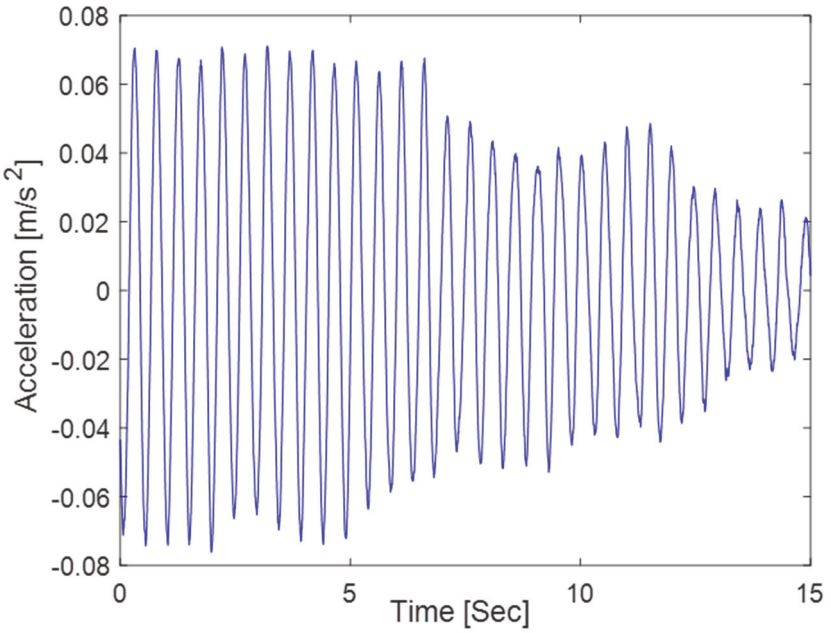

(a) Dynamic response of the vehicle

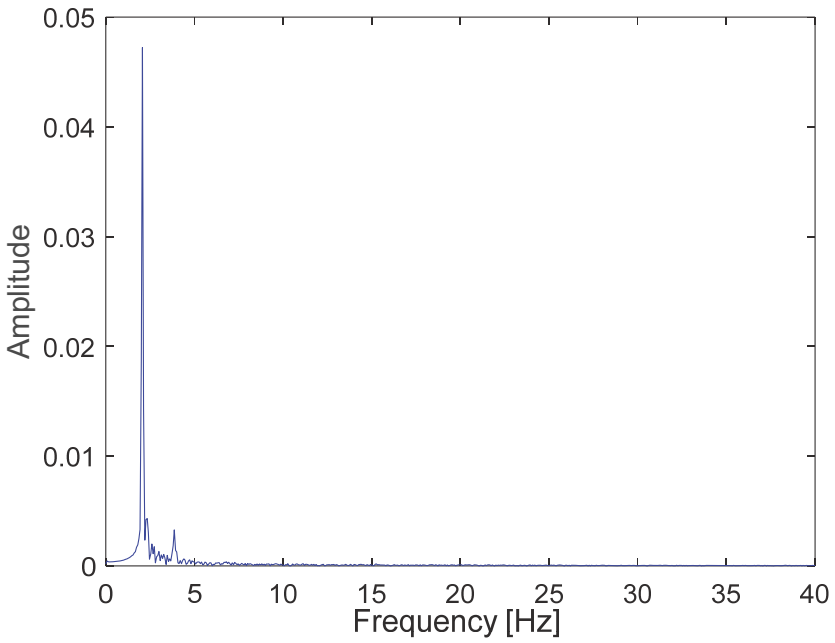

(b) Spectrum of response

Figure 4.11 Vehicular response and spectrum

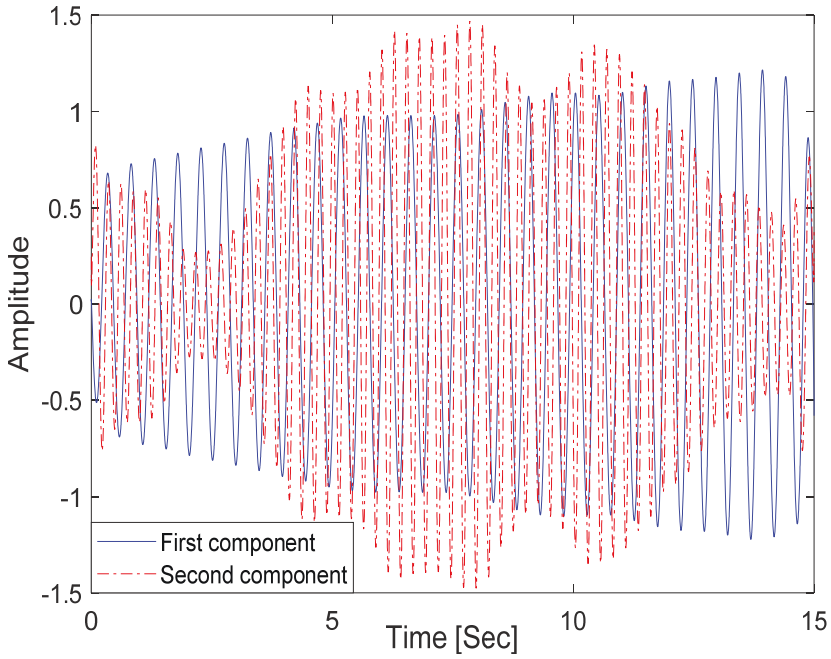

(a) The first two response components

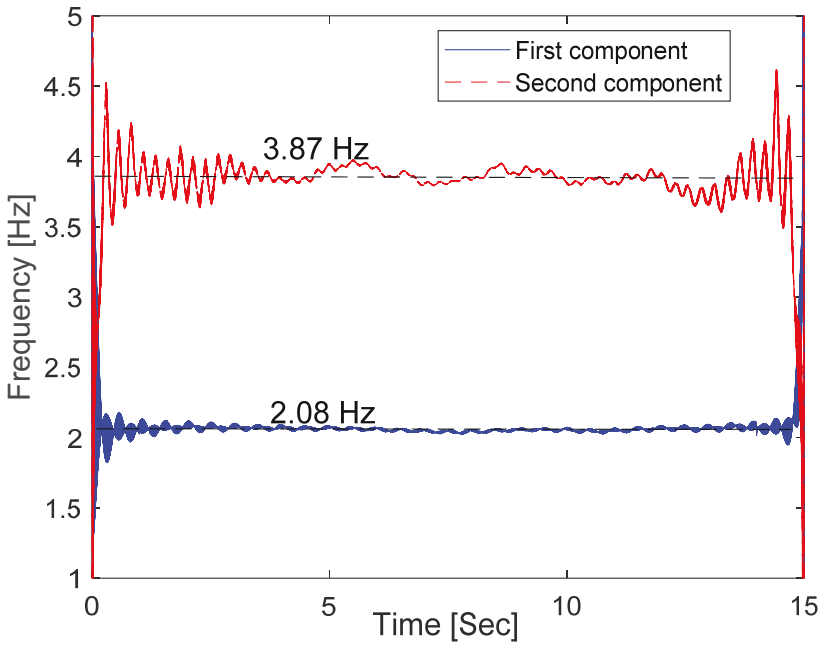

(b) The instantaneous frequencies

Figure 4.12 Vehicular response components and instantaneous frequencies

CHAPTER 5 Time-varying characteristics of a vehicle-bridge interaction system

5.1 Overview

The extraction of bridge modal frequencies from bridge or vehicle responses are mostly conducted based on the assumption that the frequencies of the vehicle and bridge are constant and/or the responses are stationary during the interaction process. However, the vehicle and bridge frequencies are time-varying during the VBI process. This is an important factor that must be investigated for the purpose of bridge SHM especially when using frequency-based indicators for damage assessment.

Time-frequency analysis is an effective tool to analyse nonstationary signals. The classical linear methods, such as short time Fourier transform and wavelet transform can expand a one-dimensional time-series signal into the two-dimensional TF plane. From the TF plane, the time-varying features can be observed and signal decomposition can be performed. However, TF representations generated via conventional methods are often blurry, and it is difficult to provide a precise time frequency description for a time-varying signal. The Wigner-Ville distribution gives optimal concentration for mono-component linear frequency modulation, but it produces undesirable cross-terms for non-linear frequency modulated or multi-component signals (Boashash and Aïssa-El-Bey, 2018). Advanced methods have been developed to improve the performance of conventional methods in the analysis of time varying signal, *e.g.*, Synchrosqueezing transform (SST) (Daubechies et al., 2011) and high-order SST (Wang et al., 2014). Recently, a TFA technique termed SET has be proposed (Yu et al., 2017). It improves the energy concentration of the TFRs by retaining only the time-frequency information that is most

related to the time-varying features of the signal. It outperforms the STFT in this aspect. The measured response from the vehicle has multiple components that are related to vehicle frequency, bridge frequency and the road surface roughness. The bridge response is a superposition of several vibration modes. Decomposing the multicomponent signal into the mono-component mode is an effective way to study the natural phenomena of their individual behaviours. Each mono-component mode in a well-separated multicomponent signal can be extracted from the TFR (Meignen et al., 2016) based on which the IF can be estimated (Thakur and Wu, 2011).

This chapter discusses the variability in the vehicle and bridge frequencies due to VBI with the TF analysis using the SET. The effects of vehicle properties, moving speed, road surface roughness and measurement noise on the frequency evolution were studied numerically.

5.2 Time-varying characteristics of the VBI system

The equation of motion of the VBI system can be expressed in a general form as

$$\boldsymbol{M}\ddot{\boldsymbol{Y}}(t) + \boldsymbol{C}\dot{\boldsymbol{Y}}(t) + \boldsymbol{K}\boldsymbol{Y}(t) = \boldsymbol{F}(t) \tag{5.1}$$

where $\boldsymbol{M}$, $\boldsymbol{C}$ and $\boldsymbol{K}$ are the mass, damping and stiffness matrices of the system respectively. $\boldsymbol{Y}$ is the displacement response vector and $\boldsymbol{F}$ is the force vector. The stiffness matrix of the coupled interaction system is time-dependent according to the location of the interacting force and the frequencies of the two sub-systems are time-varying. Considering only the first bridge vibration mode, Yang et al. (2013a) derived the solutions of the vehicle and bridge instantaneous frequencies, *i.e.*, ω_v and ω_b as follows:

For $\omega_{v0} > \omega_{b0}$

$$\omega_v^2 = \frac{\omega_{v0}^2}{2} + \frac{\omega_{b0}^2}{2} + \frac{m_v\omega_{v0}^2}{\rho L}\sin^2\left(\frac{\pi x_c}{L}\right) + \sqrt{\left(\frac{\omega_{v0}^2}{2} + \frac{\omega_{b0}^2}{2} + \frac{m_v\omega_{v0}^2}{\rho L}\sin^2\left(\frac{\pi x_c}{L}\right)\right)^2 - \omega_{v0}^2\omega_{b0}^2} \quad (5.2a)$$

$$\omega_b^2 = \frac{\omega_{v0}^2}{2} + \frac{\omega_{b0}^2}{2} + \frac{m_v\omega_{v0}^2}{\rho L}\sin^2\left(\frac{\pi x_c}{L}\right) - \sqrt{\left(\frac{\omega_{v0}^2}{2} + \frac{\omega_{b0}^2}{2} + \frac{m_v\omega_{v0}^2}{\rho L}\sin^2\left(\frac{\pi x_c}{L}\right)\right)^2 - \omega_{v0}^2\omega_{b0}^2} \quad (5.2b)$$

For $\omega_{v0} < \omega_{b0}$

$$\omega_v^2 = \frac{\omega_{v0}^2}{2} + \frac{\omega_{b0}^2}{2} + \frac{m_v\omega_{v0}^2}{\rho L}\sin^2\left(\frac{\pi x_c}{L}\right) - \sqrt{\left(\frac{\omega_{v0}^2}{2} + \frac{\omega_{b0}^2}{2} + \frac{m_v\omega_{v0}^2}{\rho L}\sin^2\left(\frac{\pi x_c}{L}\right)\right)^2 - \omega_{v0}^2\omega_{b0}^2} \quad (5.2c)$$

$$\omega_b^2 = \frac{\omega_{v0}^2}{2} + \frac{\omega_{b0}^2}{2} + \frac{m_v\omega_{v0}^2}{\rho L}\sin^2\left(\frac{\pi x_c}{L}\right) + \sqrt{\left(\frac{\omega_{v0}^2}{2} + \frac{\omega_{b0}^2}{2} + \frac{m_v\omega_{v0}^2}{\rho L}\sin^2\left(\frac{\pi x_c}{L}\right)\right)^2 - \omega_{v0}^2\omega_{b0}^2} \quad (5.2d)$$

where ω_{v0} and ω_{b0} are the original vehicle and bridge natural frequency, respectively, and x_c is the location of the vehicle on the bridge. Yang et al. (2013a) has reported that the largest deviation of the vehicle and bridge frequencies occur when the vehicle is close to mid-span of the bridge deck.

5.3 Extraction of the time-varying characteristics of the VBI system with SET

5.3.1 The SET theory

The STFT of a signal $s(t)$ with respect to the real and even window h is defined as

$$X_w(t,\omega) = \int_{-\infty}^{\infty} s(\tau)h(\tau - t)e^{-i\omega\tau}\, d\tau \quad (5.3)$$

where $h(\tau - t)$ denotes the moved window and $s(\tau)$ is the measured signal. The STFT expands a 1-D time-series signal into the 2-D TF plane so that the time-frequency information can be observed. For a purely harmonic signal $s_h(t) = Ae^{i\omega_0 t}$ with frequency ω_0 and invariant amplitude A, the STFT can be expressed as

$$X_h(t, \omega) = A * \hat{h}(\omega - \omega_0) * e^{i\omega_0 t} \tag{5.4}$$

where $\hat{h}(\omega - \omega_0)$ is the FT of the window function. In the time and frequency domain, the window function has a bandwidth, resulting in an energy-blurred spectrogram. Hence, it is difficult to characterize the time-varying feature of a signal precisely. In this study, the IF trajectory is adopted to improve the resolution of the time-frequency representation in the framework of SST. To obtain the IF of the STFT, the derivative of $X_h(t, \omega)$ with respect to time is calculated as

$$\partial_t X_h(t, \omega) = X_h(t, \omega) * i * \omega_0 \tag{5.5}$$

A 2-D IF $\omega_0(t, \omega)$ for any (t, ω) and $X_h(t, \omega) \neq 0$, can be obtained by

$$\omega_0(t, \omega) = -i * \frac{\partial_t X_h(t,\omega)}{X_h(t,\omega)} \tag{5.6}$$

Yu et al. (2017) proposed to generate a novel TF representation using only the TF coefficient in the IF trajectory $\omega = \omega_0$ similar to SST as

$$Te(t, \omega) = X_h(t, \omega) * \delta(\omega - \omega_0(t, \omega)) \tag{5.7}$$

where

$$\delta\big(\omega - \omega_0(t, \omega)\big) = \begin{cases} 1, & \omega = \omega_0 \\ 0, & \omega \neq \omega_0 \end{cases} \tag{5.8}$$

This post-processing procedure extracts the TF coefficient of $X_h(t, \omega)$ only in the IF trajectory $\omega = \omega_0$, and the rest of the TF coefficients are removed. In this study, only the

largest TF coefficients to generate a novel TFR, such that the effect of noises on the TF result can be minimized.

5.3.2 Time-frequency representation of response of the VBI system

The response of the VBI system can be expressed as

$$s(t) = \sum_{k=1}^{n} s_k(t) = \sum_{k=1}^{n} A_k(t) * e^{i\varphi_k(t)} \tag{5.9}$$

where $\varphi_k(t)$ and its one-order derivative $\varphi'_k(t)$ are the instantaneous phase and the instantaneous frequency of the *kth* component. The STFT of $s(t)$ can be represented with the first-order approximation as (Meignen et al., 2016)

$$X_h(t,\omega) \approx \sum_{k=1}^{n} A_k(t) * \hat{h}(\omega - \varphi'_k(t)) e^{i\varphi_k(t)} \tag{5.10}$$

For a well-separated measured response, the IF of each mode can estimated by

$$\varphi'(t,\omega) = \sum_{k=1}^{n} \varphi'_k(t) = -i * \frac{\partial_t X_h(t,\omega)}{X_h(t,\omega)} \tag{5.11}$$

The SET expression can then be written as

$$Te(t,\omega) = X_h(t,\omega) * \delta(\omega - \varphi'(t,\omega)) \tag{5.12}$$

and the signal can be reconstructed approximately by

$$s(t) \approx \sum_{k=1}^{n} Te\big(t, \varphi'_k(t)\big)/\hat{h}(0) \tag{5.13}$$

Each mode can be decomposed with first-order approximation as

$$s_k(t) \approx e\big(t, \varphi'_k(t)\big)/\hat{h}(0) \tag{5.14}$$

5.3.3 Time-varying characteristics of the VBI system using ridge detection

A popular multi-ridge detection algorithm (Thakur et al., 2013) was employed to decompose the measured response and to estimate all IF trajectories at the same time. This technique aims at finding the best frequency curve (denoted as $\Omega_i(t)$) in the TFR X_h, which maximizes the energy with a smoothness constraint through a total variation penalization term expressed as

$$\widehat{\Omega} = \underset{\Omega}{\operatorname{argmax}} \int |X_h(t,\Omega)|^2 dt - \lambda \int \left|\frac{d\Omega}{dt}(t)\right|^2 dt \tag{5.15}$$

where λ controls the importance of the smoothness constraint. For multi-component extraction, this method can be iterated after setting X_h equals to null in the vicinity of the previously detected ridge (Fourer et al., 2017).

5.3.4 A simply supported beam subjected to white noise excitation

A simply supported beam subjected to a white noise excitation is shown in Figure 5.1. The beam properties were: $L = 30\ m, \rho = 6000\ kg/m$, $EI = 2.5e10\ Nm$, and damping was neglected. White noise excitation was applied at Node 9 vertically, and the vertical acceleration response at Node 4 was calculated with the Newmark-β method at the sampling rate of 100 Hz. Five percent white noise was added to the calculated acceleration responses to simulate the measured data. Figure 5.2 shows the applied force, and Figure 5.3 shows the vertical acceleration response at Node 4 and the response spectrum. Two dominant peaks are found at 3.55 and 13.40 Hz corresponding to the first two modal frequencies of the beam. The measured data are analysed using STFT and SET with a window length of 2048, and the TFR of the signal is presented in Figure 5.4 (a) and (b). Both figures show two straight lines representing the first two beam modal

frequencies in the time-frequency domain. The solid line in Figure 5.4 (a) indicates a high energy component. The solid line is notably horizontal, indicating the invariability of the frequency under given excitation condition. The energy of TFR by SET as shown in Figure 5.4 (b) is noted more concentrated than that by direct STFT in Figure 5.4 (a). Therefore, the SET will be used for the time-frequency analysis in the rest of the chapter. The IF trajectories corresponding to the first two bridge vibration modes are given in Figure 5.5(a) and the TFR of the mono-component modes are presented in Figure 5.5(b). Both figures exhibit the stationary features of the responses.

5.4 Numerical study

5.4.1 Time-frequency analysis of vehicle and bridge responses

The VBI system as shown in Figure 3.1 is studied. The bridge properties were the same as those in Section 5.3.4 but with the inclusion of bridge damping. Rayleigh damping were assumed with $\mathbf{C}_b=\alpha_1\mathbf{M}_b+\alpha_2\mathbf{K}_b$ and $\alpha_1=0.243$, $\alpha_1=0.0001$, where $\mathbf{M}_b$, $\mathbf{C}_b$ and $\mathbf{K}_b$ are the mass, damping and stiffness matrices of the bridge respectively. Four vehicle models with parameters listed in Table 5.1 were adopted. The vehicle was assumed moving on a 50m approach road before entering the bridge. The response was obtained by solving the coupled VBI equation using Newmark-β method with 500Hz sampling rate. Five percent white noise was added to the calculated acceleration to simulate the measurement with the signal-to-noise ratio (SNR) equal to 26.

The case with vehicle 1 has a negligible mass ratio between the vehicle and bridge at 0.003. The frequency of the vehicle model is 3.20 Hz. Figure 5.6(a) shows the bridge response at Node 4, and the response spectrum when the vehicle moves at a speed of 2m/s. Figure 5.6 (b) shows the vehicle response and the spectrum assuming the bridge surface

is smooth. The identified first bridge modal frequency from the bridge and vehicle responses is 3.6 Hz. The responses were inputted to the SET to get the time-frequency information with window length of 2048. The TFRs for the bridge and vehicle responses are presented in Figure 5.7 (a) and (b), respectively. The time frequency information related to first and second bridge modes can be observed in Figure 5.7(a). However, only the time-frequency information related to first mode is noted from vehicle response in Figure 5.7(b). Figure 5.7(c) presents the IF trajectories of different modes. No clear variation in the frequency was observed due to the very small vehicle-bridge mass ratio.

In the second case with vehicle 2, both mass and stiffness were 14 times the values of Case 1 with the vehicle-bridge mass ratio equals 3.9%. The natural frequencies of the vehicles 1 and 2 are the same. Similar TF analysis was conducted and the IF trajectories extracted from the bridge and vehicle responses from the TFRs are shown in Figure 5.8(a). It contains the time-frequency information related to the first bridge vibration mode and vehicle vibration mode. Of note, the frequencies of the vehicle and bridge varied in a roughly half-sinewave form with respect to the location of the moving vehicle. The frequency related to the first bridge mode increased as the vehicle moved toward the mid-span of the bridge and decreases when moving away from mid-span. The vehicle frequency showed an opposite variation trend. For the second bridge vibration mode, no obvious frequency variation was observed. Therefore, the first bridge vibration mode and vehicle mode were studied further. Theoretical instantaneous frequencies were calculated by solving the eigenvalue problem of the equation of motion of the system. Figure 5.8(b) compares the results identified from the present analysis procedure and theoretical analysis with good agreement.

Vehicle 3 has the same mass as that of vehicle 2 with stiffness the same as that of vehicle 1. Vehicle 4 has an intermediate mass value. The time-frequency analysis on the bridge

and vehicle responses yielded IF results as shown in Figure 5.9. The case with vehicle 3 did not feature any obvious frequency variation in both the TFRs. In contrast, the case with vehicle 4 showed clear frequency variation in the vehicle and bridge frequencies. A comparison of the above results shows that the time-varying characteristics of a VBI system are affected not only by the vehicle mass.

The frequency change ratio $\frac{|\omega-\omega_0|}{\omega_0}$ can be calculated from Eq. 5.2. The maxima of bridge frequency change ratio and vehicle frequency change ratio in relation to vehicle mass and vehicle stiffness are plotted in Figure 5.10 (a) and (b). Only Case 2 and Case 4 exhibited prominent change, *i.e.*, 9.2 and 8.5 % for Case 2 and 3.2 and 3.3% for Case 4, in the bridge and vehicle frequencies, respectively. In comparison, the changes in Cases 1 and 3 were very small.

5.4.2 Effect of measurement noise

The effects of 10 and 15% noise levels in the measurement were also studied for the IF extraction with vehicle 2. The IF trajectories considering different measurement noise are given in Figure 5.11. Results show that the TF analysis results were very robust to the measurement noise.

5.4.3 Effect of different measurement locations on the bridge

Vertical accelerations collected at 3/20, 7/20 and 11/20 length from left support were analysed to study the effect of different measurement locations on the frequencies variation. Vehicle 2 was used and 5% measurement noise was included. The extracted IF

trajectories of responses at different locations are presented in Figure 5.12. The IF trajectories were the same from responses at the different measurement points studied.

5.4.4 Effect of vehicle speed

Vehicle 2, which moved at 4 m/s, was used for the study while other parameters are the same as those for the abovementioned cases (Sections 5.4.1-5.4.3). The time-frequency analysis results are given in Figure 5.13. Similar trend of frequency variation of the system can be observed. However, a higher moving speed means a shorter duration of vehicle-interaction with less measurement data collected which may reduce the resolution of the TFR. Therefore a lower moving speed of vehicle is recommended to obtain more accurate TFR of the signal from vehicle response.

5.4.5 Effect of the bridge surface roughness

A smooth bridge deck was adopted while Class A (ISO, 2016) bridge surface roughness was used in this study. Vehicle speed was 2m/s and 5% measurement noise was included. The bridge and vehicle responses in time-frequency domain obtained from SET are shown in Figure 5.14(a) and (b), respectively. The vehicle related frequency was more dominant with the effect of road roughness. The bridge related frequency from vehicle response became blurry in the time-frequency domain. By using the mode extraction technique introduced earlier (Section 5.3.3), the extracted components from vehicle responses are shown in Figure 5.15(a) and (b). Comparing with the results in Figure 5.14(b) and Figure 5.15 (b), it can be seen that the TFR related to the bridge vibration mode becomes clearer as shown in the Figure 5.15 (b).

5.5 Summary

The time-varying characteristics of the VBI system were studied numerically. SET was adopted to analyse the responses with improved time-frequency resolution. Component extraction was conducted to obtain the IF trajectories related to components of the vehicle and bridge. The effects of vehicle parameters, moving speed, road surface roughness and measurement noise on the instantaneous frequency was investigated. The instantaneous frequency variation is sensitive to the vehicle/bridge mass ratio. When the vehicle mass is negligible compared to the bridge mass, the frequency of the system is non-varying. Both the vehicle and bridge frequency variations can be observed in the instantaneous frequencies of the responses when the vehicle/bridge mass ratio is large and the vehicle/bridge frequency ratio is not too small. The time-varying characteristics of the bridge under the passage of vehicles have a big potential for bridge structural health monitoring.

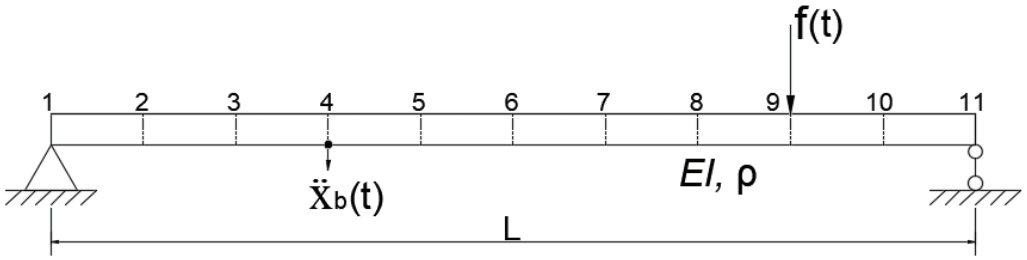

Figure 5.1 A simply supported beam under random force

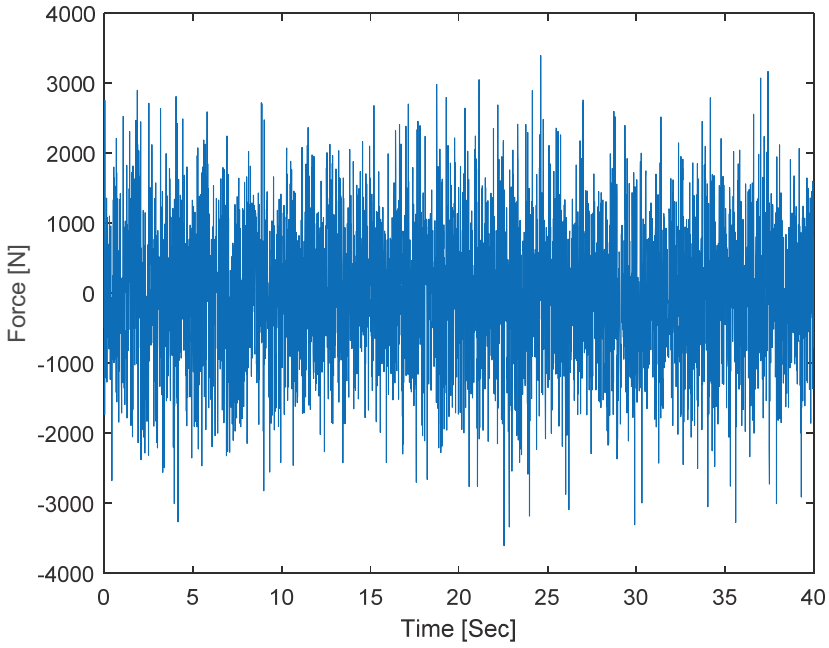

Figure 5.2 Applied force to the beam model

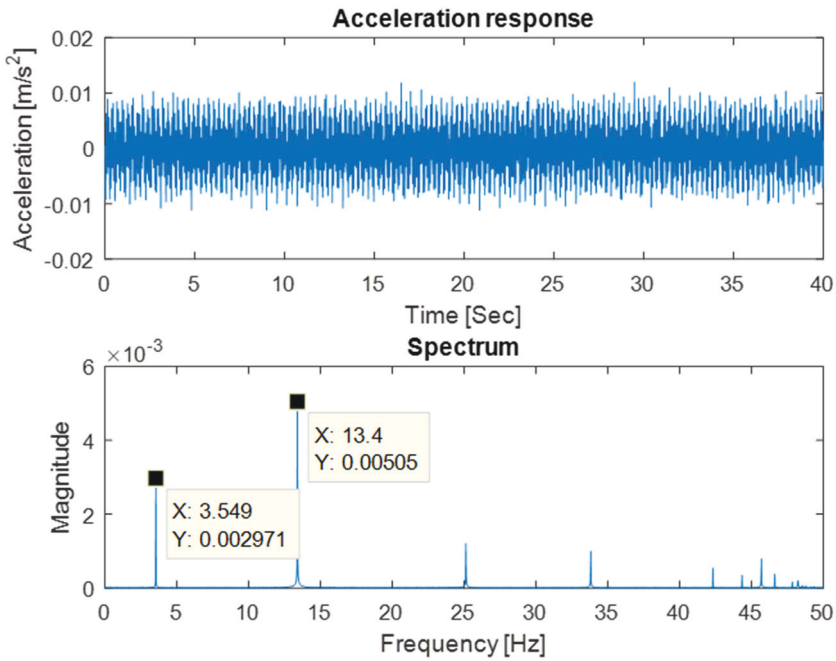

Figure 5.3 Bridge response and spectrum

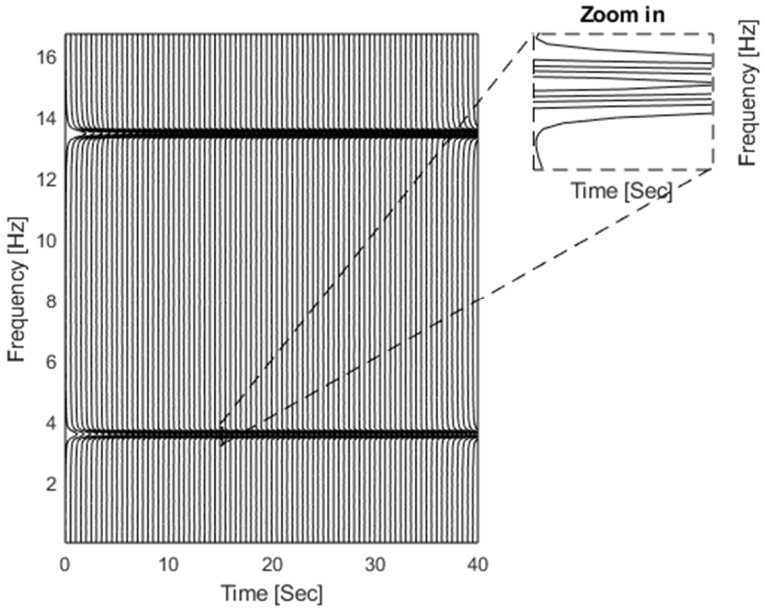

(a) TFR by STFT

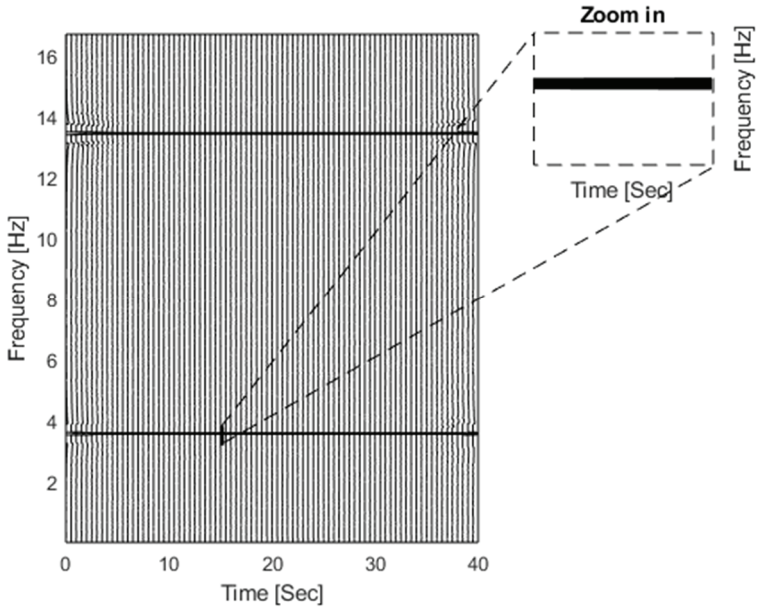

(b) TFR by SET

Figure 5.4 Time frequency representation of the bridge response

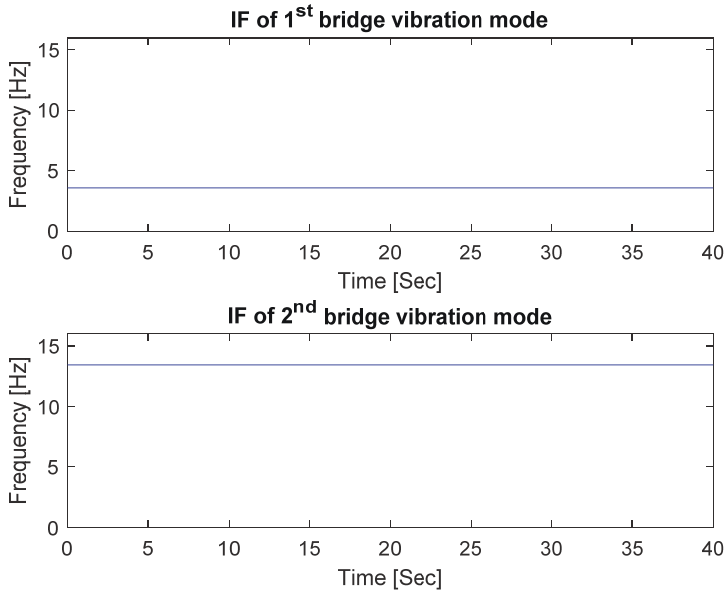

(a) IF of response components

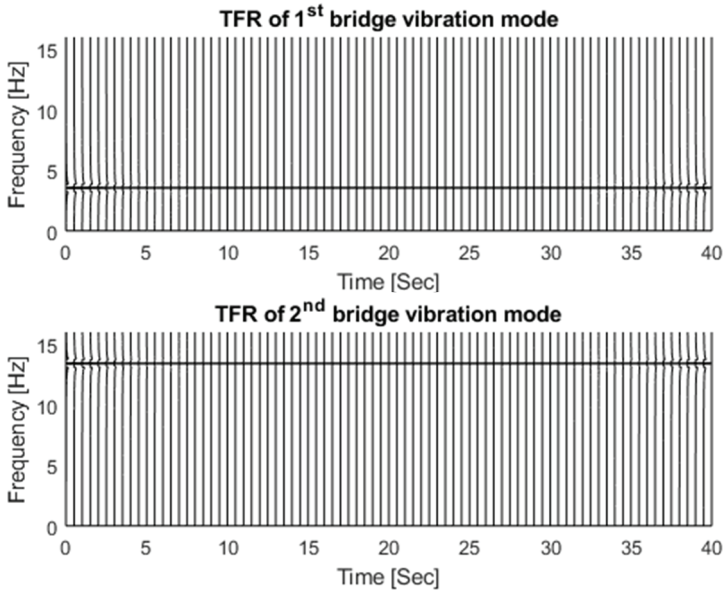

(b) TFR of response components

Figure 5.5 IF and TFR of bridge response components

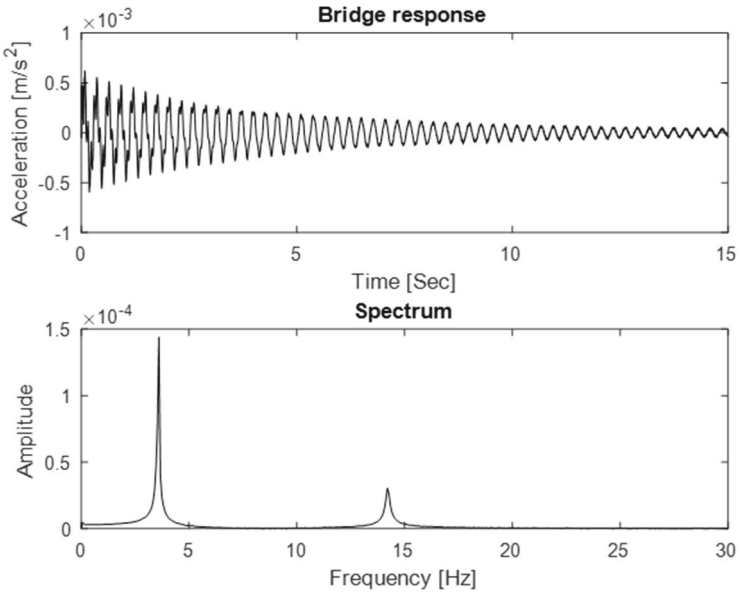

(a) Bridge response and spectrum

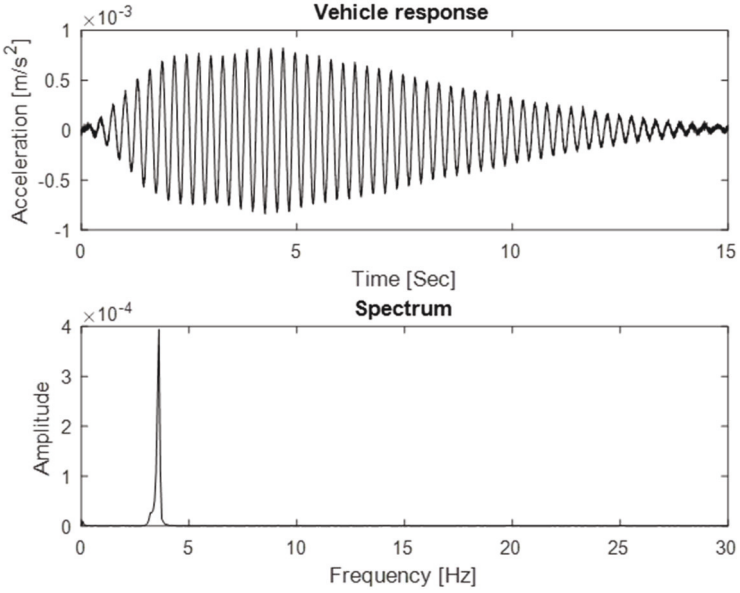

(b) Vehicle respose and spectrum

Figure 5.6 Vehicle and bridge response in the VBI system and response spectra

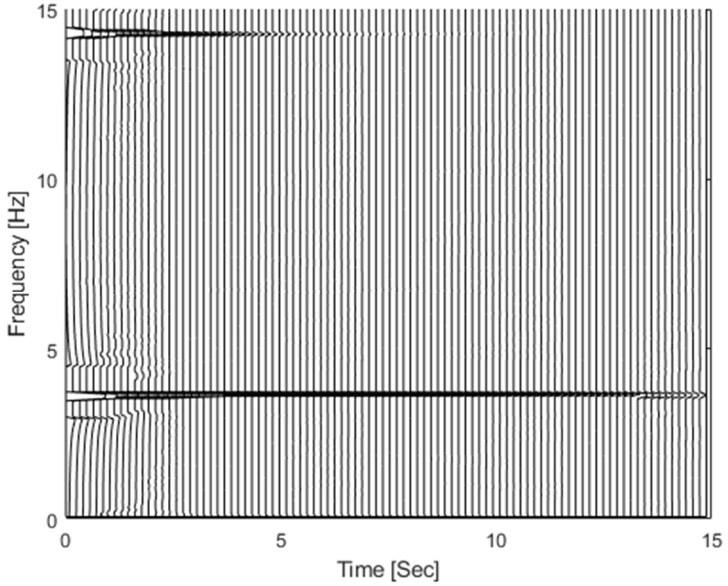

(a) TFR of bridge response

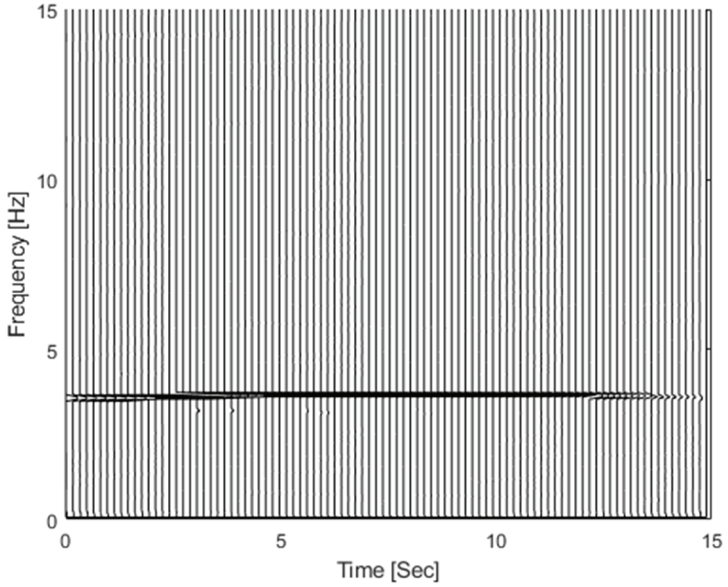

(b) TFR of vehicle response

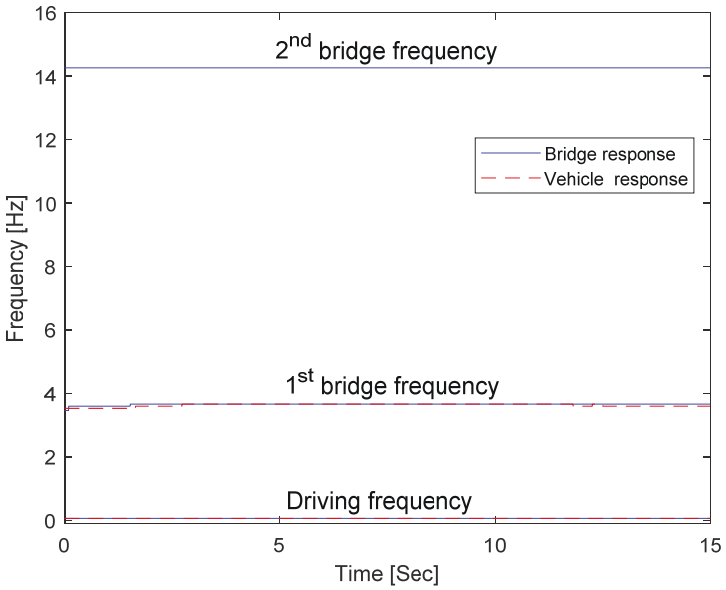

(c) IFs of the response components

Figure 5.7 TFR of the bridge and vehicle responses by SET

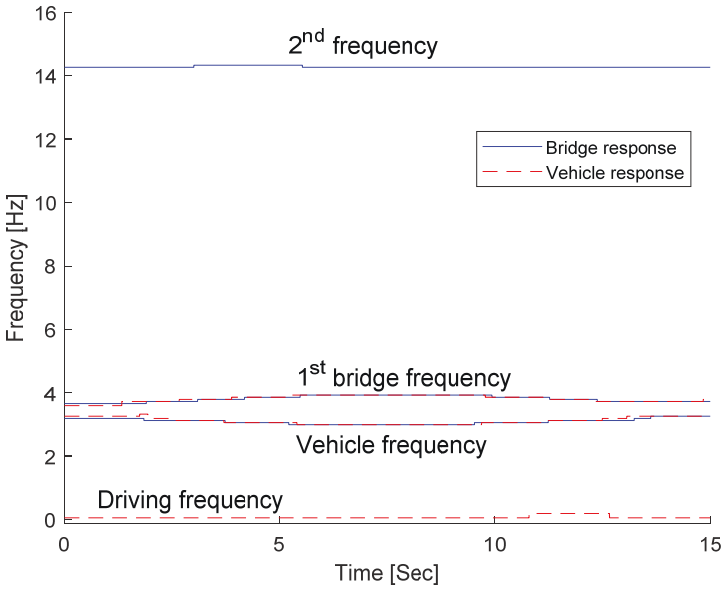

(a) TFR of bridge and vehicle response

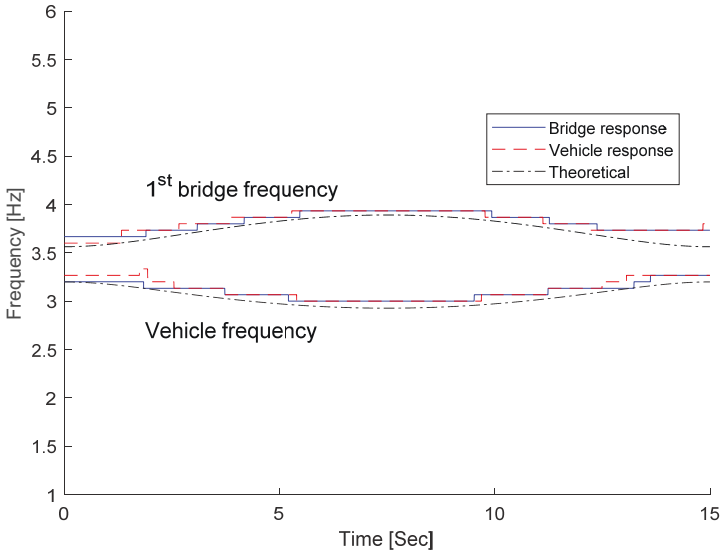

(b) Zoom in and compared with the theoretical values

Figure 5.8 TFR of the bridge and vehicle responses by SET for Case 2

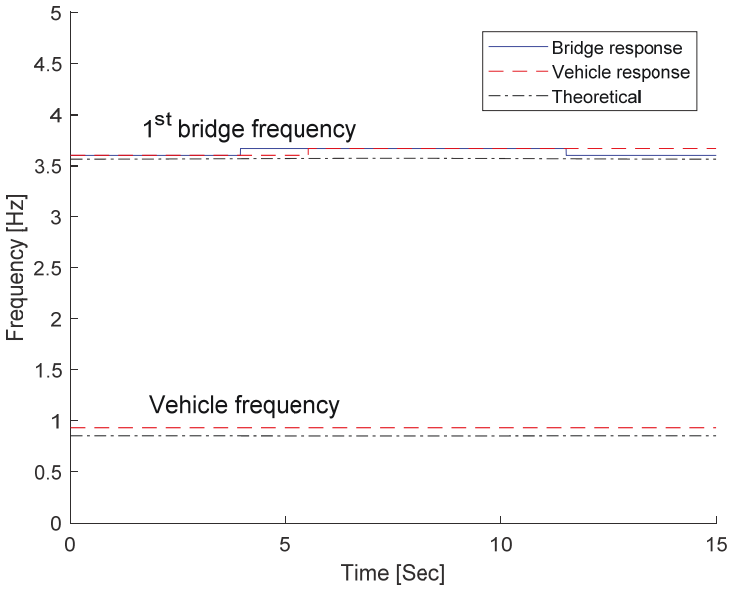

(a) Case 3

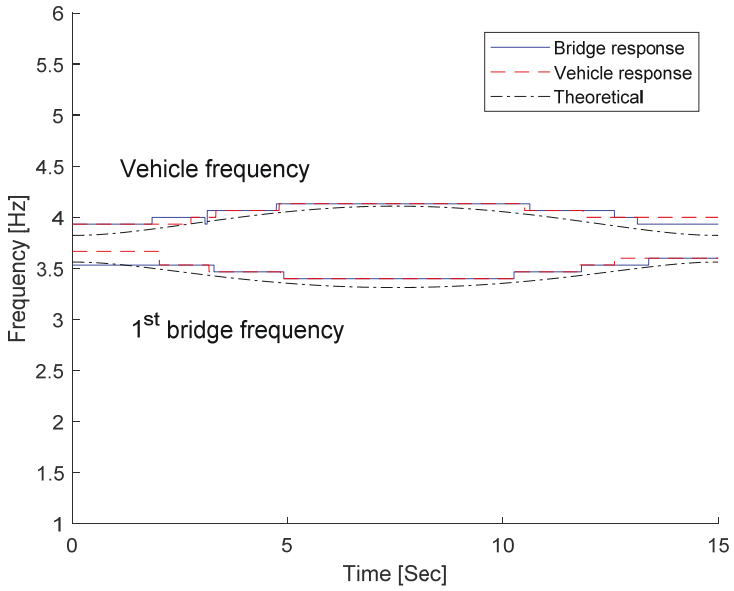

(b) Case 4

Figure 5.9 TFR of the bridge and vehicle responses by SET for Case 3 and Case 4

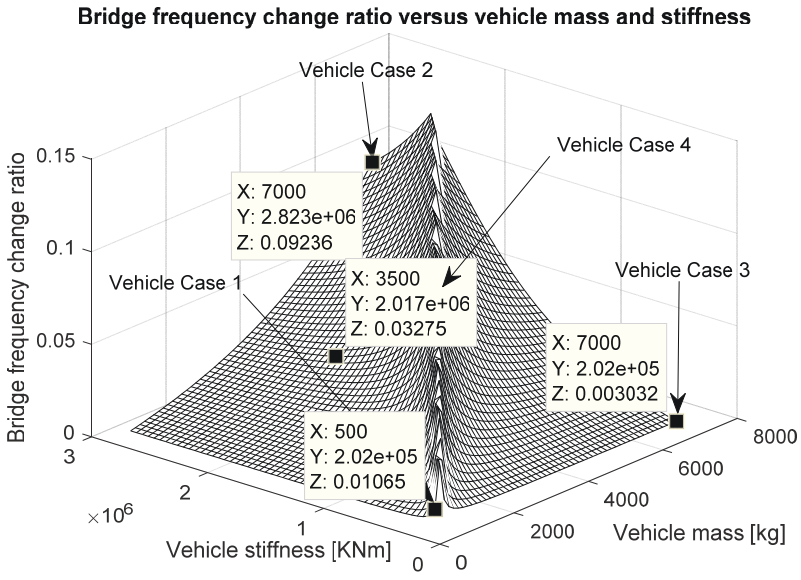

(a) Bridge frequency change ratio

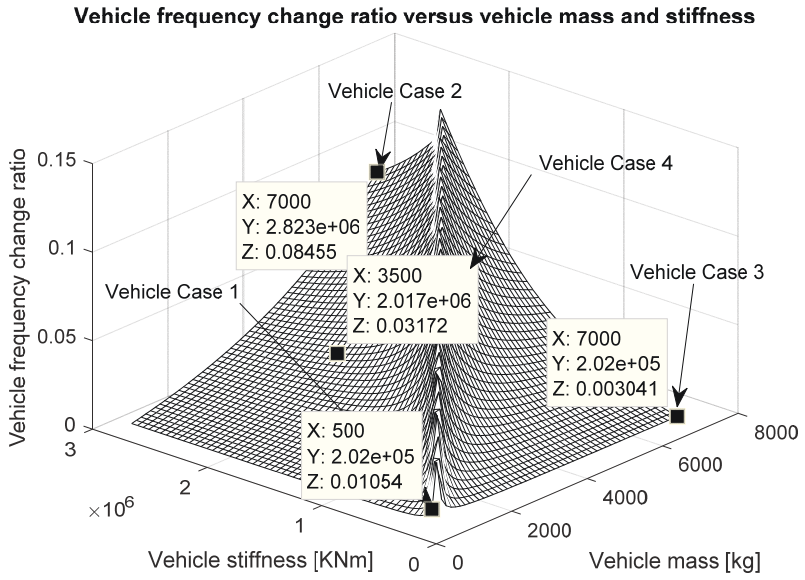

(b) Vehicle frequency change ratio

Figure 5.10 Maximum frequency change ratios in relation to vehicle properties

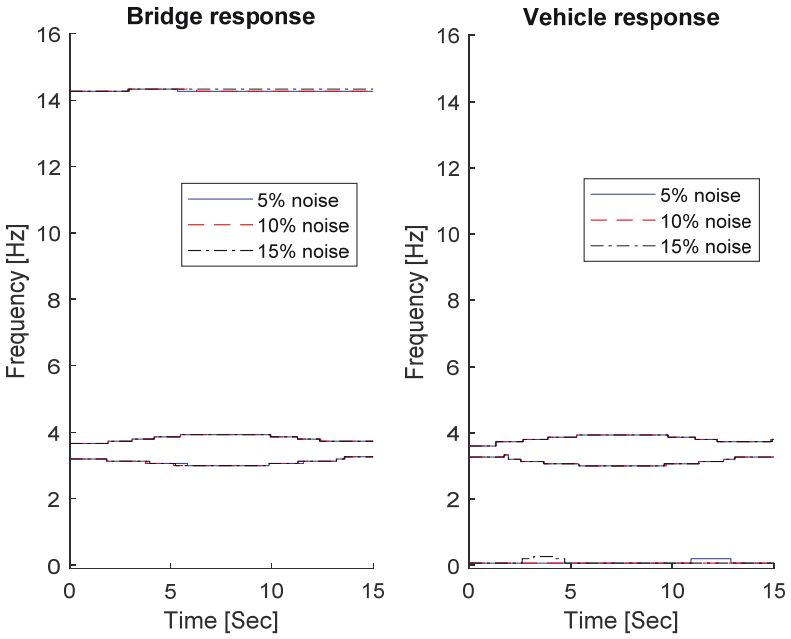

Figure 5.11 IF of modes related to bridge and vehicle frequencies from responses

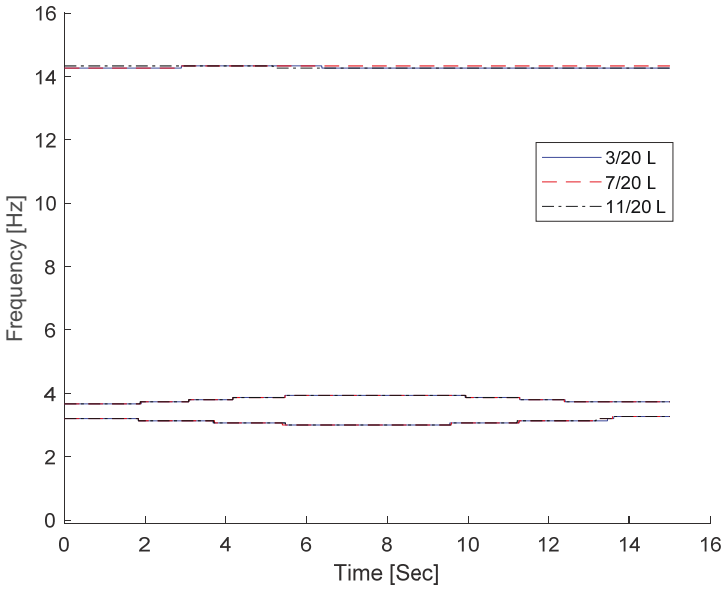

Figure 5.12 IF of vertical acceleration response measured at different points on bridge

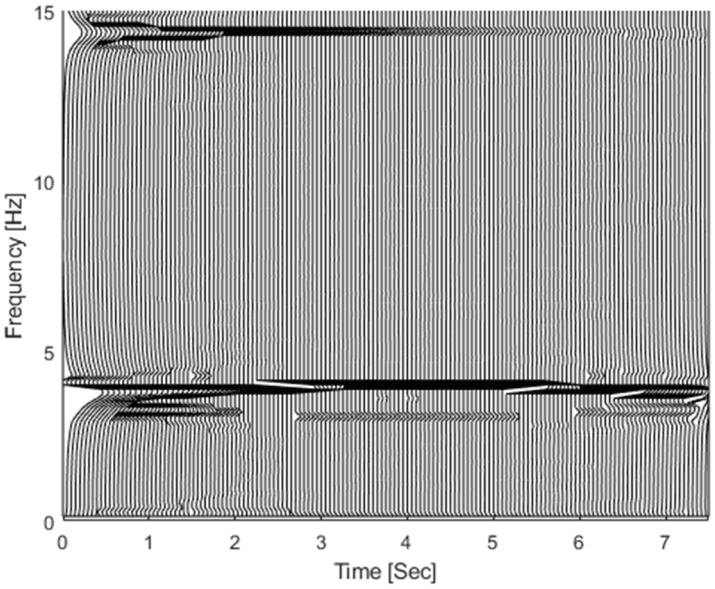

(a) TFR of bridge response

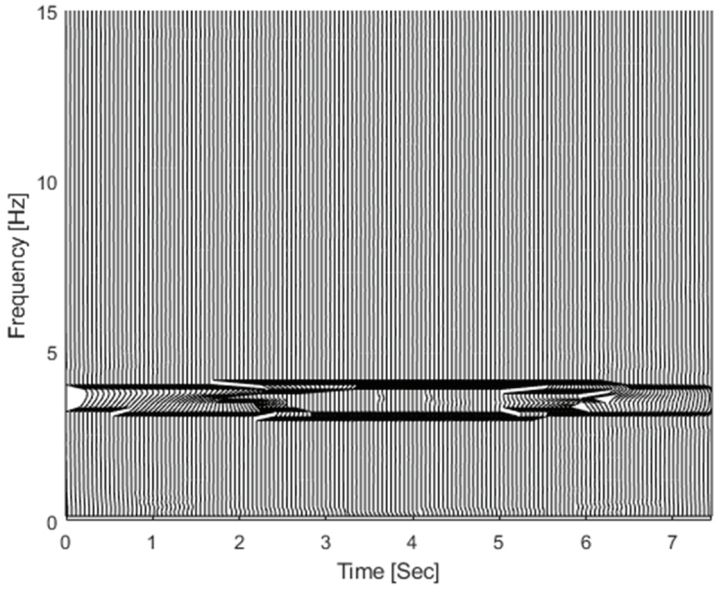

(b) TFR of vehicle response

Figure 5.13 TFR of the bridge and vehicle responses by SET for Case 2 when speed is 4m/s

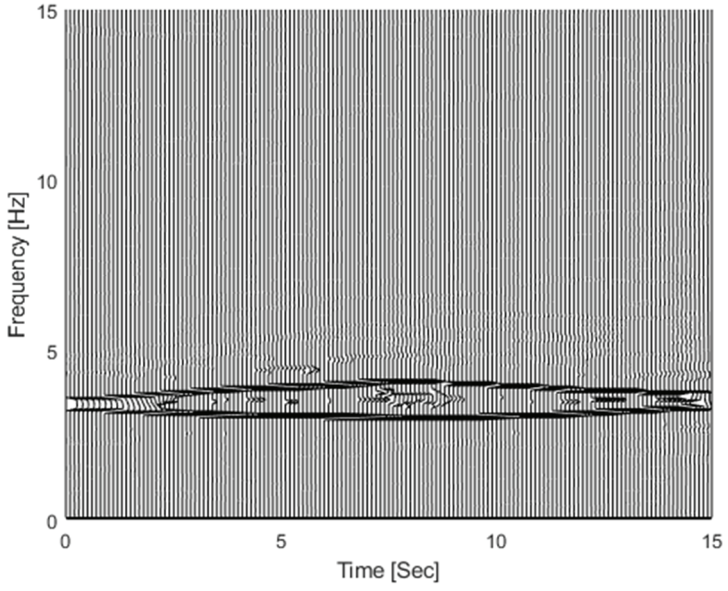

(a) TFR of bridge response

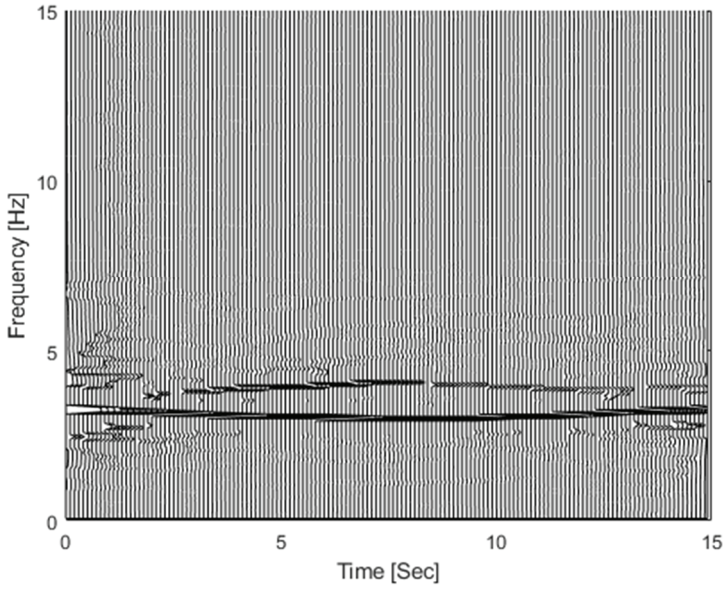

(b) TFR of vehicle response

Figure 5.14 Time frequency representation by SET considering Class A surface roughness

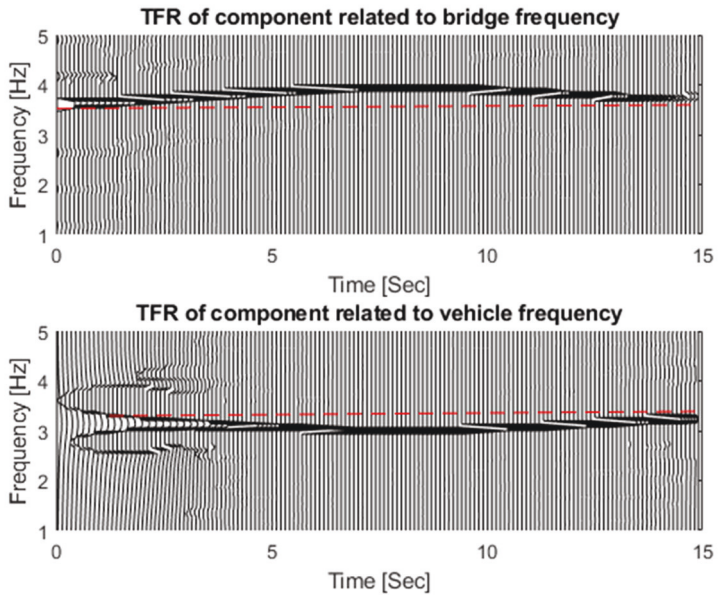

(a) TFR of components for smooth bridge surface

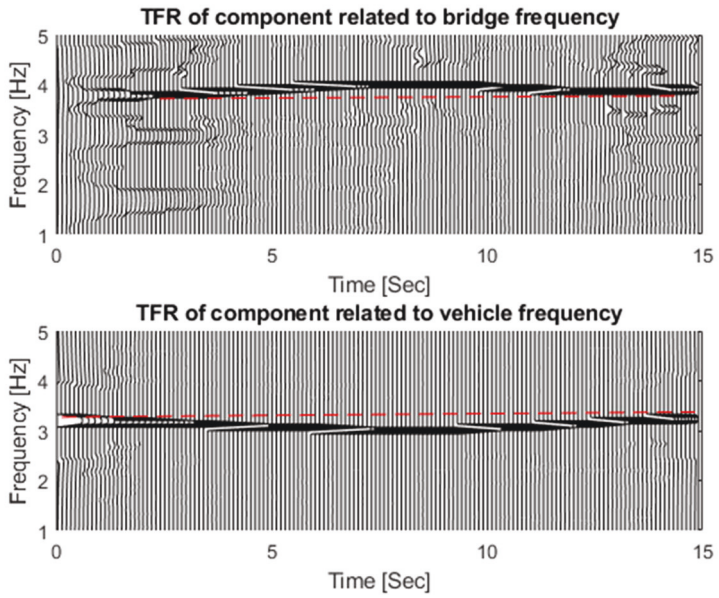

(b) TFR of components for Class A surface roughness

Figure 5.15 TFR of extracted modes related to bridge and vehicle frequencies from vehicle responses

Table 5.1 Properties of vehicle models

Case	$k_v\ (N/m)$	$m_v\ (kg)$	$c_v(\ N/m/s)$	$\omega_{v0}\ (Hz)$	Mass ratio
1	2.02e5	500	390	3.20	0.3%
2	2.82e6	7000	390	3.20	3.9%
3	2.02e5	7000	390	0.86	3.9%
4	2.02e6	3500	390	3.82	1.9%

CHAPTER 6 Indirect modal parameter identification: laboratory study

6.1 Overview

In the previous chapters, two indirect bridge modal identification methods were developed, *i.e.*, STSSI in Chapter 3 and SSA-BSS in Chapter 4. Numerical studies demonstrated the feasibility and effectiveness of the proposed methods. Chapter 5 presents the time-dependent characteristic of the VBI system numerically. In this chapter, experimental studies were conducted to validate the proposed methods. A vehicle-bridge interaction test bed was built in the laboratory. Acceleration responses were measured with a wireless sensory system for the verification.

6.2 Experimental setup

6.2.1 The bridge model

The bridge model consisted of three rectangular steel beams as shown in Figure 6.1. Those beams are 100 mm wide and 15mm deep. The main beam in the middle was continuously simply supported over two spans with 3 m each. Half-round and round steel bars were used to simulate the pinned and roller supports of the beam, respectively. A leading beam and a trailing beam was placed in front of and at the rear of the main beam to allow for acceleration and deceleration of the vehicle. The length of these beams was 3m. Figure 6.2(a) shows a photo of the bridge beam model and Figure 6.2(b) gives the dimensions of the main beam. The experimental study focused on the interaction between the vehicle and the main beam. A U-shaped aluminium section was glued along the centre of the upper surface of the beam as a direction guide for the vehicles.

6.2.2 The vehicle model

Vehicle models with different configurations including one and two-axle were manufactured for the study. One-axle vehicle was manufactured to simulate the single degree of freedom vehicle model used in the analytical program in Chapters 3 and 4. The two-axle vehicle model had four wheels. The one-axle vehicle was towed by the two-axle vehicle as they passed over the bridge. The photos of the vehicle models are given in Figure 6.3. The mass of the one- and two-axle vehicles was 2 and 4 kg, respectively. The model vehicles were pulled along the guide with an electric motor.

6.2.3 Measurement system

6.2.3.1 Wired measurement system

The PCB352C34 accelerometers from PCB Piezotronics were installed on the main beam to measure the vertical acceleration. Seven sensors are uniformly installed on each span of the main beam, resulting in a total of 14 sensors. Figure 6.4(a) shows the instrumentation on the main beam with wired accelerometers. The accelerometer were secured on a mounting base, which was attached to a location of the test beam. Figure 6.4(b) shows the installed wired accelerometer on the beam. Laser sensors were installed along the beam to record the time instants when the vehicles arrive at and exit from the main beam. These time instants were used to calculate the moving speed of the vehicle. National Instruments data acquisition system was used. The wired system was mainly used for the bridge modal testing.

6.2.3.2 Wireless measurement system

In vehicle-bridge interaction tests, a wireless sensory system was setup with devices from Beanair Gmbh. BeanDevice AX-3D wireless accelerometer was selected to measure the dynamic responses. Wireless sensors were installed on top of vehicle axles. Figure 6.4(c) shows the installation of the wireless sensor on the vehicle model. A wireless sensor was also attached to the beam as a reference sensor. BeanGateway was used to collect the data from the wireless sensors. The proposed methods are verified using the data from the wireless monitoring system.

6.3 Experimental modal testing on the bridge and vehicle

Modal testing was carried out on the vehicle and bridge models with impulse hammer as the excitation source. For the bridge modal testing, the impulse excitation and the acceleration responses were measured using the wired measurement system. The toolbox DIAMOND (Doebling et al. 1997) was used to measure the frequency response functions and Rational Fraction Polynomial method in the toolbox is used to estimate the modal parameters. The first two bridge natural frequencies were obtained as 5.68, and 8.48 Hz, respectively. Assuming that the mode shape values at the supports of the main beam were zero, the identified frequencies and their corresponding mode shapes are shown in Figure 6.5. Spectrum analysis on the vehicle responses was conducted to extract the modal frequency of the single-axle vehicle, which was 29.37 Hz. The modal frequencies for the two-axle vehicle were 32.17 and 36.01Hz with regards to the vehicle bouncing and pitching.

6.4 Experimental verification

6.4.1 Indirect modal parameter identification with STSSI of Chapter 3

6.4.1.1 Mode shape identification

The single-axle vehicle was towed by the two-axle vehicle model and pulled by the pulling system as shown in Figure 6.6. The leading two-axle vehicle was used to simulate the unknown traffic for the study. A wireless sensor was installed on the single-axle vehicle as moving sensor with the other one installed on the beam (at 1.1 m to the right support) as the reference sensor. Three different cases with varying masses of the two-axle vehicle were considered. For Case 1: no extra weight is added. For Cases 2 and 3, 2.5 and 5 kg masses were loaded on the two-axle vehicle, respectively. Notations m1, m2 and m3 were used to denote these three cases. The vehicles were pulled with three different speeds at approximately 0.10, 0.14 and 0.21 m/s, respectively. The vehicles were denoted as v1, v2 and v3, respectively, in the following discussions. Five sets of data from different test configurations were analysed including the vehicle with three different masses moving with speed v2 and weight m2 moving with two other speeds. Measurements from the moving and stationary sensors were analysed with the proposed method to identify the first mode shape of the beam in each of the five tests. Each signal was divided into eight segments. The identified operational mode shape values were compared with those from modal tests using MAC values.

Figure 6.7 presents the identified results for the three cases when the moving speed was v2. When no extra weight is added on the vehicle, the MAC value was about 0.98, which was quite accurate relative to the experimental mode shape. When the weight of the two-axle vehicle increased, the MAC value of the identified results decreased. This may be due to stronger non-stationary interaction between the vehicle and the bridge models

when the vehicle is heavy. Eq. (3.11) also shows that the effect of the vehicle weight on the total excitation term cannot be ignored when the vehicle mass is large compared to that of the bridge. Figure 6.8 shows the results for the weight m2 with three different moving speeds. The MAC value decreased from about 0.98 to 0.94 when the speed increased from 0.10 to 0.21 m/s. These experimental results provide compelling evidence that a relative low vehicle speed tends to provide more accurate identified results.

6.4.1.2 Improving the accuracy of the experimental identification results by averaging

For the mass m2 with moving speed v2, two more tests were conducted by locating the reference sensor at 1.8 and 2.6m to the right support. The MAC value of the identified result was 0.96 and 0.95 when the reference sensor is at 1.8 and 2.6 m, respectively, to the right support. The location of the latter reference sensor very close to the middle support, and the MAC value was small. The identified results are shown in Figure 6.9. However, when the three sets of identified mode shape values were averaged as shown in Figure 6.9, the MAC value improved to 0.97. This indicates that the accuracy of the identified results can be improved by averaging results obtained from different locations of the reference sensor.

6.4.2 Drive-by modal identification with SSA-BSS of Chapter 4

6.4.2.1 Frequency identification using the response of a single-axle vehicle

The response of the single-axle vehicle was used to identify the bridge frequencies with the proposed method. The window length for SSA was 500 and the time series data with the top 20% of eigenvalues were used as the input of BSS.

Figure 6.10 shows the vehicle response and its spectrum when the speed was 0.10m/s at load case m1. There was a dominant frequency observed around 30 Hz, which corresponded to the vehicle modal frequency. The decomposed components using proposed method are presented in Figure 6.11. The first component has the frequency 5.21Hz, which was close to the first modal frequency of the deck. Similarly, the frequency 8.32Hz in Figure 6.11(b) was related to the second bridge mode. The vehicle modal frequency was identified in the third component as 29.35 Hz.

Figure 6.12(a) shows the spectra of the decomposed response components with different load cases when the speed was 0.14m/s. Figure 6.12(b) shows the spectra of the decomposed components under different speeds for load m2. Table 6.1 shows the identified results for all the tests considering different speeds and weights. The vehicle-bridge weight ratios were 0.06, 0.09 and 0.13, respectively, for the three load cases studied. Results from Figure 6.12(a) and Table 6.1 show that the weight of the two-axle vehicle did not have a large effect on the identified results from the response of the single-axle vehicle. It may be concluded that the proposed method is not sensitive to operating traffic excitation. However, Figure 6.12(b) and Table 6.1 show that the vehicle speed had a large effect on the identified results. This provides experimental evidence confirming similar observation in the numerical study (Chapter 4).

6.4.2.2 Frequency identification using the response of a two-axle vehicle

Two wireless accelerometers were installed on the two-axle vehicle. One sensor on top of the front axle while another was on top of the rear axle. The dynamic responses obtained are shown in Figure 6.13. The response difference from the two accelerometers was used in the identification. All parameters were the same as those for last study

(Section 6.4.1). Figure 6.14 (a) and (b) show the spectra of the first three components with different vehicle speeds and masses, respectively. The identified bridge and vehicle frequencies are summarized in Table 6.2. The vehicle frequency and the first two bridge modal frequencies can be separately identified. Figure 6.14(a) and Table 6.2 show that an increase of the vehicle mass has no obvious effect on the identified bridge frequencies. The identified bridge frequencies in Figure 6.14(b) show small variation with the vehicle speed. This is mainly due to the reduction of the frequency resolution in the spectrum when the vehicle speed increases.

6.4.2.3 Time frequency analysis of the bridge response components

The time frequency analysis on the bridge response components using Hilbert Transform was conducted when the two-axle vehicle moves on the deck with 9 kg mass at 0.21m/s. The first two response components and their instantaneous frequencies are shown in Figure 6.15. There was no obvious oscillation in the instantaneous frequency time history, and the mean values 5.56 and 8.64Hz corresponded to the first and second modal frequencies of the bridge.

6.4.3 Time-varying characteristics of VBI system

6.4.3.1 TFA on the responses from vehicle and bridge

In this study, only the vehicle model with two axles was pulled over the beam and a 4 kg mass block was added on top of the vehicle to the centre. Wireless sensors were installed on the vehicle model above the axles as shown in Figure 6.16.

Two sets of acceleration signals – one from the sensors above the vehicle front axle and other from the sensors on the midpoint of the first beam span – were measured when the vehicle was moving at a speed of 0.61 m/s over the main beam. The signal and the spectra are shown in Figure 6.17(a). Using the TFA strategy, the components related to first bridge mode and vehicle mode were considered. The IF trajectories for the components are given in Figure 6.17(b). For the first bridge vibration mode, similar evolution trend of IF trajectory was found for the responses from bridge and vehicle. For the IF trajectory related to vehicle frequency, the results showed more fluctuation from bridge response than that directly from vehicle response.

6.4.3.2 Addition of extra mass on the midpoint of the first span of the beam

A 5 kg mass was hung beneath the beam at the midpoint of the first span to simulate the property variation of the beam model, as shown in Figure 6.18. The vehicle moved over the bridge at the same speed. The TFA results of bridge response and vehicle response are presented in Figure 6.19(a) and (b), respectively. The IF trajectory for the vehicle mode did not change significantly after adding extra mass to the beam. Based on the bridge response, the IF trajectory was generally lower than the original one for the first bridge vibration mode. Meanwhile, based on the vehicle response, the IF trajectory of the first bridge vibration mode became higher after the property variation.

6.5 Summary

A vehicle-bridge interaction test bed was fabricated in the laboratory for the verification of proposed methods. A wireless sensory system was setup to measure the acceleration responses. For the indirect bridge modal identification, the single-axle vehicle was

connected to the two-axle vehicle and pulled with different moving speeds. Experimental results showed that with measurements from one moving sensor on the vehicle and one stationary reference sensor, the bridge mode shapes can be identified efficiently with proposed STSSI method. With SSA-BSS, components related to vehicle and bridge responses was successfully extracted from one set of vehicle response. The two-axle vehicle model was used with additional mass for the analysis of time-dependent characteristic of VBI. Results show that time-varying features of the bridge frequency changes due to the extra mass added to the bridge.

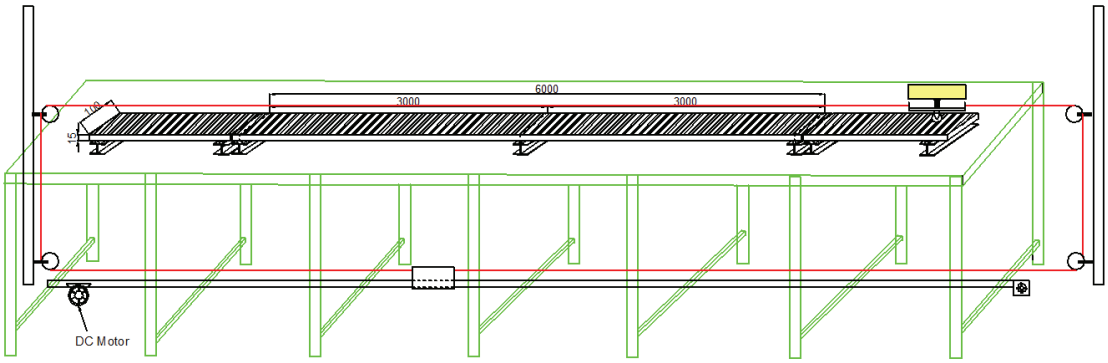

Figure 6.1 Schematic diagram of the VBI test system in the lab

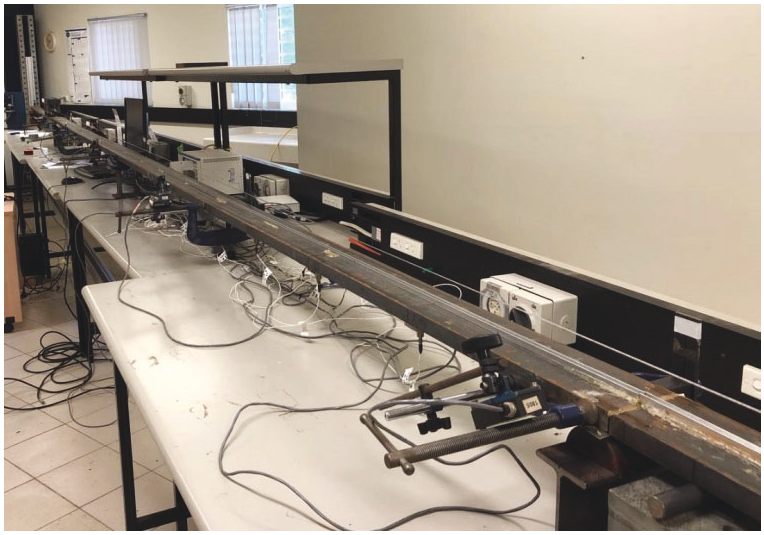

(a) Photo of the beam model

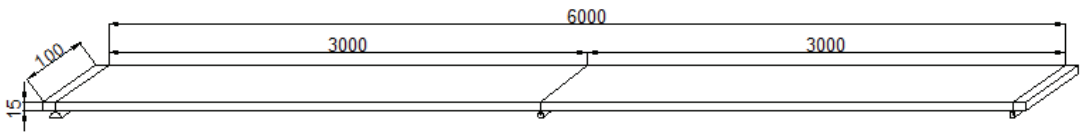

(b) Dimensions of the beam model

Figure 6.2 The main span of the bridge model

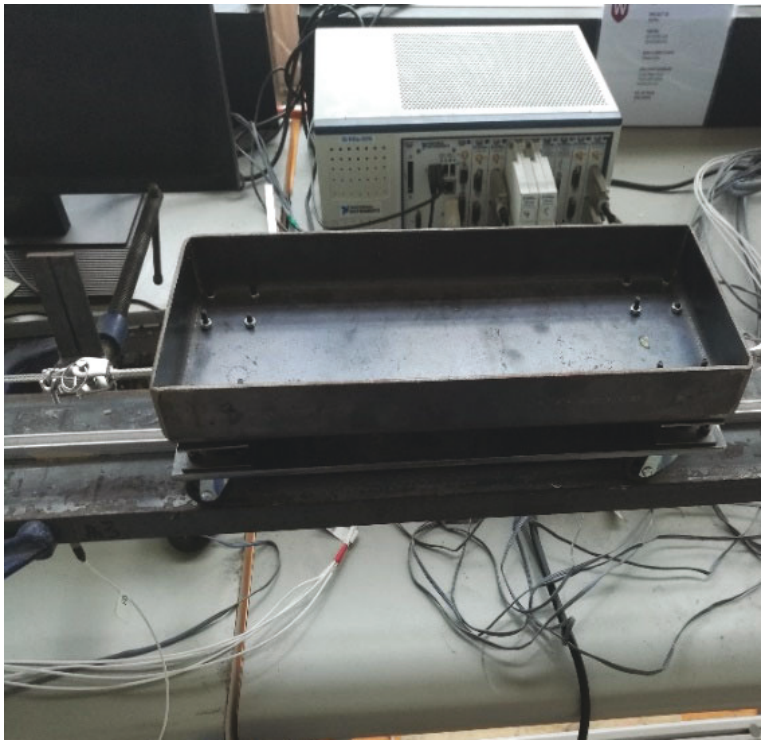

(a) Two-axle vehicle model

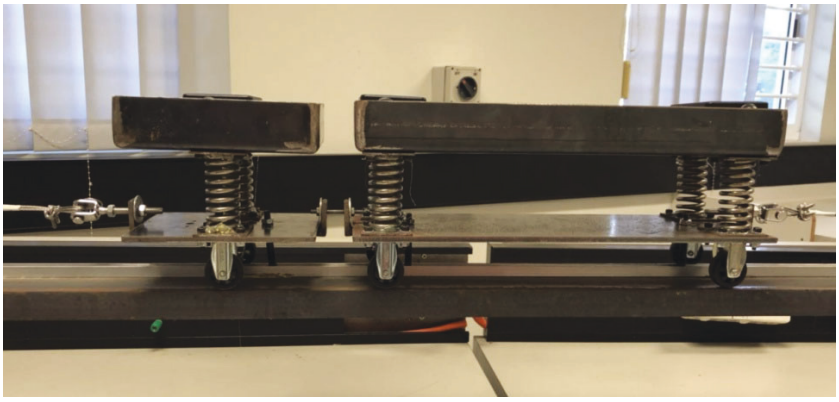

(b) Connecting the two vehicle models

Figure 6.3 Photos of vehicle models

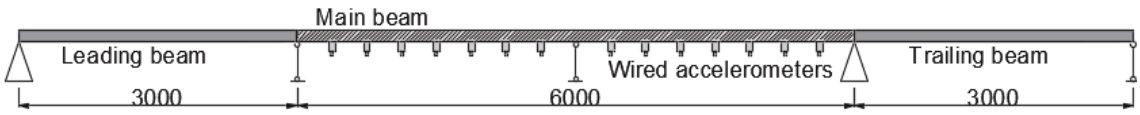

(a) Instrumentation on the main beam with wired accelerometers

(b) Sensor on the bridge

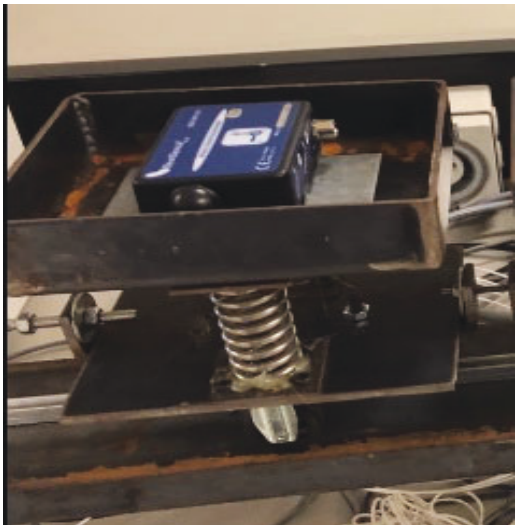

(c) Wireless sensor on the vehicle

Figure 6.4 Installation of the sensors

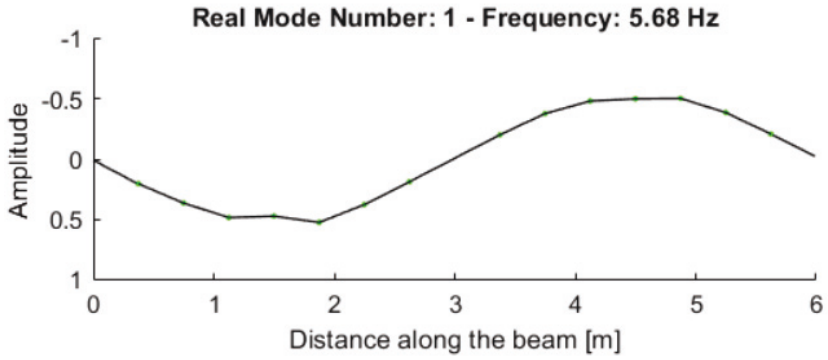

(a) The identified first bridge modal frequency and mode shape

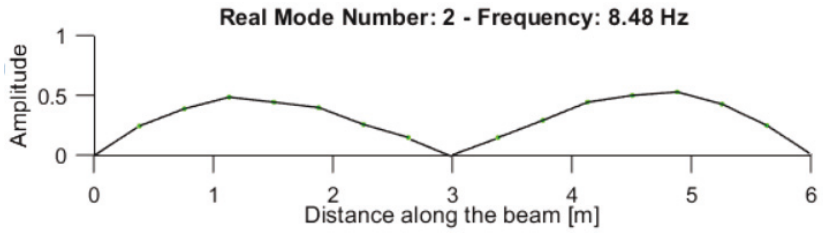

(b) The identified second bridge modal frequency and mode shape

Figure 6.5 The identified first and second modes of the bridge from modal tests

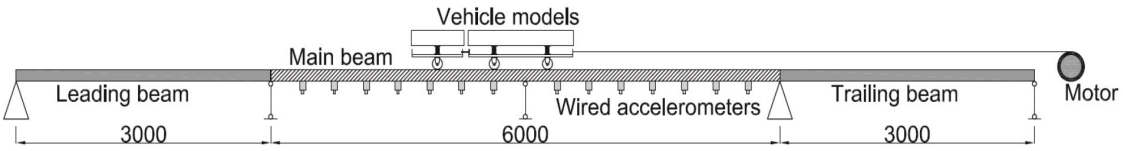

Figure 6.6 Schematic diagram of the VBI test system in the lab

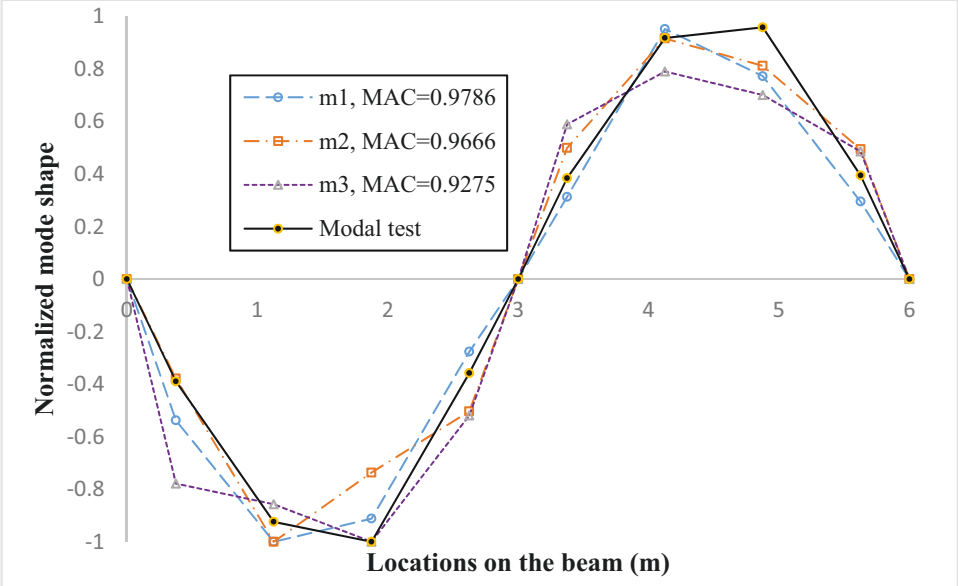

Figure 6.7 Identified mode shapes using vehicles with different weights

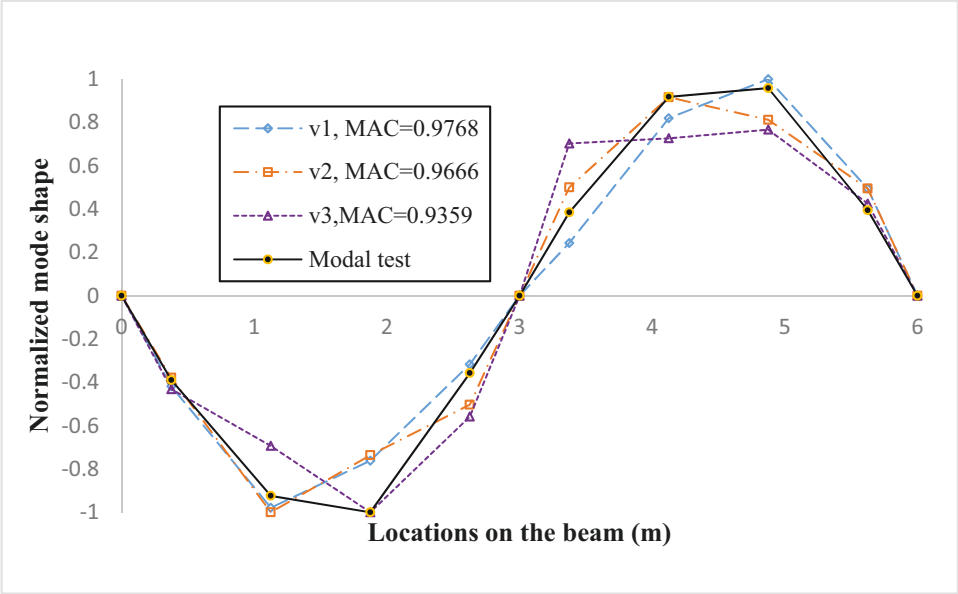

Figure 6.8 Identified mode shapes with different moving speeds

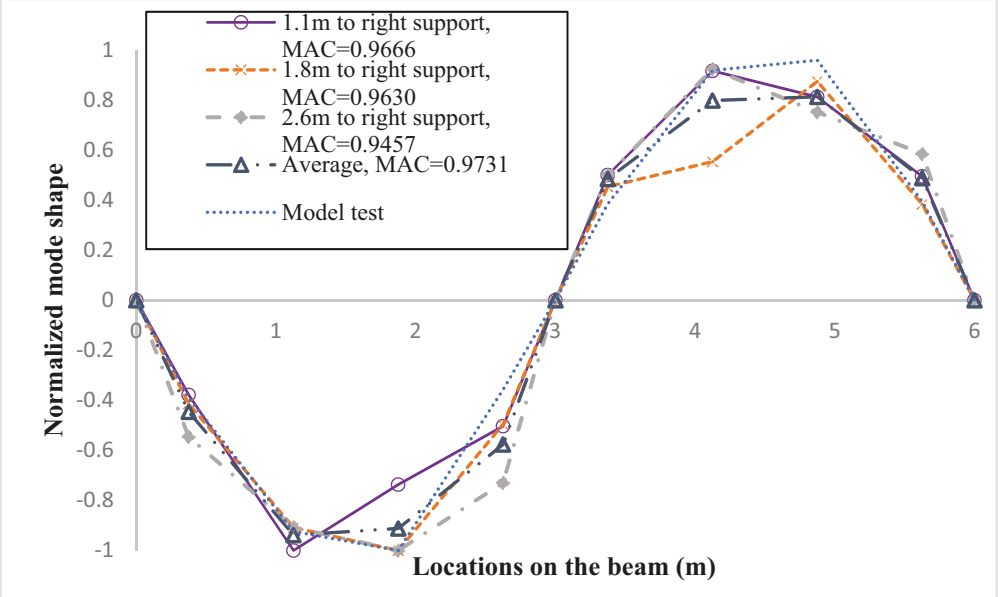

Figure 6.9 Identified mode shapes considering different locations of reference sensor

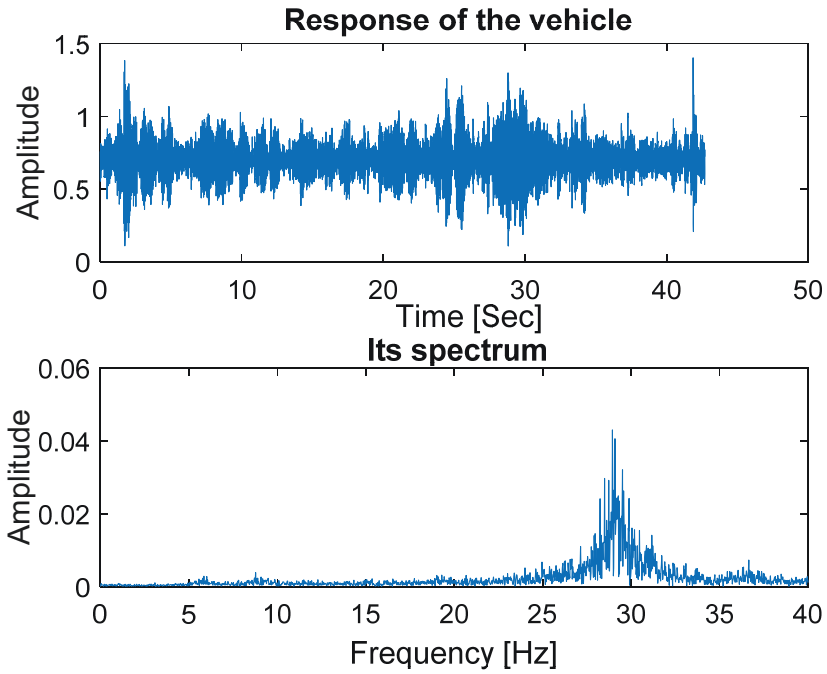

Figure 6.10 Vehicle response and its spectrum

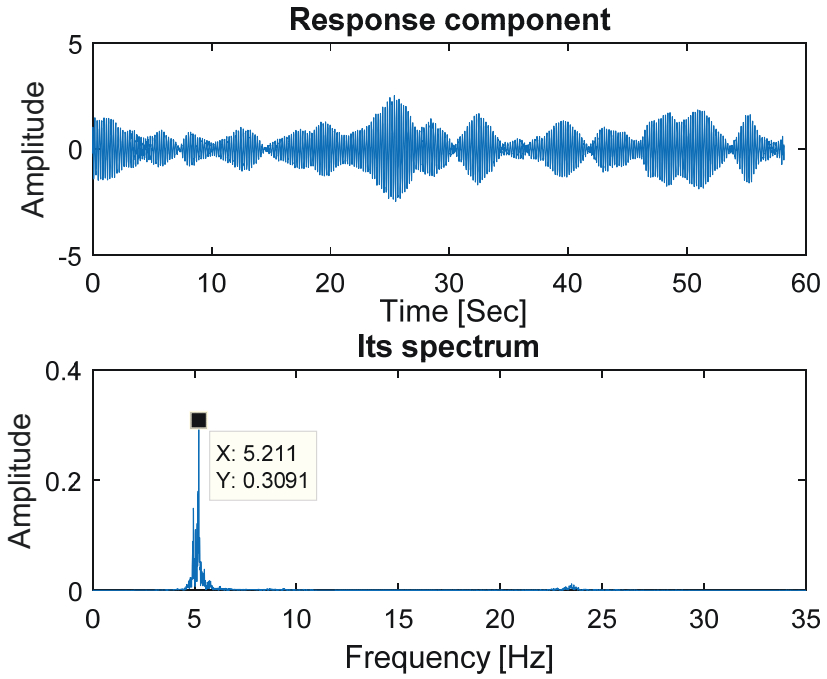

(a) First component and its spectrum

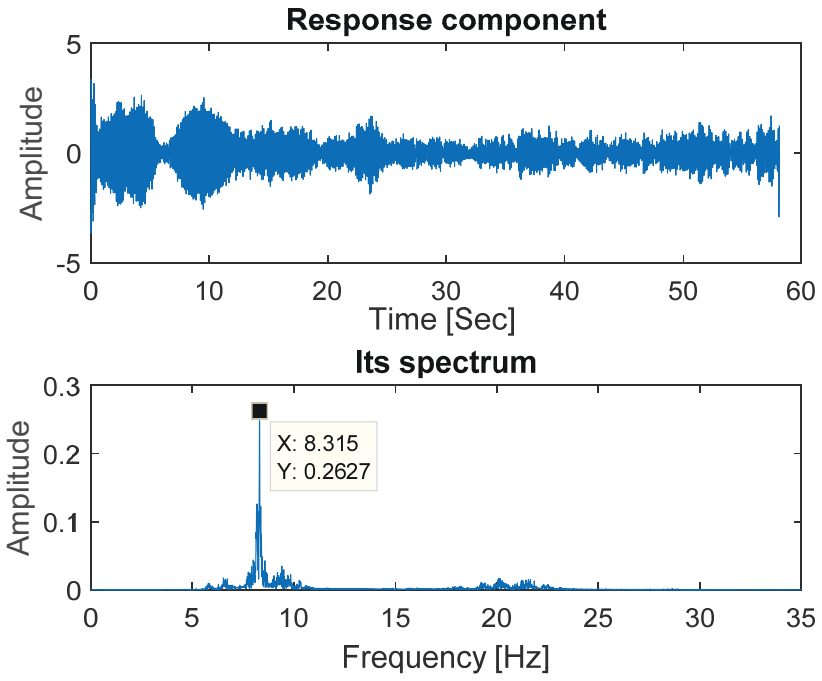

(b) Second component and its spectrum

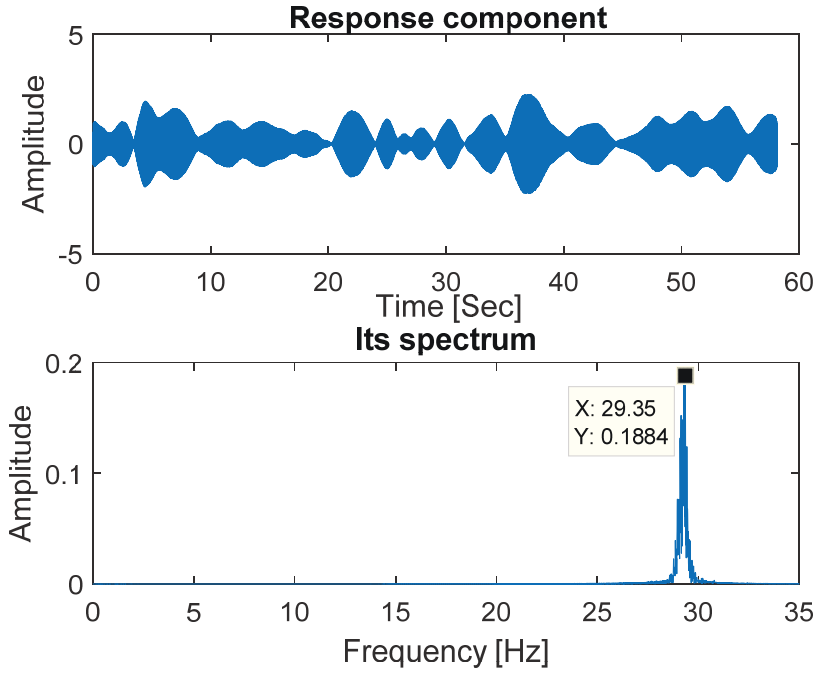

(c) Third component and its spectrum

Figure 6.11 Decomposed components and their spectra from vehicle response

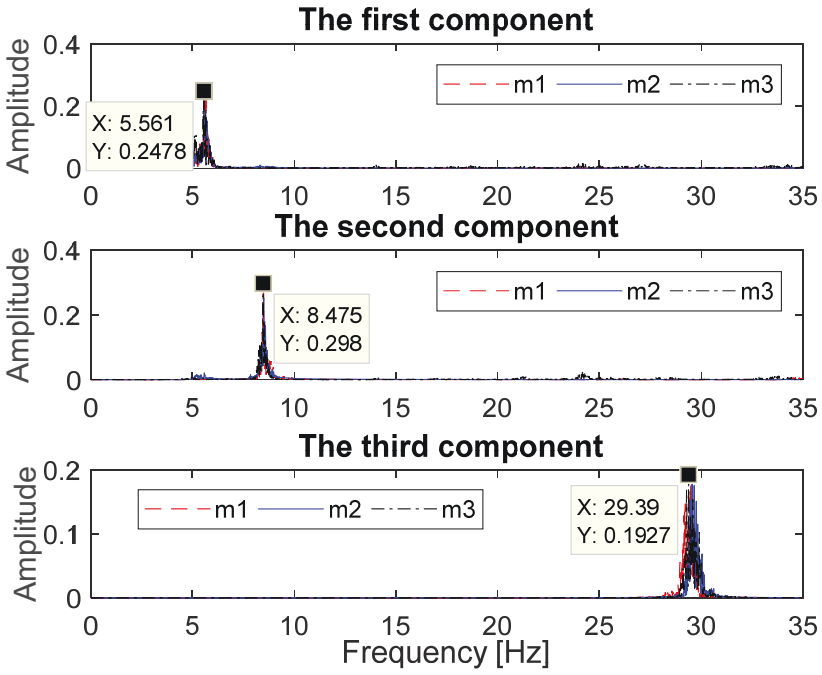

(a) Spectra of the decomposed components consider different weight of two-axle vehicle

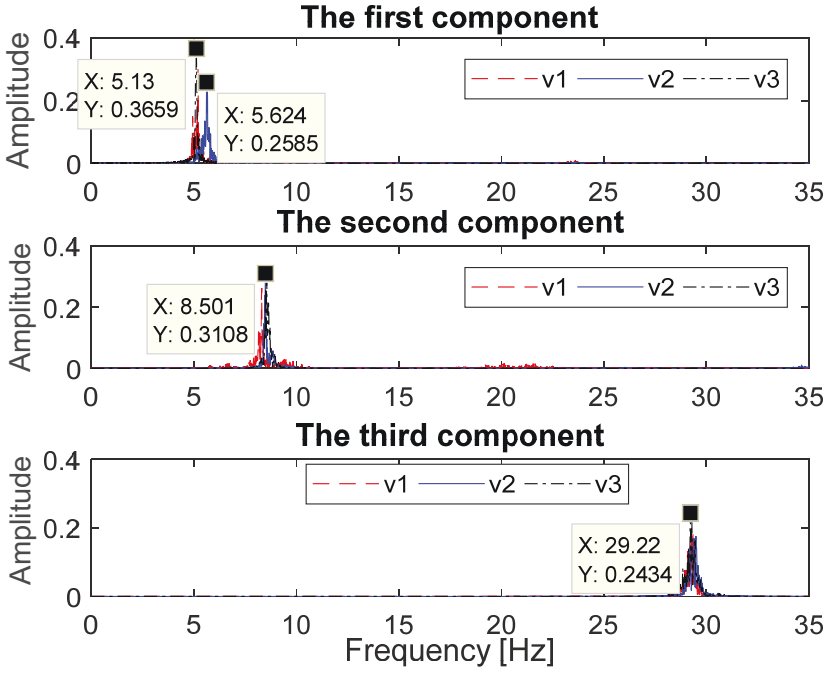

(b) Spectra of the decomposed components consider different moving speed

Figure 6.12 Spectra of the decomposed components under different test conditions

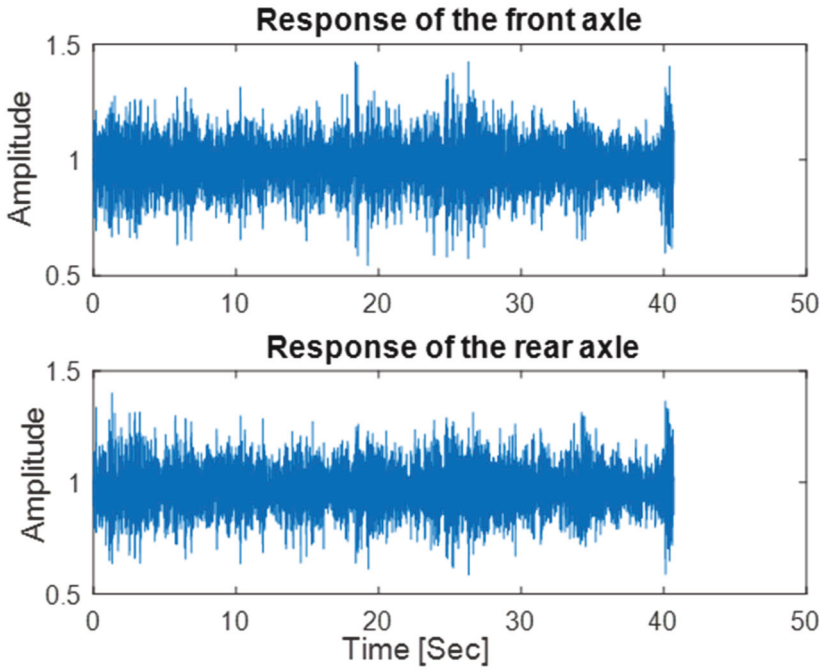

Figure 6.13 Dynamic responses of the two-axle vehicle

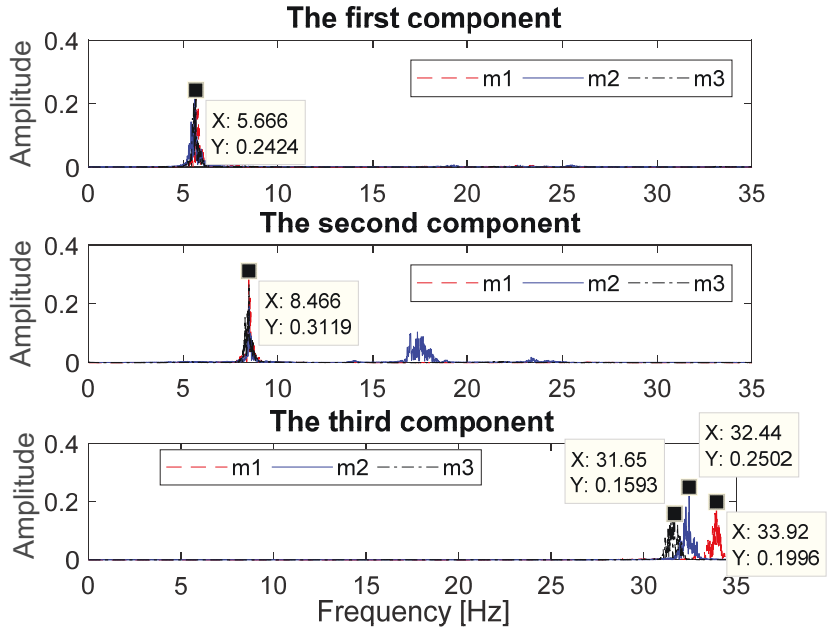

(a) Spectra of the decomposed components consider different weight of two-axle vehicle

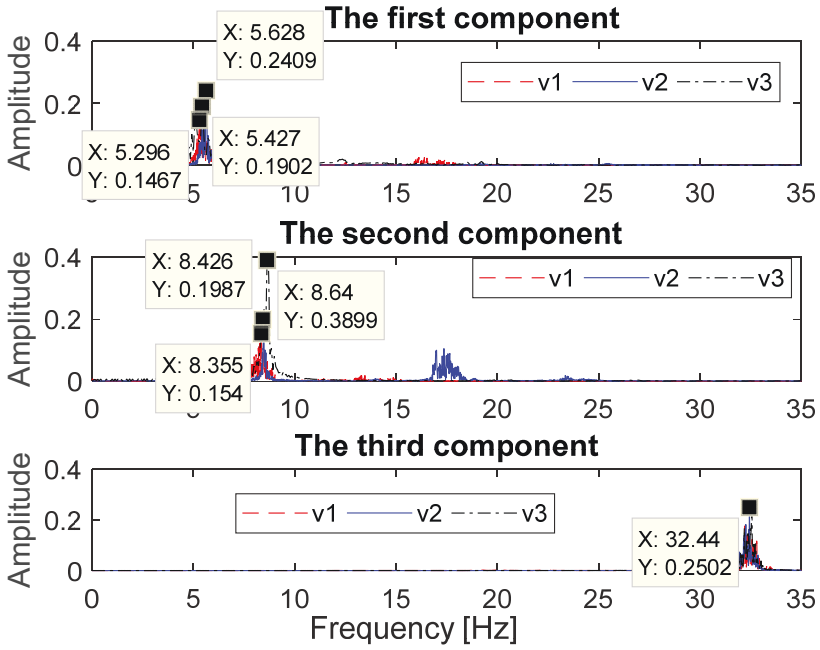

(b) Spectra of the decomposed components consider different moving speed

Figure 6.14 Spectra of the decomposed components under different test conditions

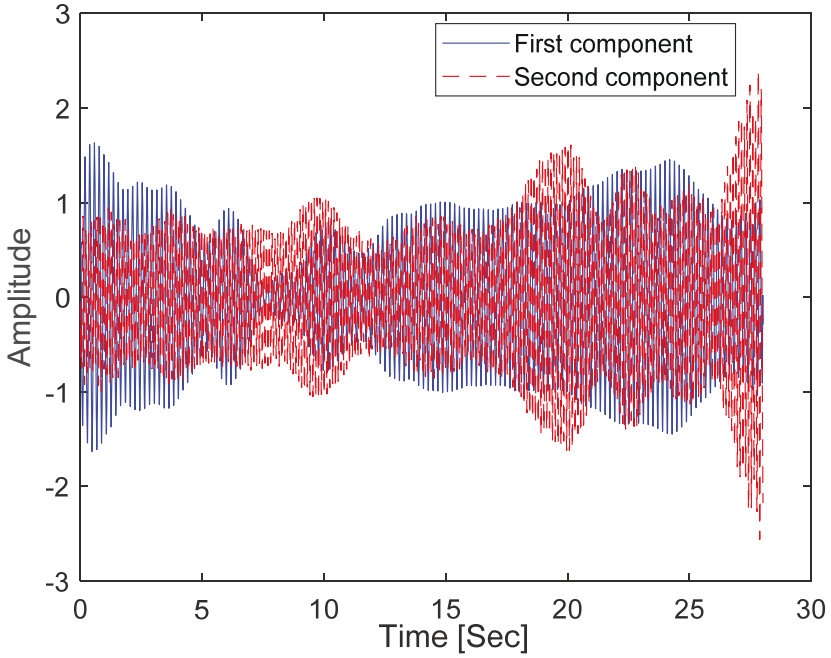

(a) The first two response components

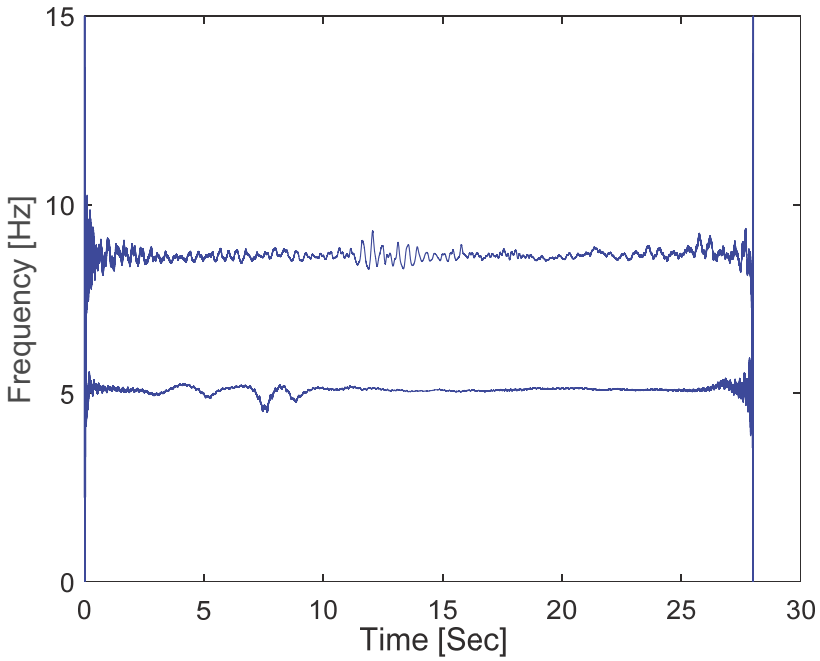

(b) The instantaneous frequencies

Figure 6.15 Response components and instantaneous frequencies

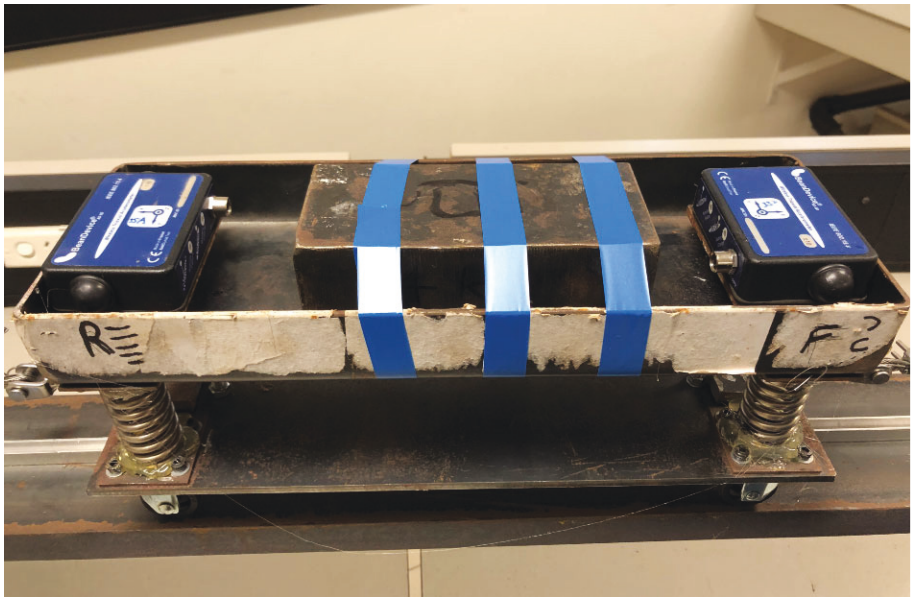

Figure 6.16 Instrumentation on the vehicle models with wireless sensors

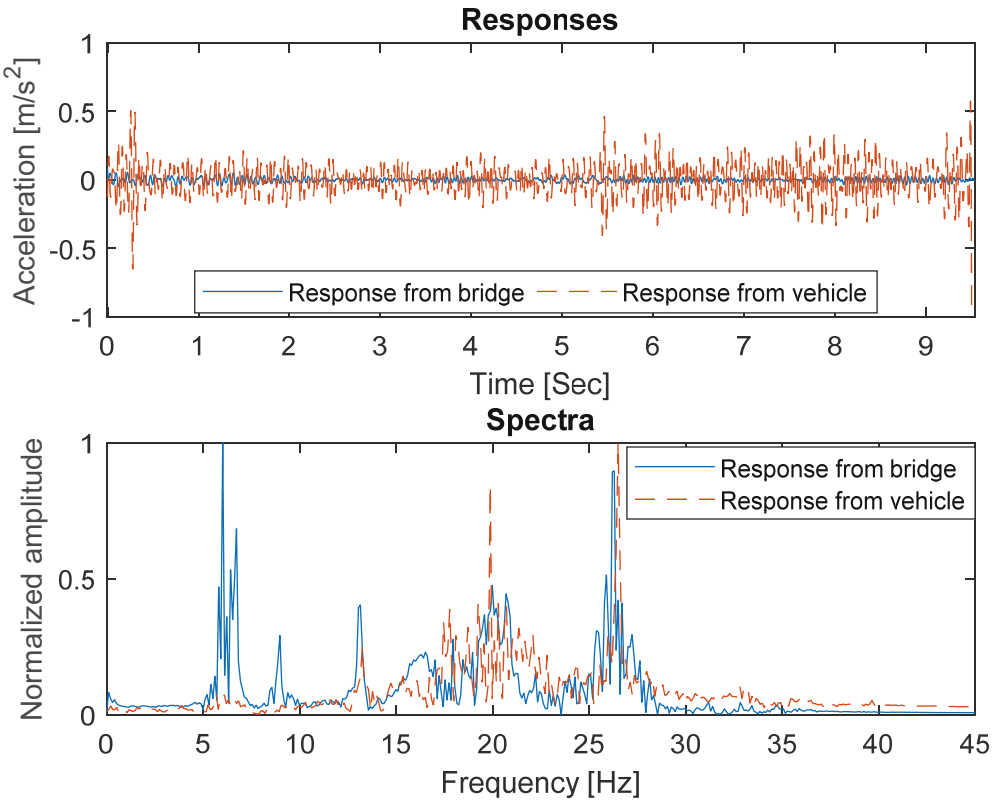

(a) Measured responses and spectrum

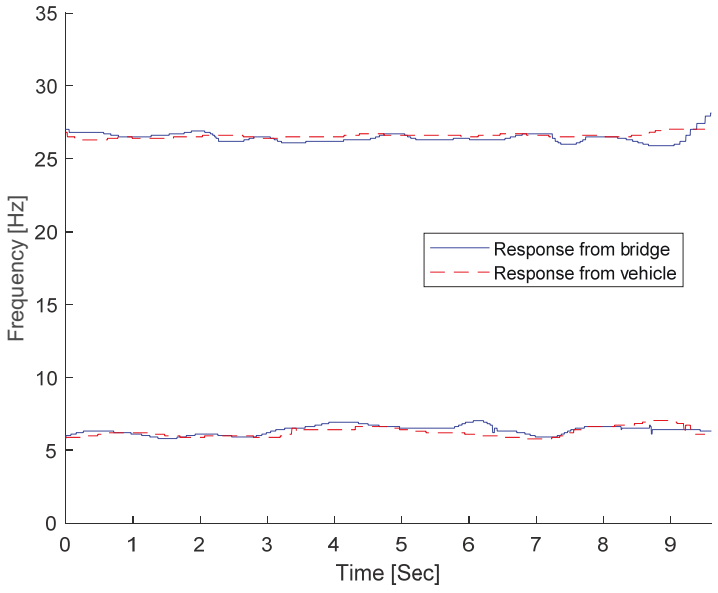

(b) IFs of the signals

Figure 6.17 Measured responses

Figure 6.18 Adding mass to the beam model

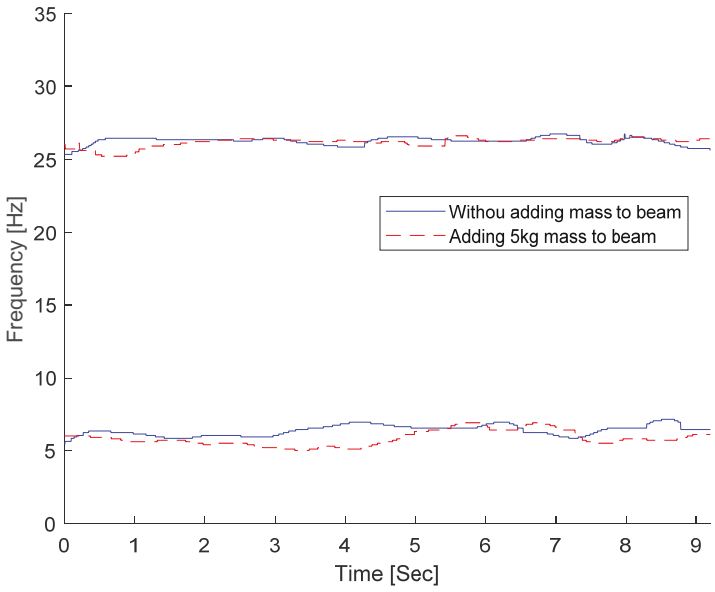

(a) From bridge response

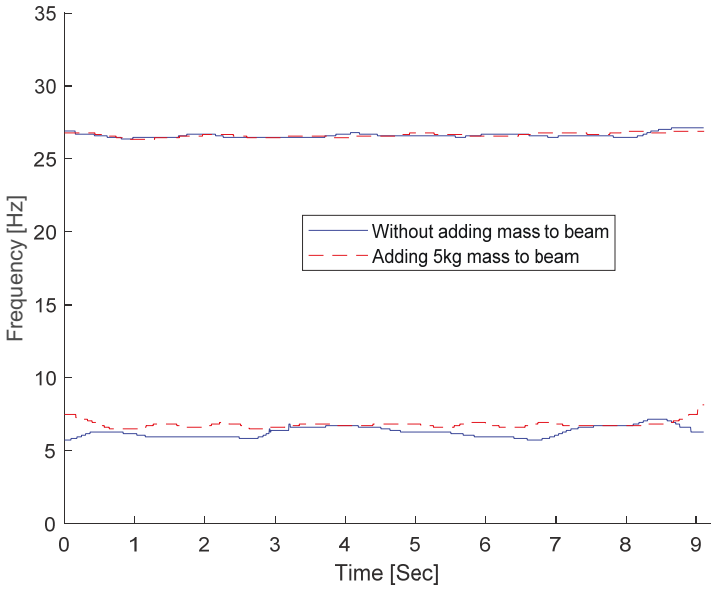

(b) From vehicle response

Figure 6.19 Instantaneous frequency

Table 6.1 Bridge and vehicle frequencies from the response of one-axle vehicle

		v1			v2			v3		
		m1	m2	m3	m1	m2	m3	m1	m2	m3
Bridge (Hz)	1st	5.21	5.22	4.93	5.62	5.59	5.55	5.12	5.12	5.09
	2nd	8.31	8.36	8.31	8.50	8.51	8.48	8.54	8.72	8.66
Vehicle (Hz)		29.37	29.40	29.30	29.58	29.56	29.68	29.53	29.39	29.65

Table 6.2 Bridge and vehicle frequencies from dynamic response of the two-axle vehicle

		v1			v2			v3		
		m1	m2	m3	m1	m2	m3	m1	m2	m3
Bridge (Hz)	1st	4.94	5.30	5.19	5.68	5.64	5.67	5.86	5.41	5.56
	2nd	8.37	8.35	8.35	8.47	8.47	8.47	8.57	8.62	8.64
Vehicle (Hz)		33.79	32.19	32.15	33.92	32.44	31.65	33.33	32.57	32.37

CHAPTER 7 A two-step drive-by bridge damage detection using Dual Kalman Filter

7.1 Overview

Drive-by bridge inspection using acceleration responses of a passing vehicle has great potential for bridge structural health monitoring. However, road surface roughness is a big challenge for the practical application of this indirect approach. This study proposes a new two-step method for the bridge damage identification using only the dynamic responses of a passing vehicle (*i.e.*, without information on the road surface roughness). In this approach, a state-space equation of the vehicle model was derived based on Newmark-β method. In the first step, the interaction forces and road surface roughness are estimated from the dynamic responses of a passing vehicle using the dual Kalman filter (DKF). In the second step, the bridge damage is identified based on the interaction force sensitivity analysis with Tikhonov regularization. In this chapter, the vehicle is modelled as a 4-DOFs half-car and the bridge is modelled as a simply supported beam with the local bridge damage simulated as an elemental flexural stiffness reduction.

Kalman filter based methods are popular for the joint input-state estimation (Yang et al., 2006; Petersen et al., 2008). Lei et al. (2012) proposed an algorithm based on sequential application of an extended Kalman estimator and least-squares estimation for the identification of the state vector of a structure and the unknown external excitations. Aucejo et al. (2019) discussed the advantages and limitations of the Kalman-type filtering for solving joint input-state estimation problems with particular focus on the applicability of the Augmented Kalman Filter (AKF). A dual Kalman filter approach was proposed for estimating the unknown input and states of a linear state-space model by using sparse

noisy acceleration measurements (Azam et al., 2015). The DKF outperformed the AKF in terms of the quality of the displacement estimates. Liu et al. (2014a) proposed a state-space model established from the explicit form of Newmark-β method which is unconditional stable with properly selected parameters. The algorithm had better performance in force identification compared to conventional state space method with zero-order-hold (ZOH) sampling technique used in (Lei et al., 2012; Azam et al., 2015). Previous studies suggested that the bridge surface roughness is a critical factor but it is usually unknown in indirect bridge SHM. It is also flexible and convenient if non-specialized testing vehicle with less instrumentation can be used to carry out the inspection. This chapter proposes to adopt previous approach (Liu et al., 2014a) to derive the state-space model of the vehicle for solving using the DKF. This strategy can identify the interaction forces and bridge surface roughness with vehicle axle responses instead of complete measurements at all degrees-of-freedom of the vehicle. Bridge damage detection can be conducted with the identified interaction forces and surface roughness.

7.2 Vehicle-bridge interaction model

The half-car model of vehicle shown in Figure 7.1 consists of four DOF. In the model, the vehicle moves over a simply supported bridge with road surface roughness at a constant speed v.

7.2.1 Equation of motion of the bridge

The supporting bridge is discretised into N Euler-Bernoulli beam finite elements. The elemental mass and stiffness matrices are obtained using Hermitian cubic interpolation shape functions. The equation of motion of the bridge structure can be written as:

$$\mathbf{M}_b\ddot{\mathbf{d}}_b + \mathbf{C}_b\dot{\mathbf{d}}_b + \mathbf{K}_b\mathbf{d}_b = \mathbf{H}_c\mathbf{P}_{int} \tag{7.1}$$

where $\mathbf{M}_b$, $\mathbf{C}_b$, $\mathbf{K}_b$ are the mass, damping and stiffness matrices of the bridge, respectively; Rayleigh damping is assumed with $\mathbf{C}_b=\alpha_1\mathbf{M}_b+\alpha_2\mathbf{K}_b$ where $\mathbf{P}_b^{\text{int}}$ is the vector of interaction forces acting on the bridge and $\mathbf{d}_b, \dot{\mathbf{d}}_b, \ddot{\mathbf{d}}_b$ are the vectors of displacement, velocity and acceleration responses of the bridge, respectively. $\mathbf{H}_c\mathbf{P}_b^{\text{int}}$ is the equivalent nodal load vector from the bridge-vehicle interaction force with

$$\mathbf{H}_c = \begin{Bmatrix} 0 \dots 0 \dots \boldsymbol{H}_1 \dots 0 \\ 0 \dots \boldsymbol{H}_2 \dots 0 \dots 0 \end{Bmatrix}^T \in R^{NN\times 2} \tag{7.2}$$

where $\mathbf{H}_c$is a matrix with null entries except at the DOF corresponding to the nodes of the beam elements on which the loads are acting. *NN* is the total number of DOF of the bridge structure after considering the boundary conditions. The components of vector $\boldsymbol{H}_i$ $(i = 1,2)$ evaluated for the *ith* interactive force on the *jth* finite element can be written in global coordinates as:

$$\boldsymbol{H}_i = \begin{Bmatrix} 1 - 3\left(\frac{\hat{x}_i(t)-(j-1)l}{l}\right)^2 + 2\left(\frac{\hat{x}_i(t)-(j-1)l}{l}\right)^3 \\ (\hat{x}_i(t) - (j-1)l)\left(\frac{\hat{x}_i(t)-(j-1)l}{l} - 1\right)^2 \\ 3\left(\frac{\hat{x}_i(t)-(j-1)l}{l}\right)^2 - 2\left(\frac{\hat{x}_i(t)-(j-1)l}{l}\right)^3 \\ (\hat{x}_i(t) - (j-1)l)\left(\left(\frac{\hat{x}_i(t)-(j-1)l}{l}\right)^2 - \left(\frac{\hat{x}_i(t)-(j-1)l}{l}\right)\right) \end{Bmatrix} \tag{7.3}$$

with $(j-1)l \le \hat{x}_i(t) \le jl$ and l the length of element.

7.2.2 Equation of motion of the vehicle model

The equation of motion of the vehicle can be written as follows based on Lagrange formulation as

$$\begin{bmatrix} \boldsymbol{M}_{v1} & 0 \\ 0 & \boldsymbol{M}_{v2} \end{bmatrix} \ddot{\boldsymbol{X}}_v + \begin{bmatrix} \boldsymbol{C}_{v11} & \boldsymbol{C}_{v12} \\ \boldsymbol{C}_{v21} & \boldsymbol{C}_{v22} \end{bmatrix} \dot{\boldsymbol{X}}_v + \begin{bmatrix} \boldsymbol{K}_{v11} & \boldsymbol{K}_{v12} \\ \boldsymbol{K}_{v21} & \boldsymbol{K}_{v22} \end{bmatrix} X_v = -\begin{Bmatrix} 0 \\ \boldsymbol{P}_{int} \end{Bmatrix} + \begin{Bmatrix} 0 \\ \boldsymbol{M}_s \end{Bmatrix} \tag{7.4}$$

where $\boldsymbol{X}_v = \{y_v, \theta_v, y_1, y_2\}^T$ is the response vector of the vehicle; $\boldsymbol{M}_{v1}$, $\boldsymbol{M}_{v2}$, $\boldsymbol{C}_{v11}$, $\boldsymbol{C}_{v12}$, $\boldsymbol{C}_{v21}$, $\boldsymbol{C}_{v22}$, $\boldsymbol{K}_{v11}$, $\boldsymbol{K}_{v12}$, $\boldsymbol{K}_{v21}$, $\boldsymbol{K}_{v22}$ are the mass, damping and stiffness sub-matrices of the vehicle model, respectively, that can be written as

$$\boldsymbol{M}_{v1} = \begin{bmatrix} m_v & 0 \\ 0 & I_v \end{bmatrix}, \qquad \boldsymbol{M}_{v2} = \begin{bmatrix} m_1 & 0 \\ 0 & m_2 \end{bmatrix},$$

$$\boldsymbol{C}_{v11} = \begin{bmatrix} C_{s1} + C_{s2} & (-C_{s1}a_1 + C_{s2}a_2)S \\ (-C_{s1}a_1 + C_{s2}a_2)S & (C_{s1}a_1^2 + C_{s2}a_2^2)S^2 \end{bmatrix},$$

$$\boldsymbol{C}_{v12} = \begin{bmatrix} -C_{s1} & -C_{s2} \\ C_{s1}a_1S & -C_{s2}a_2S \end{bmatrix}, \ \boldsymbol{C}_{v21} = \begin{bmatrix} -C_{s1} & C_{s1}a_1S \\ -C_{s2} & -C_{s2}a_2S \end{bmatrix}, \ \boldsymbol{C}_{v22} = \begin{bmatrix} C_{s1} & 0 \\ 0 & C_{s2} \end{bmatrix},$$

$$\boldsymbol{K}_{v11} = \begin{bmatrix} K_{s1} + K_{s2} & (-K_{s1}a_1 + K_{s2}a_2)S \\ (-K_{s1}a_1 + K_{s2}a_2)S & (K_{s1}a_1^2 + K_{s2}a_2^2)S^2 \end{bmatrix},$$

$$\boldsymbol{K}_{v12} = \begin{bmatrix} -K_{s1} & -K_{s2} \\ K_{s1}a_1S & -K_{s2}a_2S \end{bmatrix}, \quad \boldsymbol{K}_{v21} = \begin{bmatrix} -K_{s1} & K_{s1}a_1S \\ -K_{s2} & -K_{s2}a_2S \end{bmatrix}, \ \boldsymbol{K}_{v22} = \begin{bmatrix} K_{s1} & 0 \\ 0 & K_{s2} \end{bmatrix}$$

$\boldsymbol{P}_{int} = \{P_1(t), P_2(t)\}^T$ is the vehicle-bridge interaction force vector with

$$P_i(t) = K_{ti}(y_i - z_i) + C_{ti}(\dot{y}_i - \dot{z}_i) + \{m_i + (1 - a_i)m_v\}\mathrm{g} \tag{7.5a}$$

and

$$z_i = w(\hat{x}_i(t), t) + r\big(\hat{x}_i(t)\big), \dot{z}_i = \dot{w}(\hat{x}_i(t), t) + w'(\hat{x}_i(t), t)\dot{\hat{x}}_i(t) + r'\big(\hat{x}_i(t)\big)\dot{\hat{x}}_i(t),$$

$$\dot{w}(\hat{x}_i(t), t) = \mathbf{H}_c{}^T(\hat{x}_i(t))\dot{\mathbf{d}}_b(t), \quad w'(\hat{x}_i(t), t) = \frac{\partial \mathbf{H}_c{}^T(x)}{\partial x}\mathbf{d}_b(t)|_{x=\hat{x}_i(t)},$$

$$r'\big(\hat{x}_i(t)\big) = \frac{dr(x)}{dx}\,|_{x=\hat{x}_i(t)}, \quad \dot{\hat{x}}_i(t) = \frac{d\hat{x}_i(t)}{dt}. \qquad (i = 1, 2) \tag{7.5b}$$

where $r(x)$ is the road surface roughness at the location of the tires, $\hat{x}_1(t)$ and $\hat{x}_2(t)$ are the position of the front and rear axles respectively at time *t*. and m_v, I_v, m_1, m_2, C_{s1}, C_{s2}, C_{t1}, C_{t2}, K_{s1}, K_{s2}, K_{t1}, K_{t2} are the vehicle parameters as shown in Figure 7.1. a_1S, a_2S are the distance between the center of gravity of the vehicle body with the front and rear axles respectively and *S* is the axle spacing. g is the acceleration of gravity.

$w(\hat{x}_i(t), t)$, $\dot{w}(\hat{x}_i(t), t)$ $(i = 1,2)$ are the vertical dynamic deflection of the beam and its time derivative under the *i*th load at time *t*. $\boldsymbol{M}_s = \{M_{s1}, M_{s2}\}^T$ is the static load of the vehicle with

$$\begin{cases} M_{s1} = (m_1 + a_2 m_v)\mathrm{g} \\ M_{s2} = (m_2 + a_1 m_v)\mathrm{g} \end{cases} \tag{7.6}$$

Combining Eqs. (7.1) and (7.4), the equation of motion of the coupled vehicle-bridge system can be written as:

$$\mathbf{M}_g\ddot{\mathbf{u}} + \mathbf{C}_g\dot{\mathbf{u}} + \mathbf{K}_g\mathbf{u} = \mathbf{f} \tag{7.7}$$

where $\mathbf{M}_g$, $\mathbf{C}_g$ and $\mathbf{K}_g$ are the combined system mass, damping and stiffness matrices, respectively, and $\mathbf{f}$ is the force vector. When the vehicle and bridge parameters and the surface roughness are known, the dynamic responses of the system can be calculated at each time step using the explicit Newmark-β method.

7.3 Estimation of state vector and unknown input forces of vehicle by DKF

The DKF is used to identify the vehicle state vector and unknown excitation. Analytical recursive solutions are derived in this section with the Newmark-β method from the state space model of the vehicle system.

7.3.1 State space model of the vehicle

Eq. (7.4) can be rewritten as

$$\mathbf{M}_v\ddot{\mathbf{x}}(\mathrm{t}) + \mathbf{C}_v\dot{\mathbf{x}}(\mathrm{t}) + \mathbf{K}_v\mathbf{x}(\mathrm{t}) = \mathbf{LP}(\mathrm{t}) \tag{7.8}$$

where $\mathbf{L} = [0\ 0; 0\ 0; 1\ 0; 0\ 1]$ is the influence matrix associated with the unknown excitation vector $\mathbf{P}(\mathrm{t})$ $(= \left[f_{v,1}, f_{v,2}\right]^{\boldsymbol{T}} = \boldsymbol{M}_s - \boldsymbol{P}_{int})$ on the vehicle system; $\mathbf{M}_{\boldsymbol{v}} =$

$\begin{bmatrix} \boldsymbol{M}_{v1} & 0 \\ 0 & \boldsymbol{M}_{v2} \end{bmatrix}$, $\mathbf{C}_{\boldsymbol{v}} = \begin{bmatrix} \boldsymbol{C}_{v11} & \boldsymbol{C}_{v12} \\ \boldsymbol{C}_{v21} & \boldsymbol{C}_{v22} \end{bmatrix}$, $\mathbf{K}_{\boldsymbol{v}} = \begin{bmatrix} \boldsymbol{K}_{v11} & \boldsymbol{K}_{v12} \\ \boldsymbol{K}_{v21} & \boldsymbol{K}_{v22} \end{bmatrix}$. $f_{v,i}$ $(i = 1,2)$ is the force acting at the contact points between the vehicle and pavement, and $\mathbf{x}$, $\dot{\mathbf{x}}$ and $\ddot{\mathbf{x}}$ are respectively the vehicle displacement, velocity and acceleration responses, respectively.

The explicit Newmark-β method (Liu et al., 2014a) is based on an assumed variation of acceleration between two time instants as

$$\ddot{\mathbf{x}} = (1-\gamma)\ddot{\mathbf{x}}_i + \gamma\ddot{\mathbf{x}}_{i+1} \qquad (0 \le \gamma \le 1) \tag{7.9}$$

$$\ddot{\mathbf{x}} = (1-2\beta)\ddot{\mathbf{x}}_i + 2\beta\ddot{\mathbf{x}}_{i+1} \qquad (0 \le \beta \le 0.5) \tag{7.10}$$

Integrating the acceleration between t_i and t_{i+1}, the displacement and velocity at t_{i+1} can be obtained as

$$\dot{\mathbf{x}}_{i+1} = \dot{\mathbf{x}}_i + \Delta t\ddot{\mathbf{x}} \tag{7.11}$$

$$\mathbf{x}_{i+1} = \mathbf{x}_i + \Delta t\dot{\mathbf{x}}_i + \frac{1}{2}\Delta t^2\ddot{\mathbf{x}} \tag{7.12}$$

Substituting Eq.(7.9) into Eq.(7.11) and Eq.(7.10) into Eq.(12) to get

$$\dot{\mathbf{x}}_{i+1} = \dot{\mathbf{x}}_i + (1-\gamma)\Delta t\ddot{\mathbf{x}}_i + \gamma\Delta t\ddot{\mathbf{x}}_{i+1} \tag{7.13}$$

$$\mathbf{x}_{i+1} = \mathbf{x}_i + \Delta t\dot{\mathbf{x}}_i + \left(\frac{1}{2}-\beta\right)\Delta t^2\ddot{\mathbf{x}}_i + \beta\Delta t^2\ddot{\mathbf{x}}_{i+1} \tag{7.14}$$

Rewriting and rearranging Eqs. (7.13) and (7.14), the acceleration and velocity at t_{i+1} are derived as

$$\ddot{\mathbf{x}}_{i+1} = \frac{1}{\beta\Delta t^2}(\mathbf{x}_{i+1} - \mathbf{x}_i) - \frac{1}{\beta\Delta t}\dot{\mathbf{x}}_i - \left(\frac{1}{2\beta} - 1\right)\ddot{\mathbf{x}}_i \tag{7.15}$$

$$\dot{\mathbf{x}}_{i+1} = \frac{\gamma}{\beta\Delta t}(\mathbf{x}_{i+1} - \mathbf{x}_i) + \left(1 - \frac{\gamma}{\beta}\right)\dot{\mathbf{x}}_i + \left(1 - \frac{\gamma}{2\beta}\right)\Delta t\ddot{\mathbf{x}}_i \tag{7.16}$$

The equation of motion in Eq. (7.8) can then be rewritten in discrete form as

$$\mathbf{M}\ddot{\mathbf{x}}(t_{i+1}) + \mathbf{C}\dot{\mathbf{x}}(t_{i+1}) + \mathbf{K}\mathbf{x}(t_{i+1}) = \mathbf{L}\mathbf{P}(t_{i+1}) \tag{7.17}$$

By substituting Eqs. (7.15) and (7.16) into Eq. (7.17), the dynamic response $\mathbf{x}_{i+1}$ at t_{i+1}, can be represented as function of responses $\ddot{\mathbf{x}}_i$, $\dot{\mathbf{x}}_i$ and $\mathbf{x}_i$ at time t_i and $\mathbf{P}_{i+1}$ as

$$\mathbf{x}_{i+1} = \mathbf{A}_0\mathbf{L}\mathbf{P}_{i+1} + \mathbf{A}_d\mathbf{x}_i + \mathbf{A}_v\dot{\mathbf{x}}_i + \mathbf{A}_a\ddot{\mathbf{x}}_i \tag{7.18}$$

where $\mathbf{A}_0 = (\mathbf{K} + \frac{1}{\beta\Delta t^2}\mathbf{M} + \frac{\gamma}{\beta\Delta t}\mathbf{C})^{-1}$; $\mathbf{A}_d = \mathbf{A}_0(\frac{1}{\beta\Delta t^2}\mathbf{M} + \frac{\gamma}{\beta\Delta t}\mathbf{C})$;

$$\mathbf{A}_v = \mathbf{A}_0\left[\frac{1}{\beta\Delta t}\mathbf{M} + (\frac{\gamma}{\beta} - 1)\mathbf{C}\right]; \mathbf{A}_a = \mathbf{A}_0\left[(\frac{1}{2\beta} - 1)\mathbf{M} + \frac{\Delta t}{2}(\frac{\gamma}{\beta} - 2)\mathbf{C}\right]$$

Substituting Eq. (7.18) into Eqs. (7.15) and (7.16), respectively, the acceleration $\ddot{\mathbf{x}}_{i+1}$ and velocity $\dot{\mathbf{x}}_{i+1}$ become

$$\ddot{\mathbf{x}}_{i+1} = \mathbf{C}_0\mathbf{L}\mathbf{P}_{i+1} + \mathbf{C}_d\mathbf{x}_i + \mathbf{C}_v\dot{\mathbf{x}}_i + \mathbf{C}_a\ddot{\mathbf{x}}_i \tag{7.19}$$

$$\dot{\mathbf{x}}_{i+1} = \mathbf{B}_0\mathbf{L}\mathbf{P}_{i+1} + \mathbf{B}_d\mathbf{x}_i + \mathbf{B}_v\dot{\mathbf{x}}_i + \mathbf{B}_a\ddot{\mathbf{x}}_i \tag{7.20}$$

where $\mathbf{C}_0 = \frac{1}{\beta\Delta t^2}\mathbf{A}_0$; $\mathbf{C}_d = \frac{-1}{\beta\Delta t^2}\mathbf{A}_0\mathbf{K}$; $\mathbf{C}_v = \frac{-1}{\beta\Delta t^2}\mathbf{A}_0(\mathbf{C} + \Delta t\mathbf{K})$;

$\mathbf{C}_a = \frac{1}{\beta\Delta t^2}\mathbf{A}_0\left[(\gamma - 1)\Delta t\mathbf{C} - \beta\Delta t^2(\frac{1}{2\beta} - 1)\mathbf{K}\right]$; $\mathbf{B}_0 = \frac{\gamma}{\beta\Delta t}\mathbf{A}_0$; $\mathbf{B}_d = \frac{-\gamma}{\beta\Delta t}\mathbf{A}_0\mathbf{K}$;

$\mathbf{B}_v = \frac{\gamma}{\beta\Delta t}\mathbf{A}_0\left[\left(\frac{\beta\Delta t}{\gamma} - \Delta t\right)\mathbf{K} + \frac{1}{\gamma\Delta t}\mathbf{M}\right]$; $\mathbf{B}_a = \frac{-\gamma}{\beta\Delta t}\mathbf{A}_0\left[\left(\frac{\beta\Delta t^2}{\gamma} - \frac{\Delta t^2}{2}\right)\mathbf{K} + (\frac{1}{\gamma} - 1)\mathbf{M}\right]$.

Combining Eqs. (7.18) to (7.20), the iterative form of the explicit Newmark-β method is obtained as

$$\begin{bmatrix}\mathbf{x}_{i+1}\\ \dot{\mathbf{x}}_{i+1}\\ \ddot{\mathbf{x}}_{i+1}\end{bmatrix} = \begin{bmatrix}\mathbf{A}_0\\ \mathbf{B}_0\\ \mathbf{C}_0\end{bmatrix}\mathbf{L}\mathbf{P}_{i+1} + \begin{bmatrix}\mathbf{A}_d & \mathbf{A}_v & \mathbf{A}_a\\ \mathbf{B}_d & \mathbf{B}_v & \mathbf{B}_a\\ \mathbf{C}_d & \mathbf{C}_v & \mathbf{C}_a\end{bmatrix}\begin{bmatrix}\mathbf{x}_i\\ \dot{\mathbf{x}}_i\\ \ddot{\mathbf{x}}_i\end{bmatrix} \tag{7.21}$$

For a state vector $\mathbf{X}_i = [\mathbf{x}_i^T\ \dot{\mathbf{x}}_i^T\ \ddot{\mathbf{x}}_i^T]^T$, Eq. (7.21) can be rewritten in matrix form as

$$\mathbf{X}_{i+1} = \mathbf{A}\mathbf{X}_i + \mathbf{B}\mathbf{P}_{i+1} \tag{7.22}$$

where

$$\mathbf{A} = \begin{bmatrix} \mathbf{A}_d & \mathbf{A}_v & \mathbf{A}_a \\ \mathbf{B}_d & \mathbf{B}_v & \mathbf{B}_a \\ \mathbf{C}_d & \mathbf{C}_v & \mathbf{C}_a \end{bmatrix}, \mathbf{B} = \begin{bmatrix} \mathbf{A}_0 \\ \mathbf{B}_0 \\ \mathbf{C}_0 \end{bmatrix} \mathbf{L}.$$

7.3.2 The Output equation

Vector $\boldsymbol{y} \in R^{ns\times 1}$ represents the output of the structural system, and it can be assembled from measurements with

$$\mathbf{y} = \mathbf{R}_a\ddot{\mathbf{x}} + \mathbf{R}_v\dot{\mathbf{x}} + \mathbf{R}_b\mathbf{x} \tag{7.23}$$

where $\mathbf{R}_a$, $\mathbf{R}_v$ and $\mathbf{R}_b \in R^{ns\times N}$ are the output influence matrices for the measured acceleration, velocity and displacement, respectively, ns is the dimension of the measured responses and N is the number of DOF of the structure.

Letting $\mathbf{R} = [\mathbf{R}_d\ \mathbf{R}_v\ \mathbf{R}_a]$, Eq. (7.23) can be rewritten into the following discrete form as

$$\mathbf{y}_i = \mathbf{R}\mathbf{X}_i \tag{7.24}$$

7.3.3 State-space model of system

The state space representation of the vehicle-bridge dynamic system can be obtained from Eqs. (7.22) and (7.24) as

$$\begin{cases} \mathbf{X}_{i+1} = \mathbf{A}\mathbf{X}_i + \mathbf{B}\mathbf{P}_{i+1} + \boldsymbol{v}_i^{\boldsymbol{x}} & (7.25a) \\ \mathbf{y}_i = \mathbf{R}\mathbf{X}_i + \boldsymbol{w}_i & (7.25b) \end{cases}$$

where $\boldsymbol{v}_i^{\boldsymbol{x}}$ is the process noise that represents uncertainties in the modelling processes and $\boldsymbol{w}_i$ is the measurement noise. The vectors $\boldsymbol{v}_i^{\boldsymbol{x}}$ and $\boldsymbol{w}_i$ are assumed as Gaussian white noise with covariance $\boldsymbol{Q}^{\boldsymbol{x}}$ and $\boldsymbol{Q}^{\boldsymbol{y}}$, respectively.

The state space formulation in Eq. (7.25) is not in standard form, because knowledge of input vector at time $i+1$ is required in the state equation. A reduced state $\overline{\mathbf{X}}_i = \mathbf{X}_i - \mathbf{B}\mathbf{P}_i$ can be further formulated by transforming Eq. (7.25) as

$$\begin{cases} \overline{\mathbf{X}}_{i+1} = \mathbf{A}\overline{\mathbf{X}}_i + \mathbf{A}\mathbf{B}\mathbf{P}_i + \boldsymbol{v}_i^{\boldsymbol{x}} & (7.26a) \\ \mathbf{y}_i = \mathbf{R}\overline{\mathbf{X}}_i + \mathbf{R}\mathbf{B}\mathbf{P}_i + \boldsymbol{w}_i & (7.26b) \end{cases}$$

7.3.4 Dual Kalman Filter

Joint input-state estimation is conducted in this section. A random walk model is introduced to represent the state equation for the input $\mathbf{P}_i$ as

$$\mathbf{P}_{i+1} = \mathbf{P}_i + \boldsymbol{v}_i^{\boldsymbol{p}} \tag{7.27}$$

where $\boldsymbol{v}_i^{\boldsymbol{p}}$ is a zero mean Gaussian white process with covariance matrix $\boldsymbol{Q}^{\boldsymbol{p}}$. Combining Eqs. (7.26b) and (7.27) gives a new state-space equation for the input as

$$\begin{cases} \mathbf{P}_{i+1} = \mathbf{P}_i + \boldsymbol{v}_i^{\boldsymbol{p}} & (7.28a) \\ \mathbf{y}_i = \mathbf{R}\mathbf{B}\mathbf{P}_i + \mathbf{R}\overline{\mathbf{X}}_i + \boldsymbol{w}_i & (7.28b) \end{cases}$$

where the observation is $\mathbf{y}_i$, and the new state is $\mathbf{P}_i$. A sequential implementation of the Kalman Filter to Eqs. (7.26) and (7.28) can give the state $\mathbf{X}_i$ and input force $\mathbf{P}_i$. This procedure was named DKF (Azam et al., 2015), and can be described as follows:

1. Initialization of the state and input force at t_0

Estimation of the initial state $\overline{\mathbf{X}}_0$ and input force value $\widehat{\mathbf{P}}_0$ and their corresponding covariance matrices $\mathbf{G}_{\mathbf{0}}^{\boldsymbol{x}}$ and $\mathbf{G}_{\mathbf{0}}^{\boldsymbol{p}}$

2. For each time instant t_i, ($i = 1, \dots, N_t$)

2.1 Prediction stage for the input

Evolution of the input and prediction of covariance input with

$$\mathbf{P}_i^- = \mathbf{P}_{i-1}; \qquad \mathbf{G}_i^{p-} = \mathbf{G}_{i-1}^{p} + \boldsymbol{Q}^{p}$$

2.2 Update stage for the input

Kalman gain for input with

$$\mathbf{K}_i^{p} = \mathbf{G}_i^{p-}\mathbf{J}^{T}\left(\mathbf{J}\mathbf{G}_i^{p-}\mathbf{J}^{T} + \boldsymbol{Q}^{y}\right)^{-1}$$

where $\mathbf{J} = \mathbf{RB}$

Improved predictions of input with

$$\widehat{\mathbf{P}}_i = \mathbf{P}_i^- + \mathbf{K}_i^{p}(\mathbf{y}_i - \mathbf{J}\mathbf{P}_i - \mathbf{R}\overline{\mathbf{X}}_{i-1}); \qquad \mathbf{G}_i^{p} = \mathbf{G}_i^{p-} - \mathbf{K}_i^{p}\mathbf{J}\mathbf{G}_i^{p-}$$

2.3 Prediction stage for the state:

Evolution of state and prediction of covariance of state with

$$\overline{\mathbf{X}}_i^- = \mathbf{A}\overline{\mathbf{X}}_{i-1} + \mathbf{AB}\widehat{\mathbf{P}}_i; \qquad \mathbf{G}_i^{x-} = \mathbf{A}\mathbf{G}_{i-1}^{x}\mathbf{A} + \boldsymbol{Q}^{x}$$

2.4 Update stage for the state

Kalman gain for state

$$\mathbf{K}_i^{x} = \mathbf{G}_i^{x-}\mathbf{R}^{T}(\mathbf{R}\mathbf{G}_i^{x-}\mathbf{R}^{T} + \boldsymbol{Q}^{y})^{-1}$$

Improved predictions of state

$$\overline{\mathbf{X}}_i = \overline{\mathbf{X}}_i^- + \mathbf{K}_i^{x}(\mathbf{y}_i - \mathbf{R}\overline{\mathbf{X}}_i^- - \mathbf{J}\widehat{\mathbf{P}}_i); \qquad \mathbf{G}_i^{x} = \mathbf{G}_i^{x-} - \mathbf{K}_i^{x}\mathbf{R}\mathbf{G}_i^{x-}$$

Of note, the procedure needs *a priori* information on expected value and covariance of the state and input at time t_0. The value of the process noise $\boldsymbol{Q}^{p}$ in Eq. (7.27) must be properly chosen so that an accurate estimate of the unobserved state and the unknown input could be approximated. The process noise covariance matrices $\boldsymbol{Q}^{x}$ and $\boldsymbol{Q}^{p}$ represent the suitability of the formulated model of the system. The lower they are, the more accurate the model. The observation noise covariance $\boldsymbol{Q}^{y}$ represents the accuracy of the acquired measurements.

The vehicle model is assumed accurate and the process noise for the vehicle state is set to a small value $\boldsymbol{Q^x} = 10^{-20} \times \mathbf{I}$, where $\mathbf{I}$ is an identity matrix with dimension equal to 4 corresponding to the DOF of the vehicle system. The initial values of the covariance of the state are taken the same as for the process noise. Since the vehicle system is assumed at rest at the beginning of simulations, the expected values for the initial conditions are assumed null.

The expected value and covariance of the input force are also needed. $\boldsymbol{Q^p}$ is a tuning parameter to smooth the variation of the time history of the input. Its value significantly affects the quality of the estimated solutions (Azam et al., 2015), and it is determined as follows:

The current state update is directly related to the innovation $\mathbf{I}_{\boldsymbol{nov}}^{\boldsymbol{i}} = \mathbf{y}_i - \mathbf{R}\overline{\mathbf{X}}_{\boldsymbol{i}}^{-} - \mathbf{J}\widehat{\mathbf{P}}_{\boldsymbol{i}}$ from the Kalman filtering algorithm presented above. The innovation can be seen either as the prediction error of the state given the measurements or as a measure of the information brought by a new measurement. L-curve method is used (Aucejo et al., 2019) to calibrate the process noise for the input estimation. The optimal value $\widehat{\boldsymbol{Q}}^{\boldsymbol{p}}$ can be determined by minimising the innovation norm as,

$$\widehat{\boldsymbol{Q}}^{\boldsymbol{p}} = \underset{\boldsymbol{Q^p}}{\operatorname{argmin}} \quad \sum_{i=1}^{N_t} \left\| \mathbf{y}_i - \mathbf{R}\overline{\mathbf{X}}_{\boldsymbol{i}}^{-} - \mathbf{J}\widehat{\mathbf{P}}_{\boldsymbol{i}} \right\|_2^2 / N_t \tag{7.29}$$

7.4 Damage identification via interaction forces

The damage index α_s^j is defined as a fractional change in the *j*th elemental flexural stiffness of the bridge deck, and the damaged parameter is defined as

$$(EI)_d^j = (EI)_0^j \left(1 - \alpha_s^j\right) \qquad (0 \le \alpha_s^j \le 1, j = 1,2, \dots m) \tag{7.30}$$

where $(EI)_0^j$ is the parameter of the *j*th element when the bridge is intact.

Taking the first derivative of Eq. (7.7) with respect to the damage index α_s^j of the bridge to have

$$\boldsymbol{M}_g\ddot{\boldsymbol{S}} + \boldsymbol{C}_g\dot{\boldsymbol{S}} + \boldsymbol{K}_g\boldsymbol{S} = \overline{\boldsymbol{P}} \tag{7.31}$$

where $\ddot{\boldsymbol{S}} = [\frac{\partial \ddot{\mathbf{d}}_b}{\partial(\alpha_s^j)}; \frac{\partial \ddot{\mathbf{x}}_v}{\partial(\alpha_s^j)}]$, $\dot{\boldsymbol{S}} = [\frac{\partial \dot{\mathbf{d}}_b}{\partial(\alpha_s^j)}; \frac{\partial \dot{\mathbf{x}}_v}{\partial(\alpha_s^j)}]$, $\boldsymbol{S} = [\frac{\partial \mathbf{d}_b}{\partial(\alpha_s^j)}; \frac{\partial \mathbf{x}_v}{\partial(\alpha_s^j)}]$ are the response sensitivity matrices with respect to the damage index α_s^j; $\overline{\boldsymbol{P}} = \begin{bmatrix} \frac{-\partial K_b}{\partial(\alpha_s^j)}\mathbf{d}_b - \alpha_2\frac{-\partial K_b}{\partial(\alpha_s^j)}\dot{\mathbf{d}}_b \\ \mathbf{0} \end{bmatrix}$.

They can be obtained by solving Eq. (7.31) using Newmark integration method.

The sensitivity of the interaction $\boldsymbol{S}_f$ can be derived from Eq. (7.8) as the first partial derivative with respect to the stiffness parameters as

$$\boldsymbol{S}_f = \frac{\partial \mathbf{f}_{int}}{\partial(\alpha_s^j)} = (\mathbf{L}^T\mathbf{L})^{-1}\mathbf{L}^T\left(\mathbf{M}_v\frac{\partial \ddot{\mathbf{x}}_v}{\partial(\alpha_s^j)} + \mathbf{C}_v\frac{\partial \dot{\mathbf{x}}_v}{\partial(\alpha_s^j)} + \mathbf{K}_v\frac{\partial \mathbf{x}_v}{\partial(\alpha_s^j)}\right) \tag{7.32}$$

Zero initial values for the vector of damage index are assumed as $\boldsymbol{p_0} = \{\alpha_s^1, \alpha_s^2 \ldots, \alpha_s^m\}^T = \mathbf{0}$. The difference between the measured and the analytical interaction forces then becomes

$$\Delta\mathbf{f}_r = \mathbf{f}_m - \mathbf{f}_r \quad (r = 0,1,2,\ldots) \tag{7.33}$$

where subscript *r* denotes the value at the *rth* iteration. Quantities with subscript *r*=0 refer to the set of initial values. The vector of flexural stiffness change, $\Delta\boldsymbol{p}_r$, can be solved from the following sensitivity equation as:

$$\boldsymbol{S}_{f,r}\Delta\boldsymbol{p}_r = \Delta\mathbf{f}_r \quad (r = 0,1,2,\ldots) \tag{7.34}$$

The updated damage index vector $\boldsymbol{p}_{r+1} = \boldsymbol{p}_r + \Delta\boldsymbol{p}_r$ is calculated in the next iteration followed by the calculation on the interaction forces and sensitivity. The above process

is repeated until the identified damage index increment in the successive iteration is smaller than a predefined tolerance level.

$$\|\Delta \boldsymbol{p}_r\| < tolerance \tag{7.35}$$

where $\|\cdot\|$ is the norm of the matrix.

The set of damage index increments $\Delta \boldsymbol{p}_r$ obtained from Eq. (7.34) using a straightforward least-squares method would be unbound. Tikhonov regularization is used for optimizing the following objective function as

$$\mathrm{J}(\Delta \boldsymbol{p}_r, \boldsymbol{\lambda}_p^r) = \left\| \boldsymbol{S}_{d,r} \Delta \boldsymbol{p}_r - \Delta \mathbf{f}_r \right\|^2 + \boldsymbol{\lambda}_p^r \|\Delta \boldsymbol{p}_r\| \tag{7.36}$$

7.5 Studies on interaction force identification and surface roughness estimation

7.5.1 Numerical example

Properties of the target bridge model studied were: $L = 30\ m, \rho A = 6.0 \times 10^3\ kg/m$, $EI = 2.5 \times 10^{10} Nm^2$. The coefficients for Rayleigh damping were $\alpha_1 = 0.343$ and $\alpha_2 = 0.001$. Parameters of the vehicle were: $m_v = 17735\ \mathrm{kg}, I_v = 1.47 \times 10^5\ kgm^2, S = 4.2\ m, a1 = 0.519, a2 = 0.481,\ m_1 = 1500\ \mathrm{kg},\ k_{s1} = 2.47 \times 10^6\ N/m,\ k_{t1} = 3.74 \times 10^6\ N/m,\ c_{s1} = 3.00 \times 10^4\ N/m/s,\ c_{t1} = 0.00\ N/m/s,\ m_2 = 1000\mathrm{kg},\ k_{s2} = 4.23 \times 10^6\ N/m,\ k_{t2} = 4.60 \times 10^6\ N/m,\ c_{s2} = 4.00 \times 10^4\ N/m/s,\ c_{t2} = 0.00 N/m/s$. The bridge deck was represented by ten finite elements and acceleration responses of the moving vehicle axles were calculated as the measured signals with sampling frequency of 1000Hz. All these parameters were adopted for the following studies unless otherwise stated.

7.5.1.1 Force identification and surface roughness estimation

Figure 7.2 shows the vehicle axle responses when it is moving at 20m/s on top of the bridge deck with Class B surface roughness. The proposed method was applied for the identification of the axle forces. L-curve technique was used to determine the value of $\boldsymbol{Q^p}$. Figure 7.3 shows the mean innovation norm obtained using the acceleration time histories of the vehicle axles as list in Eq. (7.29). The optimal value of $\boldsymbol{Q^p} = 5 \times 10^{23}$ was chosen which corresponds to the minimum mean error norm.

A relative percentage error (RPE) was used to evaluate the identified results as

$$RPE = \frac{\|\boldsymbol{P}_{est} - \boldsymbol{P}_{true}\|}{\|\boldsymbol{P}_{true}\|} \times 100\% \tag{7.37}$$

where $\boldsymbol{P}_{est}\ and\ \boldsymbol{P}_{true}$ are the estimated and the true time series respectively; $\|\cdot\|$ is the norm of vector. Figure 7.4 (a) and (b) show the identified interaction forces and the road surface roughness, respectively. The results matched the true curves well. It may be concluded that the proposed strategy is able to identify the interaction forces and bridge surface roughness with high accuracy when no measurement noise is considered.

The effect of measurement noise was studied next. White noise was added to the calculated acceleration responses to simulate the polluted measurement. Random noise of 2, 5 and 10% were added to the responses separately when the vehicle moved over a Class B surface roughness at a speed of 20 m/s. Figure 7.5(a) presents the identified interaction forces for the case with 5% measurement noise. Figure 7.5 (b) and (c) show the identified bridge surface roughness and its PSD respectively. The RPE for the identified forces and road surface roughness are given in Table 7.1. The identified surface roughness deviated from the true values. The PSDs of the identified road profile in Figure 7.5(c) shows that the discrepancies mainly exist at high frequency. The measurement noise had a large effect on the identification results. It may be concluded that when the

level of measurement noise is low, *i.e.* not larger than 5%, the identified results are acceptable.

7.5.1.2 Effect of moving speed and sampling frequency

The effects of vehicle moving at the speed of 10 and 30m/s on deck with Class B road surface roughness were studied. Measurement noise of 5% was considered. Sampling frequency of 1000 and 5000Hz were used. The RPE values for the identified results are tabulated in Table 7.2. Figure 7.6 shows the identified interaction forces and bridge surface roughness when sampling frequency of 1000Hz for different vehicle speeds. Results from both the table and Figure 7.6(b) show that a higher moving speed reduces the deviation of the identified surface roughness with improved accuracy. Figure 7.7 shows that a higher sampling frequency reduces the RPE in the force identification. An inspection of Figure 7.7(a) also shows that the identified force values at the peaks and valleys using a higher sampling frequency are more accurate than those by using a lower one. The above results demonstrates that a high vehicle speed would be beneficial for a quick pavement surface inspection to reduce the traffic interruption.

7.5.2 Experimental investigation

Experimental study was conducted on the VBI test bed in the laboratory to verify the feasibility of the proposed method on the identification of interaction forces and the surface roughness. The two-axle vehicle model was used and the wireless sensors were installed above the vehicle axles. The vehicle was simplified as a two-degree-of-freedom model with mass of $m_v = 4.9\ kg$. The estimated rotational inertia of the vehicle body was $I_v = 0.06 kgm^2$ and the stiffnesses of the vehicle axles were $k_{s1} = k_{s2} = 1.3 \times$

$10^5 N/m$. These values were estimated from modal test on the vehicle. The wireless sensory system was setup to measure the vehicle responses during its moving over the beam. The sampling frequency for the measurement was 500 Hz.

Plastic strips with three levels of thicknesses were attached to the surface of the beam as shown in Figure 7.8 to simulate bumps on the road. The thickness and locations of the strips are summarized in Table 7.3. The '1/8' in the table denotes the location at 1/8 length of the first main span from its left support.

The measured responses when the moving vehicle was on the main beam with a speed 0.35 m/s are given in Figure 7.9. The proposed method was used for force identification using the vehicle model described above with $\boldsymbol{Q^p} = 1 \times 10^{20}$. The dynamic interaction forces can also be calculated directly by using the acceleration responses and integration technique due to the simplicity of vehicle model. Both the identified and calculated dynamic interaction forces are presented in Figure 7.10(a). The two sets of forces match each other quite well. The spectra of the identified force in Figure 7.10(b) has two dominant peaks at around 29.4 and 36.7 Hz corresponding to the two modal frequencies of the vehicle model. The apparent profile is defined as the profile of displacement at the contact point between the tire and the bridge surface (ElHattab et al., 2017) and it is calculated using the interaction forces and identified displacement at top of the two axles. A band pass filter with cut-off frequencies from 1.0 to 100.0 Hz was used to process the apparent profile to estimate the beam surface unevenness. The identified unevenness from two vehicle axles are shown in Figure 7.11. The locations of the installed plastic strips were all identified, and the values are presented in presented in Table 7.3. The identified results from the front and rear axles are highly consistent. The values from the front axle are generally larger than those from the rear axle.

7.6 Studies on damage detection

The same vehicle-bridge interaction system for numerical studies in Section 7.5.1 was considered, and local damages were introduced into the finite elements of the bridge model. Two damage cases were studied with (a) single damage scenario - 20% damage is introduced in Element 2, *i.e.*, $\alpha_s^2 = 0.20$; and (b) multiple damage case - Elements 4 and 8 are assumed to have damage with $\alpha_s^4 = 0.15, \alpha_s^8 = 0.20$. The algorithm described in Section 7.4 is adopted for the identification with the tolerance in Eq. (7.35) equals to 5×10^{-4} in the numerical example.

7.6.1 Damage detection with a smooth bridge surface

Measurement noise of 5% was added into the calculated vehicle responses. The cases with three different vehicle moving speeds, *i.e.*, 10, 20 and 30 m/s, were studied. The identified damage detection results in Figure 7.12 show that the damage location were identified correctly for all vehicle speeds. The identified damage extents were very close to the true values. However, a lower vehicle speed provided better identification results when the bridge surface is smooth.

To further study the effect of measurement noise on the identification, another example was studied with 10% measurement noise and 20 m/s moving speed. The identified results were compared with those for 5% measurement noise, as shown in Figure 7.13. The damage location and extent were accurately identified. It may be concluded that when the bridge surface is smooth, the proposed method can be used for drive-by bridge damage detection with a high vehicle speed using noisy vehicle axle responses.

7.6.2 Damage detection when the bridge surface roughness is known

The proposed method is used for the damage detection with the identified forces. In Section 7.5.1.1, results showed that the measurement noise effect was significant to the identification. Therefore, this this study, a higher sampling rate of 5000 Hz was used. The Classes A and B bridge surface roughness were adopted. Measurement noise of 5% and a moving speed of 20 m/s were considered. The identified results are shown in Figure 7.14. When the bridge surface roughness is known, the interaction forces obtained from the vehicle axle responses with the proposed method can yield damage location and extent with acceptable accuracy. Some elements are, however, falsely identified with small stiffness variation which is due to the effect of measurement noise. The proposed method can provide reliable information on potential damage conditions of the structure when the bridge surface roughness is known.

7.6.3 Damage detection using the identified bridge surface roughness

When both the interaction forces and vehicle displacements are identified from vehicle axle responses, the roughness can be calculated from the known vehicle-bridge system. The moving speed 30m/s and the sampling frequency 5000 Hz were adopted. The damage detection results considering different measurement noise levels are shown in Figure 7.15. When the measurement noise is 2%, the identified damage location and extent were acceptable. For a higher noise level of 5%, a few false detections were noted with the designated damaged elements identified with much higher possibility of damage. When the noise level reaches 10%, the identified damage information were not reliable for the single damage case. The measurement noise is noted to have large effect on the surface roughness estimation leading to an inaccurate damage identification. The advanced signal

pre-processing is needed to reduce the measurement noise when the proposed method is applied in the practice.

7.7 Summary

Vehicle-bridge interaction force identification and bridge damage detection using vehicle responses are two powerful techniques with great potential for widespread practical use. Both require only instrumentation on the moving vehicle. A state space model of the vehicle based on Newmark-β formulation was derived in this chapter. DKF was used to identify the interaction forces between the vehicle and bridge with only the vehicle axle responses. The bridge surface roughness can be calculated using the interaction forces and bridge parameters. A method was proposed to estimate the forces and road surface roughness with measurement noise in the responses. The interaction forces obtained can then be used for bridge damage detection based on the interaction force sensitivity analysis. Numerical examples showed that the damage index of the bridge deck can be identified from the interaction forces effectively when the measurement noise was less than 5%. Experimental investigation was also conducted to verify the feasibility of the proposed method for interaction force and bridge surface roughness estimation. Findings emphasize that measurement noise in the responses must be reduced before using the proposed method for damage detection in practice.

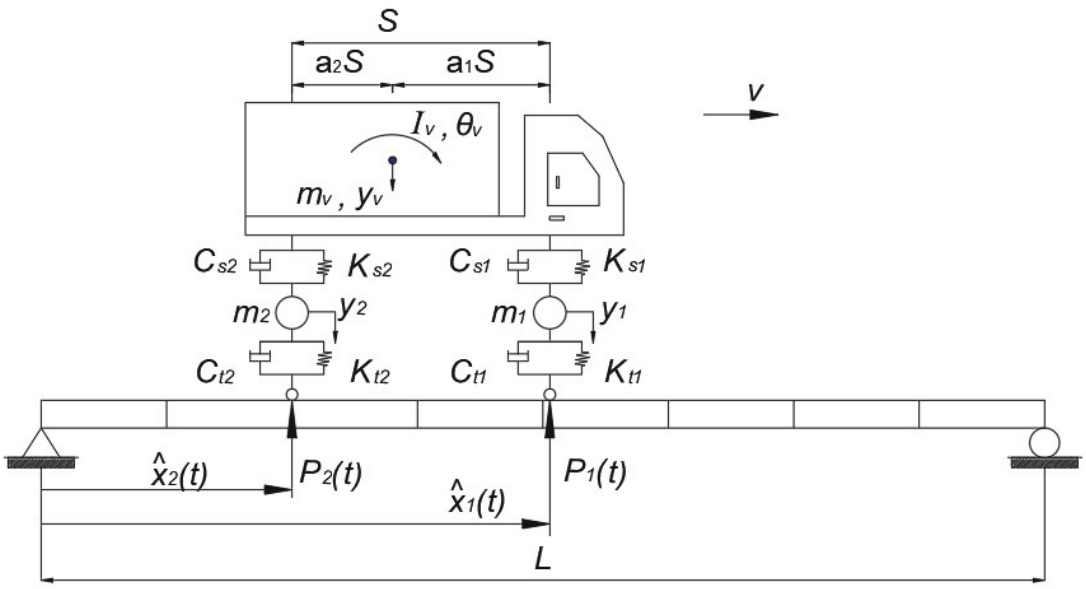

Figure 7.1 Vehicle-bridge interaction model

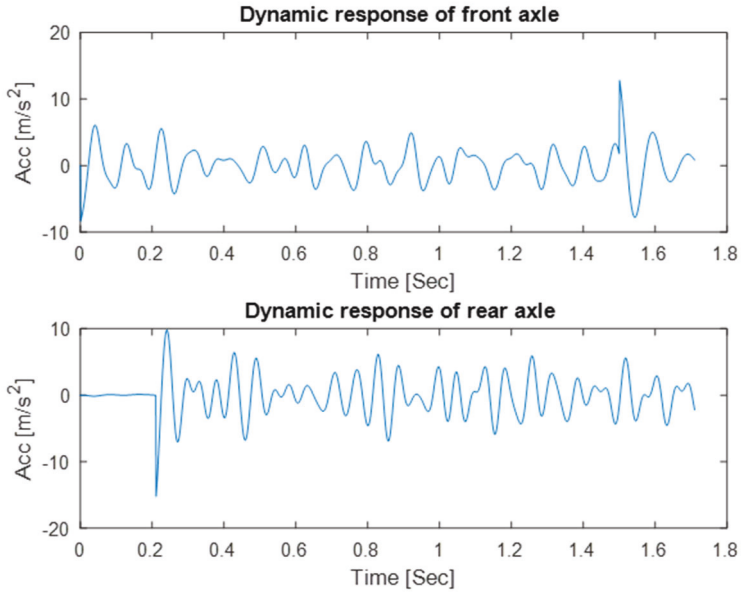

Figure 7.2 Axles responses

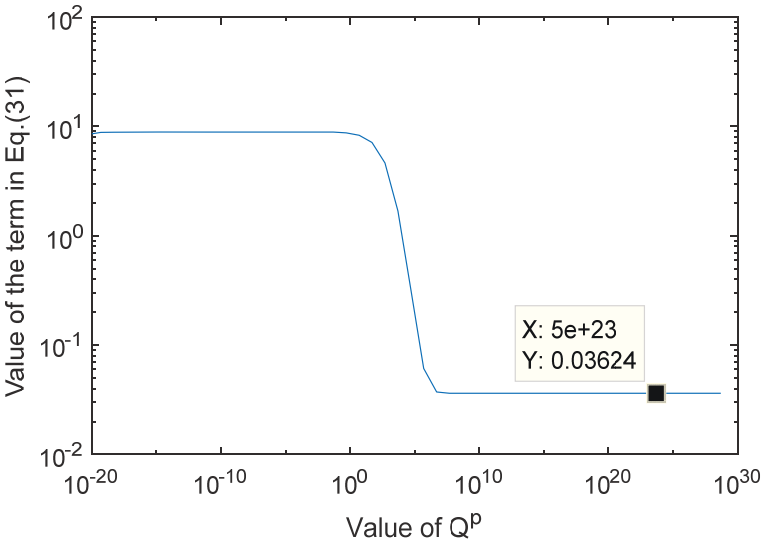

Figure 7.3 L-curve

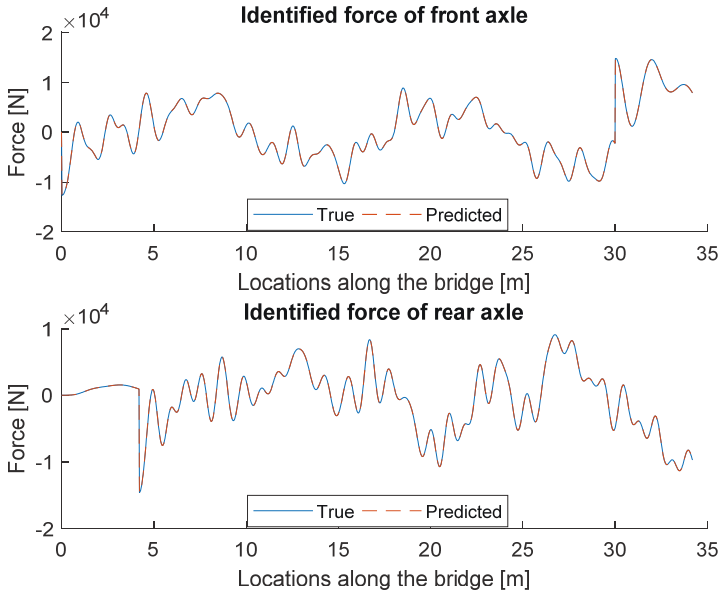

(a) Identified interaction forces

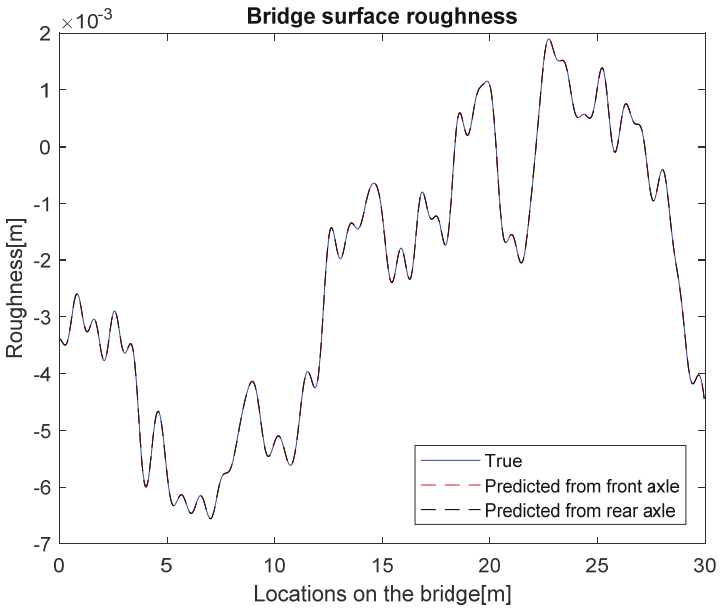

(b) Identified bridge surface roughness

Figure 7.4 Identified results with Class B roughness and v=20m/s

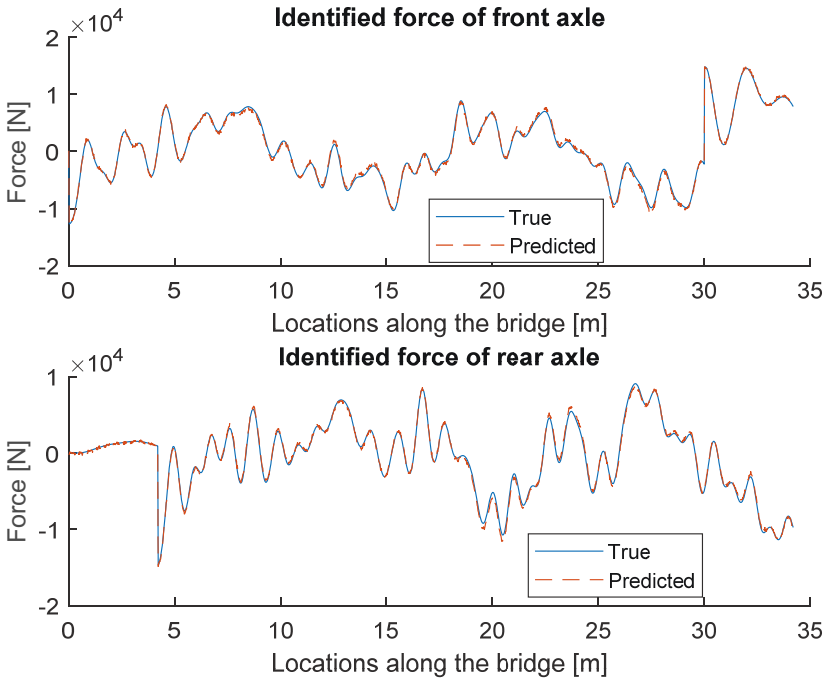

(a) Identified interacting axle forces when 5% measurement noise is added

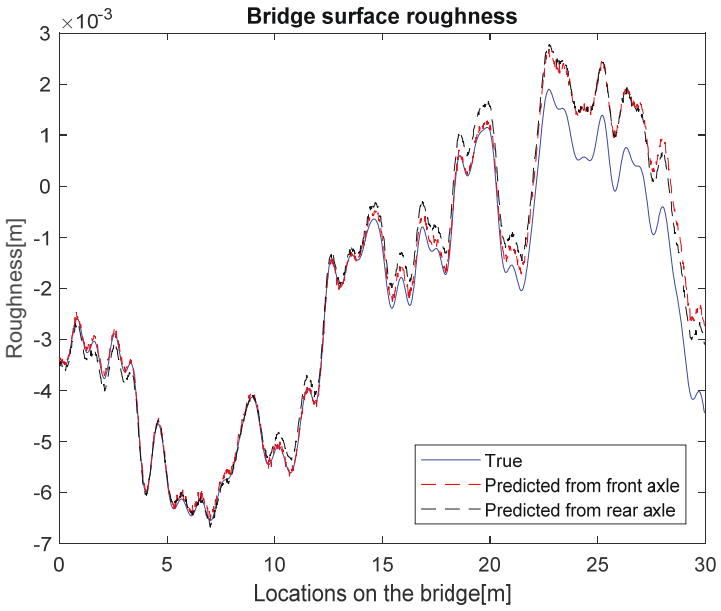

(b) Identified bridge surface roughness

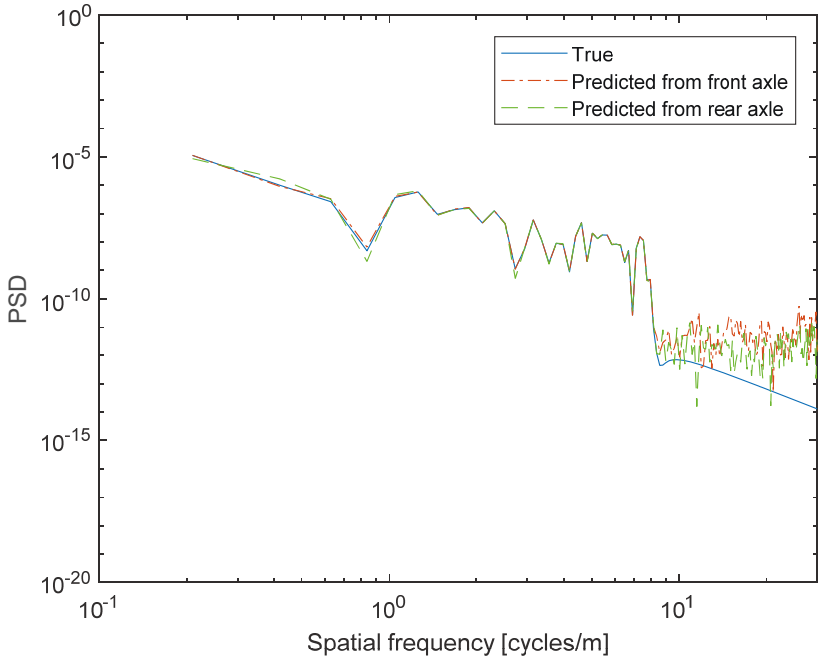

(c) PSD of surface roughness

Figure 7.5 Identified forces and surface roughness with 5% measurement noise

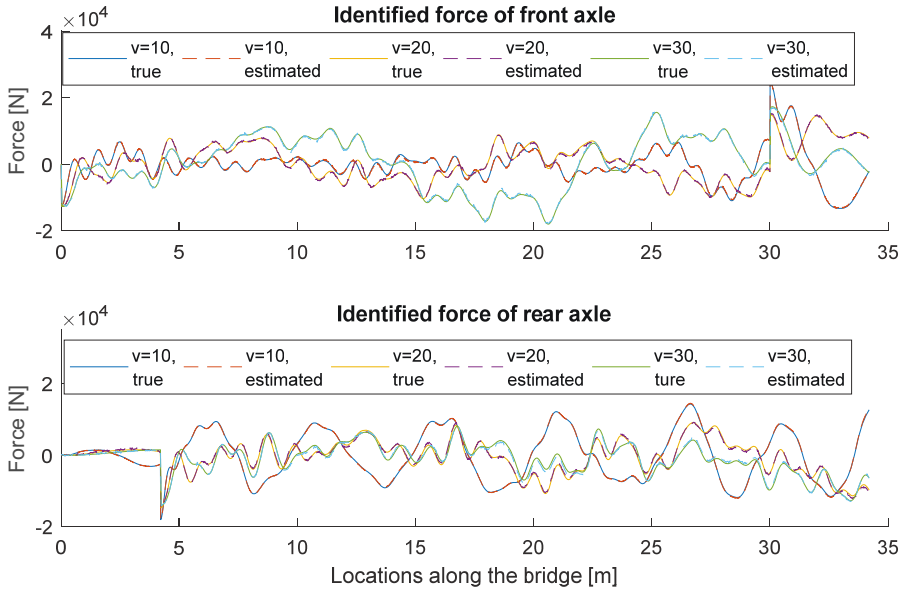

(a) Identified interaction forces

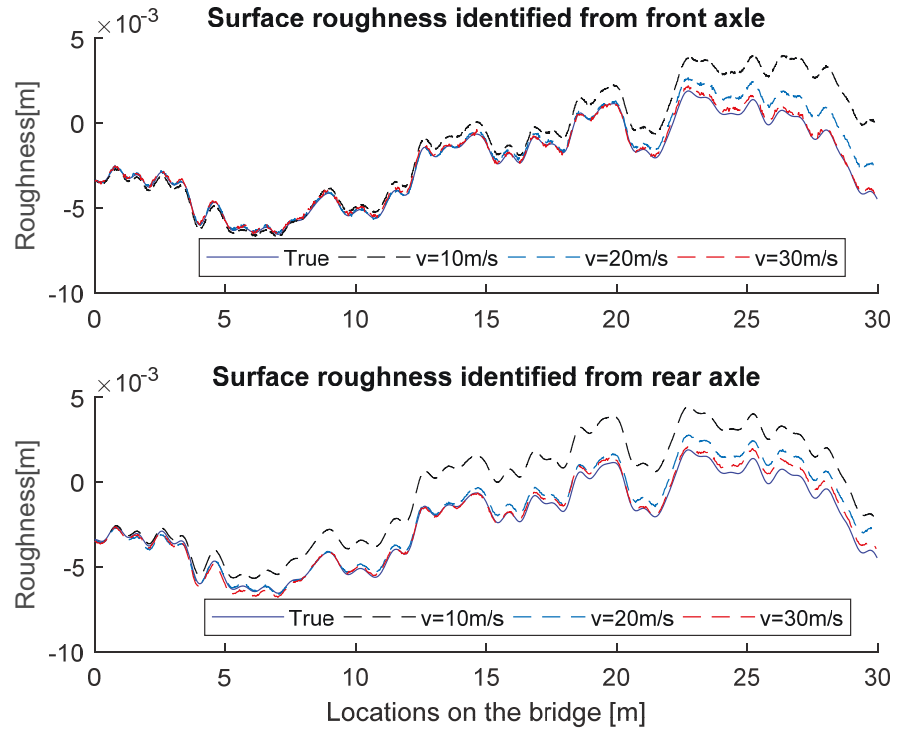

(b) Identified bridge surface roughness

Figure 7.6 Identified results considering different moving speed with Fs=1000Hz

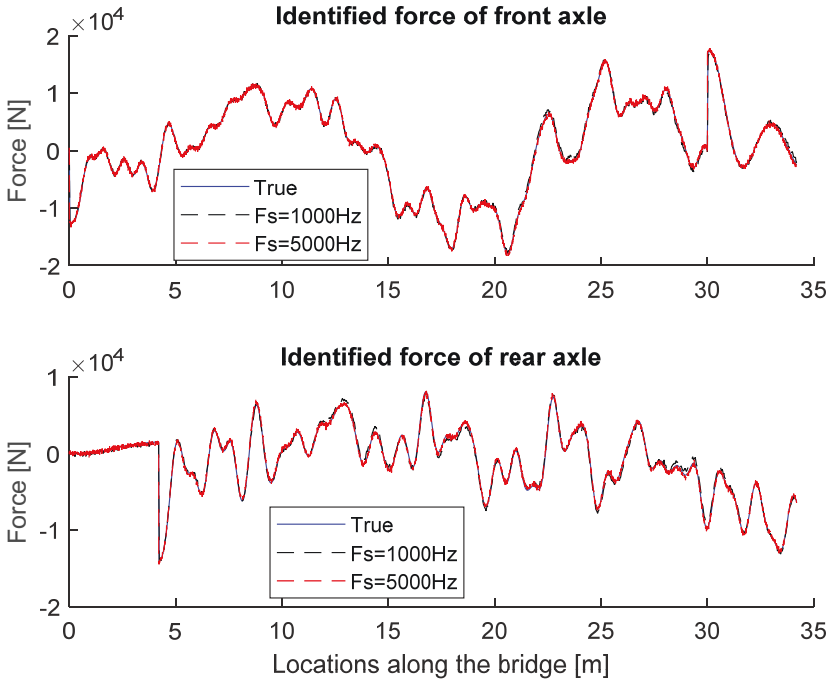

(a) Identified interaction forces

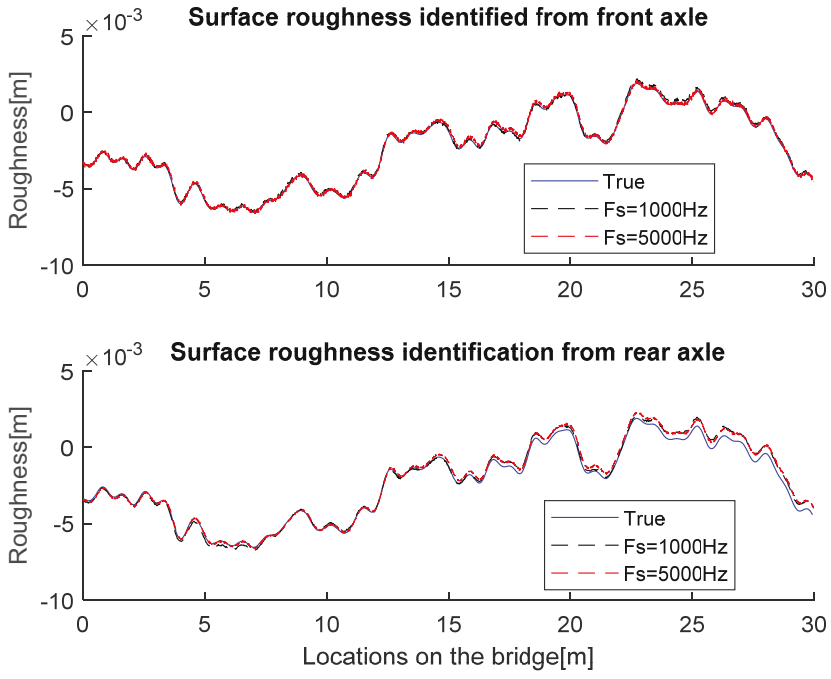

(b) Identified bridge surface roughness

Figure 7.7 Identified results considering different sampling frequency with v=30m/s

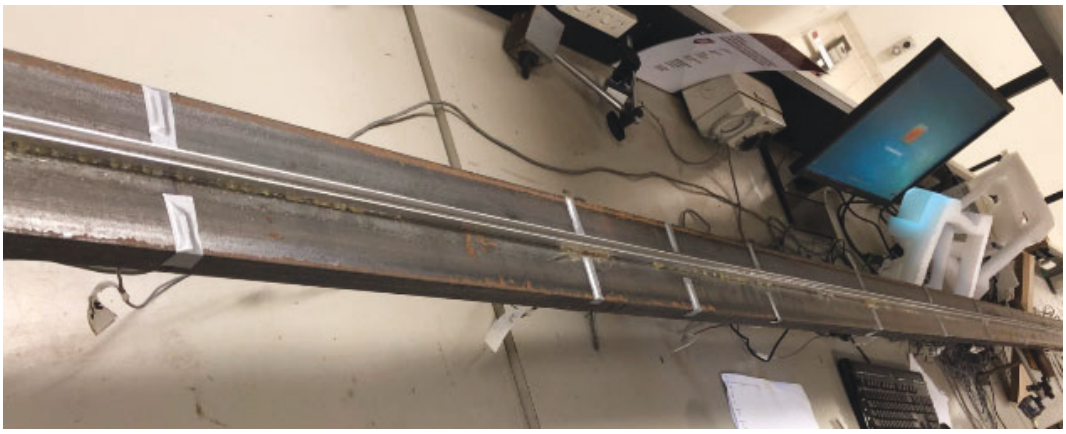

Figure 7.8 The installation of plastic strip to simulate bumps on the bridge

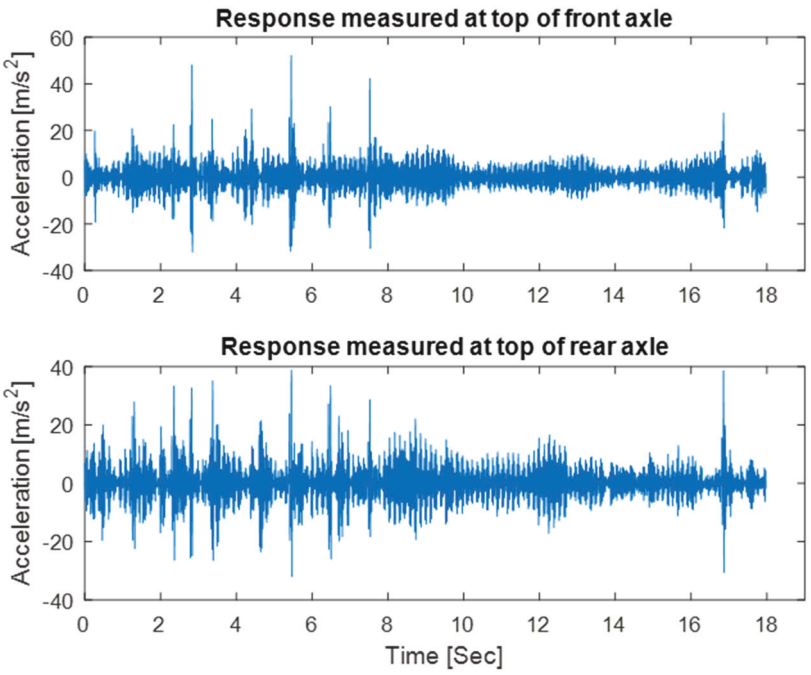

Figure 7.9 Measured responses from wireless sensors on the vehicle

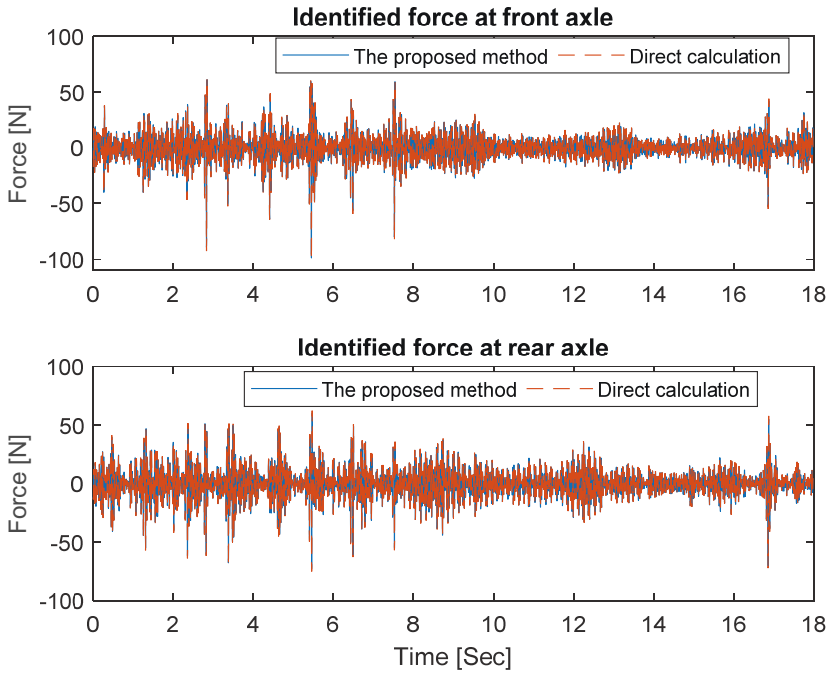

(a) Identified forces

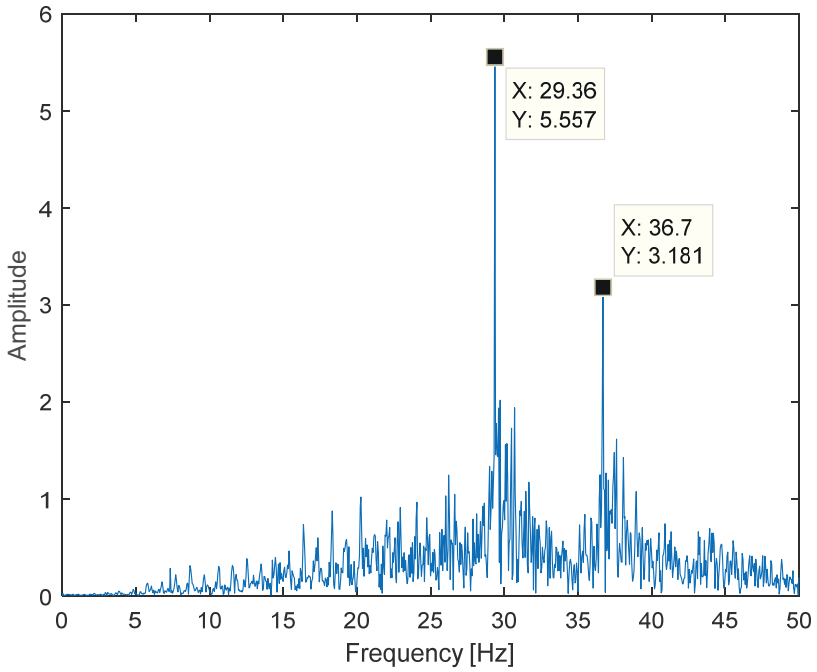

(b) Spectrum of the identified force at front axle

Figure 7.10 Identified interaction forces and the spectra at two axles

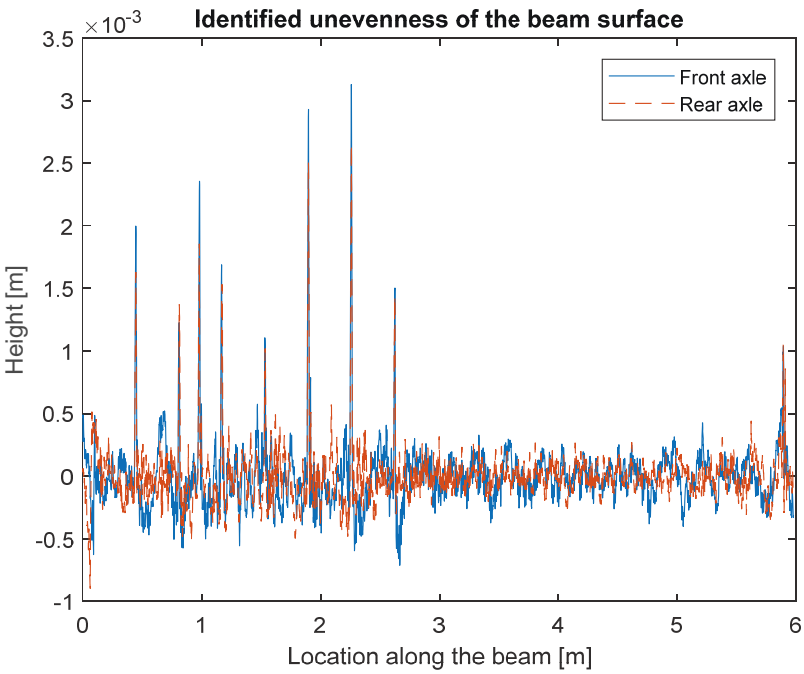

Figure 7.11 Identified unevenness on the beam surface

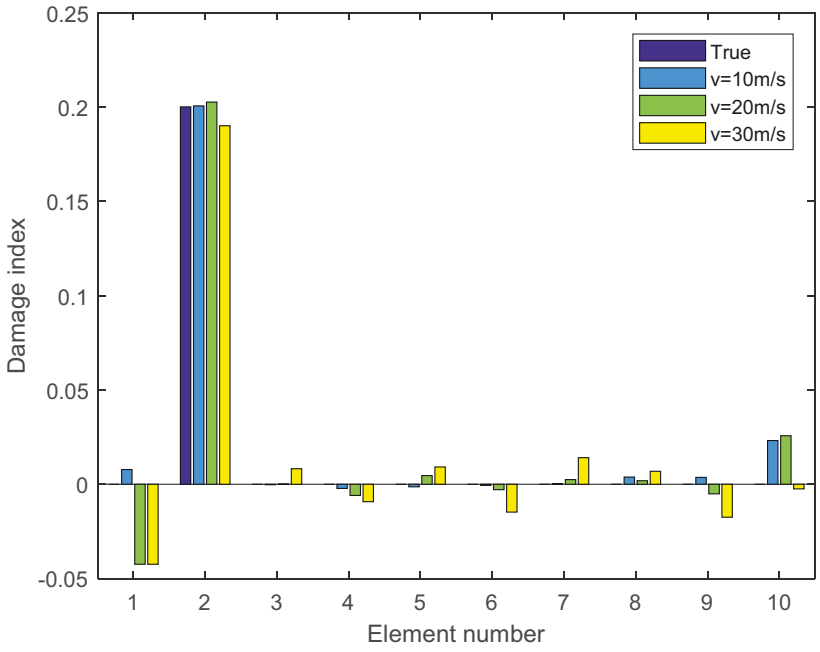

(a) Single damage case

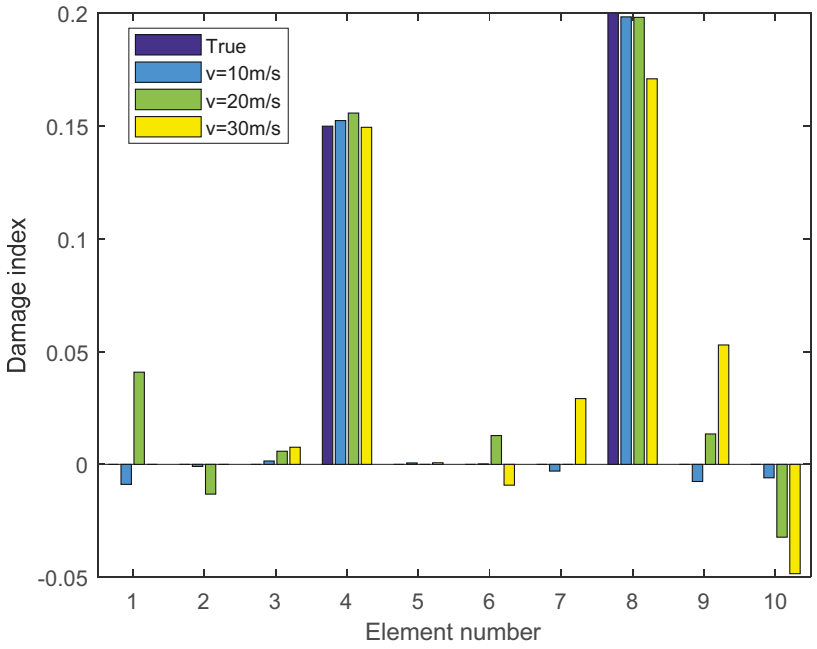

(b) Multiple damage case

Figure 7.12 Damage detection results considering different vehicle speed when bridge surface is smooth

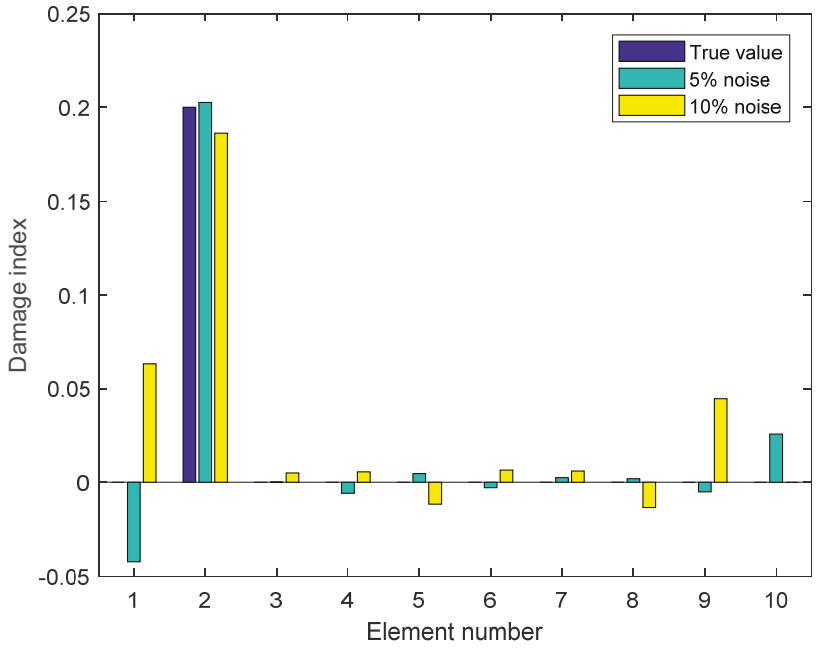

(a) Single damage case

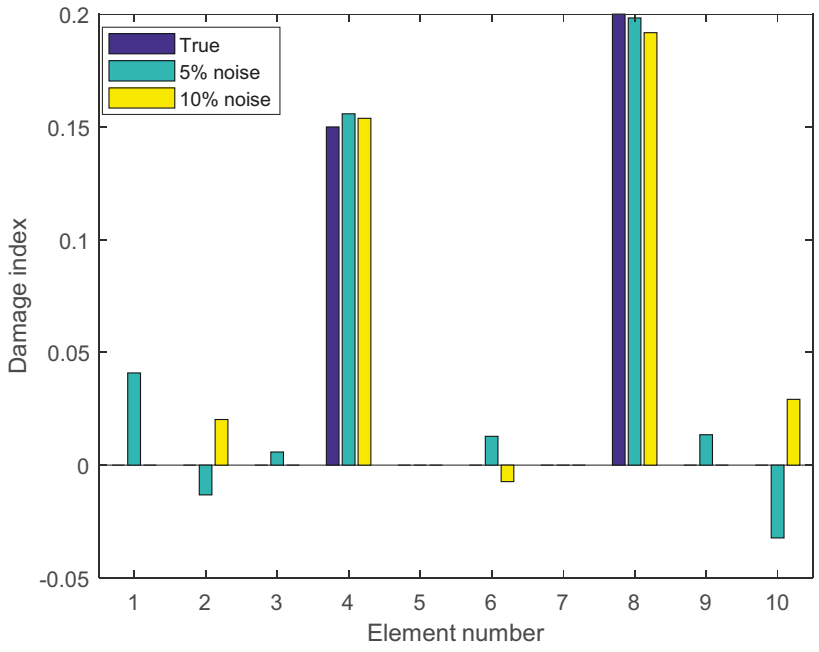

(b) Multiple damage case

Figure 7.13 Damage detection results considering different measurement noise when bridge surface is smooth

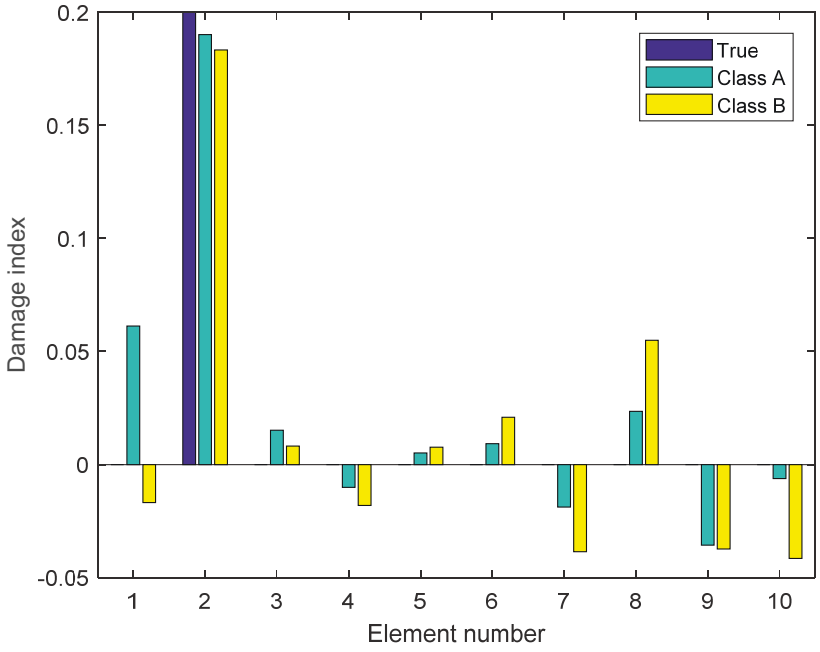

(a) Single damage case

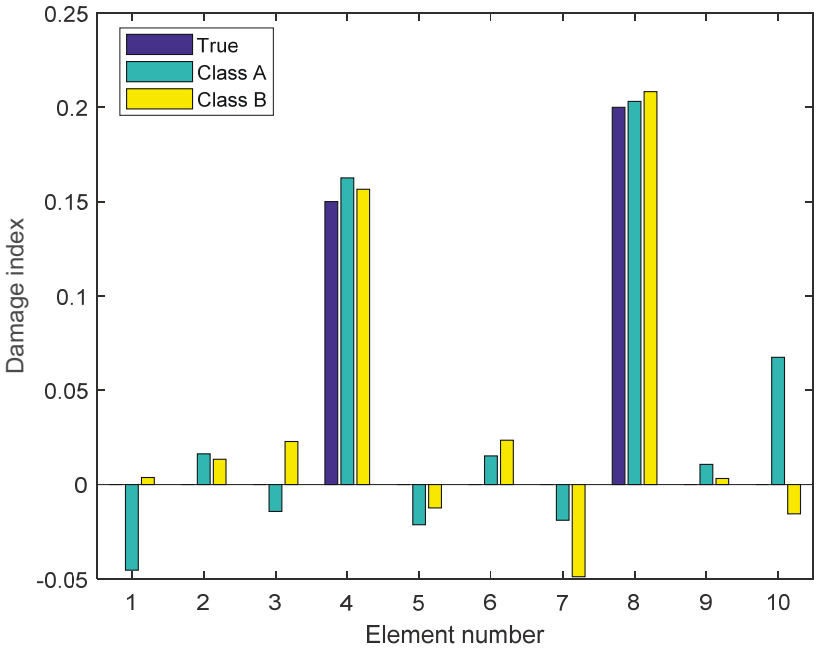

(b) Multiple damage case

Figure 7.14 Damage detection results when road surface roughness is known

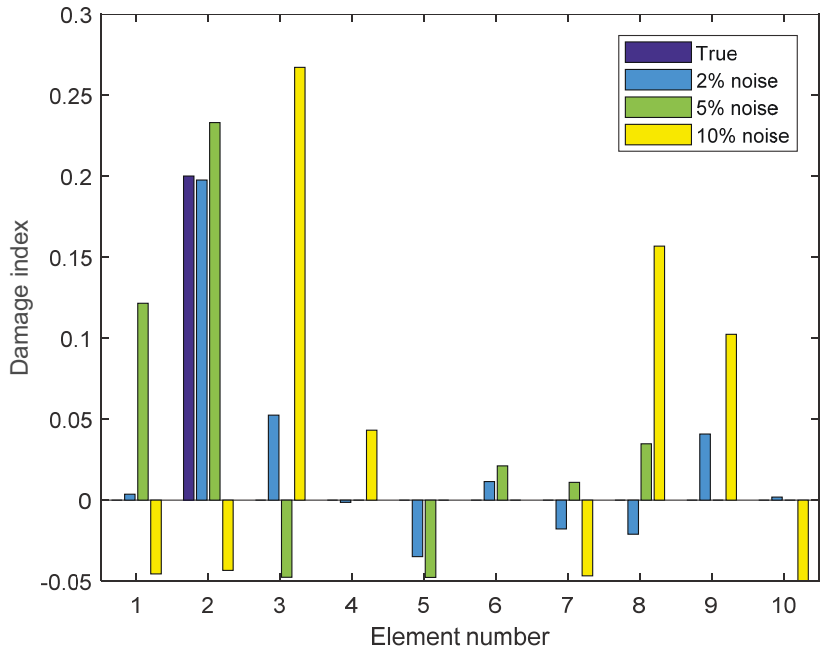

(a) Single damage case

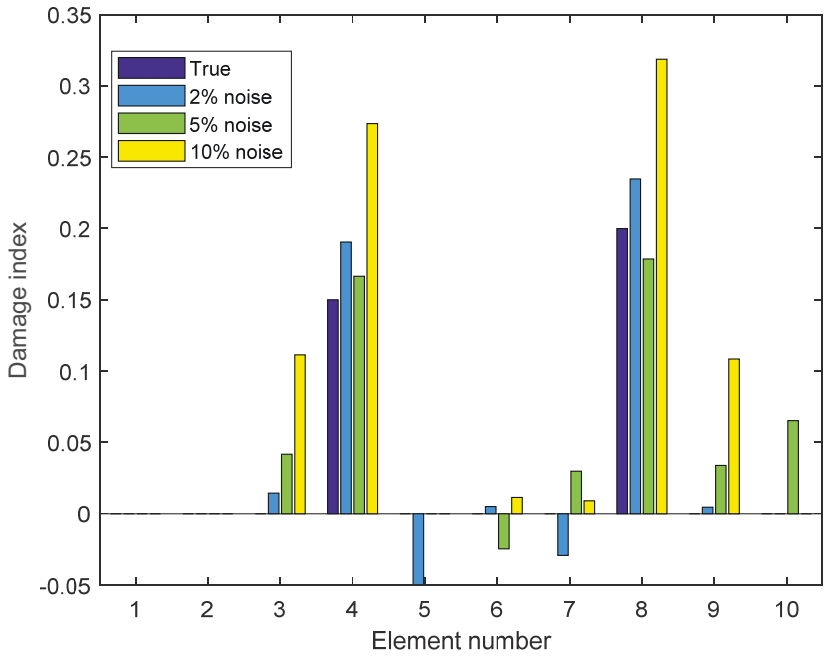

(b) Multiple damage case

Figure 7.15 Damage detection results when road surface roughness is unknown

Table 7.1 RPE of the identified results considering different measurement noise (%)

Noise level (%)	Forces		Roughness	
	Front	Rear	Front	Rear
0	0.00	0.00	2.61	2.61
2	2.06	3.25	6.86	10.41
5	5.88	6.79	18.30	17.98
10	11.75	13.59	36.3	35.72

Table 7.2 RPE of the identified results considering different vehicle speed (%)

	Sampling frequency=1000 Hz				Sampling frequency=5000Hz			
Moving speed (m/s)	Forces		Roughness		Forces		Roughness	
	Front	Rear	Front	Rear	Front	Rear	Front	Rear
10	4.78	2.79	52.97	52.36	3.07	1.72	34.81	40.84
20	5.88	6.79	18.30	17.98	4.04	4.74	13.74	27.71
30	5.12	8.98	5.23	8.68	4.14	5.96	4.91	2.91

Table 7.3 The experimental setup of the beam surface unevenness and the identification results

Experimental setup								
Label	1	2	3	4	5	6	7	8
Locations	1/8	1/4	5/16	3/8	1/2	5/8	3/4	7/8
Height (mm)	1.50	1.50	1.50	1.50	1.00	3.00	3.00	1.50
Identification results (mm)								
For front axle	2.00	1.23	2.36	1.69	1.04	2.93	3.13	1.50
For rear axle	1.63	1.37	1.87	1.53	1.02	2.50	2.66	1.44

CHAPTER 8 Further verification with an in-situ cable-stayed bridge

8.1 Overview

To examine the feasibility of the proposed methods in practical application, some methods are further verified using responses measured from a vehicle-bridge system in the field. For the indirect bridge mode shape identification using proposed STSSI method (Chapter 3), a stationary and a moving sensor are necessary and the method is applicable only when the bridge surface is not too rough. For the drive-by bridge damage detection, both the exact vehicle and bridge finite element model are required and it is also difficult to introduce damage to the in-situ bridge. Therefore, only the methods proposed in Chapters 4 and 5 are verified with the in-situ bridge. The drive-by bridge modal identification using SSA-BSS was applied to identify the modal frequencies of the actual bridge. Time-frequency analysis was performed to further investigate the time-varying characteristics of the bridge frequencies due to the vehicle-bridge interaction.

8.2 The instrumented cable-stayed bridge

8.2.1 The bridge and its measurement system

The test structure is a single lane highway bridge with a span of 46 m and a width of 6m (as shown in Figure 8.1). The composite bridge deck has four steel beams and a thickness of reinforced concrete slab of 160 mm. The bridge connects two campuses of the Western Sydney University, the South and North Campus. A long-term monitoring system was installed on the bridge. A HBM Quantum-X data logger (HBM, Darmstadt, Germany) with an embedded PC are used for signal conditioning and data logging. This hardware

combined instrument excitation, voltage regulation, digitization, anti-aliasing filters, and data logging. The logging software was Catman Version 5, which collected all channels at a default sample rate of 600 Hz (Sun et al., 2017). The dynamic monitoring system continuously recorded the vibration response of the bridge and produced a file with an acceleration time series every 10 minutes that are continuously transferred over a 4G cellular network to a database. A dense array of strain gauges (installed on each cable of the bridge deck) and accelerometers (total number of 24) were installed under the bridge deck. These were synchronized in time to measure structural responses. Figure 8.1 (b) and (c) show the sensor locations used for this study.

8.2.2 Bridge modal identification

Figure 8.2 (a) illustrates a typical acceleration time signal obtained from a 10-minute file from Channel A11 measured on 12 June 2019. A typical ambient part of the response (10-second), when there was no vehicle traveling over the bridge and a typical part of free vibration response once a moving vehicle exiting the bridge are shown in Figure 8.11 (b). From the response spectrum, it was observed that high structure vibration modes were excited due to the moving vehicle and most of the peaks are within 10 Hz. Thus, the study mainly focused on the frequencies that are smaller than 10 Hz. There were 22 accelerometers placed under the deck at the intersection of the transverse girders and the beams. While sensors A2 and A3 are installed under the beams between two transverse girders (see Figure 8.1(c)). Bridge modal analysis was conducted using the responses measured from all the accelerometers except A2 and A3. Bridge responses measured under ambient excitation and after a passing vehicle were analyzed separately. Modal analysis toolbox reported by Chang et al. (2012) was used for the identification of the bridge modal parameters with Auto-regressive technique. Figure 8.3 (a) and (b) show the

identified bridge vibration modes. Only one bridge vibration mode was identified during ambient excitation, whereas six vibration modes were identified during excitation of a passing vehicle. The first two bridge modal frequencies from modal test were 2.03 and 3.72 Hz, respectively. A finite element model of this cable-stayed bridge was established in ABQAUS by Alamdari et al. (2019). The predicted frequencies of the first two modes from the numerical model were 2.06 and 3.43 Hz, respectively. The first bridge modal frequency from the test and the numerical model were very close with a discrepancy of only 1.48%. Meanwhile, for the second mode, a larger discrepancy of 7.80% was observed between the test and simulated results.

8.3 The instrumented vehicle

For the drive-by bridge modal identification, a Hyundai Tucson 2006 model with a gross weight of 1.5 t was used as the test vehicle. A BeanDevice AX-3D wireless accelerometer was installed on the top surface of the dashboard as shown in Figure 8.4. Another wireless sensor was installed on the floor of left back seat. The modal test was conducted when the vehicle was not started on a flat ground under ambient excitation. Figure 8.5 shows the responses of the two wireless sensors for the modal test with a duration 30 seconds. SSI method was used to analyse the responses and the first three vehicle frequencies were considered. Ten sets of the response measurement from two sensors were analyzed to extract the vehicle frequencies. The stable figure of the response is shown in Figure 8.6. The identified vehicle frequencies from each set of responses are tabulated in Table 8.1. The mean values of the test results at 1.02, 1.58 and 2.31Hz were regarded as the first three vehicle frequencies, respectively.

8.4 Drive-by bridge modal identification using vehicle responses from wireless sensor

8.4.1 Vehicle responses when it is idling

Vibration at the sensor location on top of the dashboard was measured when the vehicle stopped on the road and on the bridge deck with its engine idling, respectively. Figure 8.7 shows the measured responses and the spectra. In the spectrum, two dominant peaks were visible at 17.5 and 23.3 Hz. These are the frequencies of the idle engine. When the vehicle stopped on the bridge deck, it was seen from the response spectrum that the dynamic information of the first bridge vibration mode was captured by the instrumented vehicle.

8.4.2 Drive-by bridge modal identification using SSA-BSS

The dynamic responses measured from the wireless sensor when the vehicle passes the bridge at different speeds, *i.e.*, 10, 20 and 30 km/h, were analyzed using SSA-BSS. Figure 8.8 shows the dynamic response measurement and the spectrum when vehicle passes the bridge with a speed of 10km/h. The spectrum clearly shows that besides the three vehicle frequencies V1, V2 and V3, the first bridge modal frequency B1 was distinguishable. The proposed method was used to analyse the response with window length of 1000. Figure 8.9 shows the extracted response components when the vehicle speed is 10km/h. The components can be extracted from a set of response measurements and the frequencies were identified from the components. The identified frequencies for different vehicle speeds are tabulated in Table 8.2. The identified values matched well with those obtained from the modal tests with the exception of the case when vehicle speed was 30 km/h. This was possibly because the speed of the vehicle was too high.

8.5 Time-varying characteristics of bridge modal frequency due to vehicle-bridge interaction

To study of the time-frequency characteristics of the vehicle-bridge interaction system, a truck with a gross weight of 25 t is used as shown in Figure 8.10. The vehicle-induced dynamic responses of the bridge were evaluated.

8.5.1 The case with different traffic conditions on the bridge

Responses from sensor A10 under three different traffic conditions were measured. Case 1 had no vehicle on the bridge, Case 2 had one vehicle moving on the bridge from North to South and Case 3 had one vehicle moving on the bridge from South to North. There was a roundabout at the southern entrance of the bridge. The acceleration responses and the spectra are shown in Figure 8.11. When there was no traffic on the bridge, only the first bridge frequency can be identified in the response spectrum. When there were moving vehicles, higher bridge vibration modes were prominent due to the vehicular excitations. The TF analysis of the responses under different traffic conditions are presented in Figure 8.12. The IF trajectory of the first bridge vibration mode show little variation in the absence of traffic. Meanwhile, the IF trajectories corresponding to the bridge vibration modes exhibit large variations when there was traffic. Of note, the frequency variation were lower when vehicles moved from South to North than when they moved from North to South. This may be due to a lower vehicle speed when the vehicle exited from roundabout at the South entrance of the bridge. Furthermore, the frequency variation for the first three bridge vibration modes were very small, whereas the frequency of the fourth bridge vibration mode varies periodically, *i.e.*, every6 seconds.

To better understand how the cables respond to a moving vehicle, the strain measurements on the four cables at one side of the deck were assessed. The values are given in Figure 8.13. The strain increased when a vehicle was in the vicinity of the cables, and it decreased

when vehicle moves away. This suggests that the function of the cables can be simplified as vertical spring supports at the connection points with the deck. The composite effects of vehicle and cables account for the time-varying behaviors of the bridge frequencies.

8.5.2 The time-frequency analysis results from responses at different locations

The responses measured at different locations as the vehicle moved from North to South were analyzed in TF domain. Measurements from sensors A6, A10, A14 and A18 arranged in longitudinal direction were analyzed for comparison. Similar analysis on the responses from sensors A9, A10, A11 and A12 in transverse direction was also conducted. The IF trajectories of the first two bridge vibration modes from different responses are shown in Figure 8.14. The IF trajectories form sensors A6 and A10 exhibited similar trend for the first two bridge vibration modes. Of note, they were larger than those from responses measured at A14 and A18. This may be due to lower speed when the vehicle was close to the support near the South entrance. For the sensors in transverse direction, the frequency variations obtained from the responses were almost the same for the first bridge vibration mode. However, the variations were different for the second vibration mode although the trend was similar. This is possibly because the second vibration mode consists of a mixture of torsion and bending mode from the operational modal analysis.

8.6 Summary

A drive-by modal frequency identification was applied using an actual cable-stayed bridge using instrumented vehicles. The response components related to bridge and vehicle frequencies were extracted from a set of vehicle response to identify the bridge frequencies using proposed SSA-BSS. The time-varying characteristics of the bridge

frequency due to the interaction with a heavy truck was also explored. The IF trajectories extracted from bridge response by using TF analysis technique showed complex variation trends. This study demonstrates that the combined effects from the moving vehicle and the cables have a significant effect on bridge frequency identification.

(a) The photo of cable-stayed bridge

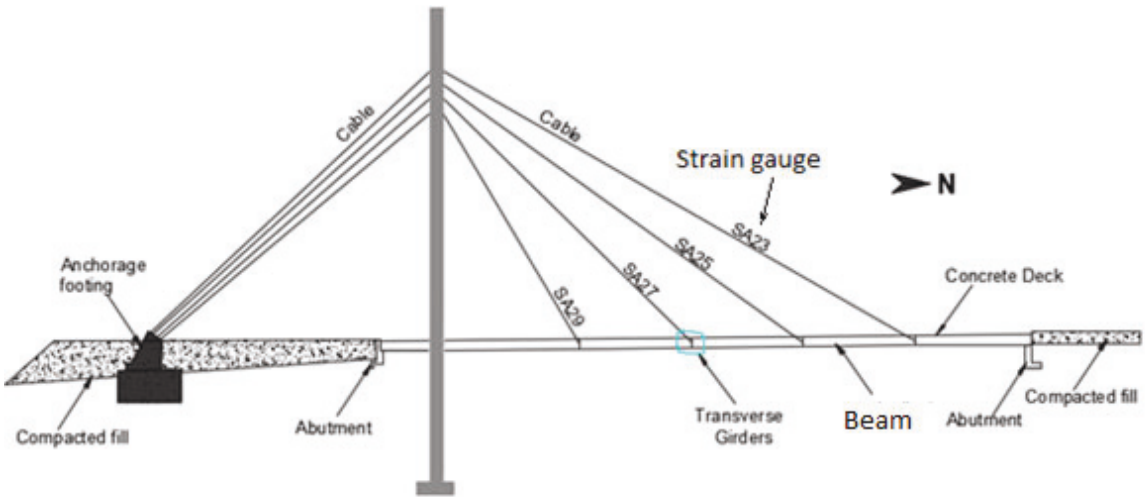

(b) The sketch of cable-stayed bridge

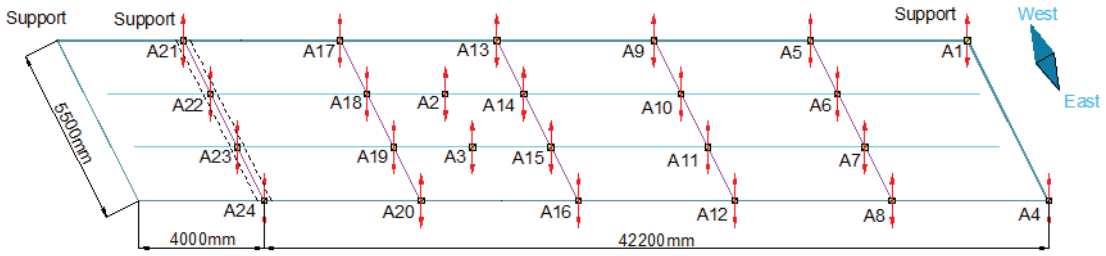

(c) Locations of accelerometers under the bridge

Figure 8.1 Instrumentation on a cable-stayed bridge in the field

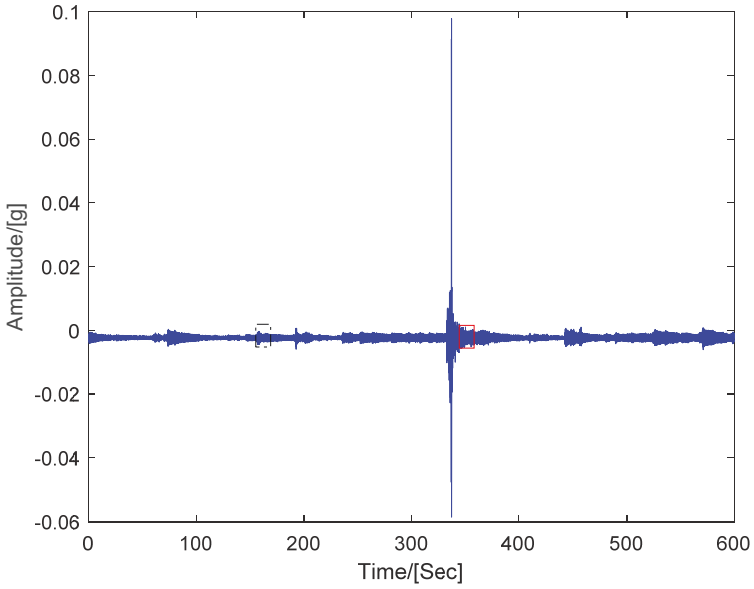

(a) A typical acceleration measurement from a 10-min file

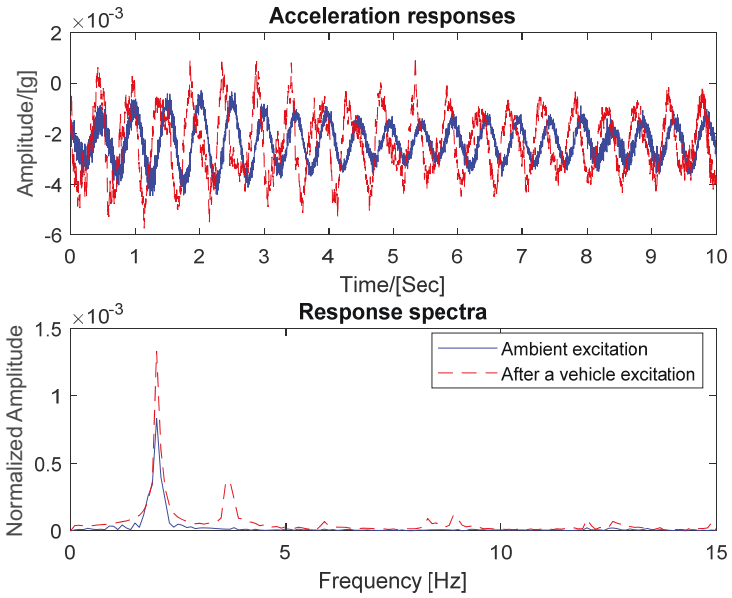

(b) Bridge response due to ambient excitation and after vehicle excitation

Figure 8.2 Bridge responses measured at Sensor A11

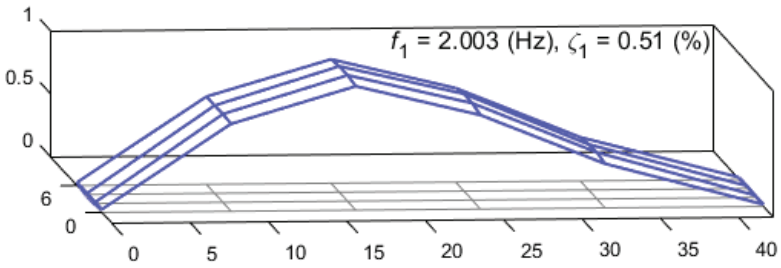

(a) Identified bridge mode under ambient excitation

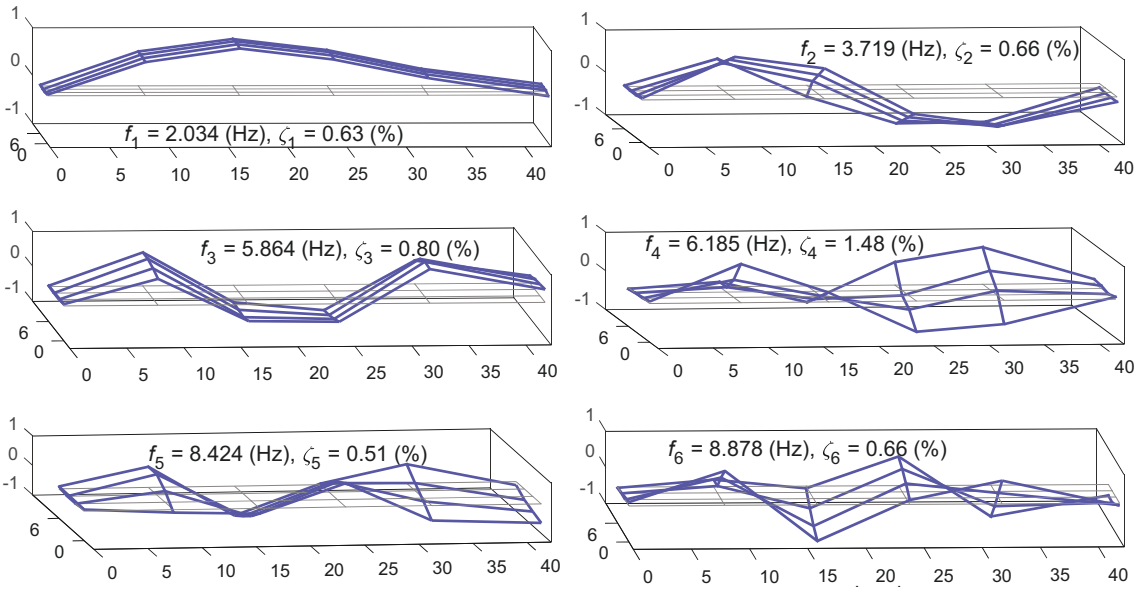

(b) Identified bridge modes after vehicle excitation

Figure 8.3 Identified bridge vibration modes under different excitations

(a) Vehicle for test (b) Vehicle instrumentation

Figure 8.4 Vehicle for test and instrumentation with wireless sensor

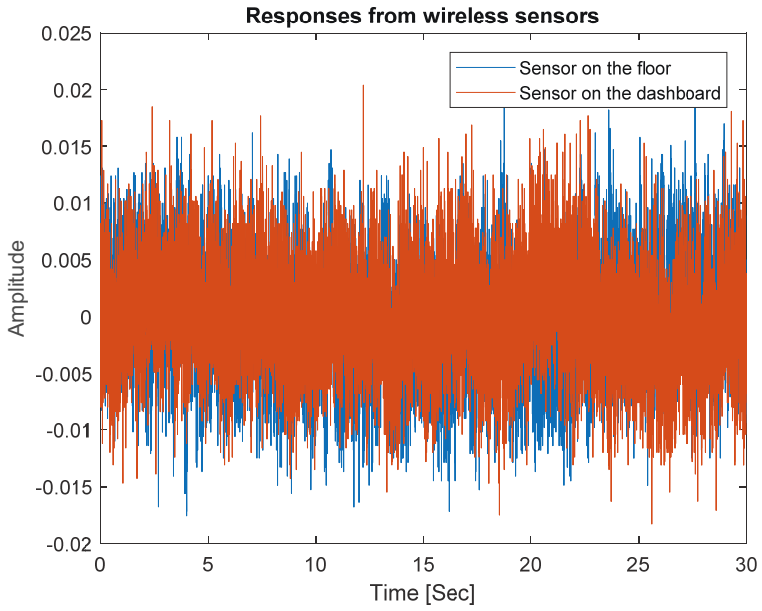

Figure 8.5 Vehicle responses for modal test

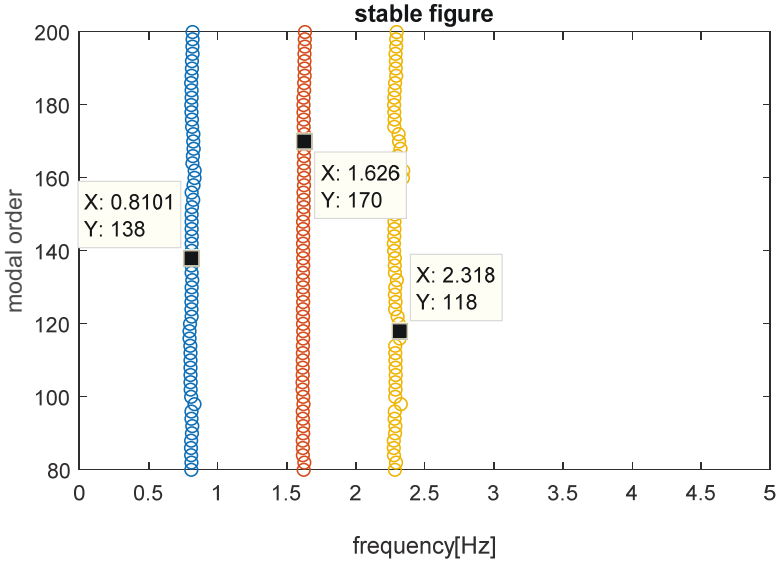

Figure 8.6 Stable figure and power spectrum of the response

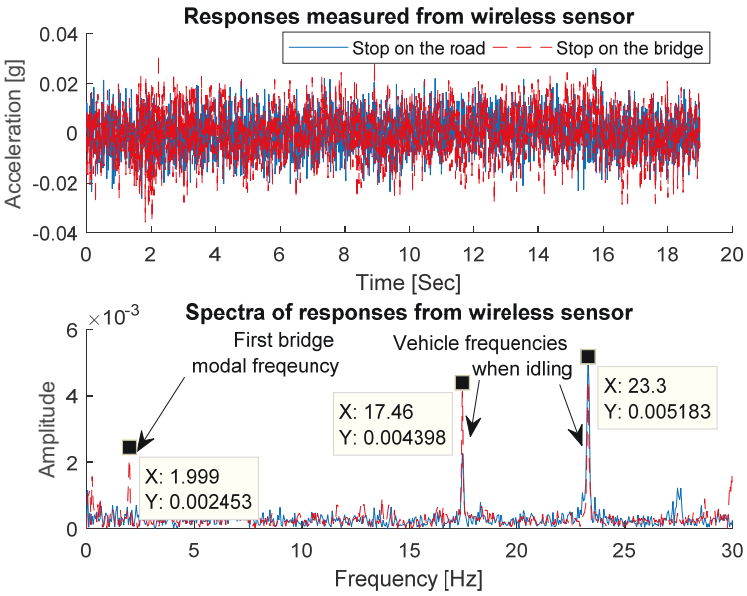

Figure 8.7 Response measurements when vehicle stops on the road and bridge

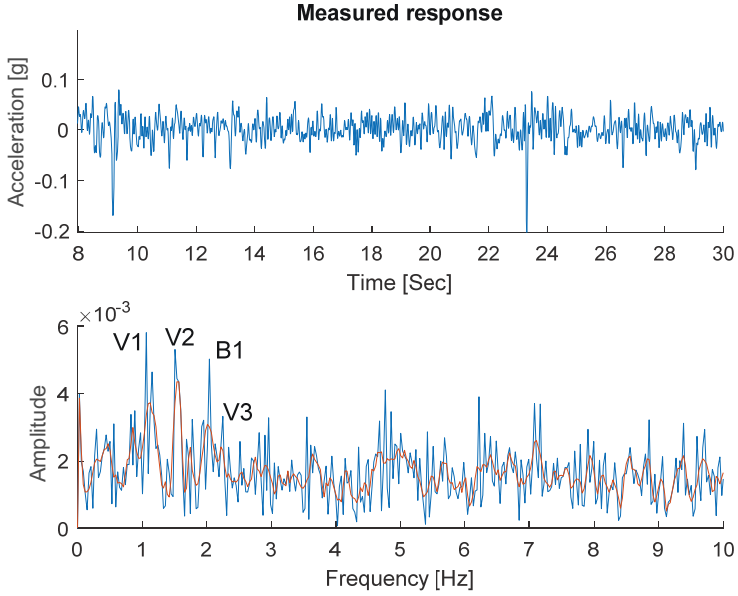

Figure 8.8 Response measurement when vehicle passing the bridge with speed of 10km/h

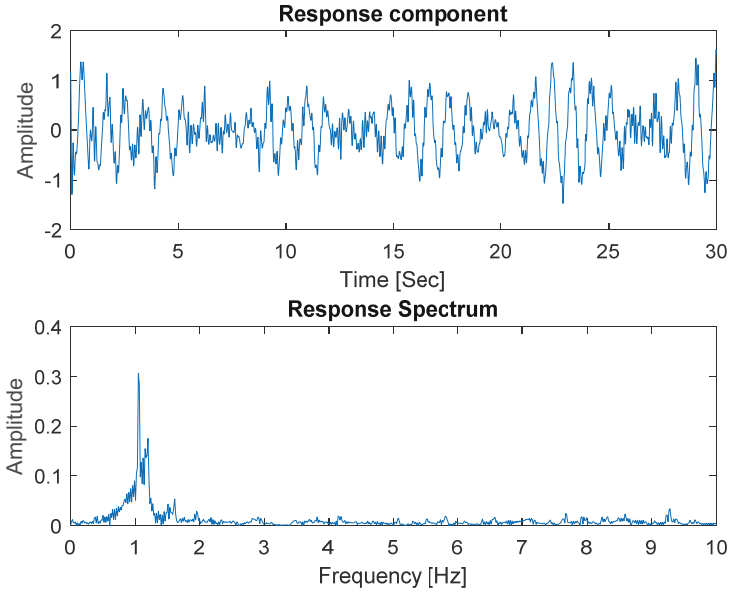

(a) First response component

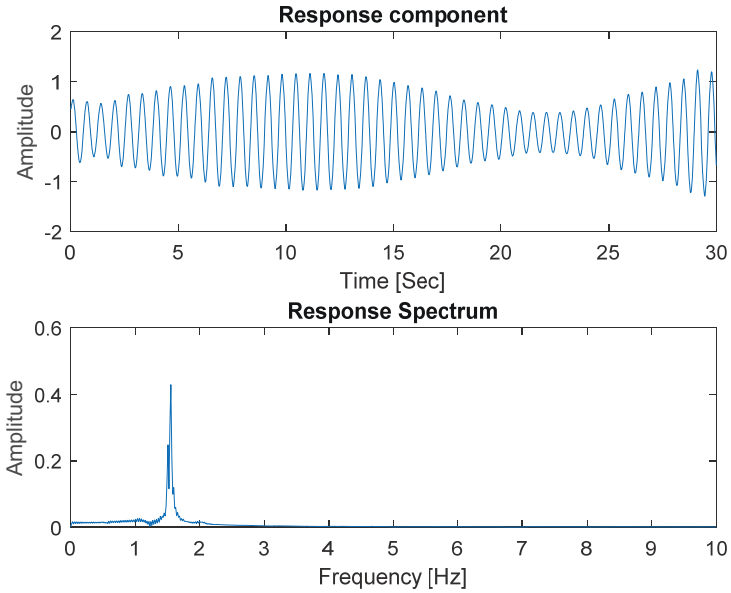

(b) Second response component

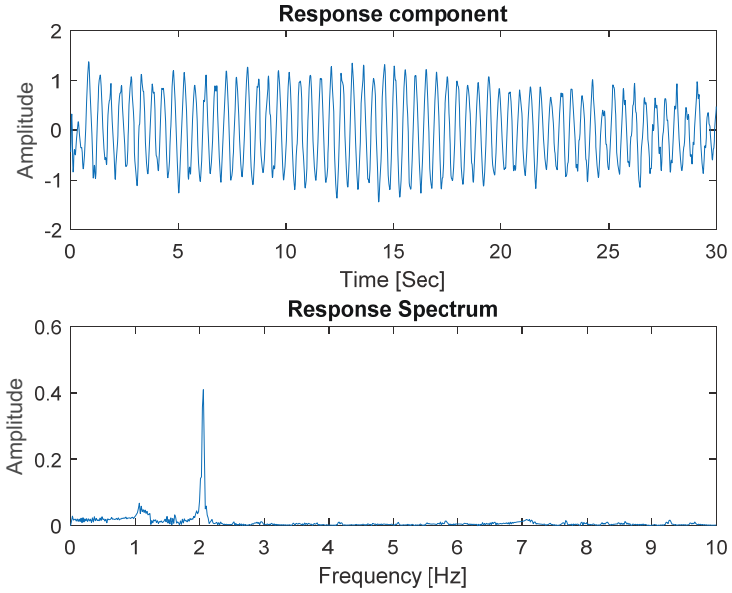

(c) Third response component

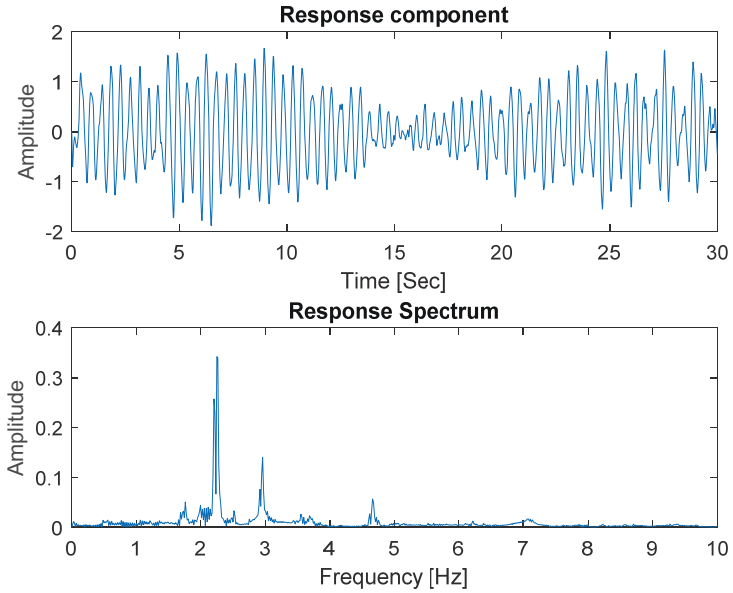

(d) Fourth response component

Figure 8.9 Extracted response components from response when vehicle speed is 10km/h

Figure 8.10 Truck for the investigation of time-varying characteristic of the VBI system

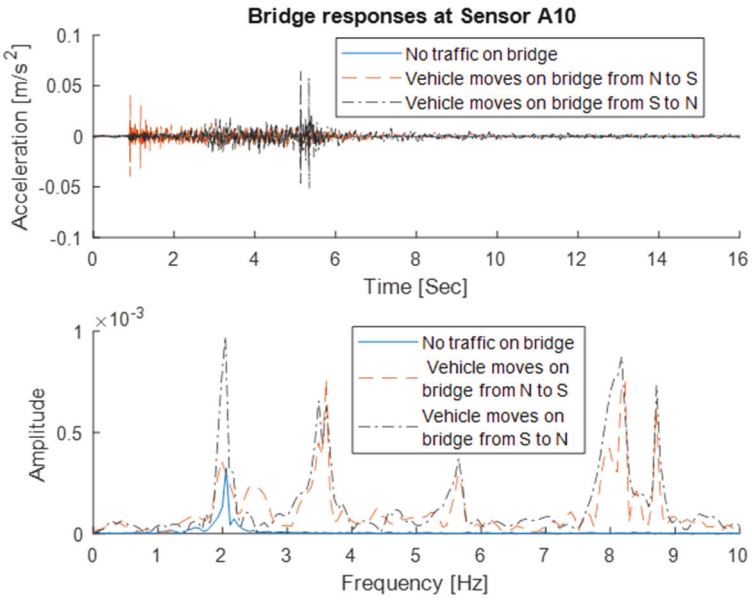

Figure 8.11 Acceleration responses and response spectra under different traffic conditions

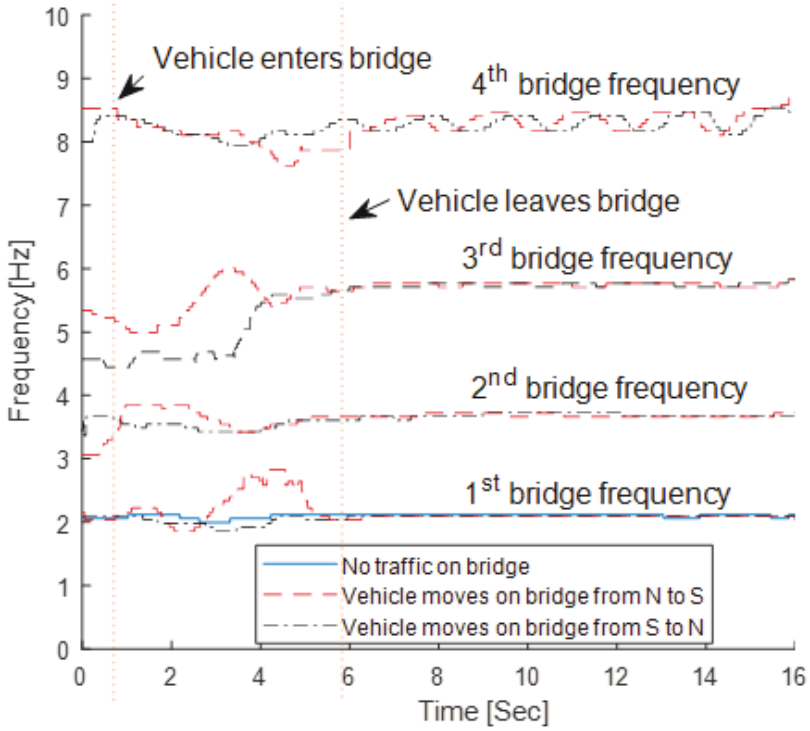

Figure 8.12 TF trajectories of responses for different traffic conditions

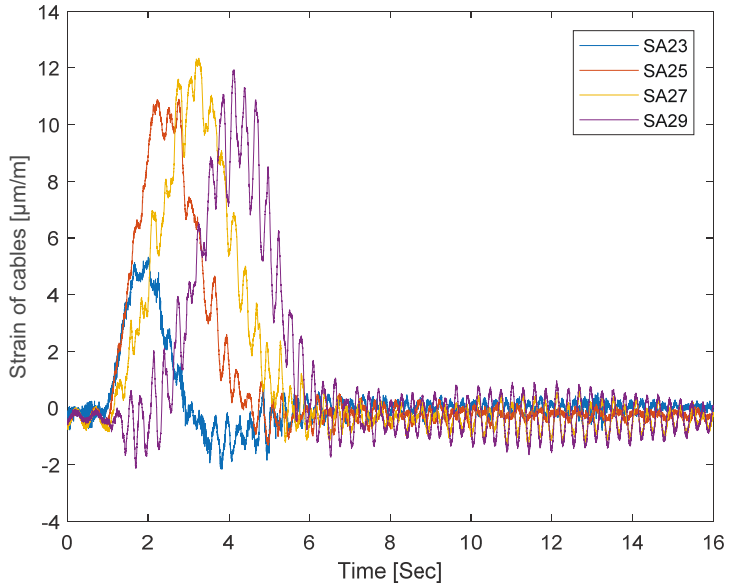

(a) Vehicle moves from North to South

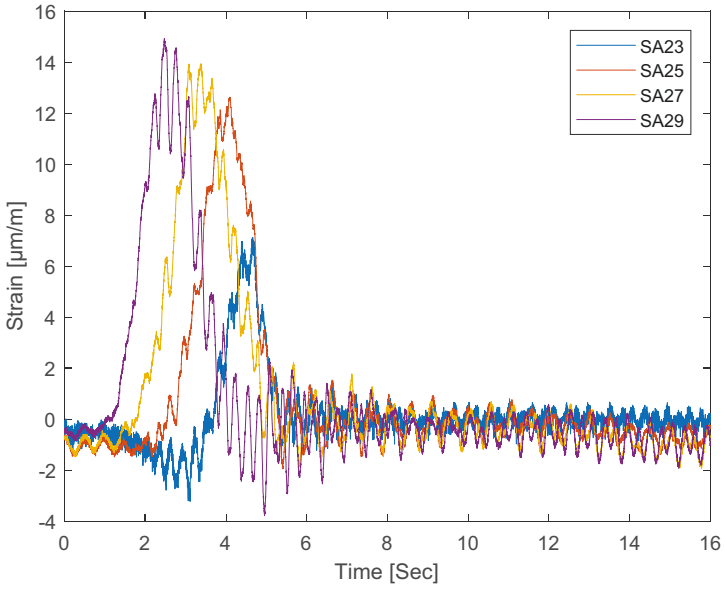

(b) Vehicle moves from South to North

Figure 8.13 Strain measurements on the cables when vehicle moves over the bridge

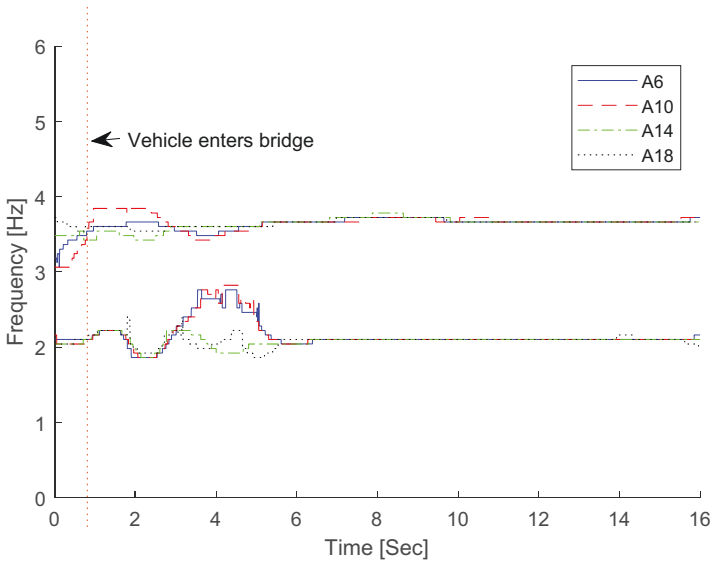

(a) Sensors along longitudinal direction

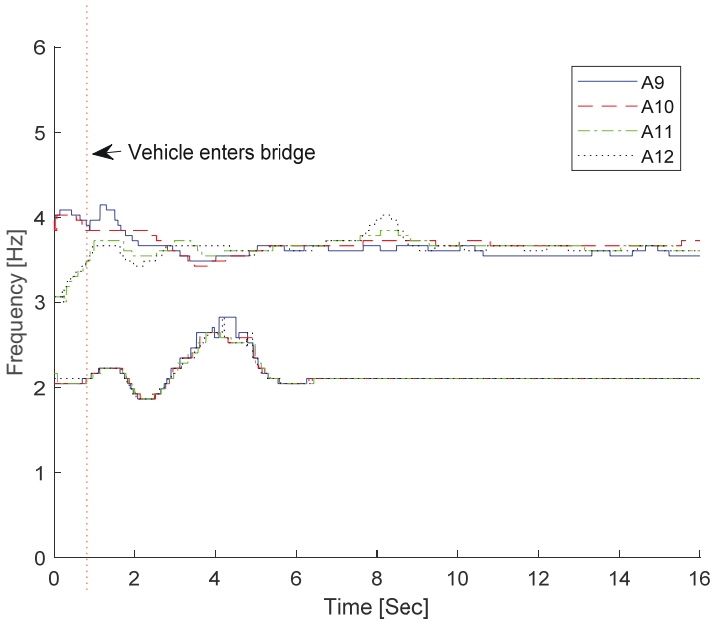

(b) Sensors along transverse direction

Figure 8.14 IFs from responses at different locations

Table 8.1 Identified vehicle frequencies via modal tests

Test number	Frequency (Hz)		
	1st	2nd	3rd
1	0.96	1.4	2.19
2	0.94	1.43	2.23
3	0.95	1.58	2.3
4	1.19	1.74	2.3
5	0.97	1.38	2.18
6	1.07	1.6	2.47
7	0.81	1.62	2.29
8	1.07	1.56	2.28
9	1.1	1.72	2.45
10	1.13	1.74	2.44
Average	1.02	1.58	2.31

Table 8.2 Identified frequencies for the components considering different vehicle speeds

Speed (km/h)	Frequency (Hz)			
	1st	2nd	3rd	4th
10	1.05	1.56	2.06	2.25
20	1.11	1.64	2.05	2.41
30	1.17	1.52	2.00	--

CHAPTER 9 Conclusions and recommendations

9.1 Summary

This study performed an in-depth investigation on the feasibility of indirect bridge SHM. Two new methods (STSSI and SSA-BSS) were proposed for the indirect identification of bridge modal frequencies and mode shapes. The novelty of these methods lie in their capacity to account for the nonstationary features of VBI. A time-frequency analysis strategy was adopted to assess the time-varying characteristics of the vehicle and bridge frequencies due to the interaction. The relationship between the time-varying frequencies and the system parameters was investigated. Numerical and experimental studies were conducted to verify the proposed methods. In the numerical study, the VBI system was modelled with a simply supported beam and a single-degree-of-freedom vehicle model. In the experimental study, a vehicle-bridge interaction testbed was constructed and used for testing. A wireless sensory system was built to monitor the acceleration data. Finally, a two-step drive-by damage detection method is proposed to detect the location and severity of the bridge local damages using vehicle axle responses.

9.2 Conclusions

Results from the numerical and/or experimental studies and lessons learnt in the development of this thesis are summarized as follows:

1) In the new indirect bridge modal parameter identification method with stochastic subspace identification, two instrumented vehicles were used to measure the bridge responses with one moving over the bridge deck and the other remain stationary on the

bridge structure. White noise excitations to the bridge supports were included to consider the effect of on-going traffic on the bridge structure in the numerical simulation. Measured accelerations were segmented and formed into a state space model. Reference-based SSI was used to obtain the local mode shape values. A rescaling procedure was implemented to the local mode shape values to obtain the global mode shapes of the bridge. Numerical and experimental results obtained clearly indicates that the proposed method can identify the bridge mode shapes effectively and accurately. However, the proposed method cannot be used directly when the bridge surface roughness is Class B or worse.

2) The proposed blind modal identification with singular spectrum analysis method decomposes the acceleration response acquired from the sensor on the moving vehicle. The measured response was decomposed into a multichannel data set using singular spectrum analysis, and it was further input to the blind modal identification to extract the bridge-related response components. The bridge modal frequencies were identified from these related components. Numerical and experimental studies showed that the method is effective and robust to the measurement noise for the drive-by bridge frequency identification. The bridge frequencies can also be identified even with a Class B surface roughness. The method was also verified successfully using responses from the vehicle-bridge interaction system in the field.

3) The time-frequency analysis technique SET was adopted to analyse the time-varying characteristics of the vehicle-bridge interaction system numerically and experimentally. The trajectories of instantaneous frequency of the system were extracted. The instantaneous frequency was sensitive to the vehicle/bridge mass ratio. When the vehicle mass was negligible compared to the bridge mass, the modal frequencies of the system were unchanged. Both vehicle and bridge frequency variations can be observed in

the IFs of the responses when the vehicle/bridge mass ratio was large and the vehicle/bridge frequency ratio was not too small. The time-varying characteristics of the vehicle-bridge interaction was also noted in experimental study. Analysis on the responses of an in-situ cable-stay bridge shows that the instantaneous frequencies are affected by the combined effects of moving vehicle and cables.

4) A two-step method was proposed for drive-by bridge damage detection from vehicle axle responses. The Newmark-β method was used to derive the state space representation of the vehicle model. DKF was then adopted to solve the state space model and obtain the unknown interaction forces and the vehicle states. The bridge surface roughness was calculated with known bridge parameters in its intact state. Numerical and experimental results indicates that the proposed method can identify the interaction forces and road surface roughness with high accuracy. Further detection of local damages in the bridge deck can be realised based on the interaction force sensitivity analysis with the interaction forces and roughness obtained in the first step. Numerical results showed that the location and severity of the bridge damages can be detected accurately when the measurement noise is low. The proposed damage detection method is sensitive to measurement noise.

9.3 Recommendations for future study

The indirect bridge inspection using vehicular moving sensory system has shown its potential as an efficient, effective and economic bridge SHM strategy. However, there are technical challenges that must be overcome before this approach can be widely applied. Future investigation on the following topics are recommended:

1) Structural modal frequencies and mode shapes can be obtained from indirect bridge modal identification as shown in this thesis. Bridge related components can be extracted from the vehicle responses, and they can further be used for bridge damage detection.

2) The time-varying characteristics of the vehicle-bridge interaction system is an important factor that must be considered for drive-by bridge inspection. These characteristics have the potential to be used for evaluating the bridge conditions and this needs more study.

3) More study on full-scale bridges is important and beneficial to know the problems with practical application of the indirect bridge health monitoring approaches

References

Abdeljaber O, Avci O, Kiranyaz S, et al. (2017) Real-time vibration-based structural damage detection using one-dimensional convolutional neural networks. *Journal of Sound and Vibration* 388: 154-170.

Alamdari MM, Kildashti K, Samali B, et al. (2019) Damage diagnosis in bridge structures using rotation influence line: Validation on a cable-stayed bridge. *Engineering Structures* 185: 1-14.

American Society of Civil Engineers' 2017 Infrastructure Report Card. (2017). *Bridges.* [online] Available at: https://www.infrastructurereportcard.org/cat-item/bridges/ [Accessed 20/01/2020].

Antoni J. (2005) Blind separation of vibration components: Principles and demonstrations. *Mechanical Systems and Signal Processing* 19: 1166-1180.

Asmussen J, Ibrahim S and Brincker R. (1998) Random decrement: identification of structures subjected to ambient excitation. *Society for Experimental Mechanics, Inc, 16 th International Modal Analysis Conference.*, 914-921.

Aucejo M, De Smet O and Deü J-F. (2019) Practical issues on the applicability of Kalman filtering for reconstructing mechanical sources in structural dynamics. *Journal of Sound and Vibration* 442: 45-70.

Azam SE, Chatzi E and Papadimitriou C. (2015) A dual Kalman filter approach for state estimation via output-only acceleration measurements. *Mechanical Systems and Signal Processing* 60: 866-886.

Bedon C and Morassi A. (2014) Dynamic testing and parameter identification of a base-isolated bridge. *Engineering Structures* 60: 85-99.

Belouchrani A, Abed-Meraim K, Cardoso JF, et al. (1997) A blind source separation technique using second-order statistics. *IEEE Transactions on Signal Processing* 45: 434-444.

Bilello C and Bergman L. (2004) Vibration of damaged beams under a moving mass: theory and experimental validation. *Journal of Sound and Vibration* 274: 567-582.

Boashash B and Aïssa-El-Bey A. (2018) Robust multisensor time–frequency signal processing: A tutorial review with illustrations of performance enhancement in selected application areas. *Digital Signal Processing* 77: 153-186.

Boonyapinyo V and Janesupasaeree T. (2010) Data-driven stochastic subspace identification of flutter derivatives of bridge decks. *Journal of Wind Engineering and Industrial Aerodynamics* 98: 784-799.

Brincker R, Andersen P and Cantieni R. (2001) Identification and level I damage detection of the Z24 highway bridge. *Experimental Techniques* 25: 51-57.

Bu JQ, Law SS and Zhu XQ. (2006) Innovative bridge condition assessment from dynamic response of a passing vehicle. *Journal of Engineering Mechanics ASCE* 132: 1372-1379.

Caicedo J and Casas JM. (2013) System and Method for Modal Identification Using Smart Mobile Sensors. Patent US8577628B2 .

Cantero D, Hester D and Brownjohn J. (2017) Evolution of bridge frequencies and modes of vibration during truck passage. *Engineering Structures* 152: 452-464.

Cantero D, McGetrick P, Kim C-W, et al. (2019) Experimental monitoring of bridge frequency evolution during the passage of vehicles with different suspension properties. *Engineering Structures* 187: 209-219.

Carden EP and Fanning P. (2004) Vibration based condition monitoring: a review. *Structural Health Monitoring* 3: 355-377.

Chang KC, Kim CW and Borjigin S. (2014a) Variability in bridge frequency induced by a parked vehicle. *Smart Structures and Systems* 13: 755-773.

Chang KC, Kim CW and Kawatani M. (2014b) Feasibility investigation for a bridge damage identification method through moving vehicle laboratory experiment. *Structure and Infrastructure Engineering* 10: 328-345.

Chang KC, Wu FB and Yang YB. (2010) Effect of road surface roughness on indirect approach for measuring bridge frequencies from a passing vehicle. *Interaction and Multiscale Mechanics* 3: 299-308.

Chang M, Pakzad SN and Leonard R. (2012) Modal identification using SMIT. *Topics on the Dynamics of Civil Structures, Volume 1.* Springer, 221-228.

Chen S, Cerda F, Rizzo P, et al. (2014) Semi-supervised multiresolution classification using adaptive graph filtering with application to indirect bridge structural health monitoring. *IEEE Transactions on Signal Processing* 62: 2879-2893.

Chen YB, Feng MQ and Tan CA. (2009) Bridge structural condition assessment based on vibration and traffic monitoring. *Journal of Engineering Mechanics ASCE* 135: 747-758.

Clough RW and Penzien J. (2003) *Dynamics of Structures*, Third Edition, Computers and Structures, Inc., USA.

Comanducci G, Magalhães F, Ubertini F, et al. (2016) On vibration-based damage detection by multivariate statistical techniques: Application to a long-span arch bridge. *Structural Health Monitoring* 15: 505-524.

Cruz PJ and Salgado R. (2009) Performance of vibration-based damage detection methods in bridges. *Computer-Aided Civil and Infrastructure Engineering* 24: 62-79.

Das S, Saha P and Patro S. (2016) Vibration-based damage detection techniques used for health monitoring of structures: a review. *Journal of Civil Structural Health Monitoring* 6: 477-507.

Daubechies I, Lu J and Wu H-T. (2011) Synchrosqueezed wavelet transforms: An empirical mode decomposition-like tool. *Applied and Computational Harmonic Analysis* 30: 243-261.

Doebling SW, Farrar CR and Cornwell PJ. (1997) DIAMOND: A Graphical Interface Toolbox for Comparative Modal Analysis and Damage Identification. *Proceedings of the Sixth International Conference on Recent Advances in Structural Dynamic*s, 14-17 July, Southampton, England.

Doebling SW, Farrar CR and Prime MB. (1998) A summary review of vibration-based damage identification methods. *Shock and Vibration Digest* 30: 91-105.

Döhler M, Andersen P and Mevel L. (2010) Data merging for multi-setup operational modal analysis with data-driven SSI. *Proceedings of the 28th International Modal Analysis Conference, Florida, USA*: 445-452.

ElHattab A, Uddin N and O'Brien E. (2017) Drive-by bridge damage detection using non-specialized instrumented vehicle. *Bridge Structures* 12: 73-84.

Engineers Australia (2010) *2010 Australia Infrastructure report card*, Engineers Australia, Barton, A.C.T., Australia.

Fan W and Qiao PZ. (2011) Vibration-based damage identification methods: a review and comparative study. *Structural Health Monitoring* 10: 83-111.

Farrar CR, Doebling SW, Cornwell PJ, et al. (1997) Variability of modal parameters measured on the Alamosa Canyon Bridge. *Proceedings of SPIE - The International Society for Optical Engineering* 1: 257-263.

Farrar CR and Jauregui DA. (1998a) Comparative study of damage identification algorithms applied to a bridge: I. Experiment. *Smart Materials and Structures* 7: 704-719.

Farrar CR and Jauregui DA. (1998b) Comparative study of damage identification algorithms applied to a bridge: II. Numerical study. *Smart Materials and Structures* 7: 720-731.

Fourer D, Harmouche J, Schmitt J, et al. (2017) The ASTRES toolbox for mode extraction of non-stationary multicomponent signals. *Proceedings of the 25th European Signal Processing Conference (EUSIPCO),* Greece: 1130-1134.

Gökdağ H. (2013) A crack identification approach for beam-like structures under moving vehicle using particle swarm optimization. *Materials Testing* 55: 114-120.

Golyandina N. (2010) On the choice of parameters in singular spectrum analysis and related subspace-based methods. *Statisitcs and Its Interface* 3: 259-279

González A, O'Brien EJ and McGetrick P. (2012) Identification of damping in a bridge using a moving instrumented vehicle. *Journal of Sound and Vibration* 331: 4115-4131.

Harmouche J, Fourer D, Auger F, et al. (2018) The Sliding Singular Spectrum Analysis: A Data-Driven Nonstationary Signal Decomposition Tool. *IEEE Transactions on Signal Processing* 66: 251-263.

Hassani H. (2007) Singular spectrum analysis: methodology and comparison. *Journal of Data Science* 5: 239-257.

Hassani H, Mahmoudvand R and Zokaei M. (2011) Separability and window length in singular spectrum analysis. *Comptes Rendus Mathematique* 349: 987-990.

Hazra B, Roffel A, Narasimhan S, et al. (2009) Modified cross-correlation method for the blind identification of structures. *Journal of Engineering Mechanics ASCE* 136: 889-897.

Henchi K, Fafard M, Talbot M, et al. (1998) An efficient algorithm for dynamic analysis of bridges under moving vehicles using a coupled modal and physical components approach. *Journal of Sound and Vibration* 212: 663-683.

Hester D and González A. (2012) A wavelet-based damage detection algorithm based on bridge acceleration response to a vehicle. *Mechanical Systems and Signal Processing* 28: 145-166.

Hester D and González A. (2017) A discussion on the merits and limitations of using drive-by monitoring to detect localised damage in a bridge. *Mechanical Systems and Signal Processing* 90: 234-253.

Hong AL, Ubertini F and Betti R. (2012) New stochastic subspace approach for system identification and its application to long-span bridges. *Journal of Engineering Mechanics ASCE* 139: 724-736.

Horner M, Koser K, Korneva K, et al. (2015) A wireless mobile sensor platform for structural health monitoring. *Proceedings of the Joint 6th International Conference on Advances in Experimental Structural Engineering (6AESE) and 11th International Workshop on Advanced Smart Materials and Smart Structures Technology (11ANCRiSST), Urbana-Champaign.* 1-7.

Huang NE, Huang K and Chiang W-L. (2005) HHT-based bridge structural health-monitoring method. *Hilbert-Huang Transform and Its Applications* 5: 263-287.

Huang NE, Shen Z, Long SR, et al. (1998) The empirical mode decomposition and the Hilbert spectrum for nonlinear and non-stationary time series analysis.

Proceedings of the Royal Society of London A: Mathematical, Physical and Engineering Sciences 454:903-995.

Huth O, Feltrin G, Maeck J, et al. (2005) Damage identification using modal data: Experiences on a prestressed concrete bridge. *Journal of Structural Engineering ASCE* 131: 1898-1910.

Ill GHJ, Carrie TG and Lauffer JP. (1993) The natural excitation technique (NExT) for modal parameter extraction from operating structures, *Internatioanl Journal of Analytical and Experimental Modal Analysis* 10: 260-277.

ISO 8608 (2016) *Mechanical vibration–Road surfaces profiles–Reporting of measured data*. International Organization for Standardization.

James G, Carne TG and Lauffer JP. (1995) The natural excitation technique (NExT) for modal parameter extraction from operating structures. *International Journal of Analytical and Experimental Modal Analysis* 10: 260.

Keenahan J, O'Brien EJ, McGetrick PJ, et al. (2014) The use of a dynamic truck–trailer drive-by system to monitor bridge damping. *Structural Health Monitoring* 13: 143-157.

Kerschen G, Poncelet F and Golinval J-C. (2007) Physical interpretation of independent component analysis in structural dynamics. *Mechanical Systems and Signal Processing* 21: 1561-1575.

Khorram A, Bakhtiari-Nejad F and Rezaeian M. (2012) Comparison studies between two wavelet based crack detection methods of a beam subjected to a moving load. *International Journal of Engineering Science* 51: 204-215.

Kim CW, Chang KC, McGetrick J, et al. (2017) Utilizing Moving Vehicles as Sensors for Bridge Condition Screening-A Laboratory Verification. *Sensors and Materials* 29: 153-163.

Kim CW, Isemoto R, McGetrick P, et al. (2014) Drive-by bridge inspection from three different approaches. *Smart Structures and Systems* 13: 775-796.

Kim CW and Kawatani M. (2008) Pseudo-static approach for damage identification of bridges based on coupling vibration with a moving vehicle. *Structure and Infrastructure Engineering* 4: 371-379.

Kim CY, Jung DS, Kim NS, et al. (2003) Effect of vehicle weight on natural frequencies of bridges measured from traffic-induced vibration. *Earthquake Engineering and Engineering Vibration* 2: 109-115.

Kim J and Lynch JP. (2012) Experimental analysis of vehicle–bridge interaction using a wireless monitoring system and a two-stage system identification technique. *Mechanical Systems and Signal Processing* 28: 3-19.

Kim J, Lynch JP, Lee JJ, et al. (2011) Truck-based mobile wireless sensor networks for the experimental observation of vehicle–bridge interaction. *Smart Materials and Structures* 20: 065009.

Ko J, Sun Z and Ni YQ. (2002) Multi-stage identification scheme for detecting damage in cable-stayed Kap Shui Mun Bridge. *Engineering Structures* 24: 857-868.

Kong X, Cai CS, Deng L, et al. (2017) Using Dynamic Responses of Moving Vehicles to Extract Bridge Modal Properties of a Field Bridge. *Journal of Bridge Engineering ASCE*: 04017018.

Kong X, Cai CS and Kong B. (2014) Damage detection based on transmissibility of a vehicle and bridge coupled system. *Journal of Engineering Mechanics ASCE* 141: 04014102.

Kong X, Cai CS and Kong B. (2016) Numerically extracting bridge modal properties from dynamic responses of moving vehicles. *Journal of Engineering Mechanics ASCE* 142: 04016025.

Kunwar A, Jha R, Whelan M, et al. (2013) Damage detection in an experimental bridge model using Hilbert–Huang transform of transient vibrations. *Structural Control and Health Monitoring* 20: 1-15.

Law SS and Zhu XQ. (2004) Dynamic behavior of damaged concrete bridge structures under moving vehicular loads. *Engineering Structures* 26: 1279-1293.

Law SS and Zhu XQ. (2009) *Damage Models and Algorithms for Assessment of Structures under Operating Conditions*, CRC Press, Taylor and Francis Group, UK.

Lederman G, Chen S, Garrett J, et al. (2017a) Track-monitoring from the dynamic response of an operational train. *Mechanical Systems and Signal Processing* 87: 1-16.

Lederman G, Chen S, Garrett JH, et al. (2017b) Track monitoring from the dynamic response of a passing train: A sparse approach. *Mechanical Systems and Signal Processing* 90: 141-153.

Lee JW, Kim JD, Yun CB, et al. (2002) Health-monitoring method for bridges under ordinary traffic loadings. *Journal of Sound and Vibration* 257: 247-264.

Lei Y, Jiang Y and Xu Z. (2012) Structural damage detection with limited input and output measurement signals. *Mechanical Systems and Signal Processing* 28: 229-243.

Li J, Law SS and Hao H. (2013) Improved damage identification in bridge structures subject to moving loads: numerical and experimental studies. *International Journal of Mechanical Sciences* 74: 99-111.

Li JZ, Su MB and Fan LC. (2003) Natural Frequency of Railway Girder Bridges under Vehicle Loads. *Journal of Bridge Engineering ASCE* 8: 199-203.

Li WM, Jiang ZH, Wang TL, et al. (2014) Optimization method based on Generalized Pattern Search Algorithm to identify bridge parameters indirectly by a passing vehicle. *Journal of Sound and Vibration* 333: 364-380.

Li ZH and Au FTK. (2014) Damage detection of a continuous bridge from response of a moving vehicle. *Shock and Vibration* 2014: Article ID 146802.

Lin CW and Yang YB. (2005) Use of a passing vehicle to scan the fundamental bridge frequencies: An experimental verification. *Engineering Structures* 27: 1865-1878.

Liu K, Law SS, Zhu XQ, et al. (2014a) Explicit form of an implicit method for inverse force identification. *Journal of Sound and Vibration* 333: 730-744.

Liu K, Law SS, Xia Y, et al. (2014b) Singular spectrum analysis for enhancing the sensitivity in structural damage detection. *Journal of Sound and Vibration* 333: 392-417.

Lu ZR and Liu JK. (2011) Identification of both structural damages in bridge deck and vehicular parameters using measured dynamic responses. *Computers & Structures* 89: 1397-1405.

Malekjafarian A, McGetrick PJ and O'Brien EJ. (2015) A review of indirect bridge monitoring using passing vehicles. *Shock and Vibration* 2015: Article ID 286139..

Malekjafarian A and O'Brien EJ. (2014) Identification of bridge mode shapes using Short Time Frequency Domain Decomposition of the responses measured in a passing vehicle. *Engineering Structures* 81: 386-397.

Malekjafarian A and O'Brien EJ. (2017) On the use of a passing vehicle for the estimation of bridge mode shapes. *Journal of Sound and Vibration* 397: 77-91.

Manuel M-LJ, Andrea B, Stefano M, et al. (2013) Wavelets-based damage localization on beams under the influence of moving loads. *Mechanics & Industry* 14: 107-113.

Marchesiello S, Bedaoui S, Garibaldi L, et al. (2009) Time-dependent identification of a bridge-like structure with crossing loads. *Mechanical Systems and Signal Processing* 23: 2019-2028.

Marulanda J, Caicedo JM and Thomson P. (2016) Modal Identification Using Mobile Sensors under Ambient Excitation. *Journal of Computing in Civil Engineering ASCE*: 04016051.

Matarazzo TJ and Pakzad SN. (2016) STRIDE for structural identification using expectation maximization: iterative output-only method for modal identification. *Journal of Engineering Mechanics ASCE* 142: 04015109.

McGetrick PJ, Kim CW, González A, et al. (2015) Experimental validation of a drive-by stiffness identification method for bridge monitoring. *Structural Health Monitoring* 14: 317-331.

McNeill S and Zimmerman D. (2008) A framework for blind modal identification using joint approximate diagonalization. *Mechanical Systems and Signal Processing* 22: 1526-1548.

Meignen S, Oberlin T, Depalle P, et al. (2016) Adaptive multimode signal reconstruction from time–frequency representations. *Philosophical Transactions of the Royal Society A: Mathematical, Physical and Engineering Sciences*, Royal Society 374: 1-13.

Nguyen KV. (2015) Dynamic analysis of a cracked beam-like bridge subjected to earthquake and moving vehicle. *Advances in Structural Engineering* 18: 75-95.

Nguyen KV and Tran HT. (2010) Multi-cracks detection of a beam-like structure based on the on-vehicle vibration signal and wavelet analysis. *Journal of Sound and Vibration* 329: 4455-4465.

O'Brien EJ, Carey C and Keenahan J. (2015) Bridge damage detection using ambient traffic and moving force identification. *Structural Control and Health Monitoring* 22: 1396-1407.

O'Brien EJ, McGetrick P and Gonzalez A. (2014) A drive-by inspection system via vehicle moving force identification. *Smart Structures and Systems* 13: 821-848.

O'Brien EJ, Malekjafarian A and González A. (2017) Application of empirical mode decomposition to drive-by bridge damage detection. *European Journal of Mechanics-A/Solids* 61: 151-163.

Oshima Y, Yamamoto K and Sugiura K. (2014) Damage assessment of a bridge based on mode shapes estimated by responses of passing vehicles. *Smart Structures and Systems* 13: 731-753.

Peeters B and De Roeck G. (1999) Reference-based stochastic subspace identification for output-only modal analysis. *Mechanical Systems and Signal Processing* 13: 855-878.

Petersen CD, Fraanje R, Cazzolato BS, et al. (2008) A Kalman filter approach to virtual sensing for active noise control. *Mechanical Systems and Signal Processing* 22: 490-508.

Pines D and Aktan AE. (2002) Status of structural health monitoring of long-span bridges in the United States. *Progress in Structural Engineering and Materials* 4: 372-380.

Piombo B, Fasana A, Marchesiello S, et al. (2000) Modelling and identification of the dynamic response of a supported bridge. *Mechanical Systems and Signal Processing* 14: 75-89.

Poncelet F, Kerschen G, Golinval J-C, et al. (2007) Output-only modal analysis using blind source separation techniques. *Mechanical Systems and Signal Processing* 21: 2335-2358.

Sadhu A, Narasimhan S and Antoni J. (2017) A review of output-only structural mode identification literature employing blind source separation methods. *Mechanical Systems and Signal Processing* 94: 415-431.

Sumitoro S, Matsui Y, Kono M, et al. (2001) Long span bridge health monitoring system in Japan. *Proceedings of SPIE 4337*, 517-524.

Sun M, Makki Alamdari M and Kalhori H. (2017) Automated operational modal analysis of a cable-stayed bridge. *Journal of Bridge Engineering ASCE* 22: 05017012.

Tan CJ, Uddin N, O'Brien EJ, et al. (2019) Extraction of Bridge Modal Parameters Using Passing Vehicle Response. *Journal of Bridge Engineering ASCE* 24: 04019087.

Thakur G and Wu HT. (2011) Synchrosqueezing-based recovery of instantaneous frequency from nonuniform samples. *SIAM Journal on Mathematical Analysis* 43: 2078-2095.

Thakur G, Brevdo E, Fuckar NS, et al. (2013) The Synchrosqueezing algorithm for time-varying spectral analysis: robustness properties and new paleoclimate applications. *Singal Processing* 93:1079-1094.

Van Overschee P and De Moor B. (2012) *Subspace identification for linear systems: Theory—Implementation—Applications*: Springer Science & Business Media.

Wang H, Nagayama T, Zhao B, et al. (2017) Identification of moving vehicle parameters using bridge responses and estimated bridge pavement roughness. *Engineering Structures* 153: 57-70.

Wang S, Chen X, Cai G, et al. (2014) Matching Demodulation Transform and SynchroSqueezing in Time-Frequency Analysis. *IEEE Transactions on Signal Processing* 62: 69-84.

Wang Y and Hao H. (2013) Damage identification scheme based on compressive sensing. *Journal of Computing in Civil Engineering ASCE* 29: 04014037.

Wickramasinghe WR, Thambiratnam DP, Chan TH, et al. (2016) Vibration characteristics and damage detection in a suspension bridge. *Journal of Sound and Vibration* 375: 254-274.

Xiao F, Chen GS, Hulsey JL, et al. (2017) Characterization of non-stationary properties of vehicle–bridge response for structural health monitoring. *Advances in Mechanical Engineering* 9: 1687814017699141.

Yang JN, Lin S, Huang H, et al. (2006) An adaptive extended Kalman filter for structural damage identification. *Structural Control and Health Monitoring* 13: 849-867.

Yang Y, Cheng M and Chang K. (2013a) Frequency variation in vehicle–bridge interaction systems. *International Journal of Structural Stability and Dynamics* 13: 1350019.

Yang Y and Nagarajaiah S. (2012) Time-frequency blind source separation using independent component analysis for output-only modal identification of highly damped structures. *Journal of Structural Engineering ASCE* 139: 1780-1793.

Yang YB and Chang KC. (2009a) Extracting the bridge frequencies indirectly from a passing vehicle: Parametric study. *Engineering Structures* 31: 2448-2459.

Yang YB and Chang KC. (2009b) Extraction of bridge frequencies from the dynamic response of a passing vehicle enhanced by the EMD technique. *Journal of Sound and Vibration* 322: 718-739.

Yang YB, Chang KC and Li YC. (2013b) Filtering techniques for extracting bridge frequencies from a test vehicle moving over the bridge. *Engineering Structures* 48: 353-362.

Yang YB and Chen WF. (2015) Extraction of bridge frequencies from a moving test vehicle by stochastic subspace identification. *Journal of Bridge Engineering ASCE* 21: 04015053.

Yang YB, Li YC and Chang KC. (2012a) Effect of road surface roughness on the response of a moving vehicle for identification of bridge frequencies. *Interaction and Multiscale Mechanics* 5: 347-368.

Yang YB, Li YC and Chang KC. (2012b) Using two connected vehicles to measure the frequencies of bridges with rough surface: a theoretical study. *Acta Mechanica* 223: 1851-1861.

Yang YB, Li YC and Chang KC. (2014) Constructing the mode shapes of a bridge from a passing vehicle: a theoretical study. *Smart Structures and Systems* 13: 797-819.

Yang YB and Lin BH. (1995) Vehicle-bridge interaction analysis by dynamic condensation method. *Journal of Structural Engineering ASCE* 121: 1636-1643.

Yang YB and Lin CW. (2005) Vehicle–bridge interaction dynamics and potential applications. *Journal of Sound and Vibration* 284: 205-226.

Yang YB, Lin CW and Yau JD. (2004) Extracting bridge frequencies from the dynamic response of a passing vehicle. *Journal of Sound and Vibration* 272: 471-493.

Yang YB and Yang JP. (2018) State-of-the-Art review on modal identification and damage detection of bridges by moving test vehicles. *International Journal of Structural Stability and Dynamics* 18: 1850025.

Yang YB, Zhang B, Chen YA, et al. (2019) Bridge damping identification by vehicle scanning method. *Engineering Structures* 183: 637-645.

Yang Y, Cheng Q, Zhu YH, et al. (2020) Feasibility study of tractor-test vehicle technique for practical structural condition assessment of beam-like bridge deck. *Remote Sensing* 12: 114.

Yu G, Yu M and Xu C. (2017) Synchroextracting transform. *IEEE Transactions on Industrial Electronics* 64: 8042-8054.

Zhang B, Qian Y, Wu Y, et al. (2018) An effective means for damage detection of bridges using the contact-point response of a moving test vehicle. *Journal of Sound and Vibration* 419: 158-172.

Zhang Q. (2007) Statistical damage identification for bridges using ambient vibration data. *Computers & Structures* 85: 476-485.

Zhang Q, Fan L and Yuan W. (2002) Traffic-induced variability in dynamic properties of cable-stayed bridge. *Earthquake Engineering & Structural Dynamics* 31: 2015-2021.

Zhang Y, Lie ST and Xiang ZH. (2013) Damage detection method based on operating deflection shape curvature extracted from dynamic response of a passing vehicle. *Mechanical Systems and Signal Processing* 35: 238-254.

Zhang Y, Wang LQ and Xiang ZH. (2012) Damage detection by mode shape squares extracted from a passing vehicle. *Journal of Sound and Vibration* 331: 291-307.

Zhen L, Peng D, Yi Z, et al. (2017) Underdetermined blind source separation using sparse coding. *IEEE Transactions on Neural Networks and Learning Systems* 28: 3102-3108.

Zhou W and Chelidze D. (2007) Blind source separation based vibration mode identification. *Mechanical Systems and Signal Processing* 21: 3072-3087.

Zhu D, Yi X, Wang Y, et al. (2010) A mobile sensing system for structural health monitoring: design and validation. *Smart Materials and Structures* 19: 055011.

Zhu DP, Guo JJ, Cho CH, et al. (2012) Wireless mobile sensor network for the system identification of a space frame bridge. *IEEE/ASME Transactions on Mechatronics* 17: 499-507.

Zhu XQ and Hao H. (2012) Development of an integrated structural health monitoring system for bridge structures in operational conditions. *Frontiers of Structural and Civil Engineering* 6: 321-333.

Zhu XQ, Law SS, Huang L, et al. (2018) Damage identification of supporting structures with a moving sensory system. *Journal of Sound and Vibration* 415: 111-127.

Zhu XQ and Law SS. (2006) Wavelet-based crack identification of bridge beam from operational deflection time history. *International Journal of Solids and Structures* 43: 2299-2317.

Zhu XQ and Law SS. (2015) Structural health monitoring based on vehicle-bridge interaction: accomplishments and challenges. *Advances in Structural Engineering* 18: 1999-2015.

Zhu XQ and Law SS. (2016) Recent developments in inverse problems of vehicle–bridge interaction dynamics. *Journal of Civil Structural Health Monitoring* 6: 107-128.